SCHLAGER Christoph, Bakk.rer.nat. MSc.

Generation of high-resolution wind fields from WegenerNet data and a spatial evaluation of regional climate models

DOCTORAL THESIS

to achieve the university degree of
Doktor der technischen Wissenschaften
submitted to

Graz University of Technology

Supervisor:

Ao. Univ.-Prof. i. R. Dr. phil. tit. Univ.-Prof. BARTELME Norbert
Institute of Geodesy, Working Group Geoinformation
Graz University of Technology

Co-Supervisor:

Univ.-Prof. Mag. Dr. rer. nat. KIRCHENGAST Gottfried
Wegener Center for Climate and Global Change
University of Graz

Graz, July, 2019

Eidesstattliche Erklärung
Affidavit

Ich erkläre an Eides statt, dass ich die vorliegende Arbeit selbstständig verfasst, andere als die angegebenen Quellen/Hilfsmittel nicht benutzt, und die den benutzten Quellen wörtlich und inhaltlich entnommenen Stellen als solche kenntlich gemacht habe. Das in TUGRAZonline hochgeladene Textdokument ist mit der vorliegenden Doktorarbeit identisch.

I declare that I have authored this thesis independently, that I have not used other than the declared sources/resources, and that I have explicitly indicated all material which has been quoted either literally or by content from the sources used. The text document uploaded to TUGRAZonline is identical to the present doctoral thesis.

Datum / Date	Unterschrift / Signature

Abstract

The innovations in computer science that have made possible the development of increasingly powerful computer hardware and more advanced software architectures have also allowed for the simulation of high-resolution model outputs based on regional climate models (RCMs) at the 1 km scale. At this resolution, RCMs provide more realistic simulations than lower-resolution models by explicitly resolving deep convection and representing orography more accurately. Model outputs based on 1-km-scale RCMs, however, have significant limitations and are subject to various sources of uncertainty. Furthermore, the fact that reference datasets in correspondingly high spatial and temporal resolutions are lacking makes it difficult to evaluate high-resolution outputs from RCMs.

This work focuses on the modeling of near-surface winds and includes as a first objective the development of an application for generating high-resolution wind fields based on station data. Related to this objective, it introduces a weather diagnostic application called the Wind Product Generator (WPG), which has been developed within this work. The WPG is capable of automatically generating gridded wind fields in near-real-time. In this project, the WPG is used to generate high-resolution reference wind fields using observations from two dense networks of meteorological stations, the WegenerNet Feldbach Region (FBR) network and the WegenerNet Johnsbachtal (JBT) network.

The high-density WegenerNet FBR consists of more than 150 meteorological stations distributed throughout a region characterized by hilly terrain and small differences in altitude, while the WegenerNet JBT contains 11 meteorological stations situated in a mountainous region exhibiting large differences in altitude. Reference wind fields produced for the WegenerNet FBR network are found to be reasonably accurate; reference wind fields produced for the WegenerNet JBT are reasonably accurate in terms of wind speeds, but wind directions are less accurate along mountain slopes, which are particularly challenging. In summary, the results of these studies indicate that the WPG can serve as a valuable tool for evaluating wind fields produced by high-resolution models.

Ultimately, the second main objective is the evaluation of high-resolution wind fields from selected dynamical models based on the WPG-generated wind fields. The spatial evaluation of high-resolution wind fields carried out in this study relates to geographic information science. The added value that high resolutions provide to model outputs is difficult to assess by traditional statistical methods. In this project, a novel neighborhood-based spatial wind verification methodology is introduced, allowing the evaluation of spatial differences and displacements between datasets. That this methodology is feasible for such purposes is demonstrated by means of

an intercomparison of WPG-generated wind fields with wind field analysis data taken from the Integrated Nowcasting through Comprehensive Analysis (INCA) system and with regional climate model wind field data from the non-hydrostatic climate model of the Consortium for Small Scale Modeling Model in Climate Mode (CCLM). Within this comparison, the quality and limitations of these models are evaluated using WPG wind fields for representative weather events generated for the WegenerNet FBR and WegenerNet JBT.

Zusammenfassung

Innovationen in den Computerwissenschaften, welche die Entwicklung immer leistungsfähigerer Computerhardware sowie Fortschritte in Softwarearchitekturen ermöglicht haben, erlauben mittlerweile Simulationen von regionalen Klimamodellen (RCMs) mit einer horizontalen Auflösung von bis zu 1 km x 1 km. Bei solch einer Auflösung liefern RCMs realistischere Simulationen im Vergleich zu Modellen mit einer geringeren horizontalen Gitterweite, indem die Tiefenkonvektion explizit simuliert und die Orographie genauer abgebildet wird.

Die vorliegende Arbeit fokussiert sich auf die Modellierung von oberflächennahen Winden und beinhaltet als erstes Ziel die Entwicklung einer Anwendung zur Erzeugung von hochauflösenden Windfeldern auf Basis von Stationsdaten. Im Zusammenhang mit diesem Ziel wird eine Wetterdiagnostikanwendung namens Wind Product Generator (WPG) vorgestellt, welche im Rahmen dieser Arbeit entwickelt wurde und mit Hilfe derer automatisch gitterförmige Windfelder in Nahezu-Echtzeit erzeugt werden können. In diesem Projekt wird der WPG verwendet, um hochauflösende Referenzwindfelder aus Beobachtungen von zwei dichten Netzwerken meteorologischer Stationen, dem „WegenerNet Feldbachregion (FBR)“ und dem „WegenerNet Johnsbachtal (JBT)“, zu erzeugen.

Das WegenerNet FBR besteht aus mehr als 150 meteorologischen Stationen, welche in einer Region gekennzeichnet durch hügeliges Gelände und geringe Höhenunterschiede verteilt sind, während das WegenerNet JBT 11 meteorologische Stationen in einer Bergregion mit großen Höhenunterschieden umfasst. Die für das WegenerNet FBR-Netz erzeugten Referenzwindfelder erweisen sich als angemessen genau; jene für das WegenerNet JBT sind in Bezug auf die Windgeschwindigkeiten angemessen genau, jedoch zeigen Windrichtungen entlang der besonders anspruchsvollen Berghänge größere Abweichungen im Vergleich zu Beobachtungen. Zusammenfassend zeigen die Ergebnisse der Studie, dass der WPG als wertvolles Werkzeug zur Evaluierung von Windfeldern, welche beispielsweise mittels hochauflösender Klimamodelle erzeugt werden, dienen kann.

Letztendlich ist das zweite Hauptziel die Evaluierung hochauflösender Windfelder aus ausgewählten Modellen, basierend auf den WPG-generierten Windfeldern. Die in dieser Studie durchgeführte räumliche Evaluierung hochauflösender Windfelder ist im Bereich der Geoinformationswissenschaften angesiedelt. Den Mehrwert, den hochaufgelöste im Vergleich zu niedrig aufgelösten Simulationen bieten, ist mit herkömmlichen statistischen Methoden schwer zu beurteilen. In diesem Projekt wird eine neuartige, nachbarschaftsbezogene Methodik zur räumlichen Windverifikation vorgestellt, die die Bewertung von räumlichen Unterschieden und Verschiebungen zwischen Datensätzen ermöglicht. Dass diese Methodik für solche Zwecke prak-

tikabel ist, wird durch einen Vergleich von WPG-generierten Windfeldern mit Windfeldanalysedaten erzeugt mittels des Integrated Nowcasting through Comprehensive Analysis (INCA)-System und mit Klimamodell-Windfelddaten generiert mittels des nichthydrostatischen Klimamodells des Consortium for Small Scale Modeling Model in Climate Mode (CCLM) demonstriert. In diesem Vergleich werden die Qualität und Grenzen dieser Modelle mit Hilfe von WPG-Windfeldern, erzeugt für das WegenerNet FBR und WegenerNet JBT, evaluiert.

Acknowledgements

First and foremost, I would like to thank my supervisor, founder and director of the Wegener Center for Climate and Global Change, Univ.-Prof. Mag. Dr.rer.nat. Gottfried Kirchengast, who gave me the opportunity to write my thesis at the Wegener Center. Thank you for your excellent guidance, scientific advice, constructive feedback and motivating words throughout my work at the Wegener Center. I especially want to thank my supervisor at Graz University of Technology Ao. Univ.-Prof. i. R. Dr. phil. tit. Univ.-Prof. Norbert Bartelme on having made this interdisciplinary research work possible. He has taught me a lot during my master studies and this research and guided this work in the right direction.

I'm particularly grateful to Dipl.-Ing. Jürgen Fuchsberger for his comprehensive support as co-supervisor at Wegener Center regarding technical aspects and IT issues, as well as for assistance in software development whenever needed. I also would like to express my gratitude to Heimo Truthetz, for valuable scientific discussions and advices.

Special thanks are extended to the entire Wegener Center Team for the privilege of working with you and for your help whenever I asked for it. Together, they created an incredible atmosphere and make this institute a great place to work. Some of them became good friends.

Finally, I would like to express sincere thanks to my sister for proofreading of several text passages which I wrote during the course of this thesis.

Contents

1 Introduction

In recent decades, scientific research has placed significant focus on the topics of weather and climate and the ways in which they impact ecosystems, societies, and the lives of individuals (e.g. Hansen et al. 1981; Hasselmann 1993; Govindasamy and Caldeira 2000; IPCC 2007; Shindell et al. 2012; IPCC 2012; IPCC 2014; Hughes et al. 2017). The influence of climate on natural environments and human life is most evident when it is studied on a regional to local scale (Prein 2013; Prein et al. 2013b). Regional climate models (RCMs) are well-established research tools for analyzing and understanding climate by generating key input data for climate change impact studies, as well as for strategies for adapting to climate change (Prein et al. 2013b; Rummukainen 2010; Leutwyler et al. 2016). These models are deployed to obtain regional-scale simulations of phenomena such as regional wind field patterns, precipitation, etc. and take into account important local interactions between the Earth's surface and atmosphere.

Since these models only cover limited geographical areas, information at the model's lateral boundaries is required, which is obtained from model outputs at coarser grid scales. These outputs are usually generated by Global Climate Models (GCMs), or through reanalysis, or by larger-scale RCMs. In conventional models, small-scale convective processes such as moist convection need to be parameterized. These parameterizations introduce a degree of uncertainty into the model's representations of clouds, precipitation, and small-scale wind patterns, negatively impacting the model's ability to represent climate change projections at smaller scales (Prein et al. 2013b; Randall et al. 2003; Leutwyler et al. 2016).

Innovations in computer science and increases in the power of computer hardware have allowed high-resolution outputs to be generated from RCMs at a 1 km scale. At this resolution, simulations produced from RCMs demonstrate two main improvements over lower-resolution simulations: first, these simulations are more realistic, especially for regions with complex terrain, thus allowing investigations of weather and climate in smaller sub-regions; and second, these simulations can resolve associated processes such as deep convection without requiring parameterizations. Multiple studies have demonstrated the added value of such so-called Convection-Permitting Climate Simulations (CPCSs), especially in simulations of small-scale precipitation patterns (Prein et al. 2013b; Langhans et al. 2012; Weusthoff et al. 2010; Hohenegger et al. 2008; Kendon et al. 2017). However, as new innovations are continually being developed, and CPCSs have only been used in the last several years, more research is required to make a rigorous and detailed evaluation of the quality of CPCSs.

1.1 Motivation and research design

Wind field evaluation data

The lack of datasets with spatial and temporal resolutions that match the resolutions of CPCSs produced by RCMs makes evaluating these simulations difficult. The model outputs generated by RCMs typically represent area averages of the involved processes rather than processes at specific locations. The most suitable datasets for evaluating simulations that use such models are therefore gridded fields of meteorological data, where each cell in a grid is an average of best estimates for the observation corresponding to that grid cell (Haylock et al. 2008; Haiden et al. 2011; Hiebl and Frei 2016)

The Wegener Center for Climate and Global Change at the University of Graz has helped address the lack of suitable evaluation data for these simulations by acquiring and automatically processing data from two networks of meteorological stations: the high-density WegenerNet Feldbach Region (FBR) network, located in a region of the Alpine foreland dominated by hilly terrain, and its sister network, the WegenerNet Johnsbachtal (JBT) network, located in a mountainous Alpine region characterized by highly complex terrain. The main aims of the Wegener Center in establishing these networks are to evaluate RCMs and investigate weather and climate on a local scale.

The observations acquired from these two station networks are controlled and processed by the WegenerNet Processing System (WPS), which includes four subsystems (Kirchengast et al. 2014): the Command Receive Archiving System transfers raw measurement data via wireless General Packet Radio Service (GPRS) transmission to the WegenerNet database in Graz; the Quality Control System checks the data quality; the Data Product Generator (DPG) generates regular station time series for all stations and parameters as well as gridded fields of weather and climate products for the variables temperature, precipitation, and relative humidity for the WegenerNet FBR; and the Visualization and Information System offers the data to users via the WegenerNet data portal (www.wegenernet.org). Further detailed information regarding the WPS and its subsystems can be found in Kirchengast et al. (2014) and Kabas (2012).

The work presented in this thesis focuses on evaluating simulations of near-surface winds on the basis of DPG station data, and comprises a first step towards filling a critical gap in the development of the DPG. In particular, the project implements a newly-developed wind field application named Wind Product Generator (WPG) in conjunction with the DPG. The WPG uses the California Meteorological Model (CALMET) as core tool and generates mean wind field data in near real-time at 10 m and 50 m height levels, with a spatial resolution of 100 m $\times$ 100 m and a temporal resolution of 30 minutes, based on the meteorological observations and surface-related datasets provided by the two WegenerNet regional networks. Gridded wind field data are available from the WegenerNet FBR starting in 2007 and from the WegenerNet JBT starting in 2012. The WPG application can also

be used to create wind fields based on data from other high-density networks, can serve as a tool for evaluating high-resolution wind field simulations from different types of models, and can aid investigations into the impact of airflows on a regional to local scale, among other uses (Schlager et al. 2017; Schlager et al. 2018).

A spatial verification of wind fields: Geographic information science

The main scientific contribution of this thesis to the field of geographic information science (GIS) deals with the spatial verification of high-resolution simulations of wind.

Spatial verification methods were developed mainly to address challenges that arise in the evaluation of high-resolution forecasts (Ebert 2008; Rossa et al. 2008; Gilleland et al. 2009; Gilleland et al. 2010; Gilleland 2013). The verification scores that traditional verification methods deliver often do not account for the ways in which high-resolution forecasts improve upon lower-resolution forecasts, such as the more realistic simulations they produce of the distributions and spatial structures of weather events. In general, however, high-resolution forecasts are not able to simulate the exact position of a weather event in space and time. In the case that a forecast's position is offset in relation to a reference field, a calculation of skill measures based on traditional gridpoint-based methods will yield "double penalties" that lower the forecast's score. A double penalty is a penalization that results, first, from the forecast simulating an event where it did not occur, and, second, from the forecast failing to simulate an event where it did in fact occur (Roberts 2008; Prein et al. 2013b; Skok and Hladnik 2018).

Coarser resolution models are generally favored by gridpoint-based verification methods, even if human analysts would assess the high-resolution forecasts as superior. Furthermore, gridpoint-based verification methods are not able to provide important diagnostic information about the type of error occurring in the forecast, such as whether the error results from scale-dependent or spatial properties, displacements, or structural differences between features of the forecast and the real data (Gilleland et al. 2010).

In recent years, several relatively new verification methods have been developed that largely come from the field of image analysis and computer vision studies. These new methods use distinct approaches and have different characteristics than gridpoint-based methods. For this reason, comparison of these new methods has been one of the focuses of a Coordinated Intercomparison Project (ICP) organized by the National Center for Atmospheric Research (details at www.ral.ucar.edu/projects/icp). The ICP resolves questions concerning issues such as the best methods to use for specific purposes, the best ways of obtaining information about uncertainty, and specific characteristics of particular methods (Gilleland et al. 2010).

Due to the high heterogeneity of precipitation patterns, most of these newly-developed verification methods were used to evaluate gridded fields of precipitation. Spatial verification methods for the evaluation of wind simulations, however,

have been less developed compared to spatial verification methods for verifying precipitation, a fact that has been recognized by the open collaborative MesoVICT project. This project conducts test cases for the verification of gridded fields of precipitation data, and other variables beyond that, in a region of complex terrain over the Alps. The project lists achieving progress in wind verification as one of its primary goals (Dorninger et al. 2013; Skok and Hladnik 2018).

To address shortcomings in wind verification, Skok and Hladnik (2018) have presented a novel wind verification method called the Wind Fractions Skill Score (WFSS), an extension of the Fractions Skill Score (FSS) metric (Roberts 2008) originally used for verifying precipitation.

In the present study, the WFSS is used to evaluate wind field analysis data derived using the Integrated Nowcasting through Comprehensive Analysis (INCA) system and dynamical climate model wind data derived using the non-hydrostatic climate model of the Consortium for Small Scale Modeling Model in Climate Mode (CCLM). For this purpose, the WPG-diagnosed empirical high-resolution wind fields are used as reference data. The focus of this study is on evaluating spatial differences and displacements between the datasets.

1.2 Objectives

The first overall objective of this thesis is to develop an operational diagnostic application that can be used to evaluate wind fields produced from different types of models. To accomplish this, the present study identifies two practical aims:

1. To develop an operational weather diagnostic application that automatically generates high-resolution wind fields in near real-time, namely the WPG.

2. To implement the WPG application by applying it to the two regions monitored by the WegenerNet FBR and WegenerNet JBT networks and using the application to generate high-resolution wind fields based on the observations of the two networks.

The second overall objective is the evaluation of wind fields from different types of models against the WPG-wind fields, with the focus on evaluating spatial differences and displacements between the wind field data. To accomplish the second objective, the present study identifies another two practical aims:

1. To select WPG empirical wind field data, INCA analysis data and CCLM regional climate model data for the two study areas, the WegenerNet FBR and WegenerNet JBT, for selected weather events.

2. To evaluate INCA and CCLM wind fields based on the WPG reference wind fields with use of the WFSS besides traditional grid point-based methods.

1.3 Structure of the thesis

The thesis is structured as follows. Chapter 2 outlines relevant literature with respect to near-surface flows. Section 2.1 describes atmospheric processes occurring within the planetary boundary layer that influence near-surface airflows. Starting at a synoptic scale, the processes with the largest influence on synoptic systems affecting mountainous regions are analyzed. The next part of this section discusses processes that effect regional- to local-scale flow patterns. In section 2.2, the current state of knowledge regarding climate change's impact on near-surface wind fields is outlined. Both observation-based climate effects and the results of climate simulations related to near-surface wind fields are discussed in detail. Two different modeling approaches, namely the dynamical modeling approach and the diagnostic modeling approach for near surface wind are presented in section 2.3, and the advantages, disadvantages, and limitations of each model are discussed. Finally, section 2.4 introduces spatial verification methods that are used to evaluate model results and discusses and compares the characteristics of these methods.

Chapter 3 provides an overview of the research areas and basic information about the evaluation data used in this thesis, including the newly-developed WPG application.

Chapter 4 presents the scientific approach of this thesis which is based on a cumulative publication dissertation. First, the connection of different phases of this thesis, and second a summary of all peer reviewed publications are presented in this chapter.

Chapters 5 to 8 include the results of the presented thesis. In chapter 5 the method used for analyzing the CALMET model's sensitivity to geophysical parameters is presented, and the results of this sensitivity analysis are discussed in detail. All manuscripts published within this research, as well as a summary of the manuscript and a description of the activities of each author, are presented in chapters 6 to 8.

Finally, chapter 9 summarizes the work and provides concluding remarks.

2 State of Research and Relevant Literature

This chapter reviews relevant literature. In the first part it focuses on the effects of topography on near surface flows over a wide range of scales. In the second part, the effects of climate change on near surface flows on a regional to local scale are explained. The third part gives information about two specific types of wind field modeling approaches. Finally, different spatial verification methods for the evaluation of model outputs are introduced and compared with each other.

2.1 Airflows in hilly and mountainous regions

Airflows are influenced by topography over different scales and produce circulation systems which can be classified into a hierarchy of circulation systems from synoptic to local scales. Section 2.1.1 starts on a synoptic scale, and concentrates on three major dynamic processes which are influencing airflows. In Section 2.1.2 effects of topography on regional- to local-scale are discussed. The first part of this Section describes wave motion through local gravitational effects and the second part focuses on thermally induced winds on a local scale.

2.1.1 Synoptic-scale flows

Synoptic winds are airflows caused by large-scale weather systems, such as cyclones or anticyclones, covering areas of greater than 1000 km in length. The topography of mountainous regions affects approaching synoptic systems in specific ways that influence weather conditions in these areas. These effects can be divided into three major categories (Barry 2008): the blocking of airflows and formation of barrier winds, the modification of frontal cyclones as they cross mountain ranges, and enhanced cyclogenesis in the lees of mountains.

Blocking effects and barrier winds

The mesoscale blocking of air motion by orography is called a “barrier effect” and occurs particularly where mountain ranges are high and continuous (Barry 2008). Whether the resulting modification to approaching air masses take the form of the airflow’s overflowing or being diverted depends on the height of a parcel relative to the height of the mountain, the slope and dimensions of the mountain, the static stability of the atmosphere, and the magnitude of the horizontal wind speeds. A

major factor that causes air masses to be redirected around rather than over a mountain is stable stratification (Barry 2008). The blocking effects of ridges can be expressed by the forecasting criterion, namely the local Froude number (Fr) (Nicholls 1973) which is calculated by

$$Fr = \frac{U}{Nh}, \tag{2.1}$$

where U is the undisturbed speed of flow, N the Brunt-Väisälä frequency and h the height of a mountain ridge. N describes vertical oscillations in the absence of frictional and pressure effects.

If Fr is less than the critical value of 1, then at least some depth of flow is blocked by the terrain and redirected around the barrier. A Fr larger than 0.75 indicates that a part of the approaching upper-level flow propagates upstream and leaves behind a decelerated flow at lower levels. In case where the Fr is larger than 1.5 some part of flow is decelerated to rest and a cavity of reverse flow occurs on the lees-side of the barrier, which leads to a persistent lee circulation (Pierrehumbert and Wyman 1985; Schär et al. 1998).

Furthermore, on a mesoscale, the effect of the Coriolis force on airflows cannot be neglected. In the northern hemisphere, air masses that are deflected to the left register as having lower pressure and consequently higher wind speeds than air masses diverted to the right, especially for large Fr values. Air approaching a barrier decelerates, while air crossing a summit region accelerates slightly. The upstream extent of flow blocking and the degree of declaration can be estimated by the Rossby number (R_O) (Pierrehumbert and Wyman 1985) in combination with Fr. The Rossby number is calculated by

$$R_O = \frac{U}{fL}, \tag{2.2}$$

where f is the Coriolis parameter, U the crossmountain flow component and L the mountain half-width. The major factor in limiting the upstream extent and the degree of declaration is the Coriolis force. The limitation of the upstream extent of flow blocking can be diagnosed by a distance called the Rossby Radius of deformation (L_R) (Barry 2008; Pierrehumbert and Wyman 1985) calculated by

$$L_R = \frac{Nh_m}{f}, \tag{2.3}$$

where $\mathrm{h_m}$ is the height of the mountain ridge.

Flow patterns for a large Fr are illustrated in Fig. 2.1, where L_y indicates the long dimension of a mountain ridge, L the relatively lower pressure of air masses deflected to the left, compared to air masses at higher pressure diverted to the right (H). If L_R is larger than L_y the flow splitting occurs further away from the ridge, which causes the lower flow splitting around the barrier and the upper flow passing over it (Fig. 2.1a, c). For a much smaller L_R compared to L_y, the splitting is close to the ridge and the flow is redirected to the left on the northern hemisphere, resulting in a barrier wind (Fig. 2.1 b, d).

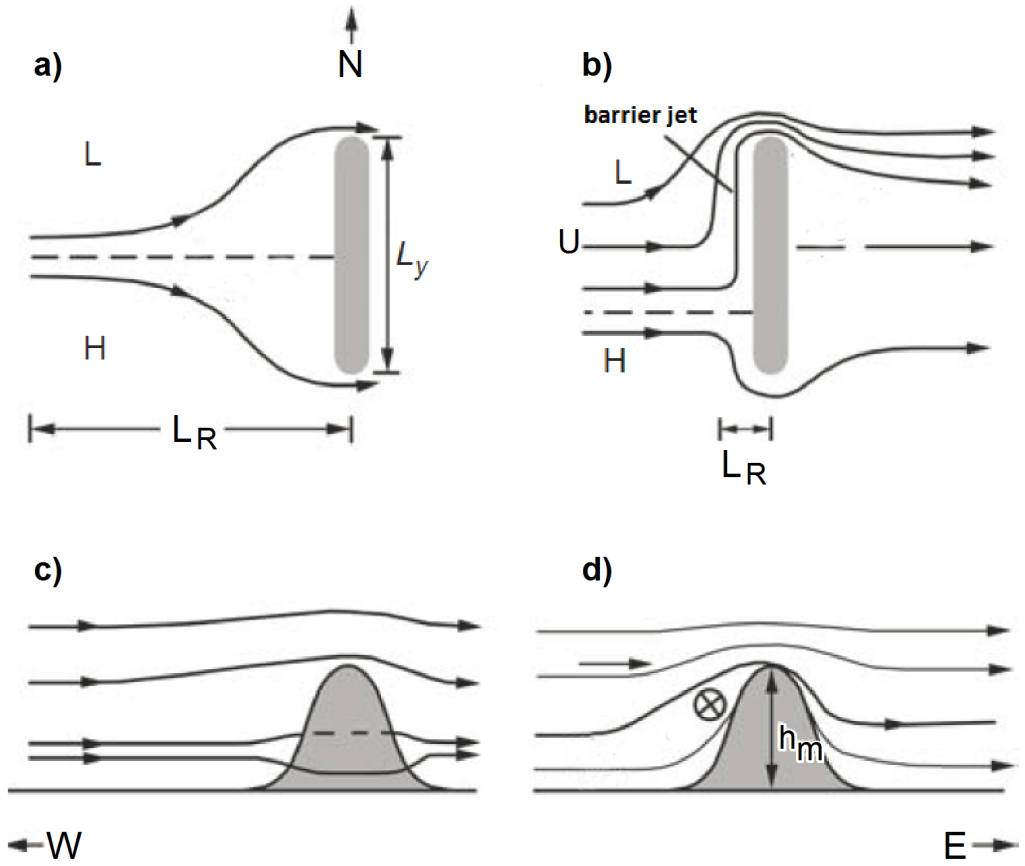

Figure 2.1: Flow blocking effects for a large Froude number for $L_R > L_y$ (a)(c) and $L_R \ll L_y$ (b)(d); (a)(b) for plan views and (c)(d) for vertical cross sections. Adapted from Barry (2008) (a)(b) based on Pierrehumbert and Wyman (1985) and (c)(d) on Shutts (1998).

Frontal modifications

Approaching fronts can be modified by orographic effects or by frontal movements themselves. Frontal characteristics can be modified by dynamic and thermodynamic effects resulting from the forced redirection of air masses by mountain barriers. Different types of mesoscale flow features are the result of the influence of mountain ranges on the propagation and structure of a front (Kljun et al. 2001).

Schultz (2005) identified ten different mechanisms for the formation of prefrontal troughs and wind shifts of cold fronts. A mechanism external to the front includes the interaction of the cold fronts with mountain barriers. Air masses of cold fronts slow down when approaching a mountain barrier, especially at lower altitudes. In this case, accumulations of air near ground-level push cold air at higher altitudes over the mountain range (Radinovic 1986). Some amount of air also passes through gaps in the mountain barrier on to the windward side of the mountain, distorting the frontal profile. The extent of a front becomes stretched as it descends the

leeward side of a mountain, which causes baroclinic instability. If moist and unstable warm air masses exist on the leeward side of the mountain, clouds form and precipitation occurs as a result of the influence of the down-flowing cold air on the warm air masses.

The retardation and blocking of an approaching cold front by a mountain is illustrated in Fig. 2.2. Dickinson and Knight (1999) performed idealized simulations of fronts which are approaching mesoscale mountain barriers and found an associated surface temperature gradient about 400 km behind the surface vorticity maximum (Fig. 2.2a). The blocking of the front on the upstream side of the mountain causes the separation between the temperature gradient and the surface vorticity, as well as the development of new vorticity in the lee of the mountain in the presence of lower-level warm advection (Fig. 2.2b, c). The vorticity maximum is reached at the lee side of the mountain, when the upper-level potential vorticity is coupled with the new surface vorticity (Fig. 2.2d) (Dickinson and Knight 1999; Barry 2008).

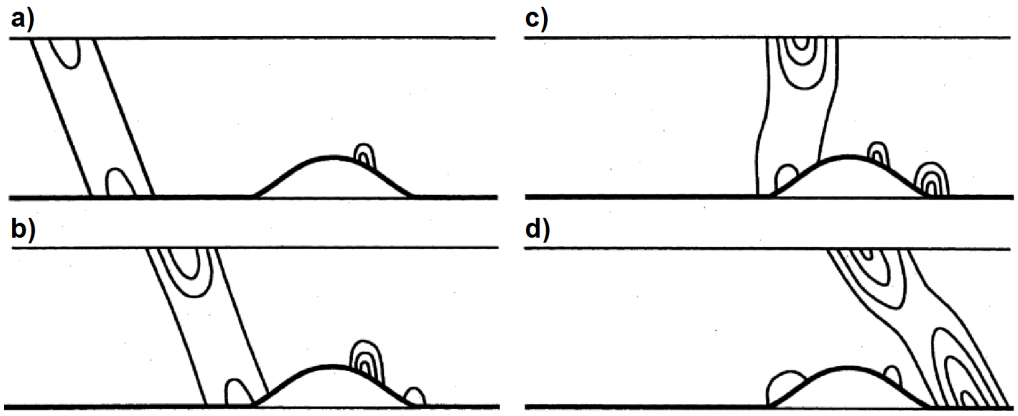

Figure 2.2: Schematic representation of a cold front moving over a mountain. The potential vorticity is illustrated by the isolines. (a) The upper- and lower-level through of a cold front are approaching a mountain barrier; (b) at the windward slope, the low-level trough of the cold front gets blocked, and a lee trough and secondary trough is developing along the lee slope; (c) the upper-level and lower-level frontal waves are separated; and (d) the upper-level frontal wave is coupled with the secondary through in the lee of the mountain. Adapted from Dickinson and Knight (1999).

Fig. 2.3 illustrates effects of mountain barriers on approaching warm fronts. Modifications occur when air ahead of a warm front is trapped on the windward slope of a barrier, slowing the motion of the lower-altitude part of the front (Fig. 2.3a, b). The underlying cold wedge of this lower part is cut off from the rest of the front, forming a stationary front that often causes continuing rainfall on the lee side of the mountain (Fig. 2.3c). Frontogenesis may also occur in pressure-trough areas in such a way that the frontal system moves away from the mountain and becomes separated from the stationary, lower part of the front (Barry 2008).

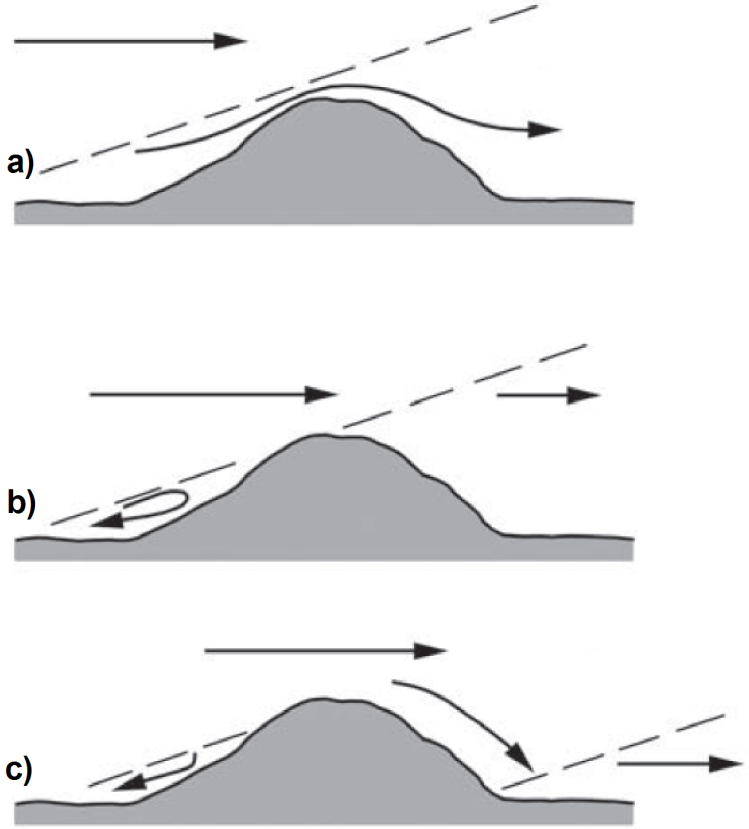

Figure 2.3: Schematic representation of a warm front moving over a mountain. (a) Approaching warm front; (b) windward retardation of approaching air masses; (c) separation. Adapted from Barry (2008).

Lee cyclogenesis

Lee cyclogenesis is the process by which cyclones are generated in the lee of mountains as a result of the orographic blocking of air masses. This type of cyclogenesis is most effective when airflows are roughly perpendicular to the main ridge of a mountain. In the Alps, for example, such airflows occur when cyclones, including their troughs or fronts approach the mountains from the west or northwest (Schär et al. 1998). When these frontal systems impinge on the Alps, new cyclones may emerge on the lee-side of the mountain as a result of the complicated three-dimensional and time-dependent evolution of airflows. These new, eastward-moving cyclones influence the climate of the eastern and southeastern areas of the Alpine regions by forming secondary storm tracks over the Mediterranean Sea (Schär et al. 1998). As part of the ALPEX studies, Pichler and Steinacker (1987) found that two particular type of weather patterns lead to lee cyclogenesis in the Alpine region: (a) the blocking of cold northwesterly air masses by the Alps, and (b) the southwesterly upper-level flow of air ahead of an eastward-moving trough. In

type (a), cyclogenesis takes place below this upper level northwesterly flow with a weakened cyclone upstream of the Alps, that gets intensified in the lee of the mountain ridge. The second type may lead to a warm front over northern Italy and a cold front in the Gulf of Genova, caused by flow blocking and splitting.

These patterns are sometimes accompanied by the south and the north föhn, the mistral, the bora, and other regional scale flow phenomena (Truhetz 2010; Barry 2008). Ahead of a cold front, a strong prefrontal flow of warm, humid, and weakly stratified air from the Mediterranean can cause the south föhn to shift to the north (Fig. 2.4a) (Schär et al. 1998). Meanwhile, as cold fronts impinge on the Alps, these fronts are slowed and modified in such a way that low-level flows are blocked and split on the windward side, shifting southerly winds in northerly and northwesterly directions; westward-deflected cold air masses then cause cold-air outbreaks along the Mediterranean Sea between the Alps and the Pyrenees (Pettre 1982; Kljun et al. 2001). Such flow patterns cause the mistral, a flow of northerly or northwesterly winds which blow through the channeling Rhone valley to the Mediterranean (Barry 2008; Kljun et al. 2001; Schär et al. 1998)(Fig. 2.4b). The splitting of westerly to northwesterly airflows in the west of the Alps leads to lee vortex development (Aebischer and Schär 1998). The slowing of surface cold fronts

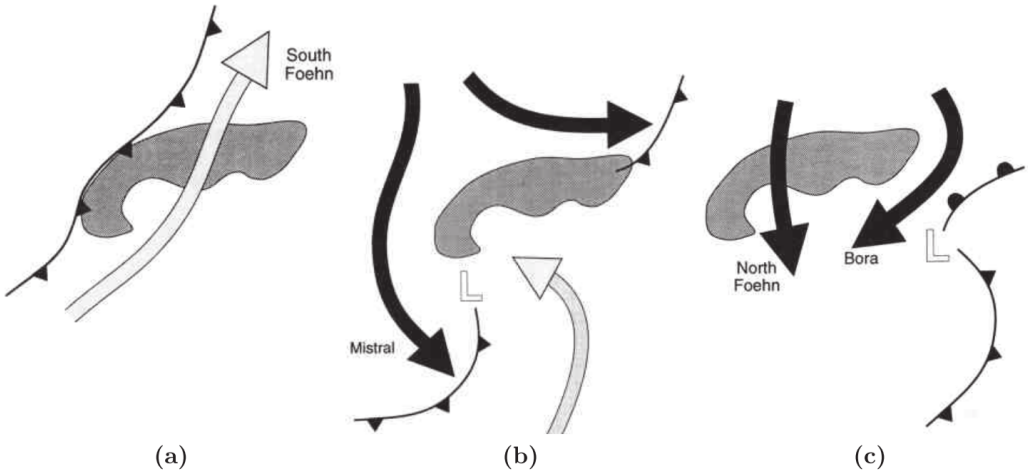

Figure 2.4: Schematic of the Alpine lee-cyclogenesis: (a) an intercepting cold front is deformed and South Föhn results from prefrontal winds, (b) cold-air breaks out into the western Mediterranean Sea (Mistral) and a lee-cyclone is formed, (c) the lee-cyclone progresses eastwards and Bora and North Föhn appear. From Schär et al. (1998)

by orography and the presence of an overtaking upper-level trough may also cause deep cyclogenesis events to develop over the gulf of Genoa (Buzzi and Tibaldi 1978). A part of the cold air mass crosses the Alps from the north or northwest, often accompanied by clouds and precipitation. The resulting dry air that falls on the southern slopes of the Alps, leading to warm, dry winds, is known as the north föhn, while eastward-deflected cold air masses in the Alpine region contribute to

the northeasterly bora winds that blow over the Dinaric Alps (Fig. 2.4c) (Smith 1987).

2.1.2 Regional- to local-scale flows

Gravitational effects

On regional to local scales of 1–100 km, the influence of the terrain on wind fields becomes increasingly important. The major factors that determine whether airflows are modified or redirected over or around obstacles are the vertical wind profile, the stability structure of the atmosphere, and the shape of the obstacle (Barry 2008). Figure 2.5 illustrates four basic types of flows that are caused by different vertical wind profiles, as outlined in Förchgott (1949). Within a laminar stream flow, air flows over an obstacle in the form of shallow waves (Fig. 2.5a). Wind speeds that are slightly stronger at higher altitudes can cause a standing eddy to form on the lee side of the barrier. Such standing eddies imply the presence of reversed, upward-directed slope flows on the lee side of the obstacle; this phenomena has often been observed in hilly terrains (Fig. 2.5b). In cases in which the vertical wind profile contains steep vertical gradients, a train of lee waves forms on the lee side of the obstacle (Fig. 2.5c). As long as flow conditions remain the same, these lee waves, which are a form of gravity wave, remain stationary, which means that the air's natural wavelength is in resonance with the size of the obstacle (Barry 2008; Schär et al. 1998; Truhetz 2010). Finally, the rotor streaming type of airflow occurs when wind speeds are strong and the direction of the wind varies according to height. In such conditions, the airflow's streamline gets separated from the ground, and turbulence occurs on the lee side of the mountain, the combination of which generates a system of quasi-stationary vortices below the wave crests (Barry 2008) (Fig. 2.5d).

In general, the vertical displacement of airflow in a stable, stratified atmosphere that is caused by mountain barriers generates disturbances, and the energy associated with the airflow is carried away from the mountains by gravity waves. The vertical and horizontal dimensions of the oscillations caused by these waves are dependent on the stability of the stratification of the atmosphere. In a stable atmosphere with weak winds, the period of an oscillation is short, with a large amplitude. In an unstable atmosphere with strong winds, however, slow oscillations with long wavelengths can generally be observed (Barry 2008; Schär et al. 1998; Truhetz 2010).

There are two basic types of mountain lee waves that can be distinguished according to the type of up-and-down oscillations the waves exhibit above and downstream of a mountain ridge; Namely vertically propagating waves and trapped lee waves. Vertically propagating waves extend to high altitudes, typically reaching the lower stratosphere, and have a horizontal wave length of 30 km or more (Durran 1990). The amplitude of these waves becomes greater at higher altitudes, and they are frequently tilted upwind (Fig. 2.6). These types of waves are produced by

conditions such as static stability increasing with height above a mountain's peak and wind speeds with small vertical gradients. In addition, synoptic-scale flows occurring perpendicular to a mountain's ridge axis produce potential energy that can allow a parcel to ascend a barrier. Strong downslope winds such as the föhn or bora often accompany vertically propagating waves. Scorer (1949) has developed the diagnostic parameter N/U = 1, where N is he Brunt-Väisälä frequency N and U is the cross-mountain wind speed. This mean of comparing stability with vertical wind profiles can also be used to compare terrain characteristics in order to identify the type of a lee wave. A value of l that is nearly constant at all heights indicates conditions that are conducive to a vertically propagating wave (Coughlin 2005).

Trapped lee waves, which occur downstream of ridges, tend to develop in cases where vertical stability decreases and wind speed increases with height. These waves occur with horizontal wavelengths of 5–35 km at a height of 1–5 km above ground-level. Resonant lee-waves may occur if the lower layer of the airflow is slower or more stable than the upper layer. A series of waves running parallel to a ridge can produce clouds in parallel, spaced lines at regular intervals (Fig. 2.7). These clouds might dissipate very slowly and propagate horizontally due to the trapped wave energy located in the stable layer of the airflow. Trapped lee waves may then develop if the vertical profile decreases sufficiently (Scorer 1949; Lin 2007; Barry 2008; Durran et al. 2015).

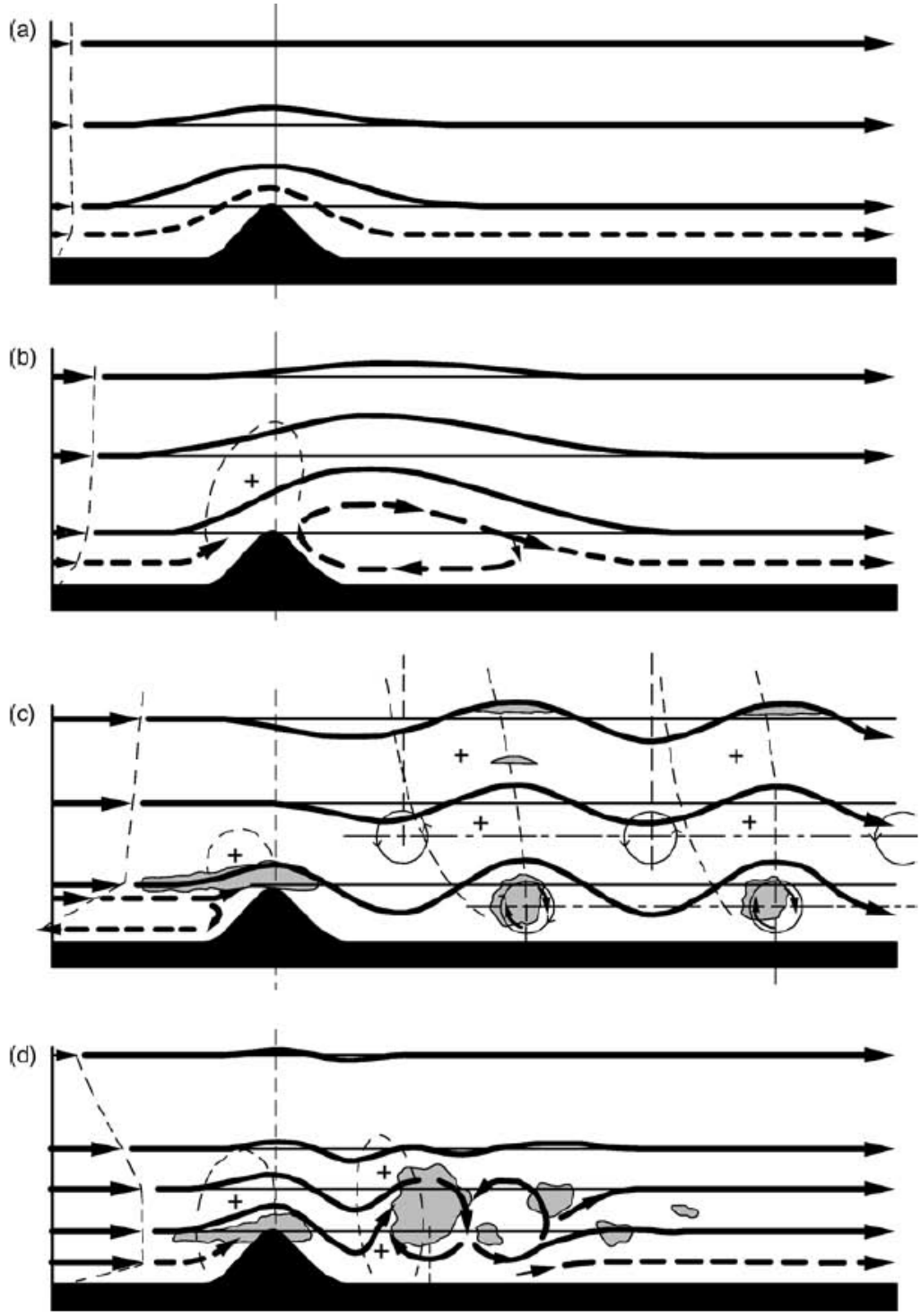

Figure 2.5: Basic types of airflow over a mountain in dependence of different vertical wind speed profiles: (a) Laminar streaming; (b) Standing eddy streaming; (c) Wave streaming, with a crest cloud and downwind rotor clouds; (d) Rotor streaming. From Corby (1954).

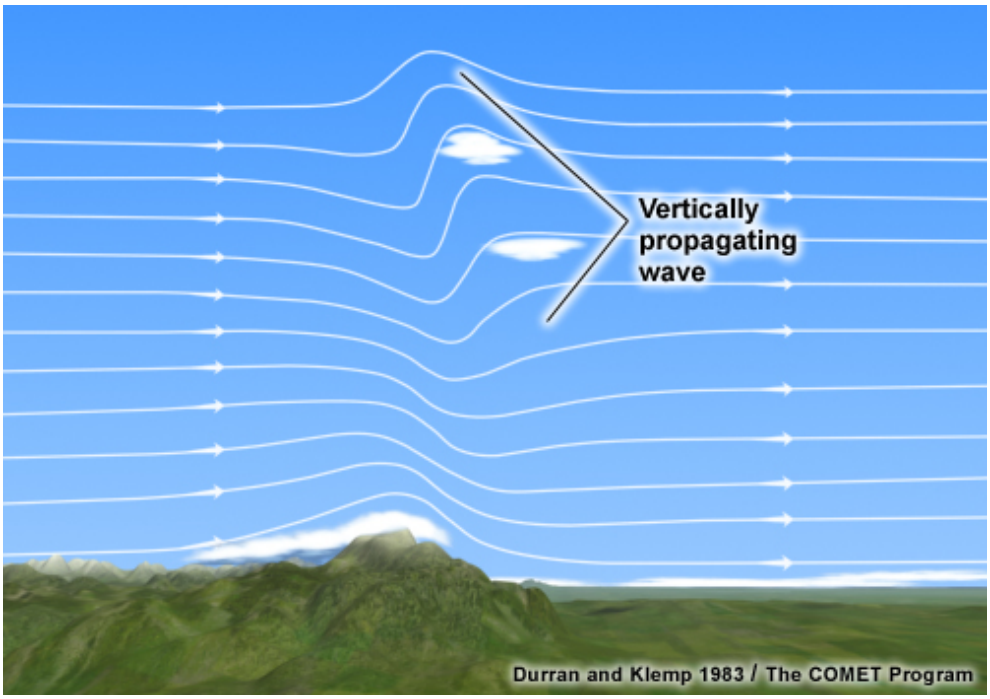

Figure 2.6: Schematic representation of vertically propagating lee waves. From EUMeTrain (2017) (© COMET Program).

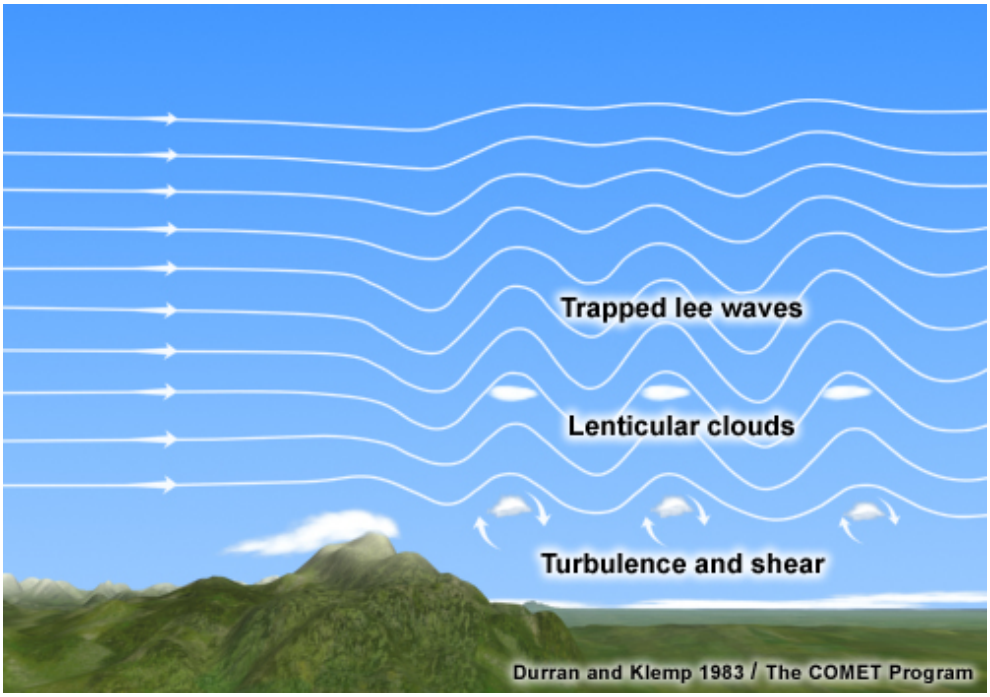

Figure 2.7: Schematic representation of vertically trapped lee waves. From EUMeTrain (2017) (© COMET Program).

Thermal induced winds

In addition to the above mentioned mainly mechanical ways in which mountain barriers influence wind fields, wind fields are also affected by small-scale temperature and pressure gradients. Especially in cases of low synoptic influences, these small-scale gradients can lead to characteristic systems of air motion (Barry 2008). The basic theory by which such thermally-induced flows are understood involves two types of wind systems (Bianco et al. 2006): slope winds and mountain-valley winds. In reality, the components of thermally-induced wind systems interact to create complex everyday flow patterns, as illustrated in Fig. 2.8.

After sunrise, upslope flow systems develop, adding to continually prevalent mountain winds. Upslope air flows, also known as anabatic winds, are generated by the heating of the slope during daylight hours. Particularly in the mornings, this heating produces a pressure gradient that causes winds to accelerate (Fig. 2.8a). As daytime heating continues, it causes strong buoyancy effects, drawing air from the interior of the valley. By means of a compensatory flow, this air is replaced by warmer air from higher altitudes over the valley. The faster warming of the valley floors compared to the plains leads near-surface air to rise, which causes a pressure drop compensation between the valley and the plain, and the mountain wind stops blowing (Fig. 2.8b).

Later, the faster warming of the air in the valley relative to that of the air in the plain causes pressure to drop upstream of the valley, and the wind begins to blow up the valley toward the mountain (Fig. 2.8c). In the late afternoon, slope winds cease, but maximum wind speeds are reached as a result of a continuing valley wind (Fig. 2.8d). At night, under calm, clear-sky conditions, radiative cooling near the ground's surface combined with the effect of gravity causes local downslope drainage in addition to the valley wind (Fig. 2.8e). The faster cooling of the valley then leads to a pressure drop compensation between the plain and the valley, and the valley wind subsequently comes to a standstill (Fig. 2.8f). Later, due to a pressure drop downstream of the valley, the mountain wind blows down the valley toward the plain (Fig. 2.8g). Before sunrise, minimum temperatures are reached in the valley, and the mountain wind dominates the circulation of airflows (Fig. 2.8h) (Bianco et al. 2006).

In general, downslope winds are divided into drainage and katabatic winds. While both types of downslope winds arise from radiative cooling and density differences, katabatic airflows include large-scale slope flows like those occurring over the ice domes of Antarctica and Greenland. The term "drainage wind" is used to refer to small-scale flows that cause the formation of cold air pockets and lakes of cold air (Barry 2008). An explanation of how downslope flows can be characterized based on the terms of momentum equations can be found in Mahrt (1982).

As described in Defant (1951), daytime up-valley winds are induced by upslope winds, while nocturnal downslope winds, in turn, feed the mountain wind. The factor with the largest influence on mountain-valley winds, however, is the shape

of the valley and the aspect of its cross-section, not the slope of the valley floor (Steinacker 1989). Compensatory flows, which run in the opposite direction of mountain-valley winds above the mountain ridge crests, close the circulation of air. These compensatory flows are not confined by topography and can be superimposed upon by stronger synoptic-scale flows. As compensatory winds are generally relatively weak and masked by prevailing synoptic winds, however, such winds are observed infrequently (Zardi and Whiteman 2013; McGowan 2004; Whiteman et al. 2000).

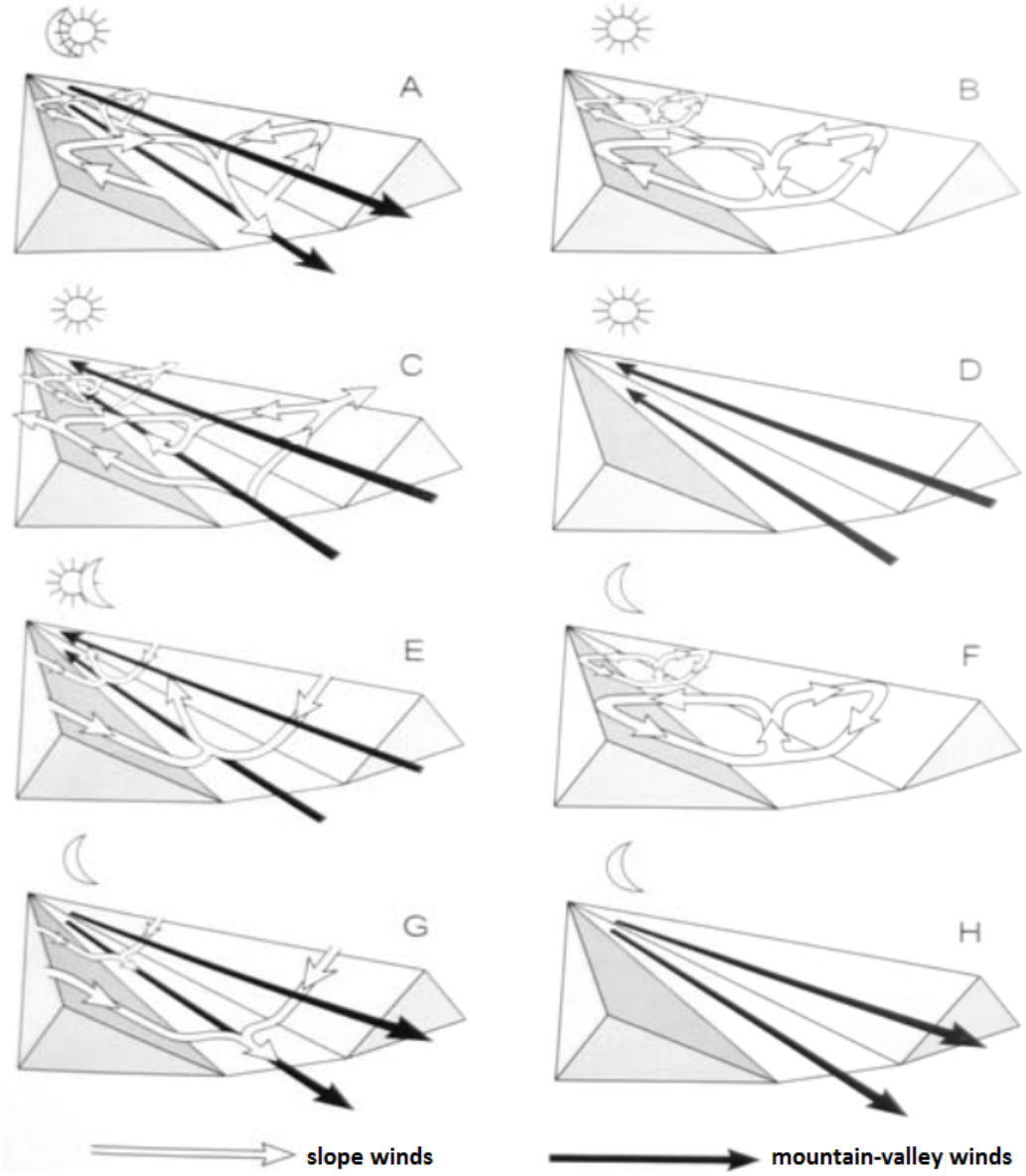

Figure 2.8: Schematic representation of diurnal valley winds for symmetrical slope warming and cooling, and autochthonous weather condition. From Bendix (2004) based on Defant (1949).

2.2 Climate change's effects on surface wind fields

The Fifth Assessment Report (AR5) of the Intergovernmental Panel on Climate Change (IPCC) indicated that confidence in long-term changes in surface and upper-air wind speeds is low. This lack of confidence was mainly the result of shortcomings in wind observation methods, the strong influence of topography on the planetary boundary layer, and uncertainty regarding the quality of data products and model outputs (IPCC 2013). Estimation of such changes is crucial, however, as severe weather events such as high wind and gust speeds pose a significant risk to property and human lives, such that failure to recognize changes may come at a considerable economic and social cost (Cheng et al. 2014). Furthermore, emission-free energy sources such as wind and solar energy are climate dependent, another reason why estimating changes in climate and weather is essential (Fant et al. 2016). This chapter focuses on the influence of climate change on near surface wind.

2.2.1 Climate change-related changes to near-surface airflows

The changes that have been observed in near-surface airflows are caused by a complex interplay of changes to driving forces and drag forces that have occurred on global, regional, and local scales. Driving forces are affected by changes in atmospheric circulation, while drag forces are altered by changes in external friction effects and internal friction effects in the atmosphere (Wu et al. 2018).

Evidence suggests that climate change has been causing shifts in atmospheric circulation. General circulation in the extratropic zones consists of jet streams, storm tracks, and atmospheric blocking (Woollings 2010). Changes in jet streams that have been noted in the last several years are considered to be driven in large part by the relatively strong warming of the Arctic region in comparison with the warming of lower latitudes (known as "Arctic amplification") (Feldstein and Lee 2014; Francis and Vavrus 2015; Barnes and Screen 2015; Meleshko et al. 2016). Observational studies confirm that jet streams have generally moved closer to the poles in either hemisphere, and also note that jet streams have weakened in the northern hemisphere (Francis and Vavrus 2015; IPCC 2013; Schneidereit et al. 2012; Archer and Caldeira 2008). It is assumed that this weakening causes jet streams to become more meandering, favors the occurrence of persistent weather patterns, and subsequently increases the likelihood of extreme events (Francis and Vavrus 2015).

The North Atlantic storm tracks have a pronounced impact on weather variability in Europe, and are often responsible for extreme weather events (Yin 2005; Bengtsson et al. 2005; Kyselý 2007; Dong et al. 2013; Catto et al. 2014; Lau and Nath 2014). The Fourth Assessment Report of the IPCC determined that northern hemisphere storm tracks were shifting northward due to the overall warming of the climate (IPCC 2012). This shift has been found to be a likely cause of the greater persistence of air circulation patterns over Europe, which has the effect of increasing the severity of temperature extremes (Kyselý 2007). Schneidereit et al.

(2012), meanwhile, has determined that the behavior of the North Atlantic storm tracks is strongly affected by the North Atlantic Oscillation.

The blocking of mid-latitude westerly flows by stationary high-pressure systems is a phenomena that is closely related to the occurrence of cold and warm temperature extremes in Europe that was just mentioned above (Cattiaux et al. 2010; Barriopedro et al. 2011; Galarneau Jr. et al. 2012; Brunner et al. 2017). Whether such blocking events occur depends on the state of atmospheric circulation, including conditions such as speed and position of jet streams or the northward shifts of northern hemisphere storm tracks described above, and is likely to be influenced by the warming of the climate (Barnes 2013; Vries et al. 2013; Dong et al. 2013; Kennedy et al. 2016).

External friction effects are mainly attributed to changes that occur to surface properties. Urbanization, for example, entails changes in land use and land cover that subsequently introduce changes in surface properties such as heat-storage capacity, heat transfer (as expressed by the Bowen ratio), and surface roughness. While quantifying the influence of drag forces on near surface flows is difficult, Vautard et al. (2010) and Wever (2012) have argued that decreasing wind speeds in the Northern Hemisphere are partly the result of an overall increase in surface roughness. Internal friction effects are mainly caused by changes in boundary layer conditions, including changes in static stability, vertical wind shear, vertical momentum transport, and local circulation. Anthropogenic-induced changes in atmospheric aerosol emissions and greenhouse gas concentrations can affect atmospheric stability and, consequently, near-surface flows (Zhao et al. 2013; Wu et al. 2018).

2.2.2 Observation-based studies

In observation-based studies of climate change that have been conducted on a global scale, most of the collected datasets contained statistically significant features. McVicar et al. (2012) reviewed 148 studies containing terrestrial near-surface wind speed observations and reported that tropical and mid-latitude winds in both hemispheres had decreased in speed by 0.14 m s^{-1} per decade. The conclusion that near-surface wind speeds are decreasing overall is supported by a separate analysis of 822 datasets recorded by land surface wind stations in northern mid-latitude zones between 1979 and 2008.

The analysis demonstrates that strong wind speeds have generally declined more than weak wind speeds during this period, and that wind speeds have declined overall by 0.1 m s^{-1}. In comparison, upper-air wind data obtained from radiosonde observations indicate that upper-air wind speeds are increasing over Europe and North America and decreasing over Central and East Asia (Vautard et al. 2010). Wu et al. (2018) recently analyzed several studies on terrestrial near-surface wind speeds spanning the last 30 years and found that near-surface wind speeds are declining most significantly in Central Asia and North America, with a mean decrease in each of these areas of 0.11 m s^{-1} per decade. Meanwhile, decreases in

near-surface wind speeds in Europe and East and South Asia correspond with a mean linear trend of a 0.08 m s^{-1} decrease per decade, while near-surface winds in Australia were found to be decreasing at the slowest rate, a mean of 0.07 m s^{-1} per decade. As observational data in Africa is lacking, wind speed trends in this continent are highly uncertain.

Kent et al. (2012) have intercompared twelve different datasets of wind speed measurements over the global ocean from 1987 to 2009, and have found that uncertainty increases when several models are used to estimate wind speeds based on heterogeneous data. For example, for the determination of marine surface wind speeds, data derived from satellites or reanalysis products is often used in combination with in situ measurements. Large variations are seen between different datasets with respect to the way in which wind speeds are represented. Speed measurements of wind fields that are studied using in situ measurements and reanalysis are stability-dependent and earth-relative, while datasets using satellite measurements and blended datasets measure wind speeds in a neutral, surface-relative form (Kent et al. 2012).

Regardless of this, several studies have reported positive and negative trend bands for wind speeds across the North Atlantic Ocean and positive trends across the west coast of North America. The trend of increasing mean wind speeds has been found to be correlated with the trend of increases in the Southern Annular Mode (Zhang et al. 2006; Compo et al. 2011; Berry and Kent 2011; IPCC 2013).

2.2.3 Climate model simulations

For the purpose of projecting climate change developments into the future, researchers have increasingly sought to develop and improve complex three-dimensional dynamical climate models. These models are typically constructed out of component models that solve mathematical equations involving five model components: atmosphere, land, ocean, sea ice, and land ice (Truhetz 2010; Armstrong et al. 2015). These components are interconnected by means of a coupler that passes information between the components of the model. The Coupled Model Intercomparison Project Phase 5 (CMIP5) is a collaborative project that provides global-scale climate simulations using GCMs, and which contributed to the Fifth Assessment Report of the IPCC.

These simulations are based on a set of standardized assumptions regarding future greenhouse gas concentrations. The CMIP5 has created four Representative Concentration Pathways (RCPs) representing distinct timelines that could result from various socioeconomic scenarios and which are based on consistent sets of forcing projections (Fig. 2.9). These four RCPs are distinguished by the Radiative Forcing (RF) levels (measured in W m^{-2}) simulated in the year 2100 and after 2100, when stabilization is reached. The RCP2.6 is the pathway in which conditions cause the lowest RF value, which peaks at approximately 3.0 W m^{-2} and decline to 2.6 W m^{-2} in the year 2100; RF levels in the pathways RCP4.5 and RCP6.0, meanwhile, stabilize after 2100 at 4.2 and 6.0 W m^{-2}, respectively, while RCP8.5

shows the highest RF levels, with an RF value of 8.3 W m^{-2} in 2100 and a rising trajectory. These absolute RF values are estimated by taking into account both, positive radiative forcing from greenhouse gases and negative radiative forcing caused by aerosols. The trends for the different RCPs, including the total positive anthropogenic greenhouse gas and anthropogenic aerosol negative RF are shown in Fig. 2.9 (Vuuren et al. 2011; Moss et al. 2010; IPCC 2013).

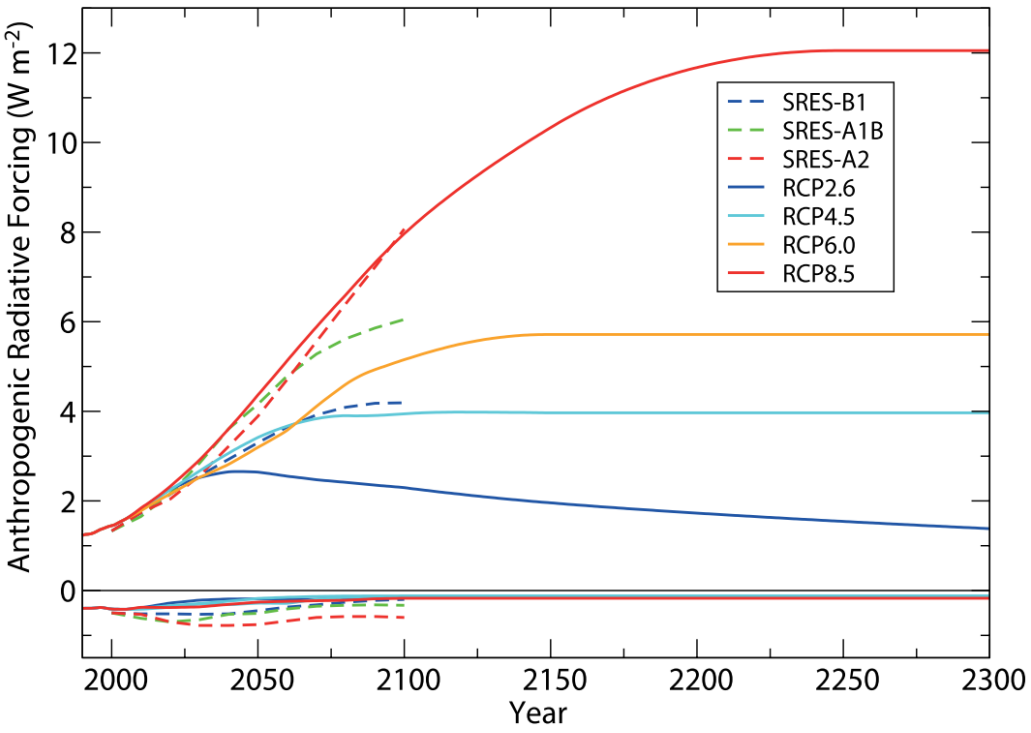

Figure 2.9: Time evolution of total anthropogenic (positive) and anthropogenic aerosol (negative) radiative forcing (RF) relative to pre-industrial (about 1765) for the representative concentration pathways (RCPs) (continuous lines) of the Intercomparison Project Phase 5 (CMIP5), and Special report on Emissions Scenarios (SRES) scenarios (dashed lines). The SRES scenarios have been used in an earlier project phase, the CMIP3. Adapted from IPCC (2013).

Analyses of the outputs of the CMIP5 models indicate that, dependent on the chosen RCP, an increase in mean surface temperatures for the projected period of 2081–2100 relative to the reference period of 1986–2008 is likely in the 5–95 % confidence range of these models. In RCP4.5, global average temperatures are expected to increase by more than 1.5 °C compared to temperatures observed in the reference period and by over 2 °C for RCP6.0 and RCP8.5 (IPCC 2013).

As for changes observed in atmospheric simulations, poleward shifts in mid-latitude jet streams of up to two degrees have been estimated by CMIP5 models by the end of the 21st century, with somewhat weaker shifts being estimated in the Northern Hemisphere. Such changes impact the transport of momentum,

energy, and water through the atmosphere, all of which is transported primarily via extratropical storm tracks (O'Gorman 2010). O'Gorman (2010) have estimated that climate change in the 21st century will be significantly affected by an intensification of southern storm tracks, an increase in storm amplitude in both hemispheres, and the complex relationship between storm-track intensity and global mean surface temperature. In addition, Kug et al. (2010) have found that a poleward shift of storm tracks in the Northern Hemisphere may amplify polar warming and moistening. Changes in sea-level pressure, meanwhile, are correlated with poleward shifts in mid-latitude storm tracks in the Southern Hemisphere, as well as with the expansion of the Hadley cell (Yin 2005; IPCC 2013).

The extent to which storm-track intensities and high surface wind speeds are correlated varies widely according to the model being used (Thompson and Wallace 2001; Yin 2005; Miller et al. 2006). Casas-Prat et al. (2018) has analyzed simulations of surface winds based on five CMIP5 models and the RCP8.5 scenario and found that the changes projected for the period 2081–2100 vary considerably from one model to another, though projections of some regions consistently exhibit statistically significant changes.

Figure 2.10 illustrates the ensemble of projected relative changes of 10 m surface wind speeds observed in Casas-Prat's study, including areas with statistically significant changes such as the mid-latitudes of the North Atlantic and Pacific; significant decreases of surface wind speeds are projected in this region, a trend that differs starkly from that projected in the storm track region in the low- to mid-latitudes, where a significant increase in wind speeds is estimated (Fig. 2.10). For the Southern Hemisphere, a study by Swart and Fyfe (2012) reports that westerly surface winds are also estimated to increase under all CMIP5 scenarios except for RCP2.6, with the largest changes occurring over the Pacific (Bracegirdle et al. 2013).

2.3 Wind field modeling methods

Regional near-surface winds are subject to a complex interplay of conditions, including large-scale atmospheric circulation, various synoptic weather phenomena, and interactions between the earth's surface and atmosphere (see Section 2.1 above). Depending on the type of model, numeric modeling approaches aim to account for all of, or at least a part of, these conditions and the associated processes (Truhetz 2010).

In this chapter, two types of modeling approaches are introduced, and their advantages and disadvantages are discussed.

Ultimately, the modeling approach described in Section 2.3.2 was used to generate wind field datasets in near real-time based on observations derived from two dense networks of meteorological stations; these generated wind fields were then used to evaluate model outputs generated using the modeling approach described in Section 2.3.1.

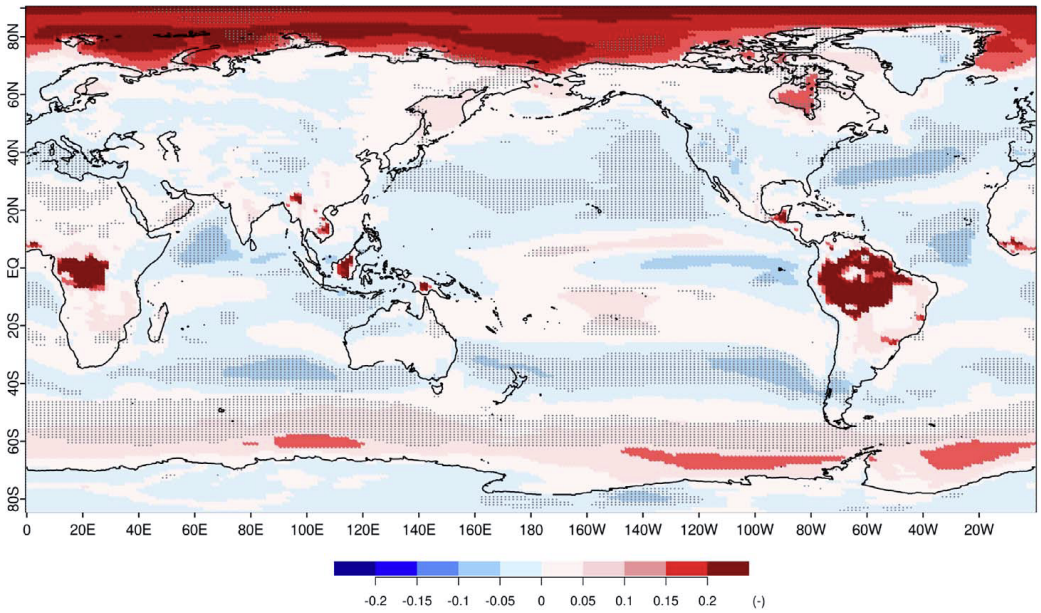

Figure 2.10: Projected relative changes of 10 m surface wind speed for 2081–2100 (relative to 1979–2005). Stippling indicates areas where projected changes are statistically significant. From Casas-Prat et al. (2018)

2.3.1 Dynamic models

Dynamic models such as GCMs and RCMs are the most sophisticated options available for determining the spatial distribution of wind. They are capable of simulating physical processes that take place in the atmosphere, ocean, cryosphere, and on the surface of the land, including synoptic processes and interactions between the earth's surface and atmosphere (Truhetz 2010). As such simulations require extensive computational resources, dynamic models with equations representing complex physical phenomena are generally simulated on supercomputers.

GCMs are designed to simulate the earth's climate over the entire planet and depict meteorological variables on a three-dimensional grid that spans the entire globe. Given the extensive computing power required to run such models, the horizontal resolutions of these models are generally limited, and the equations governing the models are simplified (Truhetz 2010; Prein 2013). Quadrupling the horizontal resolution of a given model, for example, entails that the model includes 16 times as many gridpoints. To keep simulations stable in such cases, it is necessary that the temporal resolution is four times higher. Ultimately, quadrupling a model's horizontal resolution requires 64 times as many computational steps as a simulation with the original-resolution model (Prein 2013). Nevertheless, a higher horizontal resolution is desirable because it allows for the simulation of smaller atmospheric processes and provides better representations of orography, coastlines, and surface fields. In the GCMs used in CMIP5, for example, model outputs in

horizontal grids are spaced at a distance of approximately 60 km.

An example of the way in which governing equations are simplified to reduce computing demands is seen in the hydrostatic assumption, where incompressible, rotating, stratified fluid flows are assumed to be in hydrostatic equilibrium (Gibbon and Holm 2011). On average, the earth's atmosphere is close to hydrostatic equilibrium, a state in which the vertical pressure gradient force is equal to the force of the downward gravitational pull of the Earth (Truhetz 2010; Wedi and Malardel 2010). The hydrostatic assumption is made for synoptic-scale motions and large spatial scales like those modeled in GCMs. Smaller-scale phenomena, including deep convection, flows over mountains, and the entrainment of vertical fluid by strong gravity waves, disturb this equilibrium, which means that such processes cannot be represented by hydrostatic climate models (Prein 2013). Figure 2.11 illustrates the difference between hydrostatic and non-hydrostatic solutions of high-resolution simulations of airflows over a mountain at a height of 100 m in vertically stratified atmosphere, with 10 m s^{-1} near-surface wind speeds and wind speeds increasing linearly up to 35 m s^{-1} at the tropopause (at a height of 10.5 km, or about 687 hPa).

Figure 2.11 also depicts orographically-forced gravity waves in the presence of vertical wind shear as a reference solution that can be compared to the hydrostatic and a non-hydrostatic solutions. The reference solution is provided using a state-of-the-art Eulerian/semi-Lagrangian fluid solver (Prusa et al. 2008) (Fig. 2.11a), while the hydrostatic (Fig. 2.11b) and non-hydrostatic (Fig. 2.11c) simulations are generated using the Integrated Forecast System (IFS). The hydrostatic solution is not able to reproduce the results of the EULAG simulation, and generates vertically-propagating gravity waves. The non-hydrostatic solution, is able to simulate horizontally-propagating trapped lee waves. A visual example of trapped lee waves observed off of Amsterdam Island in the southern Indian Ocean, acquired using the Moderate Resolution Imaging Spectroradiometer (MODIS), can be seen in Fig. 2.11d (Wedi and Malardel 2010).

Due do the overly coarse spatial resolution of GCMs and the simplifications they require, as explained above, significant differences may be found between GCM simulations to regional-scale climate processes. To provide higher-resolution model outputs on regional scales, RCMs are run on sub-domains. The numerical and physical principles upon which this type of regional model is based are very similar to the principles GCMs use. These models generally use larger-scale atmospheric conditions at their lateral and surface boundaries that are derived from GCMs or from RCMs with relatively coarse resolutions. This modeling approach, which is illustrated in Fig. 2.12, is referred to as dynamical downscaling.

The exchange of information between a driving model (a GCM or RCM with relatively coarse resolution) and a higher-resolution RCM can be realized through two coupling methods: RCMs can be one-way coupled to their driving model so that information from the driving model's lateral boundaries is passed into the RCM's modeling domain, but no information is passed back to the driving model; or, two-way coupled, such that information is received by the RCM and fed back

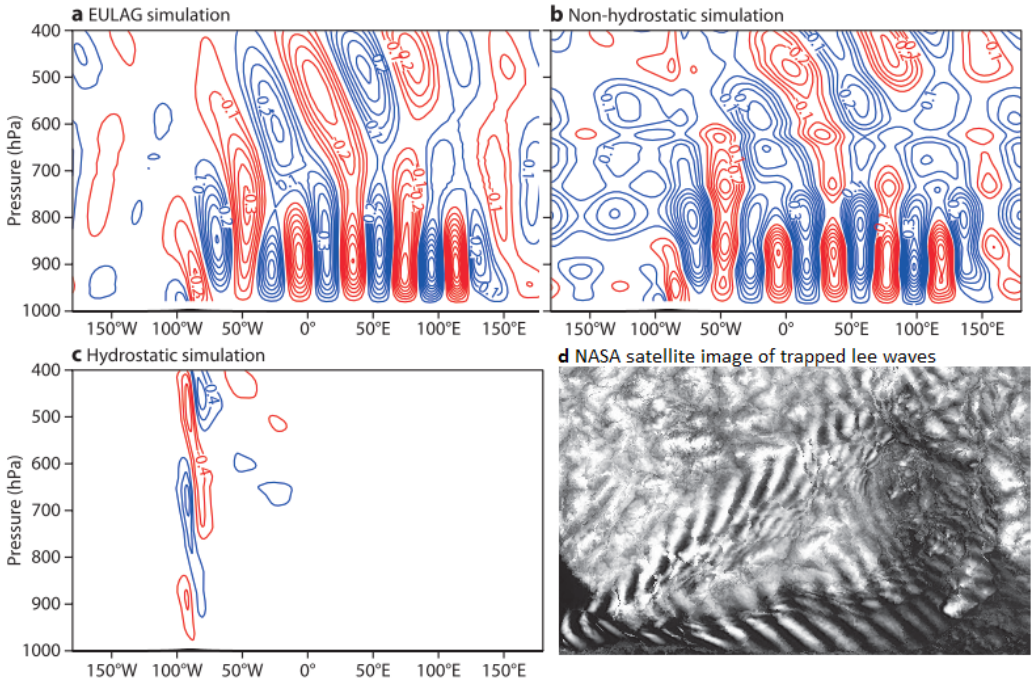

Figure 2.11: Vertical cross-sections of orographically-forced gravity waves at the equator in an idealized flow simulation (a, b, c): (a) non-hydrostatic EULAG simulation, (b) non-hydrostatic and (c) hydrostatic IFS simulations. (d) Trapped lee waves propagating at Amsterdam Island on 19 December 2009. Image taken from MODIS imager on board of the Terra satellite. Adapted from Wedi and Malardel (2010).

to the driving model to enable a smoother transition between the driving model and the RCM (Prein 2013).

Nudging is another technique by which RCMs can preserve large-scale information within the modeling domain along with lateral boundary information. This technique prevents drifts that can be caused by large-scale weather patterns in RCMs (Omrani et al. 2012; Prein 2013; Lucas-Picher et al. 2016). There are two basic types of nudging methods used to drive RCMs (e.g. Kida et al. 1991; Waldron et al. 1996; Storch et al. 2000; Radu et al. 2008a): spectral nudging, which is used at selected spatial scales, and indiscriminate nudging, which drives the RCM indiscriminately at all scales. Winterfeldt and Weisse (2009) demonstrated that spectrally nudged simulations generate instantaneous wind speeds and frequency distributions that are more accurate than driving reanalysis data. Lucas-Picher et al. (2016), have conducted a study comparing classic RCM simulations to simulations driven by large-scale nudging to reproduce weather regimes.

The results of the study revealed that classic RCMs simulate the mean statistics of weather regimes reasonably well, but daily weather regimes and seasonal anomalies are reproduced more accurately by simulations driven by large-scale nudging. Some studies, however, indicate that there are disadvantages to using large-scale nudging,

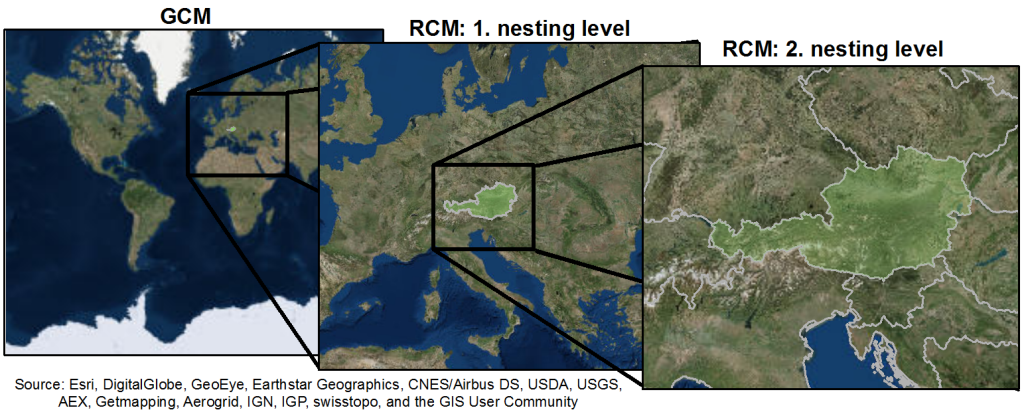

Figure 2.12: Schematic representation of a double nesting approach.

such as a slight precipitation increase in simulations of extreme precipitation events (Radu et al. 2008b; Alexandru et al. 2009).

As mentioned in Chapter 1, RCMs are becoming increasingly complex, and are now capable of generating simulations with horizontal resolutions at the 1 km scale (Awan et al. 2011; Suklitsch et al. 2011; Prein et al. 2013b; Leutwyler et al. 2016; Kendon et al. 2017). One of the most complex tasks in climate modeling is correctly representing cloud processes, including the very important process of cumulus convection. These processes develop out of the interactions of various sub-processes between the surface, the atmospheric boundary layer, and the free troposphere (Fosser et al. 2014; Khodayar et al. 2013; Prein et al. 2013b). Since convective processes are small scale-phenomena, they must be parameterized with coarse resolutions in RCMs. The parameterization schemes used for such processes were developed over the past several decades and generate known sources of errors, such as representing the onset and peak of convective processes prematurely. Using scales of 4 km or less allows to forgo most convection parameterizations and resolve deep convection explicitly (Hohenegger et al. 2008; Brockhaus et al. 2008; Bechtold et al. 2004; Fosser et al. 2014); such simulations are referred to as Convection-Permitting Climate Simulations (CPCSs), as briefly mentioned in Section 1.

Several studies have confirmed the added value of using CPCSs for numerical weather predictions, especially when representing precipitation fields in cases of moist convection in regions with complex terrain (e.g. Langhans et al. 2013; Mass et al. 2002; Miura et al. 2007; Grell et al. 2000; Richard et al. 2007; Lean et al. 2008; Schwartz et al. 2009; Weusthoff et al. 2010; Baldauf et al. 2011; Hohenegger et al. 2008; Prein et al. 2013b). Furthermore, Fosser et al. (2014) have investigated 30-year CPCSs and estimate that CRCSs of hourly intensity distributions and diurnal cycles of precipitation improve significantly upon comparable models.

2.3.2 Diagnostic models

Diagnostic models are designed to represent the actual state of the atmosphere for regional to local scales, and their vertical extent is mostly limited by the planetary boundary layer. They omit time-consuming integrations of nonlinear equations, such as the governing equations of dynamical models, and are therefore attractive for near real-time modeling (Truhetz 2010; Seaman 2000; Ratto et al. 1994). Dynamic processes such as flow splitting and grid-resolved turbulence are not simulated by these models. Such models reconstruct 3D wind fields based primarily on meteorological observations, including observations of the effects of topography on airflow, and generate mass-consistent wind fields. In diagnostic models, the most common method for determining unobserved vertical velocities is computing them using the incompressible conservation of mass equation with smoothed horizontal wind field components (Scire et al. 1998; Cox et al. 2005; Seaman 2000).

The general approach taken in diagnostic modeling involves two steps. The first step is the generation of an initial guess wind field based on meteorological observations. In the second step, the initial guess wind field is adjusted for topographic effects. Finally, to eliminate mass inconsistency caused by adjusted vertical velocities, divergence minimization schemes that satisfy the incompressible mass consistency are applied. More sophisticated diagnostic models, such as the California Meteorological Model (CALMET), apply additional parameterizations that allow the model to empirically take into account conditions such as the kinematic effects of terrain, slope flows, and terrain-blocking effects (Scire et al. 1998; Truhetz 2010).

The quality of the model wind fields that are generated depends above all on the quality and spatial and temporal resolution of the meteorological observations and surface-related datasets used (Schlager et al. 2017; Schlager et al. 2018; Morales et al. 2012; Cox et al. 2005; Gross 1996). Gross (1996) have compared the results obtained using a Mass Consistent model with no additional parameterizations and a non-hydrostatic RCM for an area of moderately complex terrain with dimensions of approximately 25 km x 25 km. The observations that supplied the Mass Consistent model were derived from the non-hydrostatic RCM's simulations, and the results indicated that the Mass Consistent model required observations from between 50 and 100 observation sites in order to reproduce detailed flow characteristics in the modeling domain.

Cox et al. (2005) have compared the simulations of three diagnostic models, namely the CALMET, the Stationary Wind Field and Turbulence model (SWIFT), and the Mass Consistent Model associated with the Second Order Closure Integrated Puff transport/dispersion model (MCSCIPUF) for a short-term period of 36 hours in a relatively non-complex terrain with an average distance of approximately 5.6 km between observation sites. The CALMET and SWIFT model exhibited nearly perfect performance measures with correlation coefficients of 0.98 and mean absolute errors in wind speed simulations of less than 1 m s^{-1}. For the MCSCIPUF

model larger errors were estimated.

Two studies by Schlager et al. (2017) and Schlager et al. (2018) have confirmed that a weather diagnostic application, the WegenerNet Wind Product Generator (WPG) in particular, can be applied to meteorological station networks. In the first of these studies, the WPG generated wind fields based on observations derived from the WegenerNet FBR, a high-density network of over 150 meteorological stations located in complex, hilly terrain. The WPG's performance was evaluated over a two-month period of representative weather conditions, and the results were found to be highly accurate (Schlager et al. 2017). In a further study (Schlager et al. 2018), the WPG was applied to a second network of meteorological stations, the WegenerNet JBT, located in a mountainous region with very complex terrain and consisting of 11 observation sites. The application's performance was evaluated again for a two-month period involving representative wind events. The estimated wind speed results exhibited strong statistical agreement estimated with the real observations.

As for wind direction, the statistical agreement with real observations varied according to the station's locations, as locations along mountain slopes proved particularly challenging. Furthermore, the WPG was evaluated in this study with respect to the nine-year climate data of the WegenerNet FBR and the five-year climate data of the WegenerNet JBT. In these evaluations the climate data generated by the WPG was of similar quality to the shorter-term simulations, with simulations for the WegenerNet FBR performing slightly better. More information regarding the WPG can be found in Sections 6.3 and 7.3.

2.4 Spatial verification methods

Most of the spatial verification methods can be classified into one of the following four categories (Gilleland et al. 2010): a) neighborhood (or fuzzy), b) scale separation (or decomposition), c) features based (or objects based), and d) field deformation. The first two methods (a, b) are further generalized as filter methods, while the second ones (c, d) are also denoted as displacement approaches.

The advantage of filter approaches is the ability to deliver a scale dependent information about the forecasting skill. In case of neighborhood based approaches, the statistics are calculated for a range of neighborhood sizes to smear out variability at smaller scales and reduce the accuracy of the forecasts (Fig. 2.13a) (Roberts and Lean 2008; Skok and Hladnik 2018). Scale separation techniques implement single-band spatial filters to deliver information about the skill as a function of the spatial scale. Therefore, phenomena of a particular size are isolated based on calculating statistics for different spectral bands. Binary differences between a forecast and observation, including constituent wavelet components are illustrated in Fig. 2.13b (Briggs and Levine 1997; Tustison et al. 2001).

Displacement methods are trying to shift a forecast field spatially with the aim to better match the observed field. In case of feature based approaches, single

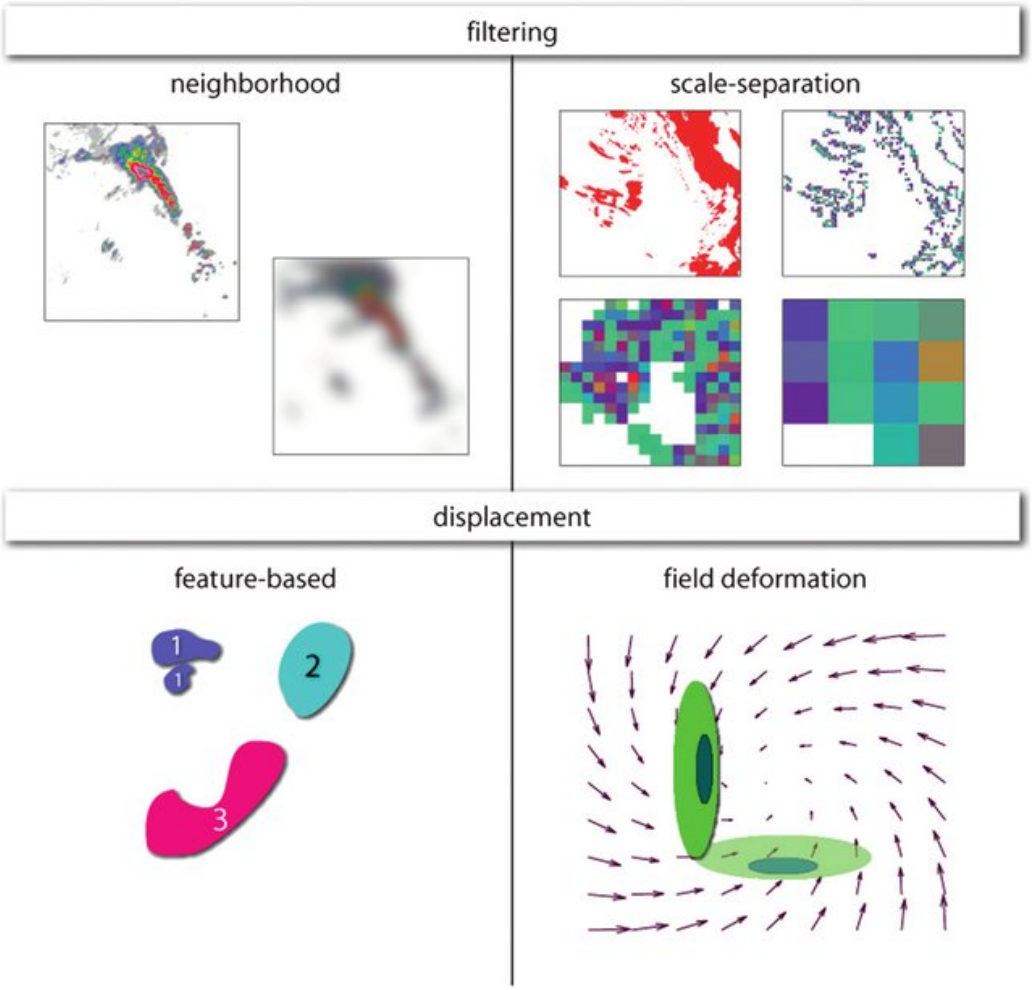

Figure 2.13: Schematic representation of characteristics of different types of spatial verification methods categorized in filtering (a, b) and displacement methods (c, d): Filtering methods apply a smoothing filter and calculate metrics at increasing spatial scales. (a) neighborhood techniques calculate statistics for increasing neighborhood sizes, whereas (b) scale-separation methods calculate statistics for different spectral bands based on a bandpass filter to estimate performance at independent scales. The displacement methods deliver information about amount and type of location errors (among others). (c) feature-based methods analyze objects and their structures within a field (see individually numbered objects), whereas (d) field deformation approaches are generally applied to the entire field as a whole unit. From Gilleland et al. (2010)

objects like a storm are identified within the field and their structures are analyzed separately (Fig. 2.13c) (Harris et al. 2001; Marzban and Sandgathe 2009; Scheuerer and Hamill 2015; Lack et al. 2010). Field deformation methods are trying to deform the forecast field to match the observation and deliver statistic about the degree of deformation (Fig. 2.13d) (Hoffman et al. 1995; Alexander et al. 1999).

In this context, the WFSS used in this work is classified as neighborhood base verification metric, and is described in detail in Section 8.3.1. A comprehensive literature review and qualitative comparison of selected methods can be found in Gilleland et al. (2010).

Table 2.1 summarizes the measured attributes by the different methods and indicates which method is useful for estimating skills for different situations. All methods include algorithms for estimating intensity errors, but they are different for each approach. As briefly mentioned above, filter methods are differing from displacement approaches in their ability of estimating scale information or location errors. Only feature-based approaches are attempting to identify structures in each field and matched features are compared based on different attributes (Gilleland et al. 2010).

Table 2.1: Types of information which can be estimated by the respective category of spatial verification metrics. Reproduced from Gilleland et al. (2010).

Category	Scales with skill	Location errors	Intensity errors	Structure errors	Occurence (hits, misses, and false alarms)
Neighborhood	yes	No	yes	No	yes
Scale separation	yes	No	yes	No	yes
Features based	No	yes	yes	yes	yes
Deformation	No	yes	yes	No	No

3 Study areas and WegenerNet data

3.1 The WegenerNet networks

The first area considered in this study, the WegenerNet FBR, is centered near the town of Feldbach (46.93°N, 15.90°E) and lies in the Alpine foreland of southeastern Styria in Austria (Fig. 3.1a). The terrain is characterized by its many hills and small range of altitude, with altitudes varying approximately 100 m between the area's valleys and crests. The area's highest peak is the Gleichenberg Kogel, with an elevation of 598 m, compared to about 250 m at the lowest point. A dense grid of 155 meteorological stations covers an area of approximately 22 km x 16 km, with the average distance between stations of approximately 1.4 km.

The stations are classified based on their sensor configurations into four different categories corresponding to the types of measurements they are capable of. All 155 stations measure air temperature, humidity, and precipitation, and 14 stations are equipped with additional sensors that permit them to measure wind speed and wind direction. The observations of the meteorological stations are available going back to the year 2007, with a 5-minute temporal resolution (Kirchengast et al. 2014; Schlager et al. 2017; Schlager et al. 2018).

This region exhibits a more Alpine climate in its valley floors, with cold winters and hot summers, and a more Mediterranean climate along the hillsides, with milder winters and hot summers as well. The area is subject to a rich variety of weather situations, including strong convective activity and extreme precipitation in summer (Wakonigg 1978; Kabas et al. 2011; Hohmann et al. 2018). Furthermore, it exhibits rich weather variability, especially through strong convective activity and severe weather in summer (Kirchengast et al. 2014; Kann et al. 2015a; O et al. 2017; O et al. 2018; Schroeer and Kirchengast 2018).

From a climatological perspective, the area is considered to be homogeneous with respect to synoptic patterns of heavy precipitation (Seibert et al. 2007). The area's sensitivity to regional climate change can already be clearly measured (Kabas et al. 2011; Hohmann et al. 2018). The winds in this study area are characterized by thermally-driven local flows and flows influenced by a dynamical process called Alpine pumping (Lugauer and Winkler 2005; Schlager et al. 2017; Schlager et al. 2018).

The second study area, the WegenerNet JBT (Fig. 3.1b), is centered near the village of Johnsbach (47.54°N, 14.58°E), named after the Johnsbach river basin and overlaying with the Gesäuse National Park in the Ennstaler Alps, lying in the eastern Alpine region in northern Styria, Austria. This mountainous region is characterized by large differences in altitude, with summits of over 2300 m and

valleys with altitudes of between approximately 600 m and 800 m (Strasser et al. 2013; Schlager et al. 2018). Eleven irregularly distributed meteorological stations are installed at various elevations within an area of about 16 km x 17 km at different elevations, including two summit stations situated at altitudes of 2191 m and 1969 m (Schlager et al. 2018). Measurements for the observed variables are recorded by the stations at a 10 minute intervals. The Alpine climate of this region causes it to have annual mean temperatures of about 8°C at lower altitudes, and below 0°C at higher elevations, and an annual precipitation sum of 1500 mm in the valley and 1800 mm in the summit regions (Wakonigg 1978; Prettenthaler et al. 2010). The area's wind system is mainly controlled by thermally-induced local flows and westerly-flow synoptic weather conditions (Schlager et al. 2018).

The data used in this study, which was acquired from the stations of the two WegenerNet regions, FBR and JBT, was automatically quality controlled and processed by the WegenerNet Processing System (WPS) with its four subsystems (Kirchengast et al. 2014): the Command Receive Archiving System, which transfers raw data via wireless transmission to the WegenerNet database in Graz; the Quality Control System, which checks data quality; the DPG, which generates regular station time series and gridded fields of weather and climate products; and the Visualization and Information System, which offers the data to users via the WegenerNet data portal (www.wegenernet.org).

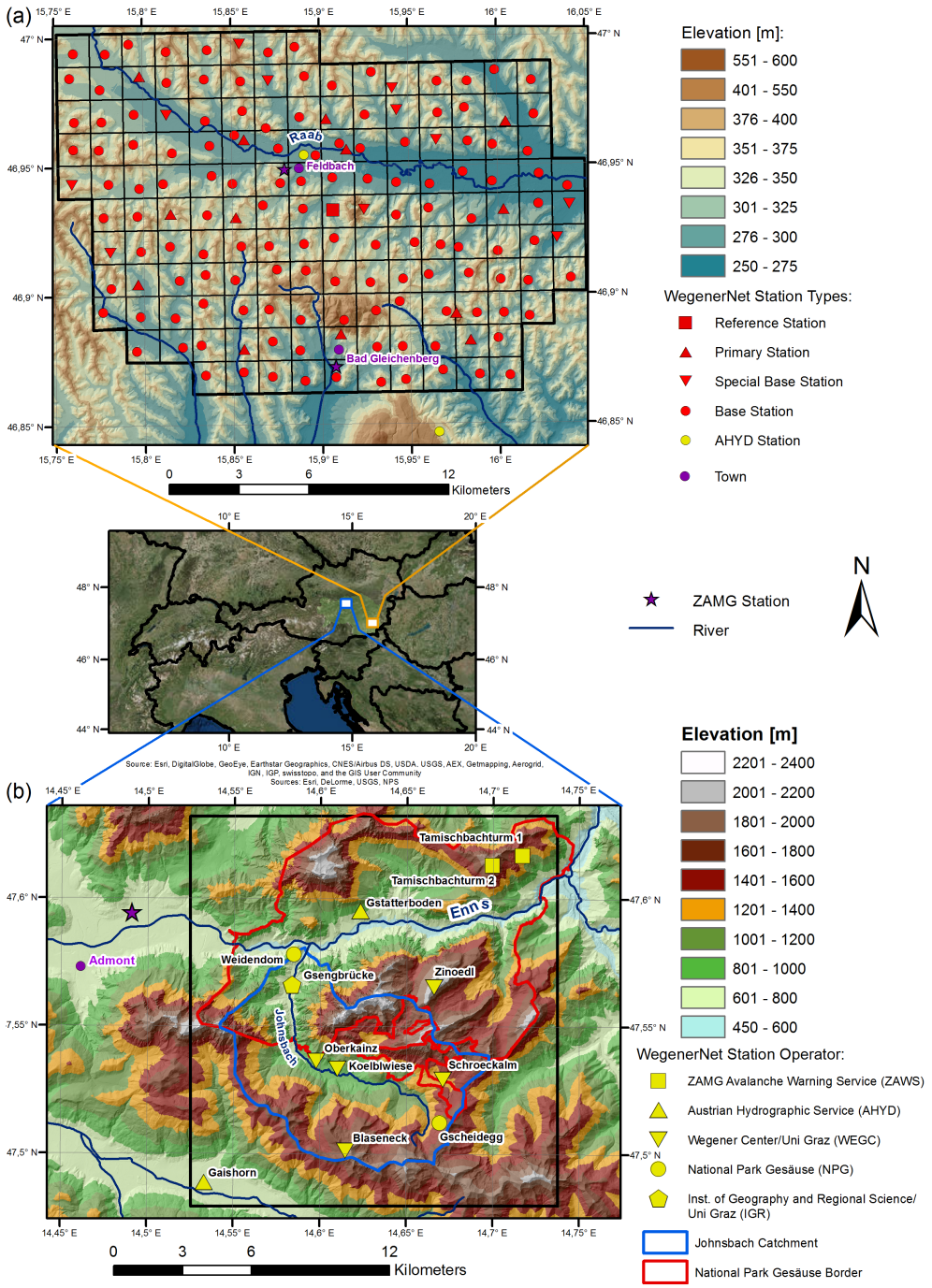

Figure 3.1: (middle panel) Location of the study areas, the WegenerNet Feldbach Region (FBR) in the southeast of Styria, Austria and the WegenerNetJohnsbachtal (JBT) region in the north of Styria, Austria (white-filled rectangles, enlarged in (a) and (b)). (a) The WegenerNet FBR with its 154 meteorological stations, with the legend explaining map characteristics and station types. (b) Map of the WegenerNet JBT region (blackrectangle) including its meteorological stations, with the legend explaining map characteristics and station operators.

3.2 The wind product generator introduction

Wind field evaluation data was generated for this study using the WPG, an application developed and integrated into the DPG over the course of preparing this thesis project. The WPG automatically generates high-resolution wind fields in near real-time based on the DPG-controlled and -processed meteorological observations and auxiliary geophysical information. A core tool for the WPG is the empirical CALMET, which is based on the modeling approach explained in Section 2.3.2 (Scire et al. 1998).

The WPG uses an enhanced version of the CALMET model, which includes algorithms for empirically calculating solar radiation-based topographic shading across different terrain heights, the slope and aspect of topography, and the position of the sun. Furthermore, the enhanced CALMET model generates temperature fields based on vertical temperature gradients estimated by the meteorological stations, and accounts for the influence of vegetation cover based on leaf area indices (Bellasio et al. 2005; Schlager et al. 2017; Schlager et al. 2018) (cf. Sections 6.3 and 7.3).

The WPG application can be applied to other high-density meteorological station networks with different landscape characteristics and terrain, but area-specific model parameters have to be adjusted according to the characteristics of those regions (cf. Table 6.3 for the WegenerNet FBR and Table 7.3 for the JBT). The CALMET model obtains geophysical information from the study areas in the form of gridded datasets that include data concerning elevations, land-use types, and relevant geophysical parameter values (see Table 6.4 for the WegenerNet FBR and Table 7.4 for the JBT).

Gridded wind field datasets are available for the WegenerNet FBR dating back to 2007 and for the WegenerNet JBT dating back to 2012, with a spatial resolution of 100 m x 100 m and a temporal resolution of 30 minutes for both regions.

4 Methodology and Scientific Approach

This chapter outlines the methodology and scientific approach and explains the connection of different research stages to achieve the two defined objectives, explained in section 1.2 above. These stages are starting from preparatory phases which include literature reviews and ending up with final phases, which include the completion of the entire work.

4.1 Scientific approach

The scientific approach to reach the first objective is separated into five phases which are illustrated in Fig. 4.1. During the preparation phase the needed knowledge is gained based on literature review and used as general input for the carried out research. In a second step, the modeling phase started with the development of the

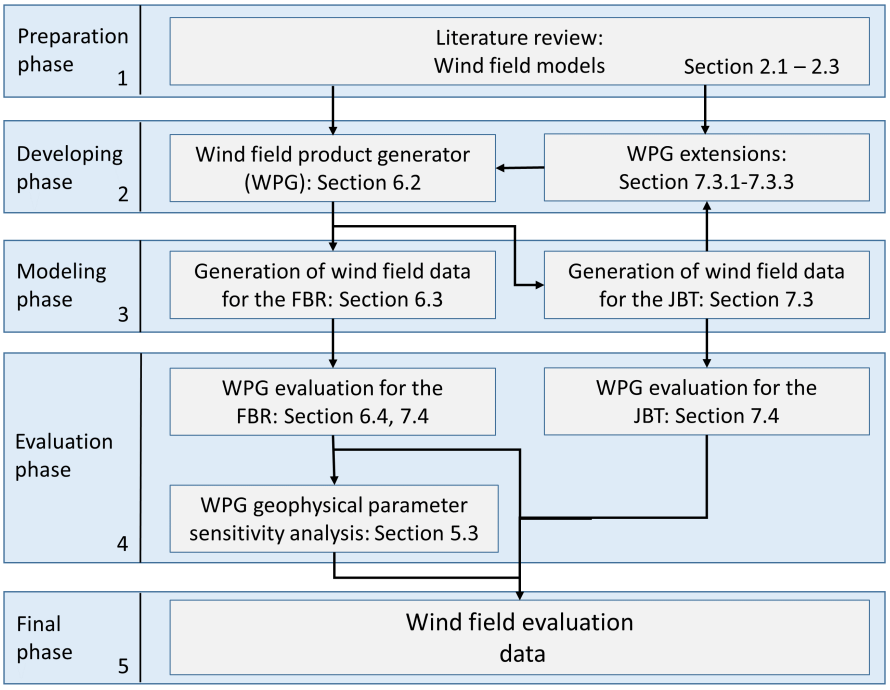

Figure 4.1: Conceptual workflow model of the scientific approach's main phases to accomplish the first objective, including references to according sections of the manuscript. The objectives are defined in section 1.2.

WPG, which has been applied to the WegenerNet FBR and WegenerNet JBT. Based on finding systematic errors in the modeled wind fields for the WegenerNet JBT, the WPG has been extended with addition functionality. During the evaluation phase, the applications performance is evaluated for the WegenerNet FBR and the WegenerNet JBT. Furthermore, the sensitivity of the CALMET model and subsequently the WPG has been investigated within this phase. Last, all steps result in the automatic generation of high-resolution wind field data for the two study areas.

The second objective has been accomplished by four different phases of the scientific approach which are illustrated in Fig. 4.2. The preparation phase includes a comprehensive literature review about data preparation and verification methods. With the obtained knowledge, methods for automatic selection and classification of wind field data have been developed. The R code for the calculation of the WFSS has been integrated into a Python environment to allow an automatic calculation of this score based on selected wind field data. During the evaluation phase, spatial verification as well as traditional gridpoint-based error measure were calculated for the selected wind field data. Finally, going through all phases led to the wind field evaluation results.

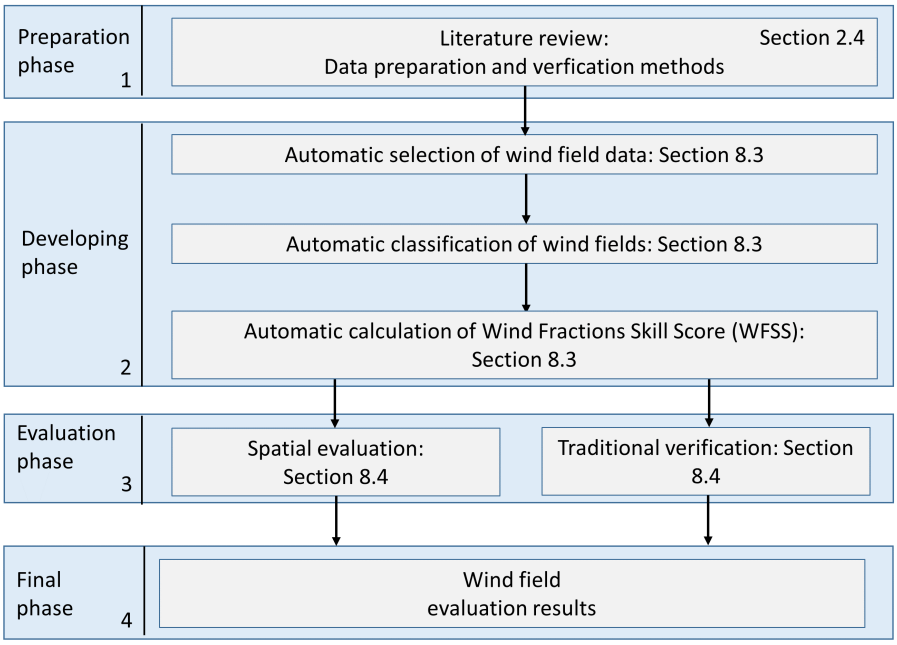

Figure 4.2: Conceptual workflow model of the scientific approach's main phases to accomplish the second objective, including a reference to according sections of the manuscript. The objectives are defined in section 1.2.

4.2 Peer reviewed publications

The study areas, methods, evaluation periods and events, as well as the results of the scientific approaches (cf. Section 4.1) are summarized in the chapters 5 to 8 and are mainly presented based on peer-reviewed publications, except the results regarding the geophysical parameter sensitivity analysis. The method and results regarding the sensitivity analysis of the CALMET model to geophysical parameters have not yet been published, but are discussed in detail in chapter 5.

The chapters 6 to 8 include the following peer-reviewed publications for which the chapter title is also the title of the publication:

Schlager, C., G. Kirchengast, and J. Fuchsberger (2017). "Generation of high-resolution wind fields from the dense meteorological station network WegenerNet in south-eastern Austria". *Wea. Forecasting* 32.4, pp. 1301–1319. doi: 10.1175/WAF-D-16-0169.1.

Contributions: Christoph Schlager collected the data, performed the analyses and modeling, created the figures and wrote the first draft of the manuscript. Gottfried Kirchengast provided guidance and advice on all aspects of the study and significantly contributed to the text. Jürgen Fuchsberger provided guidance on technical aspects of the WegenerNet networks and its data characteristics and contributed to the text.

Schlager, C., G. Kirchengast, and J. Fuchsberger (2018). "Empirical high-resolution wind field and gust model in mountainous and hilly terrain based on the dense WegenerNet station networks". *Atmos. Meas. Tech.* 11.10, pp. 5607–5627. doi: 10.5194/amt-11-5607-2018.

Contributions: Christoph Schlager collected the data, performed the analyses and modeling, created the figures and wrote the first draft of the manuscript. Gottfried Kirchengast provided guidance and advice on all aspects of the study and significantly contributed to the text. Jürgen Fuchsberger provided guidance on technical aspects of the WegenerNet networks and its data characteristics and contributed to the text.

Schlager, C., G. Kirchengast, J . Fuchsberger, A. Kann, and H. Truhetz (2019): "A spatial evaluation of high-resolution wind fields from empirical and dynamical modeling in hilly and mountainous terrain", *Geosci. Model Dev.* 12.7, pp. 2855-2873. https://doi.org/10.5194/gmd-12-2855-2019.

Contributions: Christoph Schlager collected the data, performed the analyses and modeling, created the figures and wrote the first draft of the manuscript. Gottfried Kirchengast provided guidance and advice on all aspects of the study and significantly contributed to the text. Jürgen Fuchsberger provided guidance on technical aspects of the WegenerNet networks and its data characteristics and contributed to the text. Alexander Kann provided INCA-related advice and contributed to the INCA part of the text and Heimo Truhetz provided information and advice on the CCLM model setup and characteristics and contributed to the CCLM part of the text. All authors commented on the final version of the manuscript.

5 Geophysical parameter sensitivity analysis

This section introduces the methods and results of an additional study regarding the influence of geophysical parameters on the generation of wind fields. First, the method of the CALMET model to geophysical parameters is presented and second, the results regarding this sensitivity analysis are presented in the last part of this chapter.

5.1 Method

As briefly explained in Section 3.2 above, the CALMET model includes surface characteristics in form of two-dimensional gridded fields including terrain elevations, land-use types and geophysical parameter values. A geophysical preprocessing tool constructs the gridded datasets of geophysical parameter values for the CALMET model, based on user defined geophysical parameters for existing land-use types (Scire et al. 1998).

To analyze the sensitivity of the CALMET model to geophysical parameters, wind fields were generated based on perturbations of the values of these parameters. The sensitivity test was performed with wind field data generated from WegenerNet FBR stations and geophysical parameter values for the predominant land-use types of this region (Fig. 6.2). The wind fields that were generated using perturbed parameter values were compared to reference wind fields; wind fields from August 10, 2008, generated based on the parameter values summarized in Table 6.4, were used as a reference for thermally-driven circulations with weak wind speeds, and wind fields from March 15, 2013 for strong wind speeds (Schlager et al. 2017). For generating wind fields based on perturbed parameter values, value ranges for the geophysical parameters were estimated on the basis of a literature review considering the most common land-use classes, which are summarized in Table 5.1.

For the sensitivity analysis, 60 sensitivity cases were defined, 12 for each of the 5 geophysical parameters. Table 5.2 provides a summary of these evaluation cases, including the perturbed parameter values applied for each geophysical parameter and the three-to-four most common land-use types, and the statistical results for both reference periods. The cases xMin and xMax are defined as cases corresponding to the minimum and maximum values of the geophysical parameters (Table 5.1). Furthermore, to determine the degree of linearity of the parameterization schemes that account for these parameters, two cases denoted by XMin and XMax were identified. The influence of the perturbations was assessed

by calculating the root-mean-square error (RMSE), bias (B), and mean absolute error of wind direction (MAEDIR) (Table 6.5 or Table 7.6).

Table 5.1: Value ranges of the geophysical parameters for the dominating land use types of the WegenerNet FBR (top half), and reference publications for each parameter on basis which these value ranges were estimated (bottom half).

Land use type (abbreviation)	Surface roughness length [m]	Albedo	Bowen ratio	Soil heat flux constant	Vegetative leaf area index	Area [%]
Agri. land - unirri. (AGRI)	0.10-0.50	0.10-0.60	0.30-2.00	0.10-0.30	0.20-3.20	57
Forest land (FOR)	0.50-1.50	0.10-0.50	0.20-2.00	0.00-0.20	0.60-8.00	35
Discon. urban fabr. (DUF)	0.50-1.50	0.10-0.40	0.50-4.00	0.20-0.40	0.40-2.20	5
Pastures (PAS)	-	0.10-0.60	0.30-2.00	-	-	3

Reference publications per geophys. parameter

Surface roughness length:	Gao et al. (2015), Cheng and Byun (2008), Kalyanapu et al. (2009), Nicholas and Lewis (1980), and EPA. (2004)
Albedo:	Sütterlin et al. (2016), Salifu and Agyare (2012), Cheng and Byun (2008), Lamptey (2010), and EPA. (2004)
Bowen ratio:	Lin et al. (2016), Cheng et al. (2015), Lamptey (2010), Frey et al. (2011), and EPA. (2004)
Soil heat flux constant:	Lamptey (2010), Gao et al. (2015), Tsuang (2005), and Takashi et al. (1989)
Leaf area index:	Salifu and Agyare (2012), Knote et al. (2009), and Sun and Schulz (2017)

5.2 Results

For thermally-driven circulations, the generated wind fields were found to be most sensitive to changes in the surface roughness length parameter, followed by changes in the Bowen ratio and albedo parameters. The results estimated for strong wind speeds indicated that these three parameters are again the most influential, but in the opposite order, as wind fields with high speeds were found to be most sensitive to changes in Bowen ratio values, followed by changes to the albedo measure and to surface roughness length. Changes to the values of the soil heat flux constant parameter and leaf area index parameter had hardly any influence on generated wind fields on either day.

The results also revealed that changes to parameters had a slightly larger influence on thermally-driven circulations than on strong winds, especially with respect to wind direction. A direct correlation was observed between the influence of changes made to parameters and the total area dedicated to the corresponding land-use type, with the exception of surface roughness length when applied to areas with discontinuous urban fabric (DUF) under weak conditions (cases rough_duf_xMin, rough_duf_xMax, rough_duf_XMin, rough_duf_XMax). Changes in parameters were found to have the strongest estimated impact in the rough_duf_XMin case for August 10, 2008, where an RMSE value of 0.153 m s^{-1}, a B value of 0.103 m s^{-1} and a MAEDIR value of 4.220° were estimated. The high sensitivity of the wind

fields to parameters under weak conditions is caused by the downward extrapolation of observations from the WN44 station, which is located in an area classified as DUF and measures wind parameters at a height of 55 m.

Table 5.2: Statistical performance measures calculated for the WegenerNet FBR, for perturbations applied to the parameter values, for the 10 August 2008 and 15 August 2013.

			10 August 2008			15 March 2013		
Sensitivity case (per geophys. param.)	Land use type[a]	Param. value[b, c]	RMSE [m s^{-1}]	B [m s^{-1}]	MAE_{dir} [°]	RMSE [m s^{-1}]	B [m s^{-1}]	MAE_{dir} [°]
Surface rough. length [m]								
rou_duf_xMin	DUF	1.00|0.50	0.0321	0.0197	0.9563	0.0025	0.0000	0.0062
rou_duf_xMax	DUF	1.00|1.50	0.0245	-0.0145	0.7620	0.0017	0.0000	0.0042
rou_duf_XMin	DUF	1.00|1e-4	0.1526	0.1028	4.2196	0.0157	-0.0001	0.0383
rou_duf_XMax	DUF	1.00|2.50	0.0585	-0.0370	1.9842	0.0039	0.0001	0.0107
Mean value			0.0669	0.0178	1.9805	0.0060	0.0000	0.0149
rou_agr_xMin	AGR	0.25|0.01	0.0602	0.0397	1.4159	0.0321	-0.0046	0.2958
rou_agr_xMax	AGR	0.25|0.50	0.0150	-0.0075	0.2717	0.0061	0.0008	0.0594
rou_agr_XMin	AGR	0.25|1e-4	0.0602	0.0397	1.4159	0.0321	-0.0046	0.2958
rou_agr_XMax	AGR	0.25|1.00	0.0329	-0.0175	0.6390	0.0124	0.0017	0.1349
Mean value			0.0421	0.0136	0.9356	0.0207	-0.0017	0.1965
rou_for_xMin	FOR	1.00|0.50	0.0023	-0.0001	0.0943	0.0054	0.0002	0.0495
rou_for_xMax	FOR	1.00|1.50	0.0022	0.0001	0.0889	0.0039	-0.0001	0.0359
rou_for_XMin	FOR	1.00|1e-4	0.0072	0.0001	0.4971	0.0324	0.0022	0.2830
rou_for_XMax	FOR	1.00|2.50	0.0048	0.0005	0.3035	0.0089	-0.0001	0.0937
Mean value			0.0041	0.0002	0.2460	0.0127	0.0006	0.1155
Albedo [1/1]								
alb_duf_xMin	DUF	0.18|0.10	0.0008	0.0000	0.0018	0.0004	0.0000	0.0001
alb_duf_xMax	DUF	0.18|0.40	0.0041	-0.0002	0.0168	0.0064	0.0000	0.0019
alb_duf_XMin	DUF	0.18|0.00	0.0011	0.0001	0.0036	0.0005	0.0000	0.0002
alb_duf_XMax	DUF	0.18|0.70	0.0080	-0.0006	0.0465	0.0146	0.0000	0.0079
Mean value			0.0035	-0.0002	0.0172	0.0055	0.0000	0.0025
alb_agrpas_xMin	AGR|PAS	0.15|0.10	0.0019	0.0001	0.0288	0.0015	-0.0001	0.0025
alb_agrpas_xMax	AGR|PAS	0.15|0.60	0.0103	-0.0005	0.4230	0.0343	0.0024	0.0807
alb_agrpas_XMin	AGR|PAS	0.15|0.00	0.0029	0.0002	0.0696	0.0024	-0.0002	0.0063
alb_agrpas_XMax	AGR|PAS	0.15|1.00	0.0449	-0.0057	1.6910	0.0936	0.0125	0.3916
Mean value			0.0150	-0.0015	0.5531	0.0330	0.0037	0.1203
alb_for_xMin	FOR	0.10|0.10	0.0000	0.0000	0.0000	0.0000	0.0000	0.0000
alb_for_xMax	FOR	0.10|0.50	0.0091	0.0005	0.2634	0.0234	-0.0010	0.0407
alb_for_XMin	FOR	0.10|0.00	0.0020	0.0000	0.0357	0.0018	0.0001	0.0032
alb_for_XMax	FOR	0.18|0.90	0.0404	0.0039	1.1565	0.0736	-0.0068	0.2235
Mean value			0.0129	0.0011	0.3639	0.0247	-0.0020	0.0669
Bowen ratio [1/1]								
bow_duf_xMin	DUF	1.50|0.50	0.0015	-0.0001	0.0054	0.0007	0.0000	0.0003
bow_duf_xMax	DUF	1.50|4.00	0.0012	0.0001	0.0039	0.0006	0.0000	0.0002
bow_duf_XMin	DUF	1.50|0.00	0.0041	-0.0004	0.0270	0.0090	0.0000	0.0051
bow_duf_XMax	DUF	1.50|7.50	0.0015	0.0001	0.0056	0.0007	0.0000	0.0004
Mean value			0.0021	-0.0001	0.0105	0.0028	0.0000	0.0015
bow_agrpas_xMin	AGR|PAS	1.00|0.30	0.0504	-0.0002	1.8859	0.0550	-0.0069	0.9310
bow_agrpas_xMax	AGR|PAS	1.00|2.00	0.0507	0.0007	1.8100	0.0548	-0.0075	0.9247
bow_agrpas_XMin	AGR|PAS	1.00|0.00	0.0525	-0.0022	2.3541	0.0628	-0.0066	1.0205
bow_agrpas_XMax	AGR|PAS	1.00|3.70	0.0509	0.0009	1.8508	0.0549	-0.0077	0.9286
Mean value			0.0511	-0.0002	1.9752	0.0569	-0.0072	0.9512
bow_for_xMin	FOR	1.00|0.20	0.0074	0.0004	0.1865	0.0064	-0.0005	0.0166
bow_for_xMax	FOR	1.00|2.00	0.0032	-0.0001	0.0707	0.0028	0.0002	0.0064
bow_for_XMin	FOR	1.00|0.00	0.0218	0.0012	0.5839	0.0274	-0.0008	0.0751
bow_for_XMax	FOR	1.00|3.80	0.0047	-0.0002	0.1222	0.0041	0.0003	0.0111
Mean value			0.0093	0.0003	0.2408	0.0102	-0.0002	0.0273

[a] The value ranges of Albedo and Bowen ration are similar for AGR and PAST (see also Table 5.1 for information on value ranges)
[b] Reference value|Perturbed value (see also Table 6.4 for information on reference values)
[c] Perturbed values: minimum ($xMin$) and maximum ($xMax$) values of the corresponding geophysical parameters are defined based on literature; see Table 5.1 for information about the literature sources. $XMin(lut) = 2xMin(lut) - xMax(lut)$; $XMax(lut) = 2xMax(lut) - xMin(lut)$.
In CALMET, negative values are not allowed, the surface roughness length must be greater than zero (Scire et al. 1998).

continued ...

... continued

Sensitivity case (per geophys. param.)	Land use type[a]	Param. value[b, c]	10 August 2008 RMSE [m s^{-1}]	10 August 2008 B [m s^{-1}]	10 August 2008 MAE_{dir} [°]	15 March 2013 RMSE [m s^{-1}]	15 March 2013 B [m s^{-1}]	15 March 2013 MAE_{dir} [°]
Leaf area index [1/1]								
lai_duf_xMin	DUF	0.20|0.40	0.0000	0.0000	0.0000	0.0001	0.0000	0.0000
lai_duf_xMax	DUF	0.20|2.20	0.0000	0.0000	0.0000	0.0001	0.0000	0.0000
lai_duf_XMin	DUF	0.20|0.00	0.0001	0.0000	0.0001	0.0001	0.0000	0.0000
lai_duf_XMax	DUF	0.20|4.00	0.0001	0.0000	0.0001	0.0001	0.0000	0.0000
Mean value			0.0001	0.0000	0.0000	0.0001	0.0000	0.0000
lai_agr_xMin	AGR	3.00|0.20	0.0000	0.0000	0.0000	0.0000	0.0000	0.0000
lai_agr_xMax	AGR	3.00|3.20	0.0002	0.0000	0.0001	0.0001	0.0000	0.0000
lai_agr_XMin	AGR	3.00|0.00	0.0003	0.0000	0.0003	0.0004	0.0000	0.0003
lai_agr_XMax	AGR	3.00|6.20	0.0003	0.0000	0.0005	0.0002	0.0000	0.0002
Mean value			0.0002	0.0000	0.0002	0.0002	0.0000	0.0001
lai_for_xMin	FOR	7.00|0.60	0.0008	0.0000	0.0007	0.0005	0.0000	0.0004
lai_for_xMax	FOR	7.00|8.00	0.0001	0.0000	0.0001	0.0001	0.0000	0.0000
lai_for_XMin	FOR	7.00|0.00	0.0008	0.0000	0.0007	0.0005	0.0000	0.0004
lai_for_XMax	FOR	7.00|15.4	0.0002	0.0000	0.0004	0.0002	0.0000	0.0002
Mean value			0.0005	0.0000	0.0005	0.0003	0.0000	0.0002
Soil heat flux const. [1/1]								
shfc_duf_xMin	DUF	0.25|0.20	0.0005	0.0000	0.0007	0.0002	0.0000	0.0000
shfc_duf_xMax	DUF	0.25|0.40	0.0009	-0.0001	0.0022	0.0004	0.0000	0.0001
shfc_duf_XMin	DUF	0.25|0.00	0.0011	0.0001	0.0032	0.0005	0.0000	0.0002
shfc_duf_XMax	DUF	0.25|0.60	0.0016	-0.0001	0.0056	0.0007	0.0000	0.0003
Mean value			0.0010	-0.0000	0.0029	0.0005	0.0000	0.0002
shfc_agr_xMin	AGR	0.15|0.10	0.0013	0.0001	0.0136	0.0011	0.0000	0.0013
shfc_agr_xMax	AGR	0.15|0.30	0.0023	-0.0002	0.0438	0.0020	0.0001	0.0041
shfc_agr_XMin	AGR	0.15|0.00	0.0022	0.0001	0.0391	0.0019	-0.0001	0.0037
shfc_agr_XMax	AGR	0.15|0.50	0.0040	-0.0004	0.1123	0.0034	0.0003	0.0106
Mean value			0.002	-0.0001	0.0522	0.0021	0.0001	0.0049
shfc_for_xMin	FOR	0.15|0.00	0.0022	-0.0001	0.0373	0.0019	0.0001	0.0034
shfc_for_xMax	FOR	0.15|0.20	0.0013	0.0000	0.0133	0.0011	0.0000	0.0012
shfc_for_XMin	FOR	0.15|0.00	0.0022	-0.0001	0.0373	0.0019	0.0001	0.0034
shfc_for_XMax	FOR	0.15|0.40	0.0033	0.0001	0.0724	0.0029	-0.0002	0.0065
Mean value			0.0024	-0.0000	0.0401	0.0020	0.0000	0.0036

[a] The value ranges of Albedo and Bowen ration are similar for AGR and PAST (see also Table 5.1 for information on value ranges)
[b] reference value|perturbed value (see also Table 6.4 for information on reference values)
[c] Perturbed values: minimum ($xMin$) and maximum ($xMax$) values of the corresponding geophysical parameters are defined based on literature; see Table 5.1 for information about the literature sources. $XMin(lut) = 2xMin(lut) - xMax(lut)$; $XMax(lut) = 2xMax(lut) - xMin(lut)$.
In CALMET, negative values are not allowed, the surface roughness length must be greater than zero (Scire et al. 1998).

Figure 5.1 illustrates the spatial distribution of mean wind speed bias for the cases in which sensitivity to surface roughness length, the albedo measure, and the Bowen ratio value were highest, for both thermally driven wind (Fig. 5.1a) and strong wind (Fig. 5.1b). The highest sensitivity was estimated for XMin or XMax cases. As mentioned above, a correlation between the degree of sensitivity to perturbations and the total area dedicated to the relevant land-use type could be observed in all cases, expect for the rough_duf_XMin case on August 10, 2008. In this case, the influence of the surface roughness length parameter, which was used as input for the vertical extrapolation of half-hourly surface observations, is evident.

In CALMET, the observed wind measurements are extrapolated from the heights of the meteorological stations' sensors to predefined vertical levels (10 m and 50 m) before horizontal spatial interpolation is performed for the purpose of generating the first guess wind field (Scire et al. 1998; Schlager et al. 2017; Schlager et al. 2018). The similarity theory (Van Ulden and Holtslag 1985) was selected as an extrapolation method for this study. The distribution of the rough_duf_XMax

case exhibits the largest bias values for thermally-induced wind events in the area nearby the WN 44 station (see the upper-left panel of Fig. 5.1a). This station is located in an area classified as DUF and measures wind parameters at a height of 55 m. The relatively large B values in this case are caused by the low surface roughness length values belonging to DUF areas, which are accounted for in the downward extrapolation of wind speeds to the 10 m height level.

It is important to note that the XMin and XMax evaluation cases represent unrealistically low and unrealistically high parameter values, respectively, and are outside expected value ranges that occur in nature. Furthermore, the results of the estimations for minimum (xMin cases) and maximum values (xMax cases) of the geophysical parameters, which reflect more realistic value ranges all generally exhibit low sensitivity to parameter perturbations, with a maximum RMSE value of about 0.06 m s^{-1} for both periods. The B values, range from -0.01 to 0.04 m s^{-1} for thermally-induced winds, and from -0.008 – 0.002 m s^{-1} for strong winds. Regarding MAEDIR values, ranges from 0 – 1.89° are estimated for thermally-induced winds, and from 0 – 0.93° for strong winds.

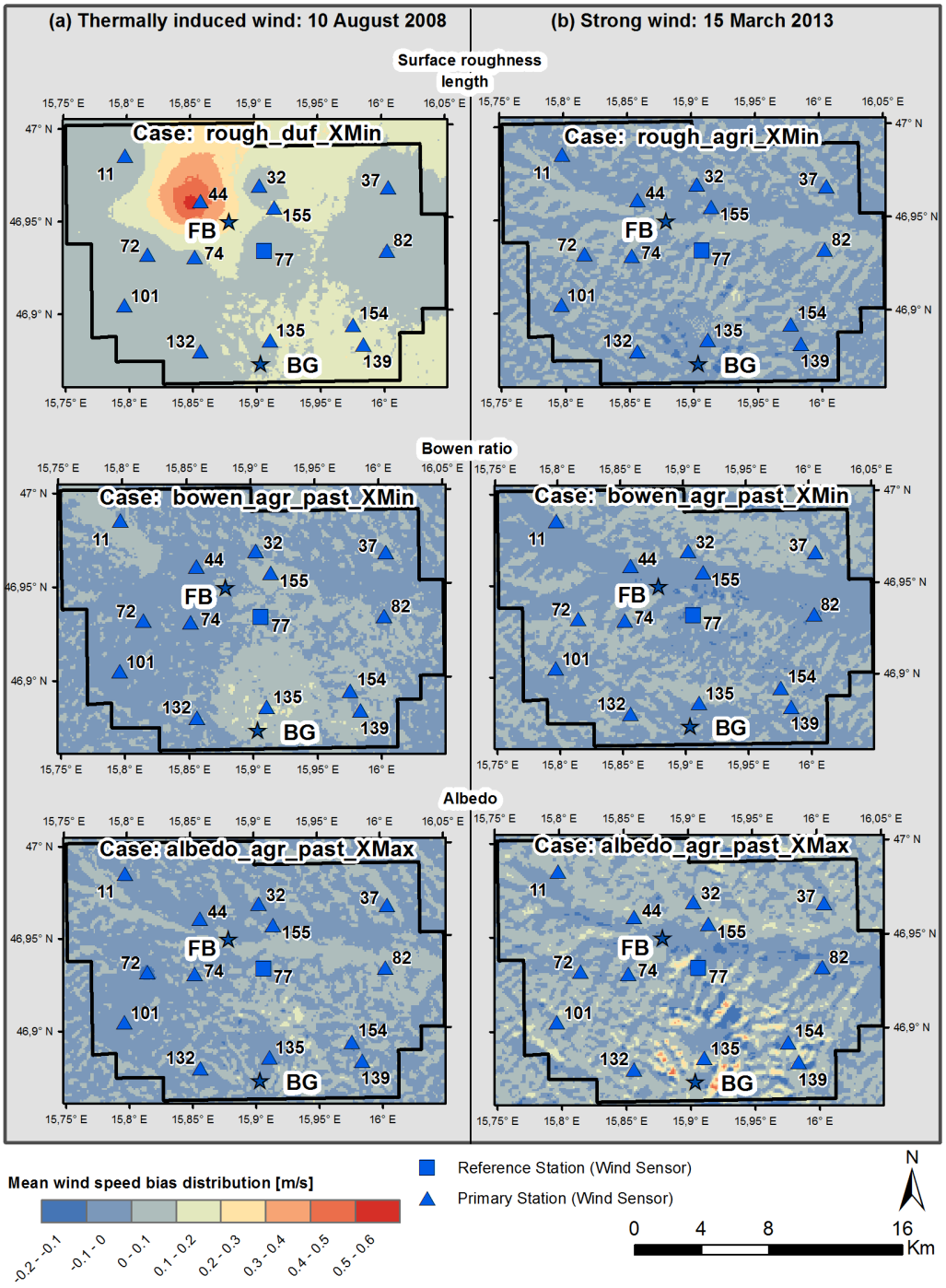

Figure 5.1: Mean wind speed bias distribution for the WegenertNet FBR, for cases with highest sensitivity (see Table 5.2 for definition of cases):(a) for thermally induced wind events and (b) strong wind events.

6 Generation of high-resolution wind fields from the WegenerNet dense meteorological station network in southeastern Austria

The first publication introduces the WPG which has been developed and applied to the WegenerNet FBR during the research phases as illustrated in Figure 4.1. Furthermore, it illustrates the application's performance, which has been evaluated for two months including mainly representative weather conditions. Table 6.1 clarifies the respective contributions of all authors of this publication.

Table 6.1: Author contributions of the first peer-reviewed publication (Schlager et al. 2017).

Title:	Generation of high-resolution wind fields from the dense meteorological station network WegenerNet in south-eastern Austria
Reference:	Schlager, C., G. Kirchengast, and J. Fuchsberger (2017). "Generation of high-resolution wind fields from the dense meteorological station network WegenerNet in south-eastern Austria". *Wea. Forecasting* 32.4, pp. 1301–1319. doi: 10.1175/WAF-D-16-0169.1
Author contributions:	
Christoph Schlager:[a,b]	Collected the data, performed the analyses and modeling, created the figures and wrote the first draft of the manuscript
Gottfried Kirchengast:[a,b]	Provided guidance and advice on all aspects of the study and significantly contributed to the text
Jürgen Fuchsberger:[a,b]	Provided guidance on technical aspects of the WegenerNet networks and its data characteristics and contributed to the text

[a] Wegener Center for Climate and Global Change (WEGC), University of Graz, Graz, Austria.
[b] Institute for Geophysics, Astrophysics, and Meteorology/Institute of Physics, University of Graz, Graz, Austria.

Generation of High-Resolution Wind Fields from the WegenerNet Dense Meteorological Station Network in Southeastern Austria

CHRISTOPH SCHLAGER, GOTTFRIED KIRCHENGAST, AND JÜRGEN FUCHSBERGER

Wegener Center for Climate and Global Change, and Institute for Geophysics, Astrophysics, and Meteorology/Institute of Physics, University of Graz, Graz, Austria

(Manuscript received 15 September 2016, in final form 8 February 2017)

ABSTRACT

An operational weather diagnostics application for automatic generation of wind fields in near–real time from observations delivered by the high-density WegenerNet meteorological station network in the Feldbach region of Austria is introduced. The purpose of the application is to empirically provide near-surface wind fields of very high spatial and temporal resolution for evaluating convection-permitting climate models as well as investigating weather and climate variability on a local scale. The diagnostic California Meteorological Model (CALMET) is used as the core tool. This model computes 3D wind fields based on observational weather data, a digital elevation model, and land-use categories. The application first produces the required input files from the WegenerNet stations and subsequently runs the CALMET model based on this input. In a third step the modeled wind fields are stored in the WegenerNet data archives every 30 min with a spatial resolution of 100 m × 100 m, while also generating averaged weather and climate products during postprocessing. The performance of the modeling against station observations, for which wind speeds were classified into weak and strong wind speeds, is evaluated and reasonably good results were found for both wind speed classes. The statistical agreement for the vector-mean wind speed is slightly better for weak wind speeds than for strong ones while the difference between modeled and observed wind directions is smaller for strong wind speeds than for weak ones. The application is also a valuable tool for other high-density networks.

1. Introduction

Progression in computer technology and the growing power of computers in data processing leads to more complex and accurate nonhydrostatic climate models for high-resolution simulations, with horizontal resolutions at a scale of 1 km (Prein 2013; Suklitsch et al. 2011; Hohenegger et al. 2008). Because of this higher resolution, such nonhydrostatic and convection-permitting modeling (NHCM) provides more realistic simulations, especially for regions with complex terrain (Awan et al. 2011; Suklitsch et al. 2011; Prein et al. 2013).

The evaluation of regional climate models (RCMs) and further model improvements require, among other needs, meteorological observations and gridded datasets with correspondingly high spatial and temporal resolutions (Kirchengast et al. 2014). RCMs generally simulate area-averaged rather than point-scale processes (Osborn and Hulme 1998). Therefore, the most appropriate data for evaluation are gridded datasets where each grid value is a best estimate average of the grid-box observations (Haylock et al. 2008). For example, the European Climate Assessment and Data (ECA&D) activity provides the daily gridded observational dataset (E-OBS) based on station datasets and other archives, consisting of temperature, precipitation, and sea level pressure for Europe. This dataset is used on a regional scale for evaluating RCMs, monitoring climate change, and for studies regarding climate variability (Haylock et al. 2008; Klok and Klein Tank 2009; Brunner et al. 2017).

The Wegener Center at the University of Graz, Graz, Austria, established the long-term field experiment WegenerNet Feldbach region, a dense grid of more than 150 meteorological stations within an area of about 20 km × 15 km for investigating weather and climate on a local scale as well as evaluating RCMs (Kirchengast et al. 2014; O et al. 2017; Kabas 2012; Kabas et al. 2011). The processing system developed to control and manage observations from the meteorological stations is called the

Corresponding author: Christoph Schlager, christoph.schlager@uni-graz.at

DOI: 10.1175/WAF-D-16-0169.1

WegenerNet Processing System (WPS) and consists of four subsystems. The Command Receive Archiving System (CRAS) is used to transfer the raw data via general packet radio service (GPRS) to the WegenerNet Database, the quality control system (QCS) checks the quality of the data, the data product generator (DPG) produces gridded fields of weather and climate products, and the visualization and information system (VIS) offers the data to users via the WegenerNet data portal (www.wegenernet.org).

Products already implemented in the DPG are gridded weather and climate products generated by a point-specific interpolation of the main variables of temperature, precipitation, and relative humidity. In the case of the temperature, fields 2 m above the ground are produced, including calculated temperature lapse rates from the observational datasets. The gridded fields of relative humidity are constructed by an inverse-distance weighted interpolation and for precipitation the inverse-distance-squared algorithm is used. Detailed information related to the WPS and its DPG subsystem can be found in Kirchengast et al. (2014) and Kabas (2012).

The application introduced in this study fills a critical gap in the DPG. Gridded wind fields generated from the existing wind observations of the 12 WegenerNet stations that are well distributed within the 20 km × 15 km area have not yet been implemented into the DPG. Wind is often considered as one of the most difficult meteorological variables to model and depends on many different conditions, including surface properties such as topography and surface roughness. Therefore, a simple interpolation of wind station data can only be performed in cases of uniform characteristics of landscape and an additional tool is needed to determine the spatial distribution of the wind parameters (Abdel-Aal et al. 2009; Sfetsos 2002).

The key goal of this study is therefore the development of an adequately realistic and robust operational application for the automated generation of gridded high-resolution wind fields from the observational data of the WegenerNet.

In general, to determine the spatial distribution of wind speed and wind direction, different types of model simulations are used (Morales et al. 2012). Dynamic mesoscale models like the Weather Research and Forecasting (WRF) Model or the Integrated Nowcasting through Comprehensive Analysis (INCA) are the most sophisticated options, since they are capable of physically simulating synoptic processes and interactions between the earth's surface and the atmosphere (Truhetz 2010). These complex prediction models solve prognostic equations and require extensive computational resources. Therefore, because of the considerable computing time and power needs, the spatial and temporal resolution is limited (Jancewicz 2014; Truhetz et al. 2007). An alternative model type was selected for being able to develop wind fields with high spatial and temporal resolution in near–real time without the need for extensive computing resources.

Empirical diagnostic models, used to represent the actual state of the atmosphere based on the data, are such an adequate alternative (Morales et al. 2012). They apply parameterizations to empirically take into account processes like the kinematic effects of terrain, slope flows, and terrain-blocking effects. They also include divergence minimization schemes for satisfying the incompressible mass consistency. Dynamic processes, like flow splitting, grid-resolved turbulence, etc. are not taken into account by these diagnostic models (Truhetz 2010; Wang et al. 2008; Truhetz et al. 2007). Thus, they need much less computing time for modeling.

In this study we employ the freely distributed diagnostic California Meteorological Model (CALMET) for the development of high-resolution wind fields. CALMET is an empirical model originally developed by the California Air Resources Board to provide wind fields for the pollutant dispersion model called CALPUFF (Scire et al. 1998; Cox et al. 2005). The model reconstructs 3D wind fields based on meteorological observations, terrain elevations, and land-use information. The quality of the modeled wind fields depends on the quality and spatial resolution of the observations from in situ meteorological station measurements as well as of the surface-related datasets, which comprise digital elevation model data and land-use-type data (Morales et al. 2012; Cox et al. 2005).

The operational requirement for our application is that the wind fields are automatically generated from the observational data of the WegenerNet in near–real time and stored to the WegenerNet archives with a spatial resolution of 100 m × 100 m and a time resolution of 30 min. Furthermore, the model performance of these produced wind fields has to be evaluated for periods with representative weather conditions.

Reporting this work, the paper is structured as follows. Section 2 provides a description of the study area, the WegenerNet Feldbach region in Austria with its over 150 meteorological stations. Section 3 presents the methodology for the empirical wind field modeling, where first the characteristics of the CALMET model and the application (developed in Python) for the automated production of the wind fields are explained. Second, a description of atmospheric weather conditions during the model evaluation periods is given. Section 4

describes the results of the wind field modeling for the selected periods in August 2008 and March 2013. Finally, section 5 provides the conclusions and prospects of the study and the next steps of follow-on work.

2. Study area and WegenerNet data

The WegenerNet Feldbach region (Fig. 1) is located in the Alpine foreland of southeastern Styria, Austria, centered near the town of Feldbach (46.93°N, 15.90°E), a region with high weather and climate variability (Kirchengast et al. 2014; Kabas et al. 2011). The terrain of this study area has many low hills and is characterized by generally small differences in altitude with maximum values of about 100 m between the valleys and crests. The highest peak is the Gleichenberger Kogel, with an elevation of 598 m, and most of the area is used for agriculture, as illustrated by Fig. 2a.

The climate of this southeastern Alpine foreland region is more Alpine at valley floors with cold winters and hot summers, and more Mediterranean along the hillsides with milder winters and hot summers (Kabas 2012; Wakonigg 1978). Heavy convective rainfall from thunderstorms, with frequent hailstorms, dominates the precipitation in summer. Strong storms can occasionally occur in the winter season (Kabas 2012; Prettenthaler et al. 2010; Wakonigg 1978). Typical for the region are thermally induced local flows and the influence of thermally-driven regional wind systems with weak wind speeds, caused by a dynamical process called Alpine pumping (Lugauer and Winkler 2005).

The hills and valleys of the region exhibit temperature contrasts, which the temperature fields produced using a modified version of CALMET for fine-resolution weather conditions are able to capture (Fig. 2b). The temperatures in the late afternoon on 10 August 2008 are shown, with higher values at lower altitudes and in the valleys and lower values along the hillsides (Fig. 2b). In this modified CALMET version, we used algorithms developed by Bellasio et al. (2005) to account for topographic shading effects and the height dependency of surface temperatures. To be consistent with the published CALMET model in this study, however, we used the original CALMET code in our wind field modeling application.

The 153 stations of the WegenerNet are used to supply in situ weather measurements as model input. These stations, with an average station distance of about 1.4 km, in an area of around 20 km × 15 km, measure meteorological parameters with a time resolution of 5 min. The stations are equipped with different sensor configurations. The 130 base stations of the network measure the main variables air temperature, relative humidity, and precipitation. Three of the stations are lacking one or two parameters (Fig. 1b; red circles). Eleven special base stations measure soil moisture and soil temperature in addition to the main variables (Fig. 1b; red triangles), 11 primary stations measure wind speed and wind direction in addition to the main variables (Fig. 1b; blue triangles), and one reference station measures wind, soil variables, air pressure, and net radiation in addition to the main variables (Fig. 1b; blue square).

All wind sensors from the primary stations and the reference station, except for stations 44, 55, and 72, are mounted on 10-m masts. Station 44 measures the wind parameters at 55-m height, station 72 at 18 m, and station 101 at 14 m (all mounted on top of silos, used in the region for storing agricultural harvests). The observations from the stations provided by the Central Institute for Meteorology and Geodynamics [Zentralanstalt für Meteorologie und Geodynamik, (ZAMG); Fig. 1b; blue stars] in Vienna, Austria, are integrated into the WPS for use as reference. Table 1 summarizes the technical characteristics of the WegenerNet stations equipped with wind sensors (Kirchengast et al. 2014; Kabas 2012).

The observations of the meteorological stations and the gridded data products produced by the DPG are available to users in near–real time since 2007, generated with a latency of about 1–2 h. The same requirements apply to the new wind field modeling application introduced here, to reproduce the wind fields since 2007 and to provide the ongoing data with a maximum latency of 2 h.

3. Methods and evaluation periods

The core part of the new operational wind field application is the CALMET model briefly introduced in section 1 above (Scire et al. 1998).

The wind fields are computed by CALMET using a two-step approach. The first step includes the adjustment of an initial guess wind field in regard to kinematic effects of terrain, slope flows, and terrain-blocking effects. Based on the settings in the CALMET control file, a user has different options to generate the initial guess wind field. In the current study we use the so-called observation-only approach in order to ensure genuinely empirical wind fields, which means that the initial guess wind field is produced by an interpolation based solely on observational data. We enhanced the original CALMET code related to the interpolation for the initial guess wind field to enable less weight (influence radius) for stations that are influenced by local terrain (the original CALMET foresees a fixed influence radius).

In a second step, the observational data are used again and blended into the step 1 wind field by an inverse distance weighting interpolation to produce the consolidated step 2 wind field. Each station site with wind observations

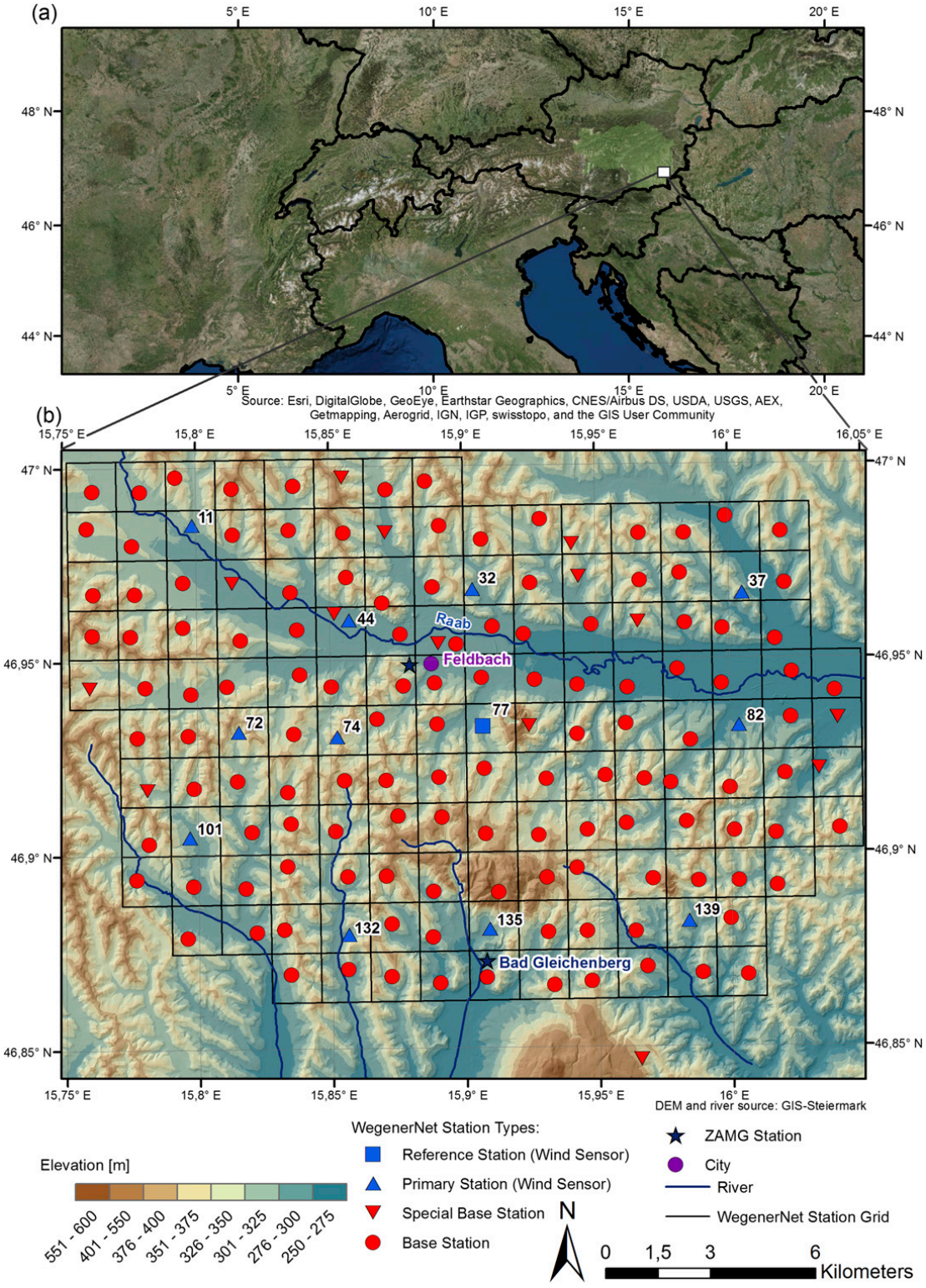

FIG. 1. (a) Overview of the WegenerNet Feldbach region study area [white rectangle; enlarged in (b)] to the southeast of Styria, Austria. (b) The WegenerNet Feldbach region with its 153 meteorological stations, with the legend explaining map characteristics and station types.

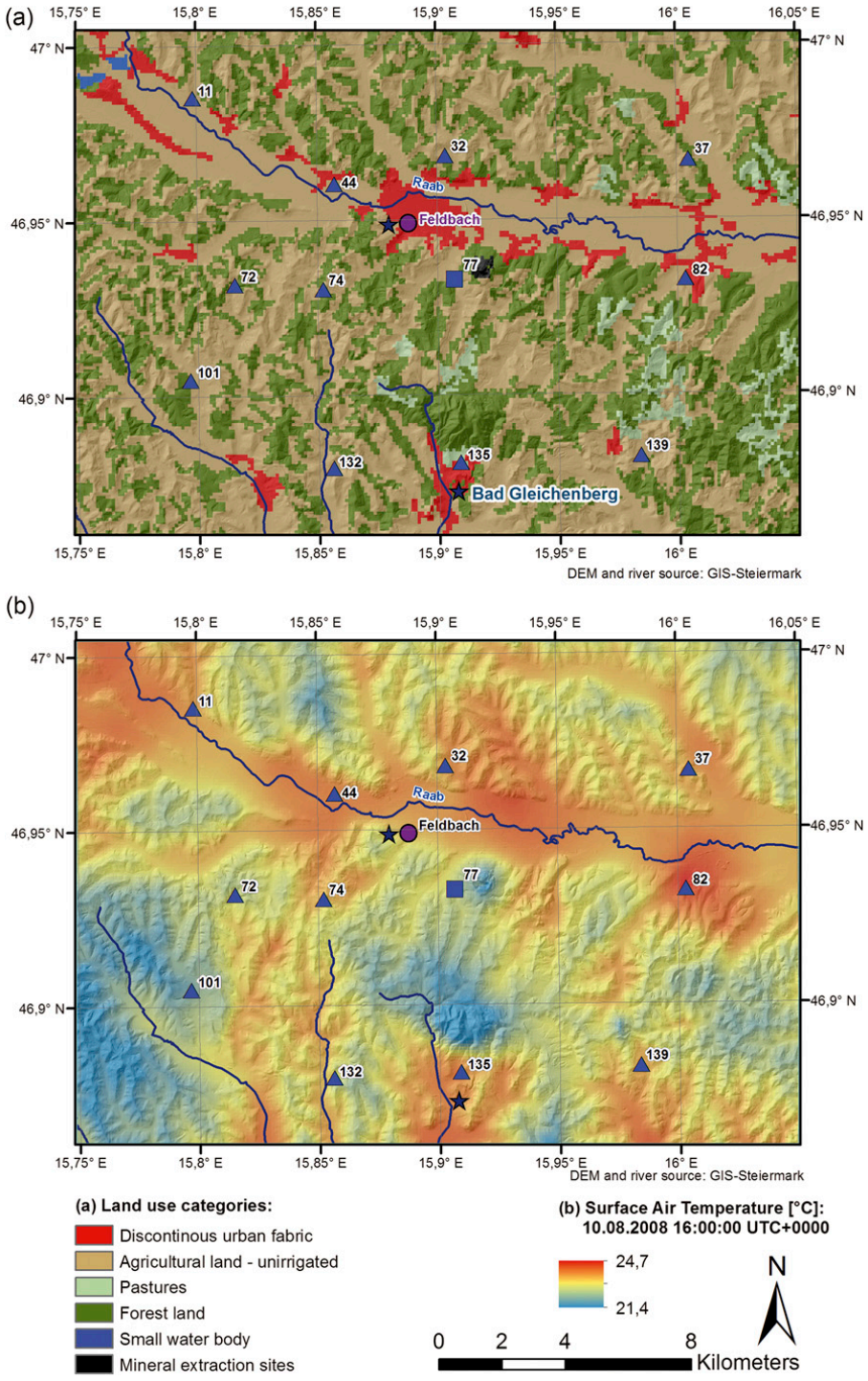

FIG. 2. (a) Land use of the study area based on the CLC 2006 raster version dataset. (b) Example temperature field of the study area (10 Aug 2008; LT = 1600 UTC + 2 h).

affects the step 2 wind field within a user-defined radius of influence. In addition, relative weighting parameters are used to weight the observations and the wind fields previously produced in step 1. To derive mass-consistent wind fields, the horizontal winds were adjusted by a divergence minimization procedure. In the observation-only approach the user has to define several critical parameters, which can affect the results of the model runs significantly.

The chosen settings for the WegenerNet Feldbach region, based on extensive sensitivity tests, and the explanation of relevant model parameters are shown in Table 2. Details related to model settings and options

TABLE 1. Characteristics of meteorological stations with wind sensors (WN, WegenerNet station; ZAMG, National Meteorological Service station).

Station ID	Lat (E)	Lon (N)	Alt (m)	Wind sensor height (m)
WN 11	15°47′52.8″	46°58′52.9″	300	10
WN 32	15°54′13.1″	46°58′05.7″	322	10
WN 37	16°00′18.1″	46°58′00.2″	330	10
WN 44	15°51′01.3″	46°57′35.2″	288	55
WN 72	15°48′55.5″	46°55′54.6″	337	18
WN 74	15°51′08.5″	46°55′49.3″	394	10
WN 77	15°54′25.6″	46°55′58.7″	302	10
WN 82	16°00′12.1″	46°55′57.5″	276	10
WN 101	15°47′48.6″	46°54′17.0″	304	14
WN 132	15°51′10.1″	46°52′44.8″	295	10
WN 135	15°54′32.5″	46°52′50.4″	305	10
WN 139	15°59′02.2″	46°52′56.2″	307	10
ZAMG FB[a]	15°52′47.0″	46°56′56.0″	322	10
ZAMG BG[b]	15°54′13.0″	46°52′20.0″	269	10

[a] Feldbach.
[b] Bad Gleichenberg.

can be found in the CALMET user's manual (Scire et al. 1998). Adjustment of our application to other regions needs repetition of the sensitivity test in those regions, as is unavoidable with this type of empirical modeling.

Figure 3 shows the flowchart of our application, implemented in Python, that automatically creates wind fields with a time resolution of 30 min and a spatial gridding of 100 m × 100 m. This application reads the meteorological data for each time step from the WegenerNet database and creates the needed surface meteorological data files and the upper-air data files in a CALMET-compliant format. This preparatory processing step of the application includes the calculation of vector-mean values from the 5-min observational wind data. The vector mean of the observed wind speed v_o and wind direction ϕ_o is estimated by

$$v_o = \sqrt{v^2 + u^2},$$

and

$$\phi_o = \begin{cases} 0^\circ & \text{when } v \geq 0 \text{ and } u = 0 \\ 180^\circ & \text{when } v < 0 \text{ and } u = 0 \\ 90^\circ - \arctan\sqrt{\left(\frac{v}{u}\right)^2} & \text{when } v \geq 0 \text{ and } u > 0 \\ 90^\circ + \arctan\sqrt{\left(\frac{v}{u}\right)^2} & \text{when } v \leq 0 \text{ and } u > 0 \\ 270^\circ - \arctan\sqrt{\left(\frac{v}{u}\right)^2} & \text{when } v \leq 0 \text{ and } u < 0 \\ 270^\circ + \arctan\sqrt{\left(\frac{v}{u}\right)^2} & \text{when } v \geq 0 \text{ and } u < 0 \end{cases},$$

where the mean values of the north component v and the east component u are calculated from six observations

TABLE 2. Settings of critical area-specific model parameters in CALMET, used in this study.

Parameter	Value	Remarks
TERRAD (km)	2.5	Radius of influence of terrain features
RMAX1 (km)	5.0	Max radius of influence over land at the surface layer
RMAX2 (km)	5.0	Max radius of influence over land aloft
R1 (km)	0.6	Relative weighting of the first guess field and observations in the surface layer
R2 (km)	0.6	Relative weighting of the first guess field and observations in the layers aloft
IEXTRP (flag)	−4	Extrapolation of surface wind observations to upper layers with similarity theory (layer 1 data at upper-air stations are ignored)
ZFACE (m)	0, 20, 80	Cell face heights on the vertical grid (the vertical levels correspond to the midlevels, 10 and 50 m, of these layer boundaries ZFACE)
BIAS ($-1 \leq$ BIAS ≤ 1)	−1.0, 0.0, 0.0, 0.0	Layer-dependent biases modifying the weights of surface and upper-air stations (negative BIAS reduces the weight of upper-air stations, positive BIAS reduces the weight of surface stations)

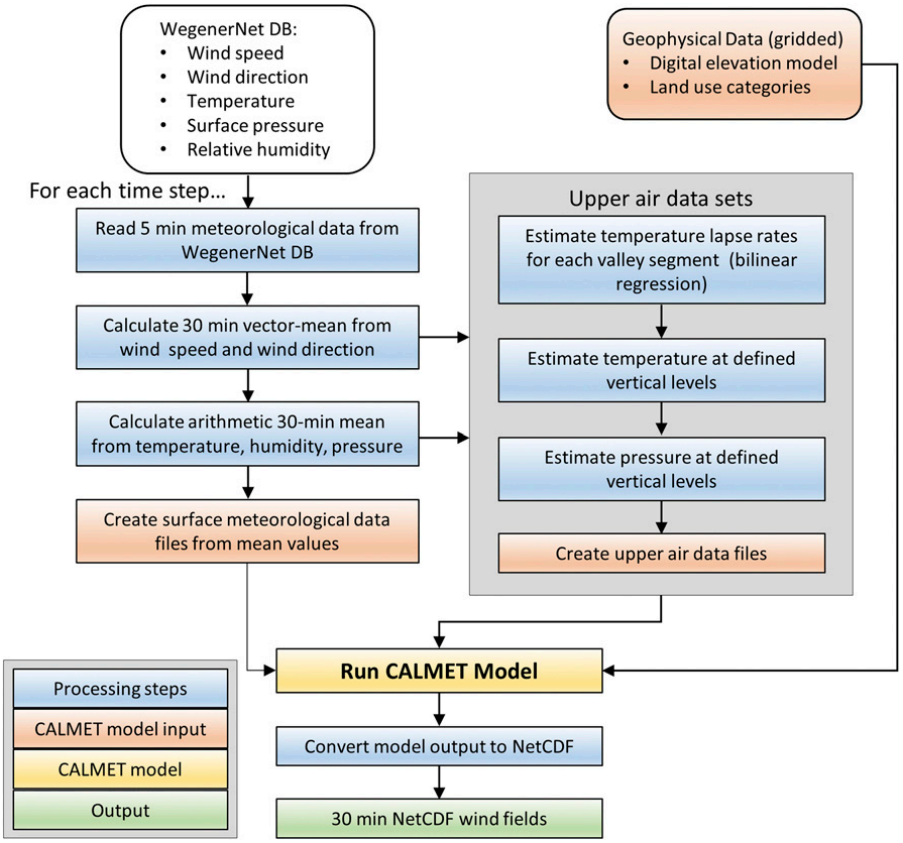

FIG. 3. Work flow for the automatic generation of high-resolution wind fields from the WegenerNet dataset.

for each CALMET time step ($N = 6$ for a temporal CALMET resolution of 30 min) by

$$v = \frac{1}{N}\sum_{i=1}^{N}(v_{o,i}\cos\phi_{o,i})$$

and

$$u = \frac{1}{N}\sum_{i=1}^{N}(v_{o,i}\sin\phi_{o,i}).$$

CALMET requires upper-air data consisting of vertical profiles of wind speed, wind direction, temperature, pressure, and elevation, usually obtained from radiosonde stations. The existing radiosonde station location in southeastern Austria is not within or nearby the study area and therefore is not representative of the WegenerNet Feldbach region. Because of the distance between radiosonde stations, and to keep the key operational input independent from data external to the WegenerNet, 12 upper-air data files are created automatically for each time step from the observed temperature, pressure, and wind measurements at the locations of the WegenerNet primary stations and the reference station.

For this purpose, temperature lapse rates are estimated based on a linear and bilinear least squares adjustment for each time step from the 153 WegenerNet temperature observations at different elevations in this hilly terrain. The bilinear fits that are composed of two lines are performed in 4-m increments of altitude z and are estimated by

$$T(z) = \begin{cases} \gamma_1 z + T_{\text{top}} & \text{when} \quad z < Z_{\text{top}} \\ \gamma_2(z - Z_{\text{top}}) + T_{\text{top}} & \text{when} \quad z \geq Z_{\text{top}} \end{cases},$$

where $T(z)$ is the temperature at altitude z. The temperature lapse rates are defined by γ_1 and γ_2, and the two lines intersect at the altitude Z_{top} with the corresponding temperature estimate T_{top}. For the linear fit we set Z_{top} to zero and fit just one line using the equation above. This linear fit is compared with the best-guess approximation of all bilinear fits, based on the performance parameter χ^2 (fit residuals). The regression parameters of the fit with the smallest χ^2 are adapted as a result for Z_{top}, T_{top}, γ_1, and γ_2. These estimates are then used to compute the temperature at the defined vertical levels (Table 2) for the WegenerNet primary stations and the reference station.

TABLE 3. Geophysical parameters based on CLC 2006 and used in this study.

Land-use type	Surface roughness length (m)	Albedo	Bowen ratio	Soil heat flux constant	Vegetative leaf area index
Discontinuous urban fabric	1.000	0.18	1.5	0.25	0.20
Agricultural land, unirrigated	0.250	0.15	1.0	0.15	3.00
Pastures	0.050	0.25	1.0	0.15	0.50
Forest land	1.000	0.10	1.0	0.15	7.00
Small body of water	0.001	0.10	0.0	1.00	0.00
Mineral extraction sites	0.050	0.30	1.0	0.15	0.05

The CALMET model uses a terrain-following vertical coordinate system, which means that its vertical levels represent the height above ground.

The upper-air pressure variables are produced for each level and time step by using the barometric law, starting from the surface pressure observed by the reference station. The air pressure P at the altitude z is calculated by

$$P(z) = \begin{cases} P_0\left(1 - \dfrac{\gamma_1 z}{T_0}\right)^{\overline{M}g/R\gamma_1} & \text{when} \quad z < Z_{\text{top}} \\ P_{z_{\text{top}}}\left[1 - \dfrac{\gamma_2(z - Z_{\text{top}})}{T_{\text{top}}}\right]^{\overline{M}g/R\gamma_2} & \text{when} \quad z \geq Z_{\text{top}} \end{cases},$$

where P_0 is the air pressure at sea level ($z = 0$ m), which is calculated from the observations of the reference station ($z = 302$ m) through the inverse of the equation above. The sea level temperature T_0 is computed for the WegenerNet primary stations and the reference station by the use of the regression parameters. Afterward, we use the equation to estimate the pressure $P(z)$ for the terrain-following vertical levels. The regression parameters Z_{top}, T_{top}, γ_1, and γ_2 are those determined by the least squares adjustment explained above. The gas constant R, mean molar mass of dry air $\overline{M}$, and the gravity acceleration g are taken to be constant with values, respectively, equal to 8.3145 J mol^{-1} K^{-1}, 0.028966 kg mol^{-1}, and 9.80795 m s^{-2}.

In the case of upper-air wind variables the measurements from the primary stations and the reference station are used for the 10-m vertical level. The upper-air wind variables for the highest defined vertical level (Table 2) are set to the observed values from the highest WegenerNet station with valid wind observations at the current time step in each file.

In addition, the CALMET model requires a preprocessed gridded geophysical data file consisting of terrain elevations and land-use categories (CALMET input data files; orange fields in Fig. 3). As our digital elevation model (DEM), a dataset derived from airborne laser scanning point clouds (provided online by gis.steiermark.at) is used, illustrated by the elevations in Fig. 1b. Before putting the data into the CALMET model, the original spatial resolution of 10 m is resampled and averaged to 100 m. Figure 2a shows the land-use map of the study area based on the Corine Land Cover 2006 dataset (CLC 2006; see EEA 2007) converted into a CALMET-compliant format. The definitions of the CLC land-use categories differ from the CALMET classes. In the entire CLC dataset the third and most detailed level contains 44 classes, while the default classification scheme of the CALMET model distinguishes up to 14 land-use types only (Oleniacz and Rzeszutek 2014). We therefore reclassified 13 CLC 2006 land-use categories of the study area into six CALMET-compliant classes, and assigned the appropriate CALMET grid code to each category. For each of these land-use categories the parameters shown in Table 3 are applied to the CALMET geophysical dataset.

The model performance is evaluated using periods with mainly two types of wind events: the thermally induced wind events and the strong wind events, which are representative of this study area. We chose the periods August 2008 and March 2013. In August 2008 the study area was mainly controlled by autochthonous weather conditions, which mainly led to thermally induced wind systems. Such weather conditions are characterized by low wind speeds, cloudless skies, low relative humidity, and increased radiation fluxes between the earth surface and the atmosphere (Prettenthaler et al. 2010). The synoptic influences are small, and the wind field is dominated by small-scale temperature and pressure gradients. In March 2013 several episodes of strong wind occurred. The wind speed was classified as *weak* ($0.5\,\text{m s}^{-1} \leq v_o \leq 2.5\,\text{m s}^{-1}$) or *strong* ($v_o > 2.5\,\text{m s}^{-1}$), to be able to estimate the performance for different conditions. Wind speeds $< 0.5\,\text{m s}^{-1}$ were classified as *calm*. In August 2008, 56% of the observed wind speeds from the WegenerNet stations were classified as weak and 8% as strong (36% being calm). In March 2013 as well 56% were weak but 19% were strong (25% being calm). The limit of $2.5\,\text{m s}^{-1}$ was chosen because it is the typical maximum wind speed in the

TABLE 4. Statistical performance parameters used for the evaluation of the wind field modeling results.

Parameter	Equation	Remarks
Bias	$B = \frac{1}{N}\sum_{i=1}^{N}(v_{m,i} - v_{o,i})$	v_m, modeled wind speed; v_o, observed wind speed
Std dev	$\mathrm{SD}_O = \sqrt{\frac{\sum_{i=1}^{N}(v_{o,i} - \overline{v_o})}{N}}$	SD_O, standard deviation of observed wind speed; v_o, observed wind speed; $\overline{v_o}$, mean observed wind speed
Root-mean-square error	$\mathrm{RMSE} = \sqrt{\frac{1}{N}\sum_{i=1}^{N}(v_{m,i} - v_{o,i})^2}$	v_m, modeled wind speed; v_o, observed wind speed
Correlation coef	$R = \frac{1}{(N-1)}\sum_{i=1}^{N}\left(\frac{v_{m,i} - \overline{v_m}}{\sigma_m}\right)\left(\frac{v_o - \overline{v_o}}{\sigma_o}\right)$	v_m, modeled wind speed; $\overline{v_m}$, mean modeled wind speed; v_o, observed wind speed; $\overline{v_o}$, mean observed wind speed; σ_m, std dev of modeled wind speed; σ_o, std dev of observed wind speed
Index of agreement	$\mathrm{IOA} = \begin{cases} 1.0 - \frac{\sum_{i=1}^{N}\lvert v_{m,i} - v_{o,i}\rvert}{c\sum_{i=1}^{N}\lvert v_{o,i} - \overline{v_o}\rvert}, & \text{when } \sum_{i=1}^{N}\lvert v_{m,i} - v_{o,i}\rvert \le c\lvert v_{o,i} - \overline{v_o}\rvert \\ \frac{c\sum_{i=1}^{N}\lvert v_{o,i} - \overline{v_o}\rvert}{\sum_{i=1}^{N}\lvert v_{m,i} - v_{o,i}\rvert} - 1, & \text{when } \sum_{i=1}^{N}\lvert v_{m,i} - v_{o,i}\rvert > \lvert v_{o,i} - \overline{v_o}\rvert \end{cases}$	v_m, modeled wind speed; v_o, observed wind speed; $\overline{v_o}$, mean observed wind speed; c, factor set to 2 (Willmott et al. 2012)
Mean absolute error of wind direction	$\mathrm{MAE}_{\mathrm{dir}} = \frac{1}{N}\sum_{i=1}^{N}\{\arccos[\cos(\phi_{m,i} - \phi_{o,i})]\}$	ϕ_m, modeled wind direction; ϕ_o, observed wind direction

study area during autochthonous days, caused by Alpine pumping (Lugauer and Winkler 2005).

For statistically evaluating the modeling skill, we use the statistical performance parameters summarized in Table 4. As an evaluation method, we use the leave-one-out cross validation for the WegenerNet and ZAMG stations with wind data as listed in Table 5 (more details in section 4 below). This evaluation methodology means that observations at one wind station are removed from the model input and generated wind fields are evaluated against the wind data from this station.

Measurements from the Feldbach and Bad Gleichenberg ZAMG stations are only used as reference for evaluation and not as model input. We compared the modeled outputs with the reference station datasets for each time step of the validation period. For each reference station location, the statistical performance parameters (Table 4) are calculated by comparing the nearest-neighbor gridpoint values to the observations at the corresponding location.

4. Results

We show typical examples of modeled wind fields for thermally driven circulations on 10 August 2008 (Fig. 4a) and strong wind speeds on 15 March 2013 (Fig. 4b), both at a height of 10 m. The top panel on the left-hand side of Fig. 4 illustrates nighttime winds with a down-valley direction caused by temperature and pressure gradients on a local scale. The middle-left panel of Fig. 4 shows the thermally induced wind field in the afternoon, caused by the Alpine pumping. This typical thermally induced regional wind of the study area is called Antirandgebirgswind and arises usually in the afternoon as a southerly wind (Wakonigg 1978). This Antirandgebirgswind, with maximum near-surface wind speeds of around 2.5 m s^{-1}, is a characteristic regional flow between the bordering mountains of the eastern Alps (Koralpe, Gleinalpe, Fischbacher Alps, and the mountainous region to the north of Graz) and the so-called Riedelland, which is the hilly country region in southeastern Styria comprising the study area and part of the Alpine Foreland (Wakonigg 1978). The bottom-left panel of Fig. 4 shows the early evening situation, where valley winds arise, generally from an up-valley direction.

Figure 4b displays a strong all-day northerly wind from 15 March 2013, with maximum 30-min wind speeds of around 8 m s^{-1} at 1000 UTC (1100 LT) (middle-right panel). It can be seen that in the area

TABLE 5. Statistical performance measures calculated for representative meteorological stations for weak and strong wind speeds (top half for August 2008; bottom half for March 2013). See Table 4 for more information on the calculations for the performance parameters. The results for ZAMG FB and WN 132 are illustrated as examples in Figs. 6–9.

	Weak wind speed: $0.5\,m\,s^{-1} \le v_o \le 2.5\,m\,s^{-1}$						Strong wind speed: $v_o > 2.5\,m\,s^{-1}$					
Station ID	B ($m\,s^{-1}$)	SD_O ($m\,s^{-1}$)	RMSE ($m\,s^{-1}$)	R (1/1)	IOA (1/1)	MAE_{dir} (°)	B ($m\,s^{-1}$)	SD_O ($m\,s^{-1}$)	RMSE ($m\,s^{-1}$)	R (1/1)	IOA (1/1)	MAE_{dir} (°)
Aug 2008												
WN 11	−0.07	0.59	0.43	0.81	0.70	25	−0.57	0.72	1.17	0.32	0.09	10
WN 32	−0.04	0.68	0.40	0.85	0.82	17	−0.59	1.03	1.18	0.42	0.17	14
WN 132	−0.03	0.66	0.40	0.84	0.79	23	−0.28	0.39	0.70	0.46	0.20	16
WN 135	−0.36	0.76	0.57	0.81	0.71	33	−1.24	0.66	1.44	0.44	−0.21	22
ZAMG FB	−0.20	0.73	0.43	0.85	0.77	14	−1.02	0.82	0.43	0.75	0.16	13
ZAMG BG	0.06	0.64	0.37	0.87	0.82	14	−0.28	0.58	0.63	0.71	0.46	14
Mean value	−0.11	0.68	0.43	0.84	0.77	21	−0.66	0.70	0.93	0.52	0.15	15
Mar 2013												
WN 11	−0.04	0.61	0.49	0.75	0.67	32	−0.81	1.43	1.35	0.66	0.57	11
WN 32	−0.05	0.76	0.48	0.83	0.78	01	−0.70	1.51	1.38	0.65	0.49	04
WN 132	0.02	0.65	0.56	0.78	0.65	30	−0.37	0.66	1.04	0.46	0.17	17
WN 135	−0.15	0.78	0.67	0.68	0.68	36	−0.78	0.99	1.32	0.59	0.31	35
ZAMG FB	−0.17	0.70	0.43	0.83	0.74	22	−0.90	1.28	1.14	0.84	0.55	07
ZAMG BG	0.01	0.68	0.66	0.67	0.58	32	−1.43	1.24	1.77	0.71	0.25	30
Mean value	−0.06	0.70	0.55	0.76	0.68	26	−0.83	1.19	1.33	0.65	0.39	17

around WegenerNet station 135 the wind direction is forced into a NW-to-W component, resulting from the observations at this station. The influence of observations from a given station, weighted by the influence radius parameter (Table 2) in step 2 of CALMET interpolation scheme (as explained in section 3 above) becomes obvious in this particular example.

The enlarged sections in Fig. 5 with an area of about 3 km × 3 km around the "Steinberg" hill display wind fields (top two rows) and vertical cross sections (bottom row) for different atmospheric stratification (for Fig. 5a the same time slice as in Fig. 4a, bottom left). In Fig. 5a the wind is again dominated by the thermally driven Antirandgebirgswind under unstable conditions, as diagnosed by CALMET based on a small value of an internal stability factor (ratio of Brunt–Väisälä frequency to wind speed) and a negative Monin–Obukhov length. Higher vertical wind speeds can be observed, especially at heights of 50 m above ground. In CALMET such terrain-forced vertical wind speeds are estimated based on a stability-dependent decay function weighted by the stability factor (Scire et al. 1998). The horizontal direction of flow remains mainly unchanged and is not modified across the local terrain. The temperature contour of the vertical cross section (Fig. 5, bottom left) shows temperature lapse rates with maximum temperatures of about 21°C in the Raab valley north of the Steinberg hill and minimum temperatures of about 20.3°C at the top of the hill.

In winter, temperature inversions occur frequently in relation to high pressure weather conditions with weak wind speeds in the study area (Fig. 5b). In Fig. 5, the top and middle panels on the right-hand side indicate the modification of the wind field in a direction around the Steinberg hill with generally low horizontal and vertical wind speeds. The temperature contour of the vertical cross section (Fig. 5, bottom right) illustrates the strong temperature inversion with maximum temperatures of about 5°C on top of the hill and minimum temperatures in the Raab valley north of the Steinberg hill of about −2°C.

Periods with rapidly changing weather conditions, such as fast-developing thunderstorms, cannot be resolved in detail by the CALMET diagnostic model because of its limited time resolution of not shorter than 30 min.

Figures 6 and 7 illustrate the model performance for the Feldbach ZAMG station and WegenerNet station 132 as typical examples of the performance of a single station. The ZAMG station is located at 330-m height near the town of Feldbach in the Raab valley, the main valley of the study area (Fig. 1b). WegenerNet station 132 is located near the Poppendorfer stream at a height of 295 m. The environment of the latter station is characterized by low-density residential areas that influence the representativity of wind observations for the 1-km scale somewhat. In the scatterplots shown, the 30-min vector mean values from the observed wind speeds are compared with the modeled 30-min nearest-neighbor grid points.

For the Feldbach station, the comparison shows a high degree of similarity between modeled and observed

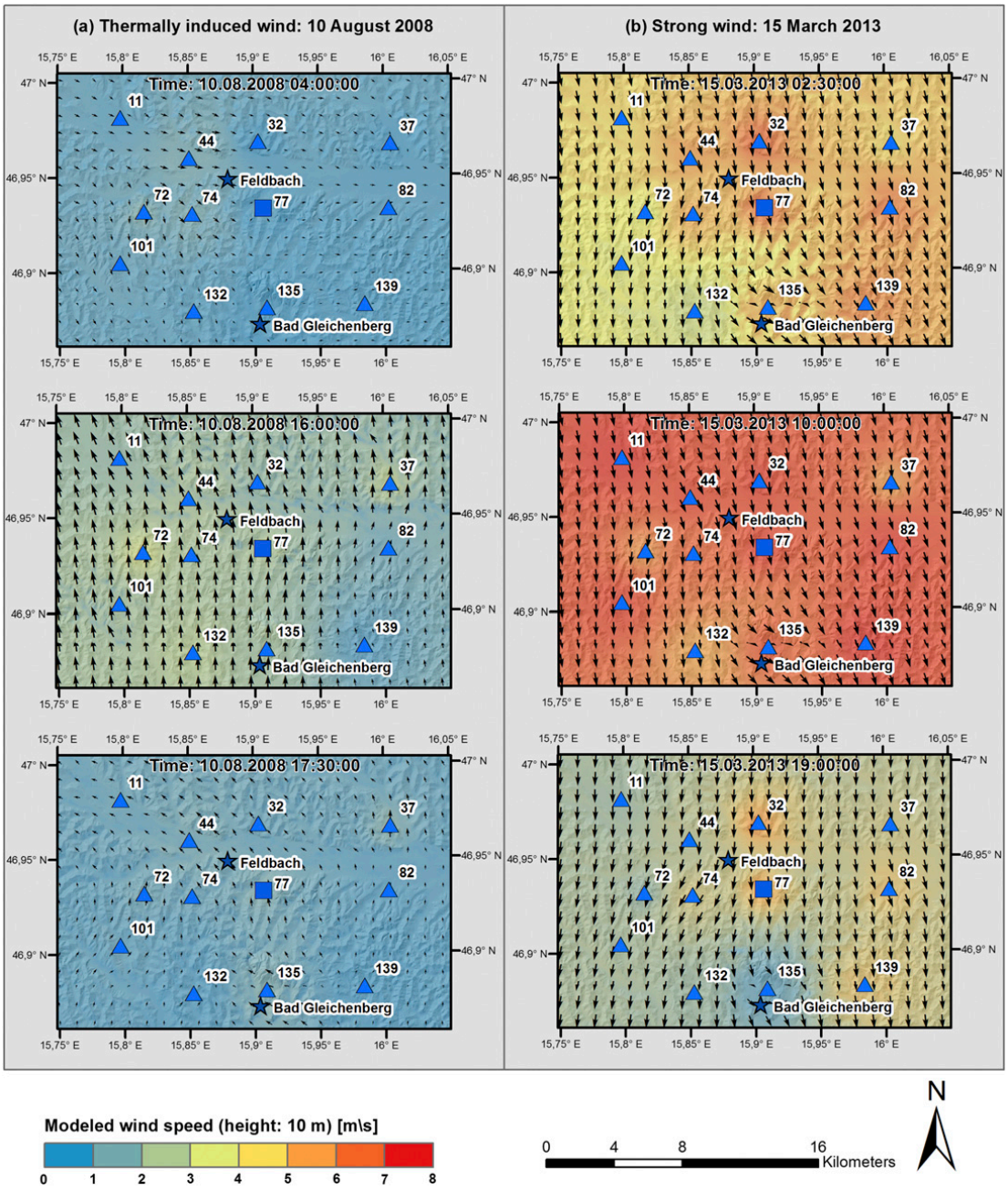

FIG. 4. Modeled wind fields typical of the study area. (a) Thermally induced wind fields (10 Aug 2008) and (b) strong region-scale winds (15 Mar 2013). Times shown are UTC (corresponding to LT − 2 h on 10 Aug 2008 and LT − 1 h on 15 Mar 2013).

wind speeds for both weak and strong conditions, with correlation coefficients ranging from 0.75 to 0.85 (Fig. 6). This indicates good representativeness for the 1-km scale. Because of the influence of local terrain on WegenerNet station 132, the results are slightly worse for this station, especially for strong wind speeds (Fig. 7). For example, the R value in August 2008 for strong conditions is 0.46 (Fig. 7a) compared with the Feldbach station with a value of 0.75 (Fig. 6a); the corresponding R value in March 2013 is also 0.46 (Fig. 7b) compared with a value of 0.84 for the Feldbach station (Fig. 6b). The mean absolute error (MAE_{dir}) of the wind direction is for both stations higher in the case of weak wind speeds, as one might expect from the challenging effects that weaker wind speeds have on wind direction estimations.

Figure 8 shows the relative frequency of wind directions from the model compared with the observed wind directions for the ZAMG Feldbach station, again for the same periods and wind speed classes. It can be seen that the distribution of wind directions is similar

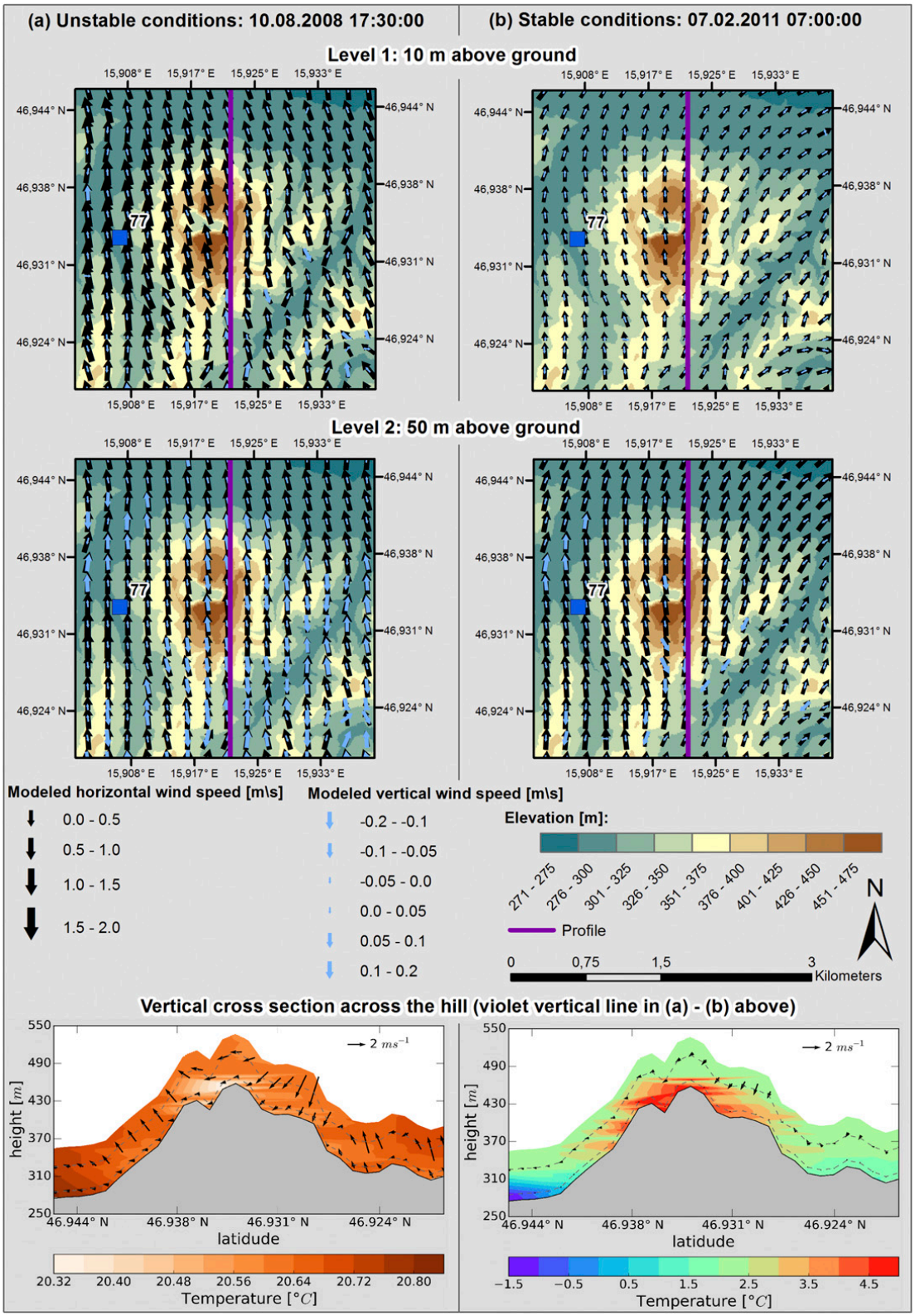

FIG. 5. Enlarged view of the subregion around the Steinberg hill east of reference station 77. (a) Thermally induced wind fields under unstable conditions (10 Aug 2008) and (b) weak winds under stable conditions (15 Mar 2013); horizontal (v, black) and vertical (w, blue) wind components at (top) 10 and (middle) 50 m above ground are indicated. (bottom) North-to-south vertical cross sections of $v - w$ wind vectors over the hill at the 10- and 50-m levels as well as temperature contours (color shading). Times shown are UTC.

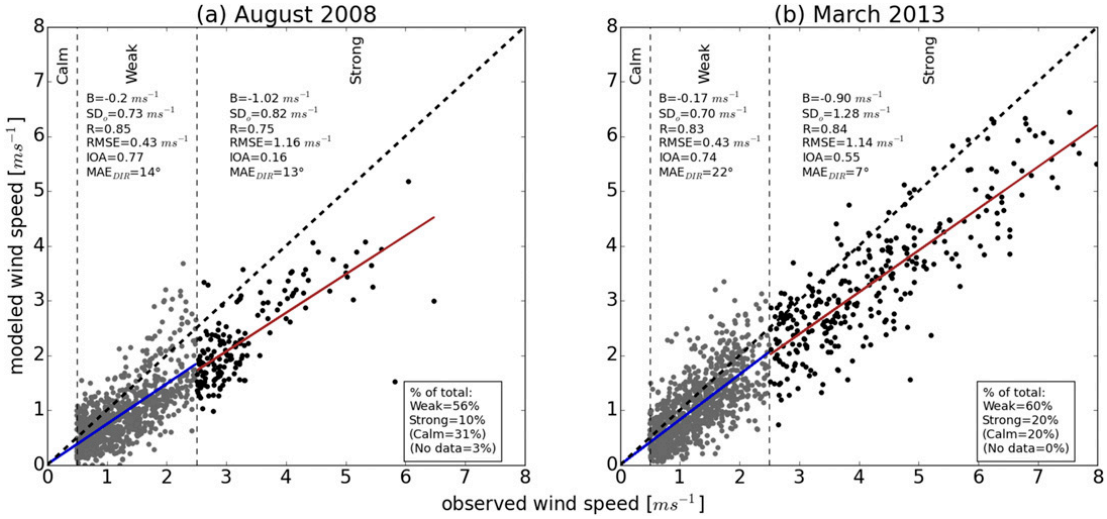

FIG. 6. Modeled vs observed wind speeds for the ZAMG station at Feldbach: (a) August 2008 and (b) March 2013 for weak ($0.5\,\mathrm{m\,s^{-1}} < v_o \leq 2.5\,\mathrm{m\,s^{-1}}$; gray dots) and strong ($v_o > 2.5\,\mathrm{m\,s^{-1}}$; black dots) wind speeds.

among the observations and modeled values, which is a satisfying result, indicating the applicability of the wind fields. The largest difference between the modeled and observed wind directions for this station can be seen in Fig. 8c in August 2008 for strong wind speeds, with a shift between the SSE and S sectors. In this case the model calculates about 40% of the wind directions for the SSE sector, while the observations show about 40% in the S sector. This shift can be explained by the influence the environment of the station has on the wind field.

Figure 9 shows wind roses divided by wind speed categories for the Feldbach ZAMG station. Again, similar patterns between observed and modeled values for weak conditions are visible. For both periods, the model properly calculates values below $2.5\,\mathrm{m\,s^{-1}}$ (Figs. 9a,b). In Fig. 9c, the shift between observed and modeled values from the S to the SSE sector for strong wind speeds can be seen in detail; for example, the 40% model wind directions in the SSE sector all have weak values below $2.5\,\mathrm{m\,s^{-1}}$, while the observations only show around 15% in this sector, with wind speeds that are all strong up to $3.5\,\mathrm{m\,s^{-1}}$. In March 2013 the strong wind case (Fig. 9) aligns very well, with the observations inclined to somewhat stronger southward wind speeds than the modeled ones.

Figures 10 and 11 show the analogous results for WegenerNet station 132. The distribution of the observed wind directions from station 132 has narrower wind corridors for weak wind speeds compared with the modeled

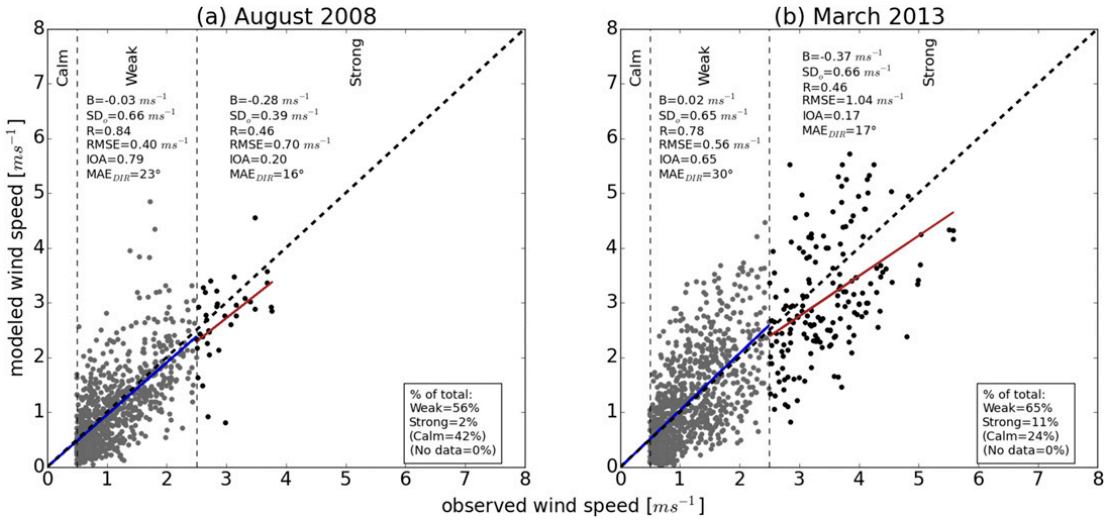

FIG. 7. As in Fig. 6, but for WegenerNet station 132.

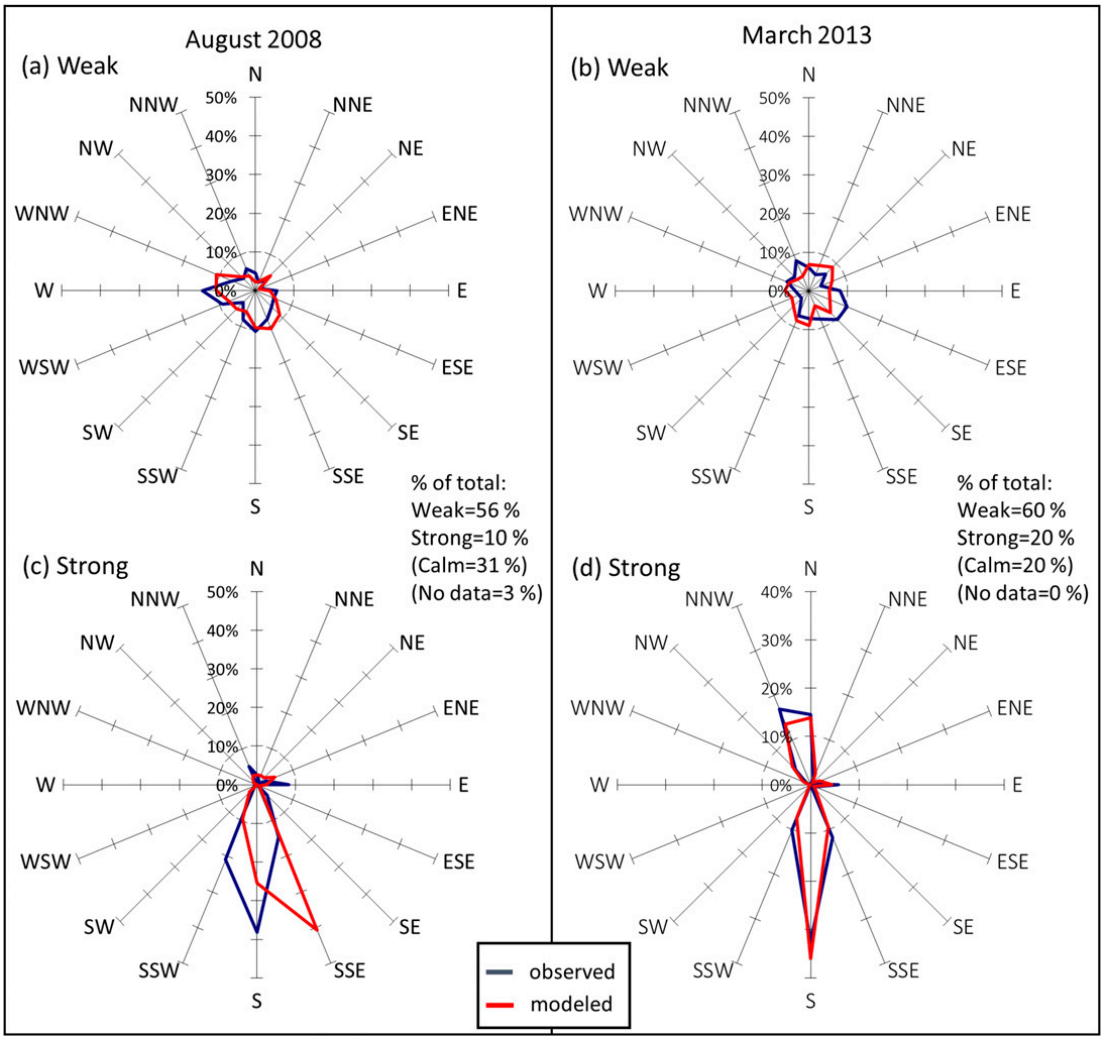

FIG. 8. Relative frequency of wind directions for observed (blue line) and modeled (red line) values for the ZAMG Feldbach station: (left) August 2008 and (right) March 2013 for (a),(b) weak ($0.5\,\mathrm{m\,s^{-1}} < v_o \leq 2.5\,\mathrm{m\,s^{-1}}$) and (c),(d) strong ($v_o > 2.5\,\mathrm{m\,s^{-1}}$) wind speeds.

wind directions (Figs. 10a,b). From Figs. 11a and 11b the same results become obvious: the corridor of the observed wind directions with weak wind speeds is narrower, with prevailing wind directions from the NNW to the N or the S sector. For the strong wind speed category the pattern of the modeled wind directions is more similar to the observed wind directions (Figs. 10c,d and 11c,d), with the modeled wind speeds somewhat underestimated (Figs. 11c,d). Because of the quite good accordance between modeled and observed wind parameters for WegenerNet station 132, the overall reasonableness of the wind field results is also underscored by this station.

Table 5 summarizes the statistical results for all of meteorological stations that were used for the performance evaluation. In fact for internal extensive evaluation, all stations were used, but the ones examined in detail and summarized in Table 5 are well representative. The results of the relative statistical parameters applied to the vector mean of the wind speed [R and index of agreement (IOA)] generally show better values for the weak wind speed class than for the strong wind speed class. On the other hand, the statistical measure applied to evaluate wind directions ($\mathrm{MAE_{dir}}$) shows better results for strong wind speeds compared to weak wind speeds. In general, the bias B is somewhat negative, except for the Bad Gleichenberg ZAMG station and for WegenerNet station 132 in March 2013 during weak conditions.

The resulting RMSE values range from 0.37 to $0.67\,\mathrm{m\,s^{-1}}$ for weak wind speeds and from 0.43 to $1.77\,\mathrm{m\,s^{-1}}$ for strong wind speeds. For the weak wind speed class the correlation coefficient is higher than 0.75 for all stations expect for the Bad Gleichenberg

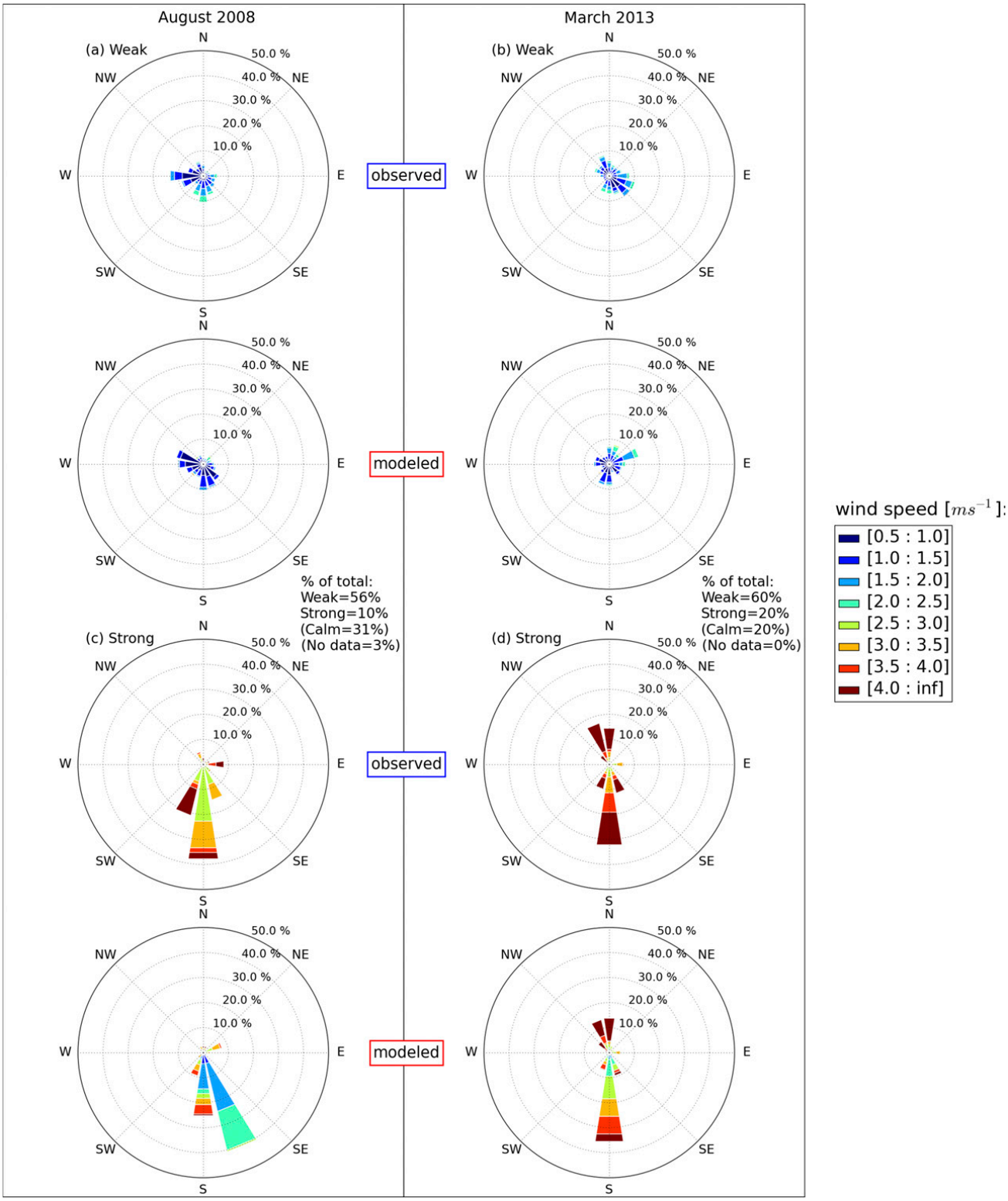

FIG. 9. Relative frequency of wind directions based on wind speed categories for (first and third rows) observed and (second and fourth rows) modeled values for the ZAMG Feldbach station: (left) August 2008 and (right) March 2013 for (a),(b) weak ($0.5\,\mathrm{m\,s^{-1}} < v_o \leq 2.5\,\mathrm{m\,s^{-1}}$) and (c),(d) strong ($v_o > 2.5\,\mathrm{m\,s^{-1}}$) wind speeds.

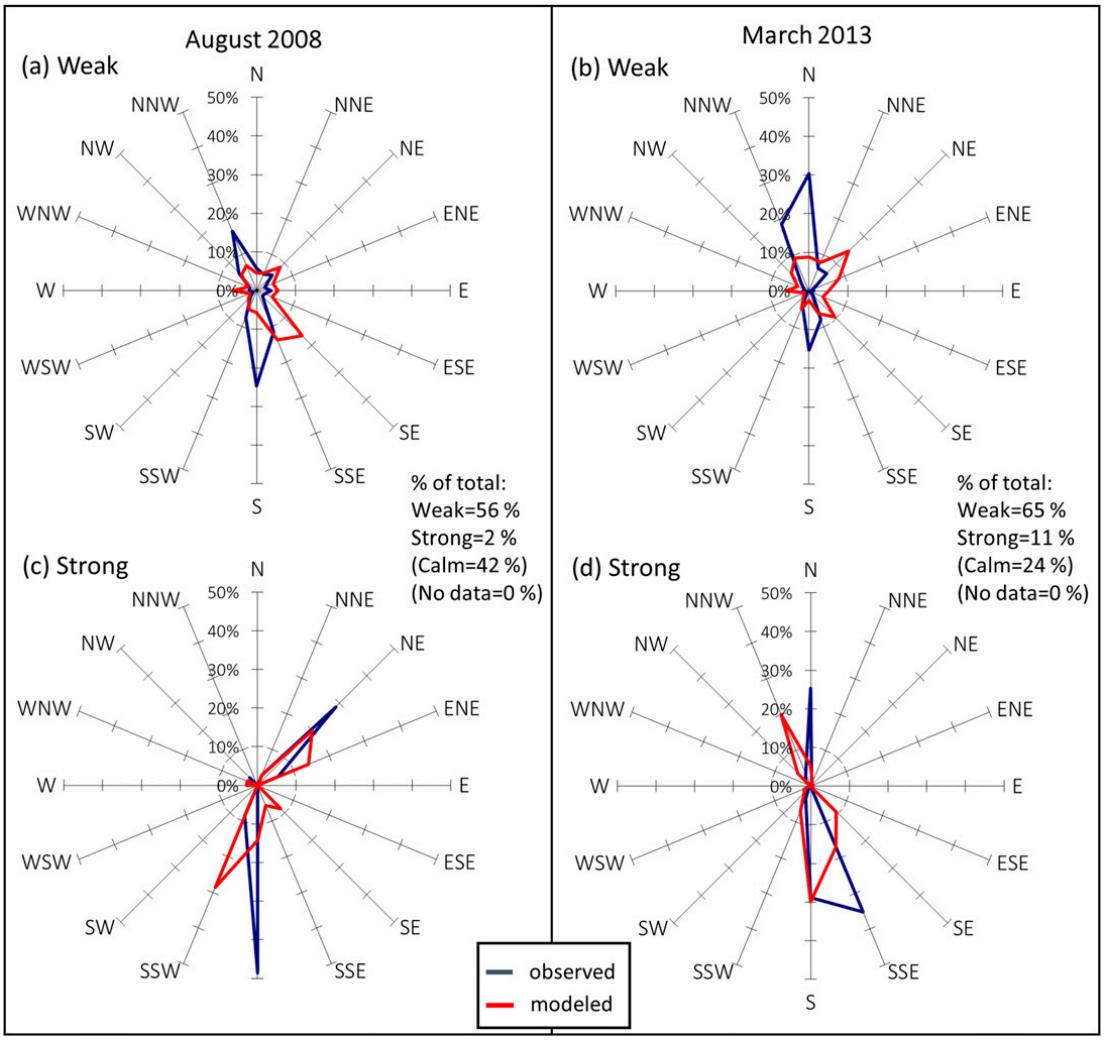

FIG. 10. As in Fig. 8, but for WegenerNet station 132.

ZAMG station and WegenerNet station 135. For the strong wind speed class the correlation coefficient is generally worse, especially for WegenerNet station 11.

Regarding the IOA, we note that in this study the IOA redefined by Willmott et al. (2012) is used with a lower limit of −1 and an upper limit of +1 with values approaching +1 representing a better degree of model performance. For example, an IOA of 0.5 means that the sum of the difference magnitudes between modeled and observed values is one-half of the sum of the observed deviation magnitudes. Conversely, an IOA of −0.5 implies that the sum of the difference magnitudes is twice the sum of the observed deviation magnitudes. Values of IOA near −1.0 mean either that the model-estimated deviations about $\overline{v_o}$ are poor estimates of the observed deviations or that there is in fact little observed variability (Willmott et al. 2012). The higher values of the IOA for weak wind speeds compared with strong wind speeds therefore indicate that the sum of the difference magnitudes compared with the observed deviation magnitudes is lower for weak wind speeds (somewhat better performance) than for strong wind speeds.

5. Conclusions and prospects

This work has introduced an operational weather diagnostics application for the automatic generation of high-resolution wind fields from the dense WegenerNet Feldbach region network of meteorological stations operated by the Wegener Center in southeastern Styria, Austria. The wind fields are computed in near–real time and stored in the WegenerNet data archives, available at 30-min temporal resolution and with a spatial resolution of 100 m × 100 m. The core part of the new application is the freely available empirical model CALMET, which we employ to simulate the wind fields based on the WegenerNet meteorological observations,

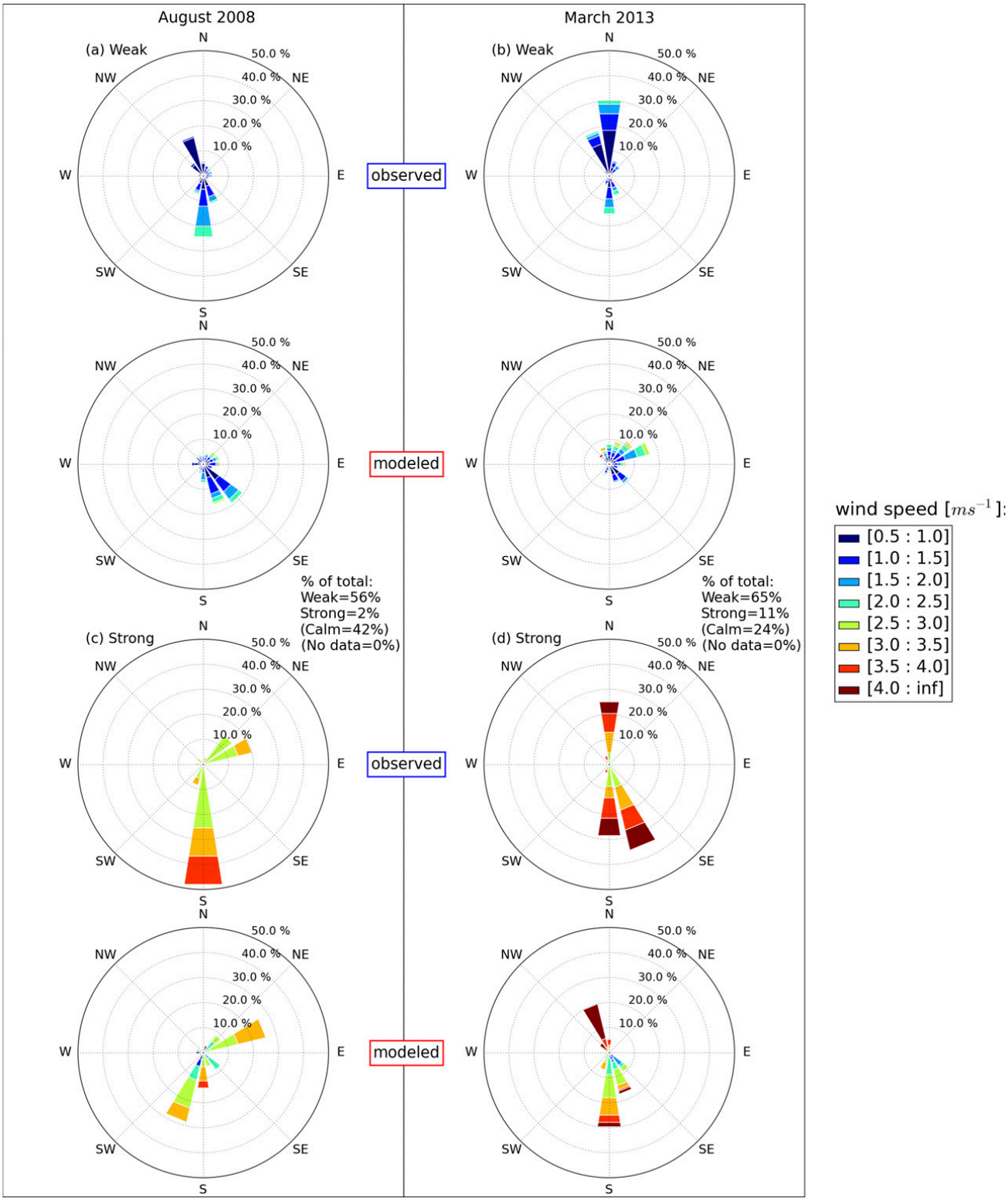

FIG. 11. As in Fig. 9, but for WegenerNet station 132.

a digital elevation model, and land-use categories. The generated half-hourly high-resolution wind fields are also averaged to further hourly and daily weather data products as well as monthly, seasonal, and annual climate data products. These data products can be used for investigating weather and climate variability on a local scale, as well as for the evaluation of convection-permitting climate models.

We evaluated the results by identifying representative monthly periods that included both frequently occurring thermally induced weak wind speeds (August 2008) and strong wind speeds (March 2013). Thanks to the dense station network, the statistics show reasonably good results for both periods and confirm the utility of the new wind fields. The statistical performance measures applied to the vector-mean wind speed show better results for weak wind speeds than for strong wind speeds. The results related to wind direction are found to be more accurate for strong wind speeds than for weak wind speeds. The application has been running operationally in the Feldbach region since mid-2016 and the earlier data since 2007 have been reprocessed.

Ongoing future work deals with applying the developed application to automatically produce wind fields for a second study area, the WegenerNet Johnsbachtal (Fuchsberger et al. 2016; Strasser et al. 2013), located to the north of Styria in an Alpine mountainous region. This second study area is characterized through a region of complex terrain with high relief energy. The original CALMET model calculates the energy balance without considering topographic shading through relief. This is a challenge in complex terrain since such shading significantly affects the energy balance and, subsequently, the wind field. Furthermore, surface temperature fields are produced by a simple inverse distance interpolation without taking the vertical temperature gradient into account.

To improve the modeling of these physical effects, for the second study area we implemented algorithms developed by Bellasio et al. (2005) into CALMET (version 6.5.0). These algorithms take into account the topographic effects for the calculation of solar radiation as well as the terrain elevation for estimating the temperature field close to the surface; detailed information on the implemented algorithms can be found in Bellasio et al. (2005). We will use the original and the enhanced CALMET model to identify and adapt the best method of generating wind fields for the WegenerNet Johnsbachtal network.

The wind fields produced based on the enhanced CALMET version will as well be cross validated for the WegenerNet Feldbach region. As a scientific application, we will then use the empirical wind fields for the evaluation of nonhydrostatic climate model simulations in the two WegenerNet regions for selected challenging weather situations. Beyond the two regions the new application can also serve, after appropriate tuning, as a valuable tool for high-resolution wind field modeling for other networks.

Acknowledgments. The authors thank Roberto Bellasio (Enviroware), Italy, for providing the modified CALMET 5.2 code, including algorithms to account for topographic shading effects and vertical temperature gradients. We also thank Heimo Truhetz (Wegener Center, University of Graz) for valuable discussions about scientific issues and the model setup, and three anonymous reviewers for valuable comments that helped to significantly improve the paper. The CALMET 6.5.0 model code was available online (www.src.com/calpuff/). CORINE Land Cover data for the study area (www.eea.europa.eu), digital elevation model data (www.gis.steiermark.at), and WegenerNet Feldbach region data (www.wegenernet.org) were available online. WegenerNet funding is provided by the Austrian Ministry for Science and Research, the University of Graz, the state of Styria (which also included European Union regional development funds), and the city of Graz; detailed information can be found online (www.wegcenter.at/wegenernet).

REFERENCES

Abdel-Aal, R., M. Elhadidy, and S. Shaahid, 2009: Modeling and forecasting the mean hourly wind speed time series using GMDH-based abductive networks. *Renewable Energy*, **34**, 1686–1699, doi:10.1016/j.renene.2009.01.001.

Awan, N. K., H. Truhetz, and A. Gobiet, 2011: Parameterization-induced error characteristics of MM5 and WRF operated in climate mode over the Alpine region: An ensemble-based analysis. *J. Climate*, **24**, 3107–3123, doi:10.1175/2011JCLI3674.1.

Bellasio, R., G. Maffeis, J. S. Scire, M. G. Longoni, R. Bianconi, and N. Quaranta, 2005: Algorithms to account for topographic shading effects and surface temperature dependence on terrain elevation in diagnostic meteorological models. *Bound.-Layer Meteor.*, **114**, 595–614, doi:10.1007/s10546-004-1670-6.

Brunner, L., G. C. Hegerl, and A. K. Steiner, 2017: Connecting atmospheric blocking to European temperature extremes in spring. *J. Climate*, **30**, 585–594, doi:10.1175/JCLI-D-16-0518.1.

Cox, R. M., J. Sontowski, and C. M. Dougherty, 2005: An evaluation of three diagnostic wind models (CALMET, MCSCIPUF, and SWIFT) with wind data from the Dipole Pride 26 field experiments. *Meteor. Appl.*, **12**, 329–341, doi:10.1017/S1350482705001908.

EEA, 2007: CLC2006 technical guidelines. European Environment Agency Tech. Rep., 66 pp. [Available online at http://www.eea.europa.eu/publications/technical_report_2007_17.]

Fuchsberger, J., G. Kirchengast, T. Kabas, and C. Bichler, 2016: Wegenernet climate station networks: Overview and examples. *LTER-Austria Conf. 2016*, Vienna, Austria, Austrian Long-Term Ecosystem Research Network. [Available online at https://wegenernet.org/downloads/poster_LTER_2016_wegnet_v2.pdf.]

Haylock, M. R., N. Hofstra, A. M. G. Klein Tank, E. J. Klok, P. D. Jones, and M. New, 2008: A European daily high-resolution gridded data set of surface temperature and precipitation for 1950–2006. *J. Geophys. Res*, **113**, D20119, doi:10.1029/2008JD010201.

Hohenegger, C., P. Brockhaus, and C. Schär, 2008: Towards climate simulations at cloud-resolving scales. *Meteor. Z.*, **17**, 383–394, doi:10.1127/0941-2948/2008/0303.

Jancewicz, K., 2014: Remote sensing data in wind velocity field modelling: A case study from the Sudetes (SW Poland). *Pure Appl. Geophys.*, **171**, 941–964, doi:10.1007/s00024-013-0698-2.

Kabas, T., 2012: WegenerNet climate station network region Feldbach: Experimental setup and high resolution data for weather and climate research (in German). Wegener Center Scientific Rep. 47-2012, 177 pp. [Available online at http://wegcwww.uni-graz.at/publ/wegcreports/2012/WCV-WissBer-No47-TKabas-Jan2012.pdf.]

——, U. Foelsche, and G. Kirchengast, 2011: Seasonal and annual trends of temperature and precipitation within 1951/1971-2007 in south-eastern Styria, Austria. *Meteor. Z.*, **20**, 277–289, doi:10.1127/0941-2948/2011/0233.

Kirchengast, G., T. Kabas, A. Leuprecht, C. Bichler, and H. Truhetz, 2014: Wegenernet: A pioneering high-resolution network for monitoring weather and climate. *Bull. Amer. Meteor. Soc.*, **95**, 227–242, doi:10.1175/BAMS-D-11-00161.1.

Klok, E. J., and A. M. G. Klein Tank, 2009: Updated and extended European dataset of daily climate observations. *Int. J. Climatol.*, **29**, 1182–1191, doi:10.1002/joc.1779.

Lugauer, M., and P. Winkler, 2005: Thermal circulation in south Bavaria climatology and synoptic aspects. *Meteor. Z.*, **14**, 15–30, doi:10.1127/0941-2948/2005/0014-0015.

Morales, L., F. Lang, and C. Mattar, 2012: Mesoscale wind speed simulation using CALMET model and reanalysis information: An application to wind potential. *Renewable Energy*, **48**, 57–71, doi:10.1016/j.renene.2012.04.048.

O, S., U. Foelsche, G. Kirchengast, and J. Fuchsberger, 2017: Validation and correction of rainfall data from the WegenerNet high density network in southeast Austria. *J. Hydrol.*, doi:10.1016/j.jhydrol.2016.11.049, in press.

Oleniacz, R., and M. Rzeszutek, 2014: Determination of optimal spatial databases for the area of Poland to the calculation of air pollutant dispersion using the CALMET/CALPUFF model. *Geomatics Environ. Eng.*, **8** (2), 57–69, doi:10.7494/geom.2014.8.2.57.

Osborn, T. J., and M. Hulme, 1998: Evaluation of the European daily precipitation characteristics from the Atmospheric Model Intercomparison Project. *Int. J. Climatol.*, **18**, 505–522, doi:10.1002/(SICI)1097-0088(199804)18:5<505::AID-JOC263>3.0.CO;2-7.

Prein, A. F., 2013: Added value of convection resolving climate simulations. Wegener Center Scientific Rep. 53-2013, 164 pp. [Available online at http://wegcwww.uni-graz.at/publ/wegcreports/2013/WCV-SciRep-No53-APrein-Jul2013.pdf.]

——, G. J. Holland, R. M. Rasmussen, J. Done, K. Ikeda, M. P. Clark, and C. H. Liu, 2013: Importance of regional climate model grid spacing for the simulation of heavy precipitation in the Colorado headwaters. *J. Climate*, **26**, 4848–4857, doi:10.1175/JCLI-D-12-00727.1.

Prettenthaler, F., A. Podesser, and H. Pilger, 2010: *Climate Atlas Styria, Period 1971–2000: An Application-Oriented Climatology* (in German). Vol. 4. Oesterreichischen Akademie der Wissenschaften, 358 pp.

Scire, J. S., F. R. Robe, M. E. Fernau, and R. J. Yamartino, 1998: A user's guide for the CALMET meteorological model (version 5). Earth Tech, Inc., 332 pp. [Available online at http://www.src.com/calpuff/download/CALMET_UsersGuide.pdf.]

Sfetsos, A., 2002: A novel approach for the forecasting of mean hourly wind speed time series. *Renewable Energy*, **27**, 163–174, doi:10.1016/S0960-1481(01)00193-8.

Strasser, U., T. Marke, O. Sass, S. Birk, and G. Winkler, 2013: John's creek valley: A mountainous catchment for long-term interdisciplinary human-environment system research in upper Styria (Austria). *Environ. Earth Sci.*, **69**, 695–705, doi:10.1007/s12665-013-2318-y.

Suklitsch, M., A. Gobiet, H. Truhetz, N. K. Awan, H. Göttel, and D. Jacob, 2011: Error characteristics of high resolution regional climate models over the Alpine area. *Climate Dyn.*, **37**, 377–390, doi:10.1007/s00382-010-0848-5.

Truhetz, H., 2010: High resolution wind field modelling over complex topography: Analysis and future scenarios. Wegener Center Scientific Rep. 32-2010, 170 pp. [Available online at http://wegcwww.uni-graz.at/publ/wegcreports/2010/WCV-SciRep-No32-HTruhetz-Apr2010.pdf.]

——, A. Gobiet, and G. Kirchengast, 2007: Evaluation of a dynamic-diagnostic modelling approach to generate highly resolved wind fields in the alpine region. *Meteor. Z.*, **16**, 191–201, doi:10.1127/0941-2948/2007/0192.

Wakonigg, H., 1978: *Weather and Climate in Styria* (in German). Technische Universitaet Graz, 473 pp.

Wang, W., W. J. Shaw, T. E. Seiple, J. P. Rishel, and Y. Xie, 2008: An evaluation of a diagnostic wind model (CALMET). *J. Appl. Meteor. Climatol.*, **47**, 1739–1756, doi:10.1175/2007JAMC1602.1.

Willmott, C. J., S. M. Robeson, and K. Matsuura, 2012: A refined index of model performance. *Int. J. Climatol.*, **32**, 2088–2094, doi:10.1002/joc.2419.

7 Empirical high-resolution wind field and gust model in mountainous and hilly terrain based on the dense WegenerNet station networks

The second publication outlines the extensions and modifications which have been implemented into the WPG. Furthermore, the application of the WPG to the WegenerNet JBT and evaluation results for two months including mainly representative weather conditions for this second study area are discussed. In addition, this publication presents evaluation results of seasonal climate data investigations from the WegenerNet JBT in comparison to the WegenerNet FBR. Table 7.1 introduces the author activities and responsibilities of this publication.

Table 7.1: Author contributions of the second peer-reviewed publication (Schlager et al. 2018).

Title:	Empirical high-resolution wind field and gust model in mountainous and hilly terrain based on the dense WegenerNet station networks
Reference:	Schlager, C., G. Kirchengast, and J. Fuchsberger (2018). "Empirical high-resolution wind field and gust model in mountainous and hilly terrain based on the dense WegenerNet station networks". *Atmos. Meas. Tech.* 11.10, pp. 5607–5627. doi: 10.5194/amt-11-5607-2018
Author contributions:	
Christoph Schlager:[a,b]	Collected the data, performed the analyses and modeling, created the figures and wrote the first draft of the manuscript
Gottfried Kirchengast:[a,b]	Provided guidance and advice on all aspects of the study and significantly contributed to the text
Jürgen Fuchsberger:[a,b]	Provided guidance on technical aspects of the WegenerNet networks and its data characteristics and contributed to the text

[a] Wegener Center for Climate and Global Change (WEGC), University of Graz, Graz, Austria.
[b] Institute for Geophysics, Astrophysics, and Meteorology/Institute of Physics, University of Graz, Graz, Austria.

Atmos. Meas. Tech., 11, 5607–5627, 2018
https://doi.org/10.5194/amt-11-5607-2018

Atmospheric Measurement Techniques
Open Access
EGU

Empirical high-resolution wind field and gust model in mountainous and hilly terrain based on the dense WegenerNet station networks

Christoph Schlager, Gottfried Kirchengast, and Juergen Fuchsberger

Wegener Center for Climate and Global Change (WEGC), and Institute for Geophysics, Astrophysics, and Meteorology/Institute of Physics, University of Graz, Graz, Austria

Correspondence: Christoph Schlager (christoph.schlager@uni-graz.at)

Received: 28 January 2018 – Discussion started: 2 July 2018
Revised: 10 September 2018 – Accepted: 13 September 2018 – Published: 15 October 2018

Abstract. A weather diagnostic application for automatic generation of gridded wind fields in near-real-time, recently developed by the authors Schlager et al. (2017), is applied to the WegenerNet Johnsbachtal (JBT) meteorological station network. This station network contains 11 meteorological stations at elevations from about 600 to 2200 m in a mountainous region in the north of Styria, Austria. The application generates, based on meteorological observations with a temporal resolution of 10 min from the WegenerNet JBT, mean wind and wind gust fields at 10 and 50 m height levels with a high spatial resolution of 100 m × 100 m and a temporal resolution of 30 min. These wind field products are automatically stored to the WegenerNet data archives, which also include long-term averaged weather and climate datasets from post-processing. The main purpose of these empirically modeled products is the evaluation of convection-permitting dynamical climate models as well as investigating weather and climate variability on a local scale. The application's performance is evaluated against the observations from meteorological stations for representative weather conditions, for a month including mainly thermally induced wind events (July 2014) and a month with frequently occurring strong wind events (December 2013). The overall statistical agreement, estimated for the vector-mean wind speed, shows a reasonably good modeling performance. Due to the spatially more homogeneous wind speeds and directions for strong wind events in this mountainous region, the results show somewhat better performance for these events. The difference between modeled and observed wind directions depends on the station location, where locations along mountain slopes are particularly challenging. Furthermore, the seasonal statistical agreement was investigated from 5-year climate data of the WegenerNet JBT in comparison to 9-year climate data from the high-density WegenerNet meteorological station network Feldbach Region (FBR) analyzed by Schlager et al. (2017). In general, the 5-year statistical evaluation for the JBT indicates similar performance as the shorter-term evaluations of the two representative months. Because of the denser WegenerNet FBR network, the statistical results show better performance for this station network. The application can now serve as a valuable tool for intercomparison with, and evaluation of, wind fields from high-resolution dynamical climate models in both the WegenerNet FBR and JBT regions.

1 Introduction

Advances in computer sciences and the growing power of computers enable highly resolved model outputs from regional climate models (RCMs) with horizontal resolutions at a scale of 1 km. At this resolution RCMs provide more realistic simulations, especially for regions with complex terrain, and allow the investigation of weather and climate in small subregions (Awan et al., 2011; Suklitsch et al., 2011; Prein et al., 2013, 2015; Leutwyler et al., 2016; Kendon et al., 2017).

To evaluate RCMs and to improve the performance of such models, meteorological observations and particularly gridded datasets in correspondingly high spatial and temporal resolutions are needed. RCMs generally represent area-averaged processes rather than on a point-scale (Osborn and Hulme, 1998; Prein et al., 2015). Therefore, gridded fields of meteorological data are the most appropriate evaluation

datasets, with each grid value being a best estimate average of the grid cell observations (Haylock et al., 2008; Haiden et al., 2011; Hiebl and Frei, 2016).

For investigating weather and climate on a local scale as well as evaluating RCMs, the Wegener Center (WEGC) at the University of Graz acquires and automatically processes data from two station networks: the WegenerNet Feldbach Region (FBR) and the WegenerNet Johnsbachtal (JBT). The WegenerNet FBR is located in southeastern Styria, Austria and covers a dense grid of more than 150 meteorological stations within an area of about 22 km × 16 km (Kirchengast et al., 2014). The terrain of the FBR is hilly and characterized by small differences in altitude, and the region is quite sensitive to climate change (Kabas et al., 2011; Kabas, 2012; Hohmann et al., 2018). It exhibits rich weather variability, especially including strong convective activity and severe weather in summer (Kirchengast et al., 2014; Kann et al., 2015; O et al., 2017, 2018). Recently, Schlager et al. (2017) also analyzed wind fields in this region.

The focus of this study is on the WegenerNet JBT, a station network consisting of 11 meteorological stations, located in a mountainous region in upper Styria, which is characterized by a very complex terrain (Fig. 1). The WegenerNet JBT has been realized through an interdisciplinary research cooperation and the stations are operated by the WEGC and several different partner organizations (indicated in Fig. 1). Details related to the cooperation, partnerships and first results can be found in Strasser et al. (2013).

All observations from the two WegenerNet regions are integrated into the WegenerNet Processing System (WPS), a system to control and manage meteorological station data (Kirchengast et al., 2014). This WPS consists of four subsystems: The Command Receive Archiving System transfers raw data via General Packet Radio Service (GPRS) wireless transmission to the WegenerNet database in Graz, the Quality Control System checks the data quality, the Data Product Generator (DPG) produces regular station time series and gridded fields of weather and climate products, and the Visualization and Information System offers the data to users via the WegenerNet data portal (http://www.wegenernet.org, last access: 3 October 2018).

The DPG-produced weather and climate products are stored to the WegenerNet data archives and have included for many years the gridded fields of the variables temperature, precipitation and relative humidity for the WegenerNet FBR. These fields are generated based on a spatial interpolation of the station observations and provided with a latency of about 1–2 h. Temperature lapse rates estimated from the observational datasets at the many different station altitudes are included in the generation of temperature fields over the hilly terrain. Technically, for temperature and relative humidity, the fields are constructed by an inverse-distance weighted interpolation and for the precipitation the inverse-distance squared weighted interpolation is used. Details related to the subsystems of the WPS can be found in Kirchengast et al. (2014) and Kabas (2012).

Furthermore, since the recent work of Schlager et al. (2017), the DPG computes spatially distributed wind fields for the WegenerNet FBR. Due to the dependence of wind on many different conditions, including surface properties such as topography and surface roughness, we use a newly developed application (named Wind Product Generator or WPG, developed in Python) to determine the gridded field of wind parameters (Abdel-Aal et al., 2009; Sfetsos, 2002; Schlager et al., 2017).

The WPG uses the freely available empirical California Meteorological Model (CALMET) as core tool and generates wind fields in near-real-time. The CALMET model reconstructs 3D wind fields (we focus on the 10 and 50 m height levels) based on meteorological observations, terrain elevations and information about land usage. Before its routine use for the WegenerNet FBR, the WPG has been evaluated for a month including mainly thermally induced events and another month with frequently occurring strong wind events; the statistics showed good results for these periods. A detailed description of the WPG application, and the statistical results for the WegenerNet FBR, can be found in Schlager et al. (2017).

The key goal of this study is the implementation, and evaluation of, the WPG to automatically produce high-resolution wind fields in near-real-time also for the second study area, the challenging WegenerNet JBT region with its terrain from about 700 to 2300 m and less wind stations than for the WegenerNet FBR. The requirement for our WPG application is to provide the JBT wind fields also with a spatial resolution of 100 m × 100 m and a time resolution of 30 min to the WegenerNet data archives. An essential goal is the evaluation of these wind fields for periods with representative weather conditions and also the estimation of wind gust fields. Furthermore, the WPG‘s performance shall be estimated first-time also for seasonal climate-averaged data for the WegenerNet JBT in comparison to the WegenerNet FBR region.

The paper is structured as follows. Section 2 provides a description of the study area, the WegenerNet JBT region with its meteorological stations. Section 3 presents the methodology for the empirical wind field modeling, where first the characteristics of the CALMET model and the extensions integrated to the WPG (Schlager et al., 2017) for the automated production of the wind fields are explained, in particular the inclusion of a few auxiliary pseudo-stations (Fig. 1). Second, the estimation method for the gust fields and a description of atmospheric weather conditions during the model evaluation periods and of the evaluation methods is introduced here. Section 4 describes the results of the wind field modeling for the selected evaluation periods, July 2014 and December 2013, for the WegenerNet JBT as well as the results of the seasonal climate datasets from the WegenerNet JBT compared to those of the WegenerNet FBR. Finally, Sect. 5

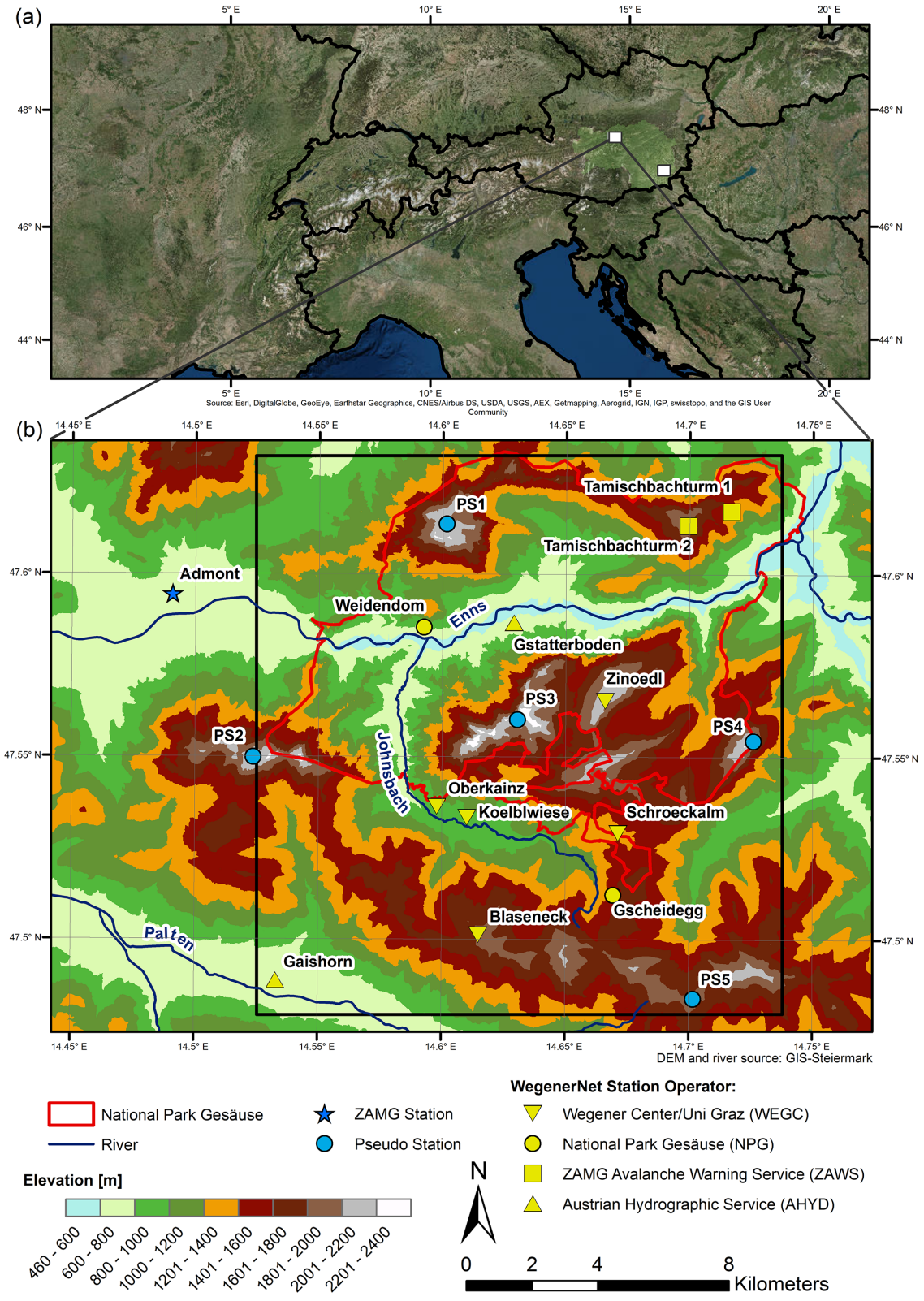

Figure 1. **(a)** Location of the study area WegenerNet Johnsbachtal (white rectangle, enlarged in **b**) in the north of Styria, Austria. The WegenerNet Feldbach Region in the Alpine forelands of southeastern Styria, Austria, is also indicated for reference in the easternmost part of the European Alpine region (details in Schlager et al., 2017; Fig. 1 therein). **(b)** Map of the WegenerNet Johnsbachtal region (black rectangle) with its meteorological stations, including the selected mountaintop pseudo-stations, with the legend explaining map characteristics and station operators.

provides the conclusions as well as prospects for the next steps of follow-on work.

2 Study area and WegenerNet data

The study area WegenerNet JBT (Fig. 1), named after the Johnsbach river basin, is located in the Ennstaler Alps, an eastern Alpine region in the north of Styria, Austria, and overlays with the National Park Gesäuse. The area is surrounded by the Gesäuse Mountains in the north, east and west and by the Eisenerzer Alps in the south. The terrain is characterized by large differences in elevation, ranging from below 700 m in the valleys to over 2300 m at the highest summits (Strasser et al., 2013). The highest peak is the Hochtor, with an elevation of 2369 m. The landscape is dominated by alpine rock formations and sparsely vegetated areas (barren land), forests and range land (Fig. 2a).

The climate is Alpine with annual mean temperatures of around 8 °C at lower elevations and below 0 °C at higher elevations and with an annual precipitation of about 1500 to 1800 mm from the valley to the summit regions (Wakonigg, 1978; Prettenthaler et al., 2010). The summer-day temperature field illustrated in Fig. 2b, produced by a modified version of CALMET (Schlager et al., 2017), shows the distinct decrease in temperatures from lower to higher elevations. We implemented algorithms developed by Bellasio et al. (2005) as part of this modified CALMET version to account for topographic shading and height dependency in surface temperatures (more details in Sect. 3). The wind field in the study area is characterized by thermally induced local flows and influenced from larger scales mainly by westerly-flow synoptic weather conditions.

The WegenerNet JBT comprises 11 irregularly distributed meteorological stations within its area of about 16 km × 17 km. The station with the highest altitude was installed in summer 2009 and is located on the summit of the Zinoedl at a height of 2191 m. A second summit station was installed in 2011 on top of the Blaseneck at a height of 1969 m (Strasser et al., 2013).

All stations are equipped with a diversity of meteorological sensors. The observed variables wind speed (v), wind direction (ϕ), air temperature (T), air pressure (p) and relative humidity (RH) are continuously recorded at a 10 min sampling rate and used as input for the WPG. Table 1 summarizes the technical characteristics of the WegenerNet JBT stations including the station operators, wind sensor heights and observed variables for each station (including the ones used). Due to a topography strongly influencing the local wind fields at the Weidendom and the Tamischbachturm 1 stations, the observations of the wind variables from these two stations are not used as input.

The observations of the Wegener JBT stations are partly available since 2010, and partly since 2007 (Table 1, first column). For this study, wind fields have been calculated within the period 2012–2017, and ongoing near-real-time data are to be provided to the users with a maximum delay of 2 h.

3 Methods and evaluation periods

3.1 Advanced CALMET model

The core tool of the operational WPG is the CALMET model (Scire et al., 1998). Based on the settings in the CALMET control file, a user has three different options for the use of the meteorological information as input data: in the no-observations approach, CALMET uses data from numerical prognostic models as input data, the hybrid approach combines data from numerical models and meteorological observations, and the observations-only approach solely uses meteorological observations. We use the observations-only approach for the WPG, to ensure genuinely empirical wind fields and to keep the key operational input independent from data external to the WegenerNet (Schlager et al., 2017; Scire et al., 1998). We consider this also the best-possible choice for later intercomparison to, and evaluation of, dynamical climate model fields.

The CALMET model computes the wind fields in a two-step approach. The first step (step 1) includes the adjustment of an initial-guess wind field for kinematic effects of terrain, slope flows and terrain blocking effects. In the observations-only approach the initial-guess wind field is produced by an interpolation of observational data.

In a second step (step 2), the observational data are introduced again and blended to the step 1 wind field by an inverse distance weighting interpolation to produce the final step 2 wind field. Observations are excluded from this interpolation method if the distance from a station location to a particular grid point is greater than a user defined radius of influence. Furthermore, relative weighting parameters are used to weight the observed wind variables to the previously computed step 1 wind field (Table 2). The procedure ensures divergence-free (mass-conserving) wind vector fields, i.e., provides physically consistent fields under assumption of incompressible flow.

Based on extensive sensitivity tests, we determined the settings for the WegenerNet JBT shown in Table 2. Comparing these to the settings of Schlager et al. (2017), Table 2 therein, for the WegenerNet FBR, one can see that we in particular found it beneficial to increase the influence of terrain features and the first-guess file in the surface layer. A detailed description related to model parameters, settings and options can be found in the CALMET Manual (Scire et al., 1998).

In the original CALMET model, the energy balance is calculated without considering topographic shading through terrain. Furthermore, height dependency of surface temperatures is not taken into account and the temperature fields are produced by a simple interpolation of point-specific observations. Especially in complex terrain like in the Wegen-

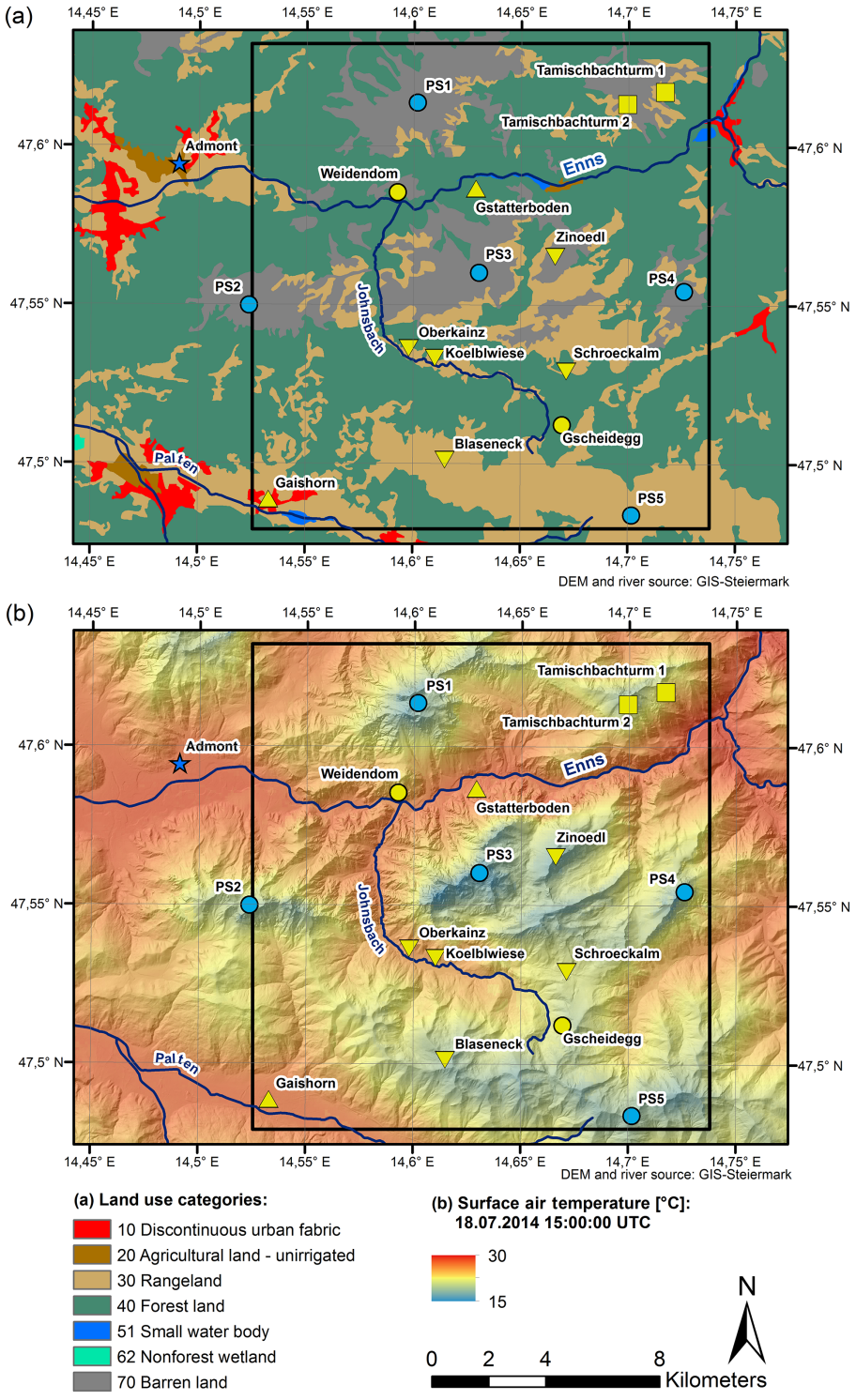

Figure 2. **(a)** Land cover and use of the WegenerNet Johnsbachtal region (black rectangle) based on the CORINE Land Cover 2006 raster version. **(b)** Example temperature field over the region during a summer day in July (18 July 2014; 15:00 UTC).

erNet JBT, such shading, vertical temperature gradients and the vegetation cover significantly affect the energy balance and subsequently the wind field.

To improve the modeling of these physical effects in this challenging region, we improved an advanced model by implementing algorithms developed by Bellasio et al. (2005).

Table 1. Characteristics of meteorological stations of the WegenerNet Johnsbachtal (JBT).

Station name, ID (start[a])	Station abbreviation	Operator	Lat (E)	Lon (N)	Alt [m]	Wind sensor height [m]	Recorded variables[b]
Oberkainz, 501 (2010)	OBK	WEGC	47°32′11.0"	14°35′52.8"	920	14	v, ϕ, v_g, ϕ_g, T, RH, P, Q_g, Q_r, s_d, s_{we}
Koelblwiese, 502 (2013)	KOE	WEGC	47°31′54.0"	14°36′37.0"	860	3	v, ϕ, v_g, ϕ_g, T, RH, P, p, Q_g, Q_r, Q_n
Schroeckalm, 503 (2010)	SCH	WEGC	47°31′45.2"	14°40′16.8"	1344	10	v, ϕ, v_g, ϕ_g, T, RH, P, p, Q_g, Q_n, ρ_s
Blaseneck, 504 (2010)	BLA	WEGC	47°29′57.7"	14°37′07.9"	1969	6	v, ϕ, v_g, ϕ_g, T, RH, Q_g, Q_n
Zinoedl, 505 (2009)	ZIN	WEGC	47°33′55.4"	14°39′57.8"	2191	6	v, ϕ, v_g, ϕ_g, T, RH, Q_g, Q_n
Weidendom, 506 (2006)	WEI	NPG	47°34′51.0"	14°35′29.3"	590	2	v, T, h, P, Q_g, wl
Gscheidegg, 507 (2008)	GSC	NPG	47°30′52.0"	14°40′28.2"	1690	6	v, ϕ, v_g, ϕ_g, T, RH, p , Q_g, s_d, ρ_s
Tamischb. 1, 508 (2008)	TA1	ZAWS	47°37′02.4"	14°43′01.2"	1431	7	v, ϕ, v_g, ϕ_g, T, RH, Q_g, T_s, s_d, T_{sn}
Tamischb. 2, 509 (2008)	TA2	ZAWS	47°36′48.4"	14°41′58.2"	1952	5	v, ϕ, v_g, ϕ_g, T, RH
Gstatterboden, 510 (2007)	GST	AHYD	47°35′29.0"	14°37′44.0"	580	–	P
Gaishorn, 511 (2007)	GAI	AHYD	47°35′29.0"	14°37′44.0"	720	–	P

[a] start year of time series (earliest year in WegenerNet archive is 2007) [b] v wind speed, ϕ wind direction, v_g peak gust, ϕ_g peak gust direction, T air temperature, RH relative humidity, P precipitation, p air pressure, s_d snow depth, s_{we} snow water equivalent, ρ_s snow density, Q_g global radiation, Q_r reflected radiation, Q_n net radiation, T_s surface temperature, T_{sn} snow temperature and wl water level

Table 2. Settings of critical area-specific model parameters in CALMET, used in this study for the WegenerNet JBT.

Parameter	Value	Remarks
TERRAD [km]	5.0	Radius of influence of terrain features
RMAX1 [km]	5.0	Maximum radius of influence over land in the surface layer
RMAX2 [km]	5.0	Maximum radius of influence over land aloft
R1 [km]	1.1	Relative weighting of the first guess field and observations in the surface layer
R2 [km]	0.6	Relative weighting of the first guess field and observations in the layers aloft
IEXTRP (flag)	−4	Extrapolate surface wind observations to upper layers with similarity theory (layer 1 data at upper-air stations are ignored)
ZFACE [m]	0, 20, 80	Cell face heights in vertical grid (the vertical levels correspond to the mid-levels, 10 m and 50 m, of those layer boundaries)
BIAS ($-1 \leq$ BIAS ≤ 1)	0.0, 0.0, 0.0, 0.0	Layer-dependent biases modifying the weights of surface and upper-air stations (Negative BIAS reduces the weight of upper-air stations, positive BIAS reduces the weight of surface stations)

These algorithms empirically take into account the topographic shading based on terrain heights, topography slope and aspect and the position of the sun for the estimation of solar radiation. In addition, temperature fields are modeled based on vertical temperature gradients, estimated from the meteorological stations located at different altitudes, and the influence of the vegetation cover is accounted for, based on the leaf area index (LAI) obtained from a geophysical dataset (Table 3). Detailed information related to these algorithms can be found in Bellasio et al. (2005).

The WPG runs this advanced CALMET model based on a surface meteorological data file, upper-air data files and a geophysical data file. In a predecessor step, the WPG automatically generates these meteorological data sets from the station observations and auxiliary geophysical information stored in the WegenerNet database. Detailed information re-

Table 3. Geophysical parameters based on the CORINE Land Cover (CLC) 2006 dataset, used in this study for the WegenerNet JBT.

Land use type	Surface roughness length [m]	Albedo	Bowen ratio	Soil heat flux constant	Vegetative leaf area index
Discontinuous urban fabric	1.000	0.18	1.5	0.25	0.20
Agricultural land – unirrigated	0.250	0.15	1.0	0.15	3.00
Rangeland	0.050	0.25	1.0	0.15	0.50
Forest land	1.000	0.10	1.0	0.15	7.00
Small water body	0.001	0.10	0.0	1.00	0.00
Non-forest wetland	0.020	0.10	0.10	0.25	1.00
Barren land	0.050	0.30	1.0	0.15	0.05

lated to the WPG, including all processing steps, can be found in Schlager et al. (2017).

The geophysical dataset consists of terrain elevations and land use categories and was created in a preparatory step. In this study we used a DEM derived from airborne laser scanning point clouds (provided online by http://gis.steiermark.at, last access: 3 October 2018), illustrated by the elevations scale in Fig. 1b. The original spatial resolution of 10 m was resampled and averaged to 50 (DEM50), 100 (DEM100), and 200 m (DEM200). In order to check the influence of the spatial resolution on the modeling performance, the model was tested with the different spatial resolutions. These sensitivity tests showed very small differences between wind field results modeled based on DEM50 and DEM100, while somewhat higher differences (from smoothing effects) were found when using DEM200. We hence selected the DEM100 as the most adequate and computationally efficient resolution and the 100 m × 100 m gridding for this study, which also matches the resolution of the land cover dataset discussed next.

Furthermore, the land use categories for the study were determined based on the CORINE Land Cover 2006 dataset (CLC 2006) (EEA, 2007). The definition and the maximum number of the land use categories of the CLC dataset differs from the classification scheme of the CALMET model. The entire CLC dataset of the third and most detailed level contains 44 different classes, while the CALMET classification scheme only distinguishes up to 14 land use types (Oleniacz and Rzeszutek, 2014). Therefore, we reclassified the 17 CLC 2006 land use categories found in the study area into seven compliant CALMET classes (Fig. 2a); the corresponding parameters summarized in Table 3 were then used as the CALMET geophysical dataset.

The observations of the three highest stations, Zinoedl, Blaseneck and Tamischbachturm 2 (Table 1), are used to create vertical profiles of wind speed, wind direction, temperature, pressure, and elevation, stored in upper-air datasets. A detailed explanation of how the creation of upper-air datasets works can be found in Schlager et al. (2017).

3.2 Auxiliary pseudo-stations for upper-air data

Based on finding a systematic underestimation of wind speed in summit regions without any station, we extended the WPG with a user option that enables the introduction of upper-air pseudo-stations in the modeling domain. These user-defined pseudo-stations are included to raise wind speed at higher altitudes. For the WegenerNet JBT we defined five pseudo-stations upon extensive sensitivity studies testing various setups, located at the unobserved summit regions (Table 4, Figs. 1 and 2). The magnitude of wind speed of a pseudo-station (v_p) is estimated for the highest defined vertical height level (z_max), which corresponds to the highest ZFACE level (Table 2; 80 m). The estimation is based on a linear interpolation between neighbor station altitudes, except for pseudo-station 5, which is located at somewhat lower altitude than its neighborhood stations. The wind speed is hence calculated by a slight downward extrapolation for this latter station. This magnitude is calculated by

$$v_\mathrm{p}(z_\mathrm{max}) = v_\mathrm{n1}(z_\mathrm{max}) + \left[\frac{v_\mathrm{n2}(z_\mathrm{max}) - v_\mathrm{n1}(z_\mathrm{max})}{z_\mathrm{n2} - z_\mathrm{n1}}\right] (z_\mathrm{p} - z_\mathrm{n1}), \quad (1)$$

where z_p is the altitude of the pseudo-station and z_n1 and z_n2 indicates the altitudes of the defined neighbor stations with real wind observations (Table 4, rightmost column).

The magnitude of the wind speeds $v_{\mathrm{n}1,2}(z_\mathrm{max})$ at the highest height level of the neighbor stations used in Eq. (1) are calculated by a logarithmic wind profile given as

$$v_{\mathrm{n}1,2}(z_\mathrm{max}) = v_{\mathrm{n}1,2}(z_{s1,2})\frac{\ln(z_\mathrm{max}/z_0)}{\ln(z_{s1,2}/z_0)}, \quad (2)$$

where $v_{\mathrm{n}1,2}(z_{s1,2})$ are the wind speeds at the neighbor stations observed at the sensor heights $z_{s1,2}$ (typically 5–10 m above surface), and z_0 is the surface roughness length at the locations of the corresponding neighbor stations (up to 1 m).

Table 4. Characteristics of upper-air pseudo-stations defined in the WegenerNet JBT region.

Station name	Station abbreviation	Latitude (E)	Longitude (N)	Altitude [m]	Neighbor stations (Table 1)
Pseudo-station 1	PS1	47°36′49.5"	14°36′06.0"	2061	TA2; ZIN
Pseudo-station 2	PS2	47°32′59.6"	14°31′24.9"	2126	BLA; ZIN
Pseudo-station 3	PS3	47°33′36.9"	14°37′45.0"	2068	BLA; ZIN
Pseudo-station 4	PS4	47°33′16.0"	14°43′33.7"	2139	BLA; ZIN
Pseudo-station 5	PS5	47°29′02.1"	14°42′06.3"	1892	BLA; ZIN

The wind direction at the pseudo-station $\phi_p(z_{max})$ is estimated through a vector-mean calculation by

$$\phi_p(z_{max}) = \begin{cases} \arctan 2(u,v) + 180° & \text{when } \arctan 2(u,v) < 180° \\ \arctan 2(u,v) - 180° & \text{when } \arctan 2(u,v) > 180° \end{cases}, \quad (3)$$

where the mean values of the south component v and the west component u are calculated from the wind directions and wind speeds at the two neighbor stations by

$$v(z_{max}) = -\frac{1}{2}\left[v_{n,1}(z_{max})\cos\phi_{n,1}(z_{max}) + v_{n,2}(z_{max})\cos\phi_{n,2}(z_{max})\right], \quad (4)$$

and

$$u(z_{max}) = -\frac{1}{2}\left[v_{n,1}(z_{max})\sin\phi_{n,1}(z_{max}) + v_{n,2}(z_{max})\sin\phi_{n,2}(z_{max})\right]. \quad (5)$$

For providing $\phi_{n1,2}$ to these equations, the wind directions at the neighbor stations are extrapolated to z_{max} based on the work of van Ulden and Holtslag (1985) by

$$\phi_{n1,2}(z_{max}) = \phi_{n1,2}(z_{s1,2}) \ \Theta \ d_1\left[1 - \exp\left(-d_2\frac{z_{max}}{z_{s1,2}}\right)\right], \quad (6)$$

where $\phi_{n1,2}(z_{s1,2})$ are the observed wind directions at the neighbor stations at the sensor heights $z_{s1,2}$. The empirical constants d_1 and d_2 take the values 1.5 and 1.0, respectively. For this extrapolation we assume neutral stability conditions, which means the turning angle Θ is set to 12°. Details can be found in van Ulden and Holtslag (1985) and the CALMET user guide (Scire et al., 1998).

Equations (2) and (6) are then used again, but in this case to compute the wind speed and wind direction at the pseudo-stations (Table 4) for the defined height levels, based on the values estimated at z_{max} from Eqs. (1) and (3).

The temperatures at the pseudo-stations are estimated from the gridded temperature field generated by an interpolation of the temperature observations. To calculate the temperatures for the defined station altitudes and height levels, temperature lapse rates are estimated from the temperature observations of the meteorological stations; for the relevant details on the generation of the upper-air datasets see Schlager et al. (2017).

An additional user option that we integrated into the WPG concerns the replacement of missing observations from meteorological stations that are used to create the upper-air datasets. If observations from such a station show invalid values, indicated by quality flags, the WPG includes an algorithm to replace these data with observations from the highest upper-air station with valid wind data. To indicate the data quality to the users, we additionally provide gridded quality flags, ranging from zero (good value) to four (bad value).

3.3 Wind gust fields as add-on product

As an additional post-processed product, we let the WPG generate gridded fields of peak gust speed and the corresponding gust direction for 10 m height above ground, based on re-scaling the gridded mean wind fields with the aid of complementary wind gust observations (v_g, ϕ_g) of the meteorological stations (Table 1). While a detailed evaluation of this add-on product is beyond the scope of this study it fits to briefly introduce its generation and some example results here, because these gust fields have also recently become routinely available via the WegenerNet data portal (http://www.wegenernet.org, last access: 3 October 2018).

More specifically, the gridded gust speeds are generated by a spatial interpolation of the ratio of the observed maximum 30 min gust speed to the 30 min average wind speed, where this speed ratio is determined at each observing station location by

$$r^v_{gm} = \frac{v_g}{v_m}, \quad (7)$$

where v_g is the peak gust speed and v_m the average wind speed. The ratio field, generated by interpolating r^v_{gm}, is then multiplied to the gridded mean speed field, yielding a gridded gust field. As interpolation method for the wind speed ratio, a simple inverse distance algorithm is employed in the WPG, which leads to a reasonably smooth gridded gust-to-mean ratio field. To avoid the generation of unrealistic high gust speeds, especially under calm weather conditions, r^v_{gm} values are excluded from the interpolation algorithm if v_m is lower than a user defined minimum average wind speed (v_{min}). Based on sensitivity tests we defined a v_{min} of 1.0 m s^{-1} for the WegenerNet JBT, and 0.2 m s^{-1} for the WegenerNet FBR (an approach that may be further refined in future). This pro-

cedure is a rough but sound approximation of how strong in any 30 min time slice the wind gustiness is pronounced, on top of the prevailing mean wind speeds.

To generate the gridded wind gust directions, the approach is essentially the same but with using direction differences instead of speed ratios. That is, the WPG determines the difference between the gust direction of the peak gust speed and the 30 min vector-mean wind direction. This wind difference is computed by

$$\Delta\Phi_{gm} = \Phi_g - \Phi_m, \quad (8)$$

where Φ_g is the direction of the peak gust speed and Φ_m the 30 min vector-mean wind direction. The spatial interpolation of these direction differences ($\Delta\Phi_{gm}$) to the grid is done in the same way as the gridded speed ratios. As interpolation method again a simple inverse distance algorithm is employed. Finally, these gridded direction difference fields are added to the mean wind direction fields to obtain the wind gust direction field.

3.4 Wind field evaluation periods

The modeling performance is first evaluated by periods with mainly two representative types of wind events: thermally induced wind events and strong wind events. We have chosen July 2014 and December 2013 as test months for this purpose.

In July 2014 the study area was mainly controlled by autochthonous weather conditions, characterized by small synoptic influences, cloudless sky, low relative humidity and increased radiation fluxes between the Earth surface and the atmosphere (Prettenthaler et al., 2010). These weather conditions mainly led to thermally induced wind systems, meaning that the wind fields were dominated by small-scale temperature and pressure gradients. In December 2013 several episodes of strong wind occurred, including wind storms with 30 min wind speeds up to around $30\,m\,s^{-1}$ and peak gusts up to $55\,m\,s^{-1}$. Wind speeds $< 0.5\,m\,s^{-1}$ were classified "calm" and discarded as to small for a reliable cross-validation.

For estimating the model performance we used a leave-one-out cross-validation, as in our previous Schlager et al. (2017) work. In this methodology, wind observations at one wind station are removed from the stations input to the WPG and generated wind fields are evaluated against the wind data from this station. More specifically, we compared the output wind field results at the station location with the observations of the respective station for each 30 min sample. We then calculated the statistical performance parameters summarized in Table 5 from all data over the full evaluation period, for all seven stations that contributed wind sensors (all wind observing stations in Table 1 except WEI and TA1).

Regarding the index of agreement (IOA) parameter we note that in this study we used a redefined IOA, which spans from -1 to $+1$ with values near $+1$ indicating best model performance (Willmott et al., 2012). An IOA of 0.5, for example, implies that the sum of the difference magnitudes between modeled and observed values is one-half of the sum of the observed deviation magnitudes. An opposite value of -0.5 indicates that the sum of the difference magnitudes is twice the sum of the observed deviation magnitudes. In case of little observed variability or poorly estimated deviations about $\overline{v_o}$, the IOA delivers a value near -1.

In addition, we calculated statistical performance parameters for 5-year seasonal data of the WegenerNet JBT and compared the results to 9-year seasonal data of the WegenerNet FBR. We used the WegenerNet independent wind measurements from the ZAMG Feldbach and Bad Gleichenberg stations, located in the FBR, and from the ZAMG Admont station, located near the JBT area (a few kilometers west of it, see Fig. 1) for this climatological evaluation. For the WegenerNet JBT we used, in addition to the ZAMG Admont station, the wind measurements from the representative "left-out" stations KOE and BLA.

4 Results

4.1 Evaluation of representative summer and winter months

Figure 3 illustrates typical examples of WPG-modeled wind fields for morning (upper panels), afternoon (middle panels) and evening (lower panels) winds at a height of 10 m. The left column (Fig. 3a) shows thermally driven circulations in course of 18 July 2014 with varying wind speeds and directions caused by temperature and pressure gradients on a local scale. The highest wind speeds typically occurred in the summit regions, with maximum 30 min wind speeds of around $7\,m\,s^{-1}$ near sunrise at 04:00 UTC (05:00 LT).

The right column (Fig. 3b) displays wind storm behavior during 7 December 2013 caused by northwesterly weather conditions. These synoptic-scale flow conditions led to strong wind speeds in the area with prevailing northwesterly wind directions and maximum 30 min wind speeds of around $30\,m\,s^{-1}$ during the early morning at 04:00 UTC (Fig. 3b, top). Later during the day slightly weaker wind speeds occur and the air flow is more influenced by the terrain and partly channeled through the valleys of the study area.

The maps in Fig. 4, shown in the same layout as Fig. 3, display the estimated distribution of the peak gust speeds and the corresponding gust directions for the same days. Note that these are neither instantaneous nor average gust fields but synthetic field estimates of maximum wind peaks and associated directions that occurred at the same time during the 30 min sample interval. The thermally driven gust field on 18 July 2014 showed maximum gust speeds of around $18\,m\,s^{-1}$ upstream to the Zinoedl summit and the ridge of TA1 at 14:30 UTC (15:30 LT) (Fig. 4a, middle). During the

Table 5. Statistical performance parameters used for the evaluation of the wind field modeling results.

Parameter	Equation	Remarks
Bias	$B = \frac{1}{N}\sum_{i=1}^{N}\left(v_{\mathrm{m},i} - v_{\mathrm{o},i}\right)$	v_m: modeled wind speed; v_o: observed wind speed
Standard deviation of observed wind speed	$\mathrm{SD_o} = \sqrt{\frac{1}{(N-1)}\sum_{i=1}^{N}(v_{\mathrm{o},i} - \overline{v_\mathrm{o}})^2}$	v_o: observed wind speed; $\overline{v_\mathrm{o}}$: mean observed wind speed
Root-mean-square-error	$\mathrm{RMSE} = \sqrt{\frac{1}{N}\sum_{i=1}^{N}(v_{\mathrm{m},i} - v_{\mathrm{o},i})^2}$	v_m: modeled wind speed; v_o: observed wind speed
Correlation coefficient	$R = \frac{1}{(N-1)}\sum_{i=1}^{N}\left(\frac{v_{\mathrm{m},i}-\overline{v_\mathrm{m}}}{\sigma_\mathrm{m}}\right)\left(\frac{v_{\mathrm{o},i}-\overline{v_\mathrm{o}}}{\sigma_\mathrm{o}}\right)$	v_m: modeled wind speed; $\overline{v_\mathrm{m}}$: mean modeled wind speed; v_o: observed wind speed; $\overline{v_\mathrm{o}}$: mean observed wind speed; σ_m: standard deviation of modeled wind speed; σ_o: standard deviation of observed wind speed
Index of agreement	$\mathrm{IOA} = \begin{cases} 1.0 - \frac{\sum_{i=1}^{N}\lvert v_{\mathrm{m},i} - v_{\mathrm{o},i}\rvert}{c\sum_{i=1}^{N}\lvert v_{\mathrm{o},i} - \overline{v_\mathrm{o}}\rvert}, \text{if } \sum_{i=1}^{N}\lvert v_{\mathrm{m},i} - v_{\mathrm{o},i}\rvert \le c\lvert v_{\mathrm{o},i} - \overline{v_\mathrm{o}}\rvert \\ \frac{c\sum_{i=1}^{N}\lvert v_{\mathrm{o},i} - \overline{v_\mathrm{o}}\rvert}{\sum_{i=1}^{N}\lvert v_{\mathrm{m},i} - v_{\mathrm{o},i}\rvert} - 1, \text{if } \sum_{i=1}^{N}\lvert v_{\mathrm{m},i} - v_{\mathrm{o},i}\rvert > c\lvert v_{\mathrm{o},i} - \overline{v_\mathrm{o}}\rvert \end{cases}$	v_m: modeled wind speed; v_o: observed wind speed; $\overline{v_\mathrm{o}}$: mean observed wind speed; c: factor set to 2 (Willmott et al., 2012)
Mean absolute error of wind direction	$\mathrm{MAE_{dir}} = \frac{1}{N}\sum_{i=1}^{N}\left\{\arccos\left[\cos\left(\phi_{\mathrm{m,i}} - \phi_{\mathrm{o,i}}\right)\right]\right\}$	ϕ_m: modeled wind direction; ϕ_o: observed wind direction

storm event on 7 December 2013, the gusts reached a tremendous speed of near 55 m s^{-1} at 04:00 UTC (Fig. 4b, top) around the Zinoedl summit and the summit pseudo-station PS2 (around 200 km h^{-1}). It is noticeable that the strongest gusts have a northerly direction whereas the average wind comes from the northwest (Figs. 4b and 3b).

Figures 5 and 6 illustrate the modeling performance at the Koelblwiese (KOE) and the Blaseneck (BLA) station, as typical examples for a valley and a summit station. The KOE station is located in the Johnsbach valley at a height of 860 m to monitor the climate at the valley floor. The environment of this station is often influenced by lakes of cold air, especially in fall and winter. The BLA station is located at a height of 1969 m on the summit of the Blaseneck. The environment of the latter station is characterized through an exposed high Alpine location were strong wind speeds can occur in all seasons. In the scatterplots we compared the observed 30 min vector-mean wind speeds to the corresponding modeled values of the nearest neighbor gridpoints (located at < 50 m distance).

For the KOE station we estimated a reasonably good model performance with a correlation coefficient R of 0.71 in July 2014 and 0.75 in December 2013. In July 2014 the maximum observed and modeled wind speeds were around 5 m s^{-1} with a slightly positive bias B between observed and modeled wind speeds (Fig. 5a). In December 2013 the maximum observed wind speeds were around 13 m s^{-1} and the estimated B is slightly negative (Fig. 5b).

The scatterplot for the BLA station indicates a wider spread of the observed and modeled wind speeds compared to the Koelblwiese station (Fig. 6). Regarding the R value we estimated similar good results with a value of 0.69 for July 2014 and 0.71 for December 2013. The mean absolute error of wind direction $\mathrm{MAE_{dir}}$ exhibits similar results for both stations and periods, with values near 40° (except for 59° at KOE in December 2013).

Figures 7 and 8 show windroses of the relative frequency of wind directions divided by wind speed categories from the model compared to the observed wind directions for the KOE and BLA station, respectively.

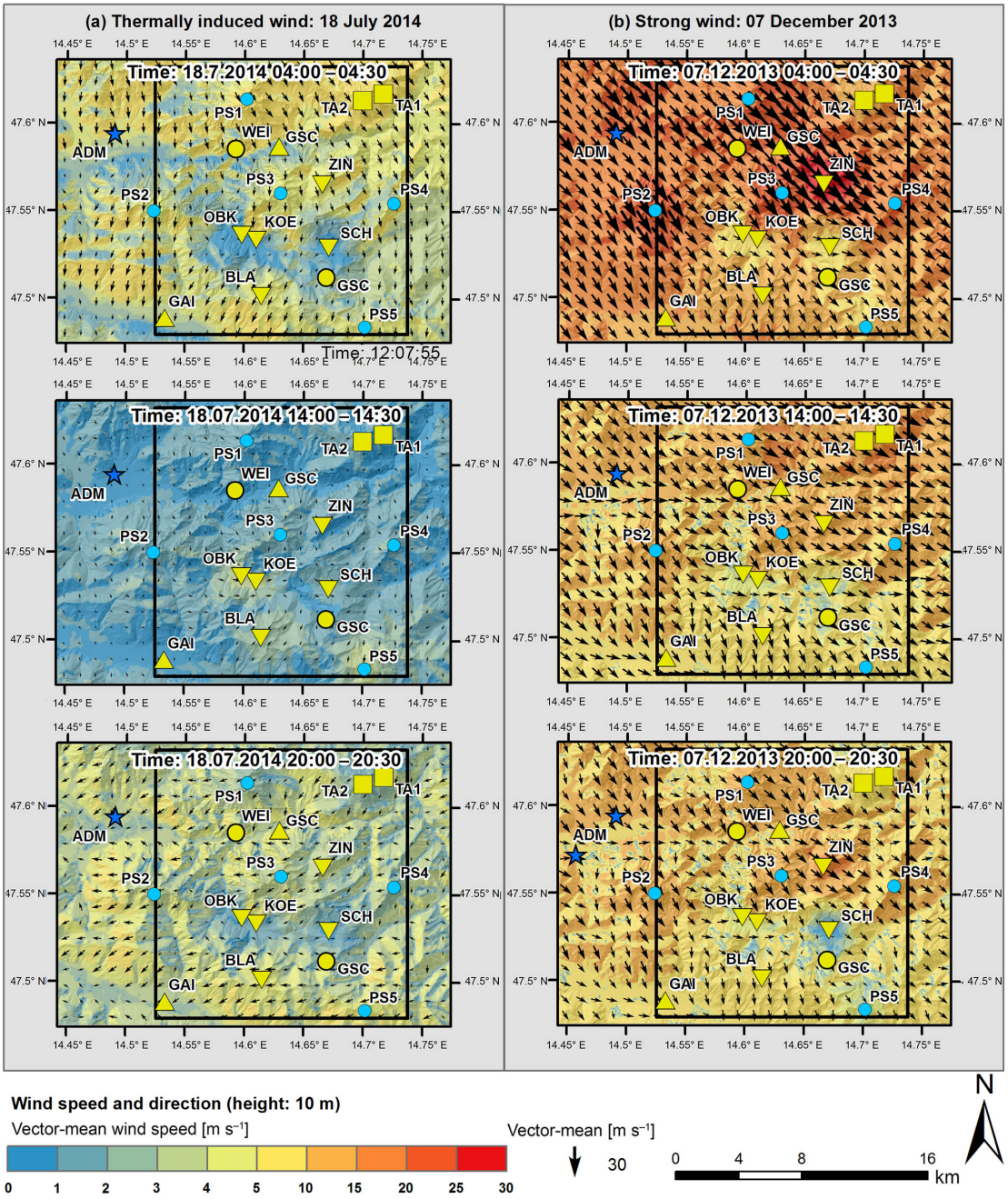

Figure 3. Modeled wind fields typical for the study area: **(a)** thermally induced wind fields (18 July 2014) and **(b)** strong region-scale winds (7 December 2013), for near-sunrise (top), afternoon (middle) and near-sunset (bottom) conditions. Time is shown as UTC (corresponding to local time minus 1 h).

Regarding the KOE station in July 2014 (Fig. 7a), a shift from the west-southwest to the west-northwest sectors can be seen in the modeled results. The observations show about 18 % in the west-southwest sector, while the model estimates just a few percent in this sector. Vice versa, the frequency of observed wind directions is 7 % for the west-northwest sector, while the model shows 23 % in this sector. This shift by about 40° in wind directions is explained by the influence of the Oberkainz (OBK) station which is located in the west-northwest in a distance of only about 1 km from the KOE station. The magnitude of the wind speed is calculated quite well by the model, with values below 5 m s^{-1} in accordance to the observations.

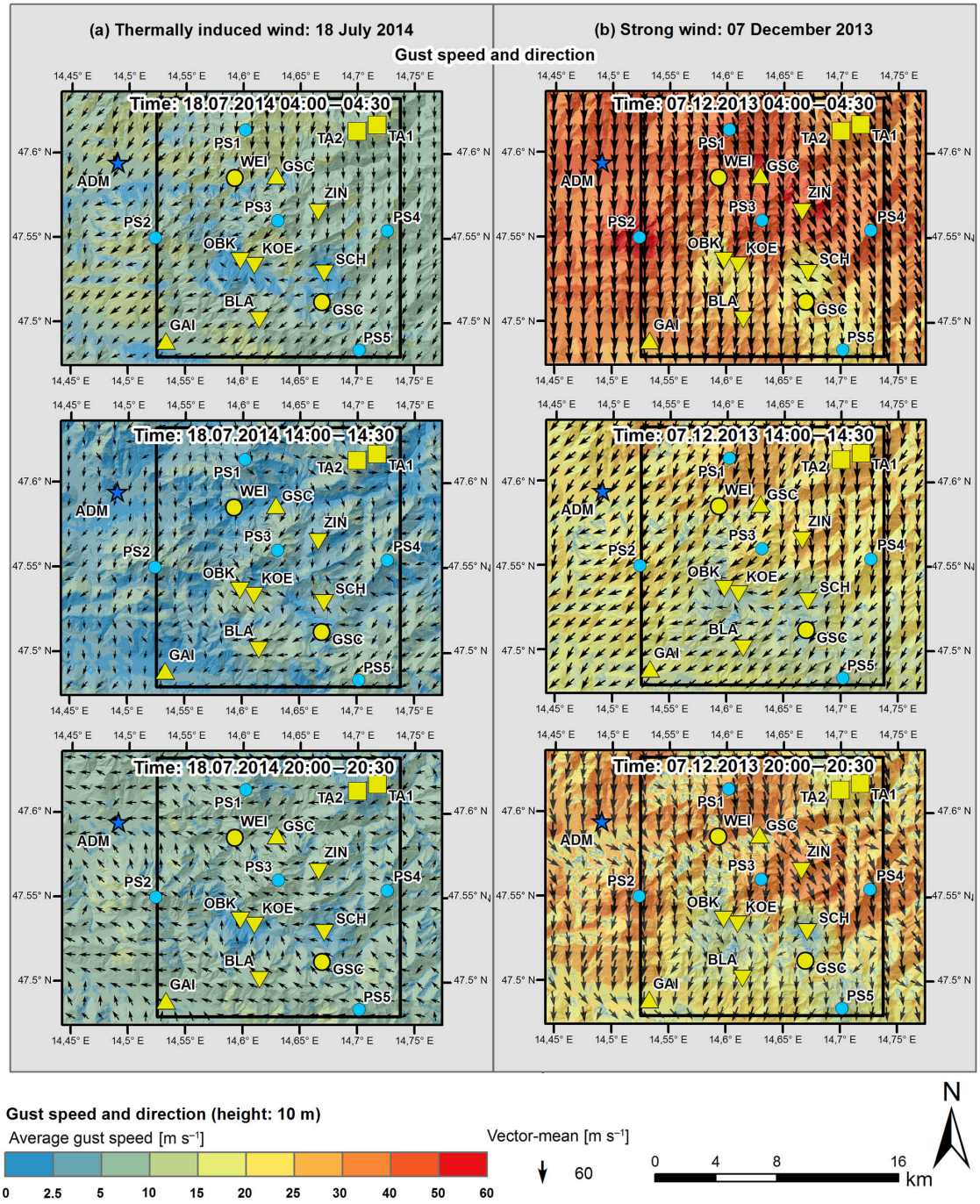

Figure 4. Modeled wind gust fields typical for the study area: **(a)** thermally induced wind fields (18 July 2014) and **(b)** strong region-scale winds (7 December 2013), for near-sunrise (top), afternoon (middle) and near-sunset (bottom) conditions. Time is shown as UTC (corresponding to local time minus 1 h).

In December 2013 (Fig. 7b) the main observed wind directions at the KOE station are from the north-northeast to the east sectors; however, wind directions with high wind speeds can be observed in the westward sectors as well. For this period, the model estimates a significantly narrower wind directions corridor, with the highest proportion of wind directions in the northwest and the east-southeast sector (each about 22 %). Evidently, the upslope flow conditions (northeast sector) cannot be captured well by the available observational information.

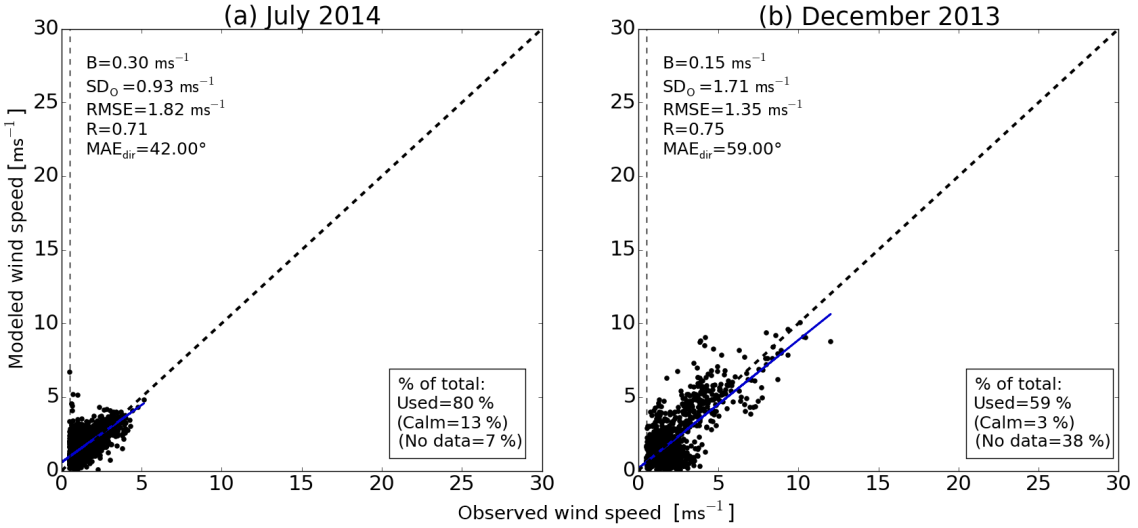

Figure 5. Scatterplot of modeled vs. observed vector-mean wind speeds for the WegnerNet Koelblwiese (KOE) station in the Johnsbach valley: **(a)** July 2014 and **(b)** December 2013.

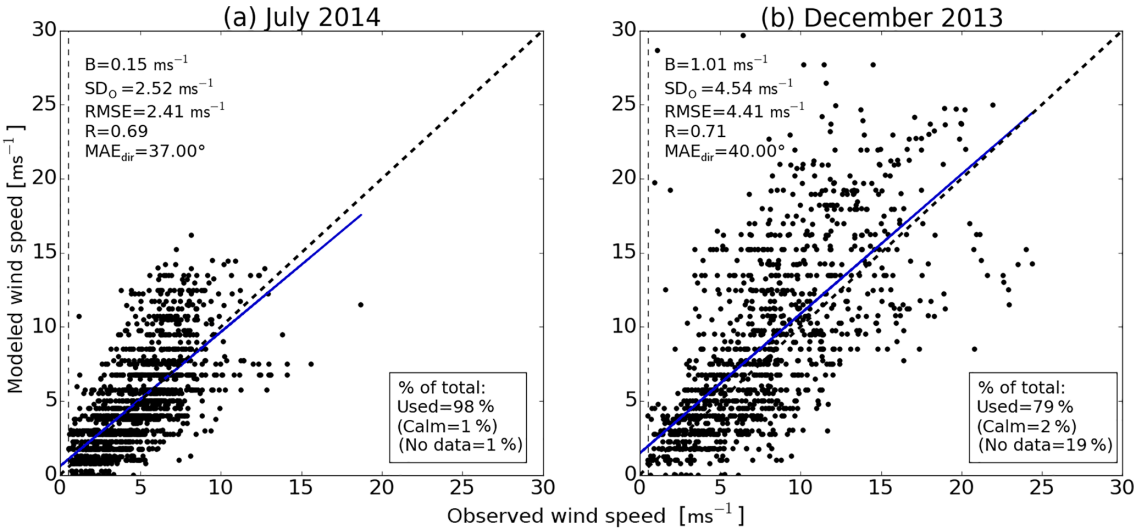

Figure 6. Same as Fig. 5 but for WegenerNet Blaseneck (BLA) station at the Blaseneck summit.

Figure 8 illustrates the BLA station results. In July 2014 (Fig. 8a), the observed prevailing wind directions are from the north-northwest to the east-northeast sectors, while the model calculates the highest proportion from the west-northwest to north sector. Regarding wind speed, the model estimates values in good agreement with the observed wind speeds, illustrated in Fig. 8 a.

In December 2013 (Fig. 8b) a shift between observed and modeled wind directions from the north-northwest to the west-northwest sector and from the SW more to the west sector can be seen. These modeled westerly flows are caused by the influence of the summit station Zinoedl (ZIN), which is mainly driven by northwesterly flows in this period. As briefly explained in Sect. 3 above, the WPG implements a function to replace missing upper-air data with valid observations from the highest upper-air station, giving the reason for the influence of this station. In case of the evaluation of the BLA station the missing upper-air data were replaced by observations from the ZIN station. For this period, again the wind speeds between the observations and the model results are in good overall agreement.

The statistical results from all meteorological stations are summarized in Table 6. The absolute statistical parameters (bias B, standard deviation SD$_o$, root-mean-square-error RMSE, and mean absolute error of wind direction MAE$_{\mathrm{dir}}$) applied to the vector-mean of wind speed show considerably higher values in December 2013, resulting from the overall higher wind speeds in this period. In general, the B values are

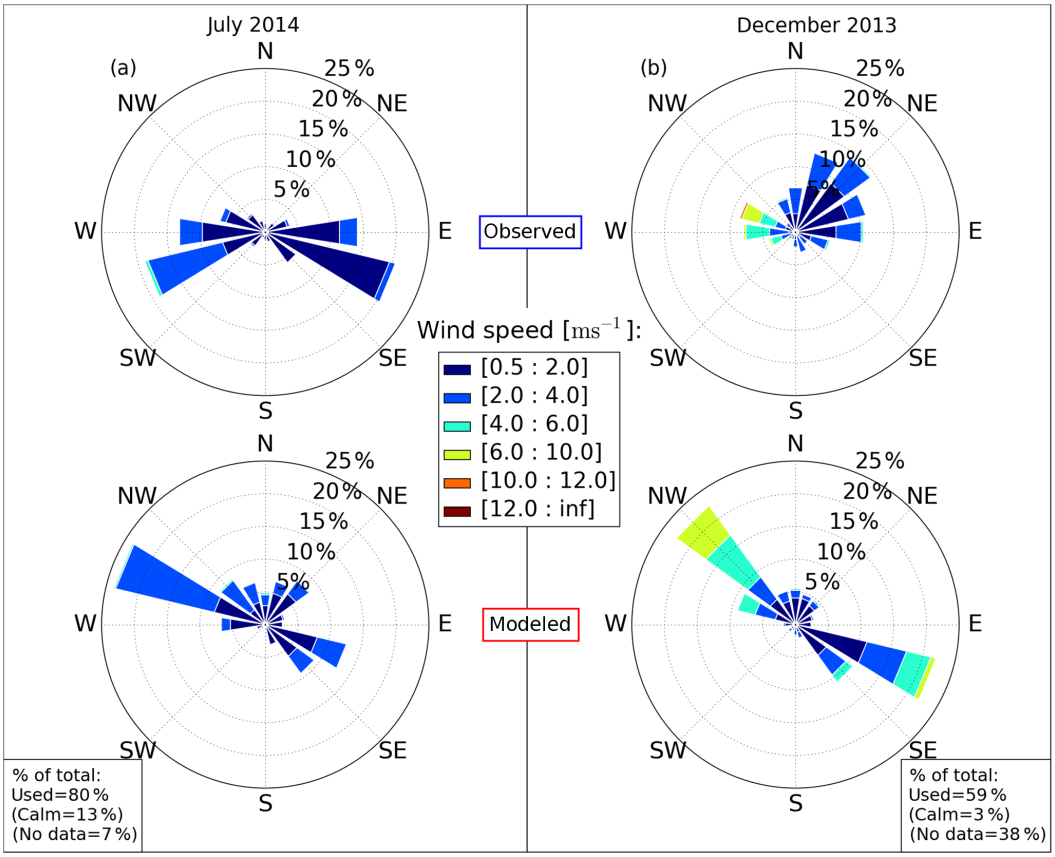

Figure 7. Relative frequency of vector-mean wind directions for a range of wind speed categories, for observed (upper row) and modeled (lower row) wind directions for the WegenerNet Koelblwiese (KOE) station in the Johnsbach valley: **(a)** July 2014 and **(b)** December 2013.

Table 6. Statistical performance measures calculated for the WegenerNet JBT meteorological stations with contributing wind sensors, for July 2014 and December 2013 from the "leave-one-out" validation analysis; see Table 5 for more information on the calculation of the performance parameters.

Station ID and abbr.	July 2014						December 2013					
	B [m s^{-1}]	SD_o [m s^{-1}]	RMSE [m s^{-1}]	R [1/1]	IOA [1/1]	MAE_{dir} [°]	B [m s^{-1}]	SD_o [m s^{-1}]	RMSE [m s^{-1}]	R [1/1]	IOA [1/1]	MAE_{dir} [°]
501, OBK	−0.10	1.23	1.24	0.42	0.57	35	1.61	1.71	3.72	0.35	0.21	51
502, KOE	0.30	0.93	0.81	0.71	0.61	42	−0.15	1.71	1.35	0.75	0.56	59
503, SCH	0.67	0.89	1.82	0.39	0.25	54	1.45	1.59	3.32	0.61	0.22	40
504, BLA	0.15	2.52	2.41	0.69	0.55	37	1.01	4.54	4.41	0.71	0.55	40
505, ZIN	−0.67	3.44	2.56	0.70	0.66	36	−3.85	6.76	6.02	0.73	0.60	38
507, GSC	0.31	1.01	1.10	0.56	0.46	74	0.83	1.28	1.85	0.62	0.32	67
509, TA2	1.40	2.47	3.01	0.62	0.46	50	0.99	4.52	4.62	0.69	0.54	37
Mean Value	0.30	1.78	1.85	0.58	0.51	47	0.27	3.16	3.61	0.64	0.43	47

positive, except for the ZIN station and for the OBK station in July 2014.

The mean R values show better results in December 2013 than in July 2014 and the estimated MAE_{dir} is similar for both periods, and found at near or below about 40°. The RMSE values range from 0.8 to 3 m s^{-1} for July 2014, with the lowest value for the KOE station and the highest value for the TA2 station. The data from December 2013 generally show higher RMSE values, with the lowest value

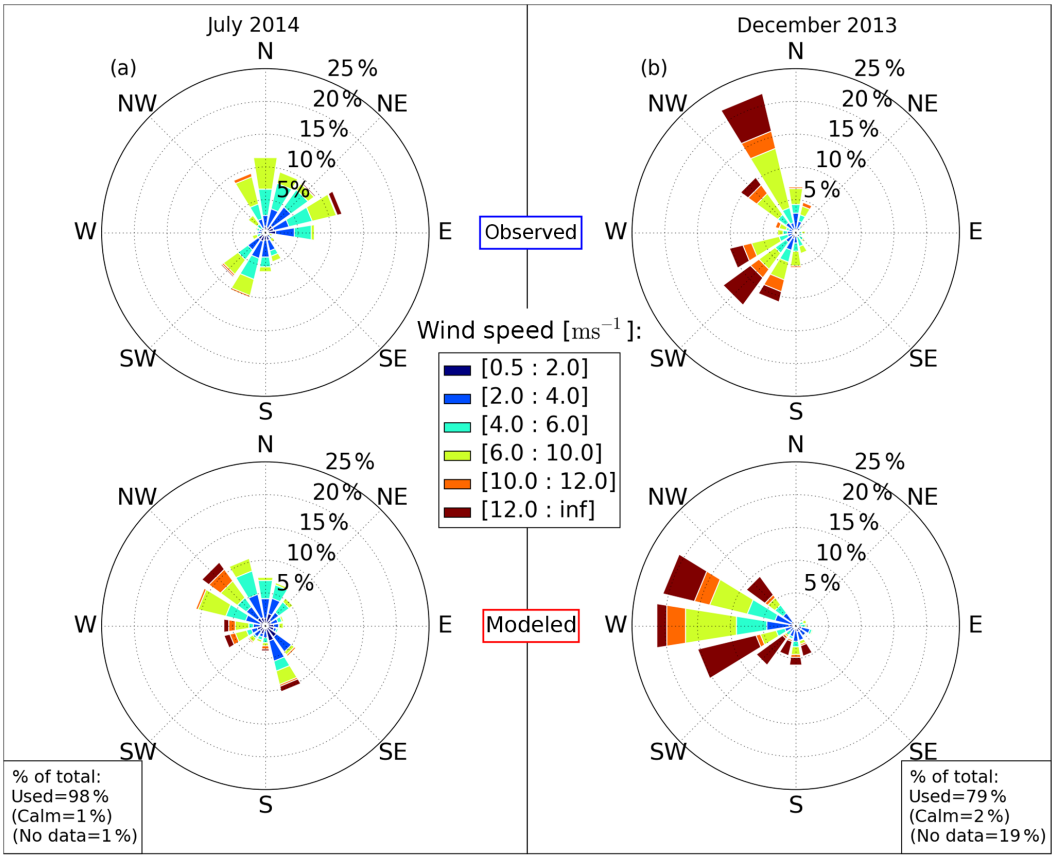

Figure 8. Same as Fig. 7 but for WegenerNet Blaseneck (BLA) station at the Blaseneck summit.

(1.35 m s^{-1}) again for the KOE station and the highest value (6 m s^{-1}) for the ZIN station.

The SD$_o$ values are of similar size for both periods. The mean R value is 0.58 for July 2014 and 0.69 for December 2013. For December 2013, the R value is higher than 0.6 for all stations except for OBK, compared to July 2014, where all stations show higher values than 0.5, except for OBK and SCH. Regarding the mean IOA, we estimated a value of 0.51 for July 2014 and 0.43 for December 2013, with again remarkably low values for the SCH station in July 2014 and for the OBK and SCH station in December 2013.

These overall statistical results, but also the example results shown in Figs. 3 to 10, illustrate the useful level of skill well but also the evident performance limits that the developed WPG application can provide for empirical wind field modeling based on a small set of seven stations in such complex terrain as the WegenerNet JBT area.

4.2 Evaluation based on multi-year climatological data

Modeled average wind fields for the WegenerNet JBT are presented in the multi-year climatological data of Fig. 9 (top panels), showing 5-year climate data for the summer and winter season. In summer, the seasonal average wind speed reaches maximum values of around 6 m s^{-1} at the highest summits and generally lower values in the valley regions, with around 3 m s^{-1}. The environment of the OBK, KOE and SCH stations exhibits the lowest average wind speeds, directly linked to the observations of these stations which are used as model input (Fig. 9a, color shading). In comparison, the winter months show generally higher average wind speeds, with a similar spatial distribution but including in particular higher values at higher altitudes and the summit regions. The maximum average wind speeds of around 8 m s^{-1} is observed at the highest summits (Fig. 9b, color shading).

The vector-mean of wind directions for the summer season has directions mainly from the south sectors with maximum vector-mean wind speeds of around 3 m s^{-1} (Fig. 9a, black arrows). In the winter season, the prevailing wind directions are from the west sectors, with maximum vector-mean wind speeds of around 5 m s^{-1} (Fig. 9b, black arrows).

The windroses of Fig. 9 bottoms show the seasonal relative frequency of wind directions for the summer and winter seasons for the KOE and BLA stations, used as examples for a valley and a summit station. The distribution of wind directions shows similar results as the distribution for the individual months July 2014 and December 2013 (cf. Figs. 7

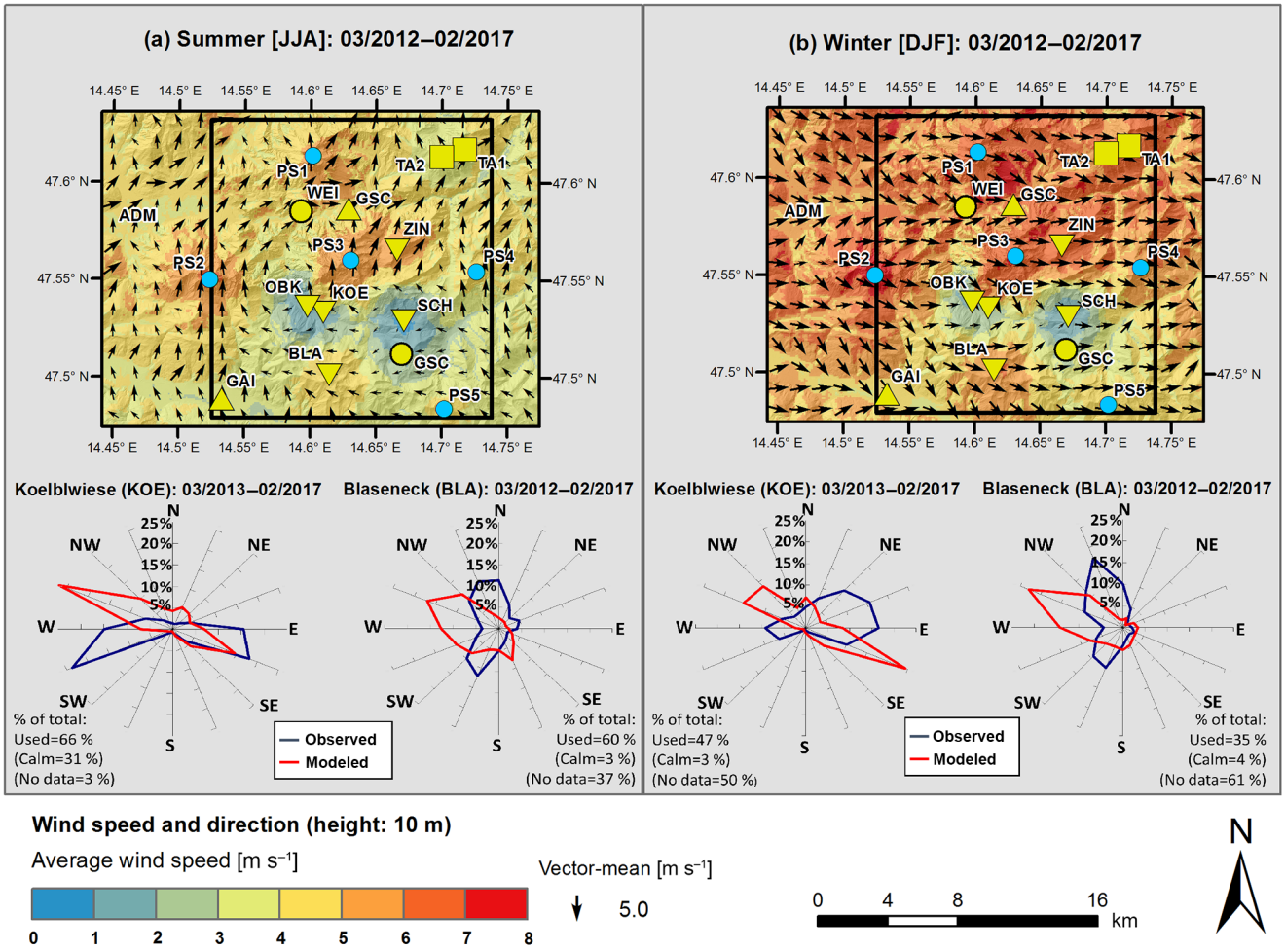

Figure 9. Modeled 5-year or 4-year seasonal mean wind fields (maps, top) and relative frequency of wind directions for the Koelblwiese (KOE) and Blaseneck (BLA) station (windroses, bottom) for the WegenerNet JBT: **(a)** summer month March 2012/(March 2013)–February 2017 and **(b)** winter month March 2012/(March 2013)–February 2017.

and 8). This similar pattern indicates a good representativeness of these months, including evidently common weather conditions in the WegenerNet JBT.

Due to the valley location of the KOE station, the observations and modeled values show narrow wind corridors with a flow mainly along the valley axis during the summer. The largest part of the observed flow is from the directions east to east-southeast and west-southwest to west, while the model estimates directions mainly from the east-southeast to west-northwest sector (bottom-left panel of Fig. 9a). In winter, most of the flow is from the northeast to the east-southeast sector. The model again estimates wind directions mainly from the east-southeast and the west-northwest to the northwest sectors (bottom-left panel of Fig. 9b). A shift between modeled and observed values from west-southwest to west-northwest directions can be seen in both seasons; this shift is caused by the observational influence of the nearby OBK station on the modeled wind fields, which is located around 1 km northwest of the KOE station (cf. also Fig. 7).

The relative frequency of observed wind directions of the BLA station shows prevailing directions from the northwest to the north in the summer and winter months, while the model mainly estimates wind directions from the west to the northwest sectors. In both seasons, the largest fraction is estimated from the west-northwest sector, with around 12 % in the summer months and around 23 % in the winter months (bottom-right panels of the second row in Fig. 9a and b). The modeled more westerly flows are caused by the influence of the ZIN station; as already indicated by the individual month results of Fig. 8.

For the WegenerNet FBR we show 9-year average wind fields again for the summer and winter season (Fig. 10), in the same format as Fig. 10 shows for WegenerNet JBT. The maximum average wind speeds occur around the highest WegenerNet FBR station 74, located at an elevation of

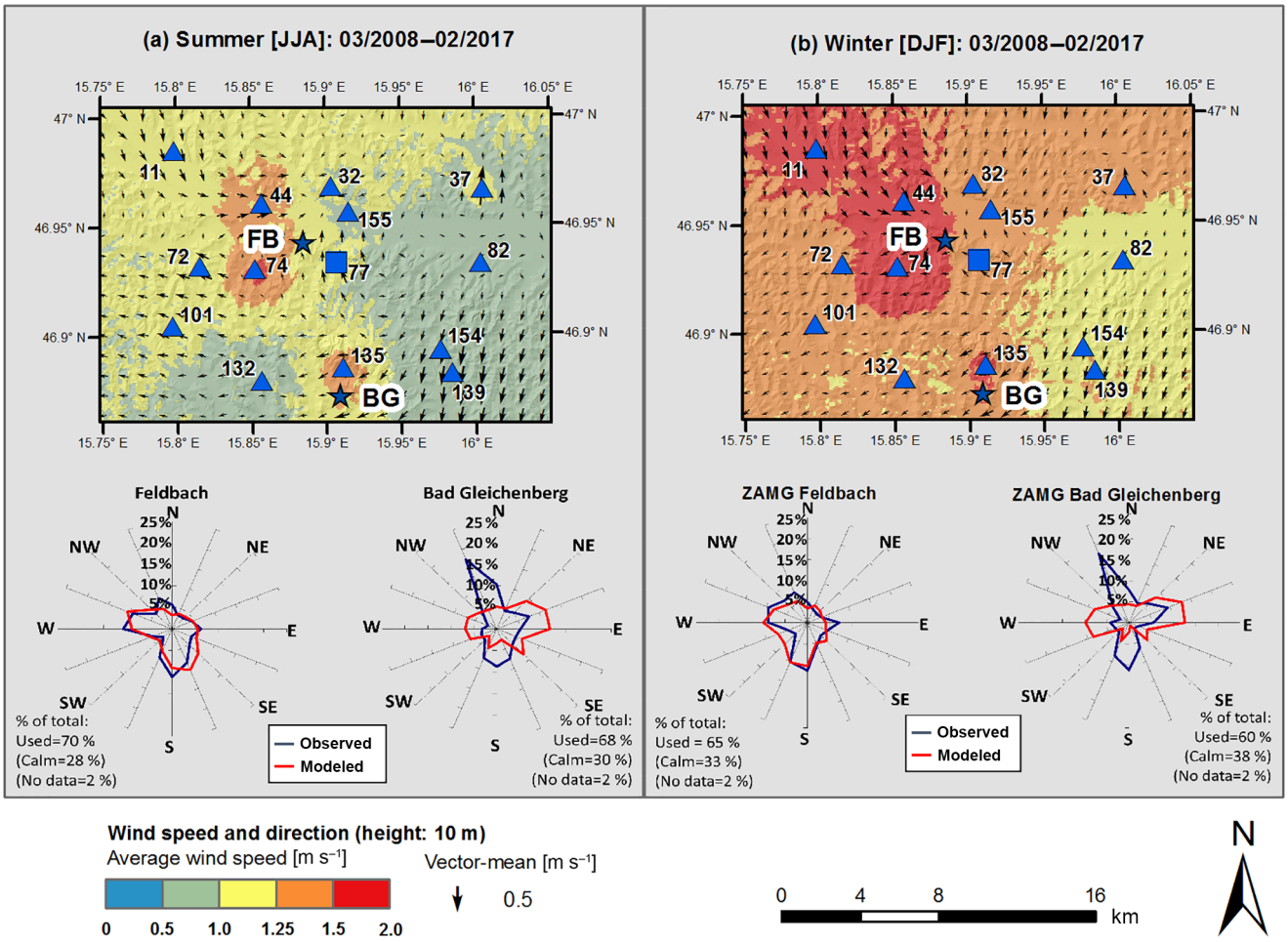

Figure 10. Same as Fig. 9 but for 9-year seasonal means in the WegenerNet FBR, and windrose results for the ZAMG Feldbach and Bad Gleichenberg stations.

394 m, with average wind speeds around 1.5 m s^{-1} in summer (Fig. 9a, top) and near 2.0 m s^{-1} in winter (Fig. 10b, top). The spatial distribution of the wind speeds exhibits slightly lower values in summer than in winter. As expected, overall both the modeled average-speed fields and the vector-mean fields from the WegenerNet FBR (Fig. 10) in the Alpine forelands show much lower wind speeds than the WegenerNet JBT (Fig. 9) with its mountainous Alpine terrain.

The seasonal relative frequency of wind directions from 9-year climate data for the ZAMG Feldbach station is similar among observations and modeled values for both seasons (bottom-left panels of Fig. 9a and b).

However, larger differences between modeled and observed values can be noticed for the ZAMG Bad Gleichenberg station (bottom-right panels of Fig. 9a and b). For this station, the model calculates the largest fraction with about 10 % to 15 % from the northeast to the east sectors for both seasons while the observed wind directions show about 17 % percent from the north-northwest sector and around 10 % from the south sector. These differences between modeled and observed values can be explained by the environment of this station bringing in local influences that degrade the representativeness of the wind observations for the 1 km scale (Schlager et al., 2017).

Table 7 summarizes the statistical results of multi-year seasonal mean data for selected stations including the ones illustrated in the bottom row of Fig. 9 and Fig. 10 and the ZAMG Admont station for JBT. The results of the statistical parameters generally show better performance for the WegenerNet FBR stations than for the WegenerNet JBT stations.

For the WegenerNet JBT stations the B is positive for all seasons, except for the KOE station in winter. The resulting RMSE ranges from about 0.9 to 1.35 m s^{-1} for this station. Due to the more frequently occurring episodes of strong wind in winter, the RMSE values are generally higher for all stations in this season. Because of the higher wind speeds at the summit regions, the RMSE shows higher values at a range from 2.7 to 5.1 m s^{-1} for the BLA station. The R value is for both the KOE and BLA stations and all seasons clearly

Table 7. Statistical multi-year climatological performance measures calculated for representative meteorological stations for the WegenerNet JBT and the WegenerNet FBR (upper half 5-year or 4-year seasonal means for three WegenerNet JBT stations; right half 9-year seasonal means for two WegenerNet FBR stations); see Table 5 for more information on the calculations of the performance parameters.

Season (per Station)	B [ms^{-1}]	SD_o [ms^{-1}]	RMSE [ms^{-1}]	R [1/1]	IOA [1/1]	MAE_{dir} [°]
WegenerNet JBT						
KOE: 03/2013–02/2017						
spring (MAM)	0.18	1.50	1.06	0.75	0.68	39
summer (JJA)	0.25	1.16	0.89	0.75	0.67	38
fall (SON)	0.16	1.35	1.10	0.68	0.63	41
winter (DJF)	−0.17	1.57	1.35	0.67	0.58	47
all	0.13	1.41	1.09	0.71	0.65	41
BLA: 03/2012–02/2017						
spring (MAM)	0.09	3.54	3.64	0.65	0.51	40
summer (JJA)	0.34	2.70	2.74	0.68	0.54	43
fall (SON)	0.74	3.50	3.67	0.67	0.52	39
winter (DJF)	0.04	4.91	5.09	0.64	0.54	41
all	0.73	3.63	3.65	0.67	0.54	41
ZAMG ADM[a]: 03/2012–02/2017						
spring (MAM)	1.33	1.38	3.28	0.38	0.19	52
summer (JJA)	0.99	1.18	2.62	0.36	0.28	53
fall (SON)	1.17	1.15	2.89	0.47	0.07	40
winter (DJF)	1.38	1.09	3.59	0.43	−0.04	36
all	1.22	1.22	3.12	0.40	0.15	38
WegenerNet FBR						
ZAMG FB[b]: 03/2008–02/2017						
spring (MAM)	−0.28	1.36	0.75	0.86	0.78	22
summer (JJA)	−0.27	1.00	0.57	0.87	0.77	19
fall (SON)	−0.25	1.05	0.57	0.87	0.78	19
winter (DJF)	−0.21	1.07	0.54	0.89	0.80	16
all	−0.25	1.15	0.61	0.88	0.79	19
ZAMG BG[c]: 03/2008–02/2017						
spring (MAM)	−0.17	1.22	0.83	0.76	0.71	31
summer (JJA)	−0.08	0.92	0.64	0.76	0.71	57
fall (SON)	−0.12	0.88	0.60	0.77	0.73	27
winter (DJF)	−0.11	0.87	0.57	0.79	0.73	26
all	−0.12	−1.00	0.67	0.78	0.72	28

[a] Admont station, [b] Feldbach station, [c] Bad Gleichenberg station

higher than 0.6. The MAE_{dir} shows for all seasons and both JBT stations similar results of near 40°.

For the ZAMG Admont station the statistical results are generally worse. Despite lower observed wind speeds compared to the other stations, the B and RMSE show high values. Additionally, the R and the IOA values indicate poor performance, with a R value only around 0.4 and IOA values in a range of just −0.04 to 0.28 for all seasons. These statistical results for an independent location outside but nearby the JBT area in the Enns valley indicate the value that an additional station with wind observations also in the Enns valley could bring to the JBT network (see also Sect. 5 below). As noted in Sects. 2 and 3, the wind observations from the existing Weidendom station, which is located in the Enns valley, are not suitable as model input due to a non-representative location.

The WegenerNet FBR stations show a somewhat negative bias (B) and generally low RMSE values for all seasons. The R values show good results for all stations, with values higher than 0.75 throughout (ZAMG Feldbach station even > 0.85). This also applies to the IOA, with values higher than 0.71. The higher values of the mean absolute error of wind directions (MAE_{dir}) for the ZAMG Bad Gleichenberg station, compared to the ZAMG Feldbach station, indicate again the local influences affecting the observations of this station (Schlager et al., 2017).

5 Conclusions

In this work we further developed an operational weather diagnostic application, the WegenerNet Wind Product Generator (WPG), recently developed by Schlager et al. (2017), and applied it to the WegenerNet Johnsbachtal (JBT), a dense meteorological station network located in a mountainous Alpine region in the north of Styria, Austria. Based on an advanced version of the CALMET model (Scire et al., 1998), the WPG automatically generates gridded high-resolution wind fields in near-real-time with a temporal resolution of 30 min and a spatial resolution of 100 m × 100 m. In addition, the WPG produces gridded wind gust fields with the same temporal and spatial resolution. As derived products, half-hourly fields are averaged to hourly and daily weather data products as well as monthly, seasonal and annual climate data products (Schlager et al., 2017).

The main purpose of the WPG products is the evaluation of wind fields from convection-permitting regional climate models and the investigation of weather and climate on a local scale, among other needs, such as monitoring of wind storms.

We evaluated the new WegenerNet JBT wind fields by identifying representative monthly periods with mainly thermally induced wind fields (July 2014) and strong wind speeds including wind storm events (December 2013). Using a "leave-one-station-out" validation approach, and then evaluating against the observed wind data at the "left-out" station, we inspected the reasonableness of individual wind fields and computed statistical performance measures such as modeled vs. observed biases, root-mean-square-errors and correlation coefficients. In case of wind speed, the statistics show reasonably good results for both periods with somewhat better values for December 2013. Compared to the wind speed, the analysis of wind direction delivers somewhat higher errors, with directional deviations in the wind sectors of typically around 40°, depending on the station location and period.

Overall the results discussed well illustrate the useful level of skill, but also the evident performance limits, that the WPG application can provide for empirical wind field modeling based on a small network of seven stations in such a complex terrain as the WegenerNet JBT area.

We also evaluated seasonal statistical performance parameters for multi-year data of both the WegenerNet JBT region and WegenerNet Feldbach region (FBR), the latter initially analyzed by Schlager et al. (2017). For the WegenerNet JBT, the statistical performance measures applied to wind speeds show reasonably good overall statistical agreement as we showed for the Koelblwiese and Blaseneck stations. The results related to wind direction show a level of directional deviation around 40°, similar to the individual month results.

For the ZAMG Admont station, an independent station nearby the area in the Enns valley, the statistics show generally poor values, reflecting the missing meteorological wind information in the valley. The installation of an additional wind-observing station in the Enns valley (no suitable JBT station currently available there) could help to significantly improve the WPG results in this subarea. Due to the denser distribution of stations in the WegenerNet FBR, and the less challenging terrain in this Alpine foreland region, the statistical evaluation shows clearly superior climatological wind field performance for this network.

Ongoing next steps of work deal with the evaluation the dynamical wind fields of non-hydrostatic weather analyses and climate model simulations for the two WegenerNet regions FBR and JBT for selected challenging weather conditions. For this purpose, we intercompare the empirical wind fields generated by the WPG with wind field analysis data from the INCA model of the Austrian weather service ZAMG (Haiden et al., 2011; Kann et al., 2015) as well as with climate model data from the non-hydrostatic model COSMO-CLM (Schättler et al., 2016). We expect the WPG application to be a valuable tool for serving this and other purposes.

Code availability. The CALMET 6.5.0 model code is available from the website http://www.src.com (last access: 3 October 2018). The overall WPG code is not in the public domain and cannot be distributed.

Data availability. CORINE Land Cover data for the study area are available from http://www.eea.europa.eu (last access: 3 October 2018), digital elevation model data from http://www.gis.steiermark.at (last access: 3 October 2018), and WegenerNet data from http://www.wegenernet.org (last access: 3 October 2018). The WegenerNet data contain the WPG wind field output data as introduced in this study on a routine basis over the entire WegenerNet data period.

Author contributions. CS collected the data, performed the analyses and modeling, created the figures and wrote the first draft of the manuscript. GK provided guidance and advice on all aspects of the study and significantly contributed to the text. JF provided guidance on technical aspects of the WegenerNet networks and its data characteristics and contributed to the text.

Competing interests. The authors declare that they have no conflict of interest.

Acknowledgements. The authors thank Roberto Bellasio (Enviroware), Italy, for providing the modified CALMET 5.2 code, including algorithms to account for topographic shading effects and vertical temperature gradients. WegenerNet funding is provided by the Austrian Ministry for Science and Research, the University of Graz, the state of Styria (which also included European Union regional development funds), and the city of Graz;

8 A spatial evaluation of high-resolution wind fields from empirical and dynamical modeling in hilly and mountainous terrain

The third paper provides the main scientific contribution of this thesis to the field of geographic information science (GIS) and uses a novel spatial verification methodology, the wind fractions skill score (WFSS). The WFSS was used to intercompare the empirical WPG wind field data with wind field analysis data from the INCA model and with dynamical climate model data from the CCLM, with the focus on evaluating spatial differences and displacements between these wind fields. Table 8.1 presents the author contributions of this publication.

Table 8.1: Author contributions of the third peer-reviewed publication (Schlager et al. 2019).

Title:	A spatial evaluation of high-resolution wind fields from empirical and dynamical modeling in hilly and mountainous terrain
Reference:	Schlager, C., G. Kirchengast, J. Fuchsberger, A. Kann, and H. Truhetz (2019): "A spatial evaluation of high-resolution wind fields from empirical and dynamical modeling in hilly and mountainous terrain", *Geosci. Model Dev.* 12.7, pp. 2855-2873. https://doi.org/10.5194/gmd-12-2855-2019
Author contributions:	
Christoph Schlager:[a]	Collected the data, performed the analyses and modeling, created the figures and wrote the first draft of the manuscript
Gottfried Kirchengast:[a,b]	Provided guidance and advice on all aspects of the study and significantly contributed to the text
Juergen Fuchsberger:[a]	Provided guidance on technical aspects of the WegenerNet networks and its data characteristics and contributed to the text
Alexander Kann:[c]	Provided INCA-related advice and contributed to the INCA part of the text
Heimo Truhetz:[a]	Provided information and advice on the CPCSs model setup and characteristics and contributed to the CPCSs part of the text

[a] Wegener Center for Climate and Global Change (WEGC), University of Graz, Graz, Austria.
[b] Institute for Geophysics, Astrophysics, and Meteorology/Institute of Physics, University of Graz, Graz, Austria.
[c] Department of Forecasting Models, Central Institute for Meteorology and Geodynamics (ZAMG), Vienna, Austria.

Geosci. Model Dev., 12, 2855–2873, 2019
https://doi.org/10.5194/gmd-12-2855-2019

Geoscientific Model Development
Open Access
EGU

A spatial evaluation of high-resolution wind fields from empirical and dynamical modeling in hilly and mountainous terrain

Christoph Schlager[1], **Gottfried Kirchengast**[1,2], **Juergen Fuchsberger**[1], **Alexander Kann**[3], **and Heimo Truhetz**[1]

[1]Wegener Center for Climate and Global Change (WEGC), University of Graz, Graz, Austria
[2]Institute for Geophysics, Astrophysics, and Meteorology/Institute of Physics, University of Graz, Graz, Austria
[3]Department of Forecasting Models, Central Institute for Meteorology and Geodynamics (ZAMG), Vienna, Austria

Correspondence: Christoph Schlager (christoph.schlager@uni-graz.at)

Received: 22 September 2018 – Discussion started: 8 October 2018
Revised: 25 May 2019 – Accepted: 19 June 2019 – Published: 11 July 2019

Abstract. Empirical high-resolution surface wind fields, automatically generated by a weather diagnostic application, the WegenerNet Wind Product Generator (WPG), were intercompared with wind field analysis data from the Integrated Nowcasting through Comprehensive Analysis (INCA) system and with regional climate model wind field data from the Consortium for Small Scale Modeling Model in Climate Mode (CCLM). The INCA analysis fields are available at a horizontal grid spacing of 1 km × 1 km, whereas the CCLM fields are from simulations at a 3 km × 3 km grid. The WPG, developed by Schlager et al. (2017, 2018), generates diagnostic fields on a high-resolution grid of 100 m × 100 m, using observations from two dense meteorological station networks: the WegenerNet Feldbach Region (FBR), located in a region predominated by a hilly terrain, and its Alpine sister network, the WegenerNet Johnsbachtal (JBT), located in a mountainous region.

The wind fields of these different empirical–dynamical modeling approaches were intercompared for thermally induced and strong wind events, using hourly temporal resolutions as supplied by the WPG, with the focus on evaluating spatial differences and displacements between the different datasets. For this comparison, a novel neighborhood-based spatial wind verification methodology based on fractions skill scores (FSSs) is used to estimate the modeling performances. All comparisons show an increasing FSS with increasing neighborhood size. In general, the spatial verification indicates a better statistical agreement for the hilly WegenerNet FBR than for the mountainous WegenerNet JBT. The results for the WegenerNet FBR show a better agreement between INCA and WegenerNet than between CCLM and WegenerNet wind fields, especially for large scales (neighborhoods). In particular, CCLM clearly underperforms in the case of thermally induced wind events. For the JBT region, all spatial comparisons indicate little overlap at small neighborhood sizes, and in general large biases of wind vectors occur between the regional climate model (CCLM) and analysis (INCA) fields and the diagnostic (WegenerNet) reference dataset.

Furthermore, grid-point-based error measures were calculated for the same evaluation cases. The statistical agreement, estimated for the vector-mean wind speed and wind directions again show better agreement for the WegenerNet FBR than for the WegenerNet JBT region. A combined examination of all spatial and grid-point-based error measures shows that CCLM with its limited horizontal resolution of 3 km × 3 km, and hence too smoothed an orography, is not able to represent small-scale wind patterns. The results for the JBT region indicate significant biases in the INCA analysis fields, especially for strong wind speed events. Regarding the WegenerNet diagnostic wind fields, the statistics show acceptable performance in the FBR and somewhat overestimated wind speeds for strong wind speed events in the Enns valley of the JBT region.

1 Introduction

Surface wind is often regarded as one of the most difficult meteorological variables to model, particularly over areas of complex terrain like the Alps (Whiteman, 2000; Sfetsos, 2002; Abdel-Aal et al., 2009; Gómez-Navarro et al., 2015). Therefore, realistic high-resolution wind fields cannot be generated with coarse-resolution models or by a simple

interpolation of wind station data onto regular grids. Innovation in computer sciences, new methods in weather analysis or nowcasting models, advanced software architectures used in regional climate models (RCMs), and the growing power of computers in the meantime led to highly resolved outputs from such models at the 1 km scale (Awan et al., 2011; Suklitsch et al., 2011; Prein et al., 2013b; Prein et al., 2015; Leutwyler et al., 2016; Kendon et al., 2017).

These models, however, contain various limitations and sources of uncertainties. In the case of weather analysis fields, which represented mixed empirical and dynamical modeling from data assimilation, these limitations and uncertainties result from too little meteorological station and remote-sensing data, and in the case of RCMs they include deviations in the driving dataset, physical and numerical approximations, as well as parameterizations of processes at the sub-grid scale (Gómez-Navarro et al., 2015).

To evaluate and improve these analyses and models, meteorological observations and especially gridded empirical datasets at high spatial and temporal resolutions are needed. The model outputs generally represent the involved processes as areal averages rather than on a point-scale (Osborn and Hulme, 1998; Prein et al., 2015). Therefore, gridded meteorological evaluation datasets, with each (aggregated) grid value being a best-estimate average of the grid cell observations, are the most appropriate evaluation datasets (Haylock et al., 2008; Haiden et al., 2011; Hiebl and Frei, 2016).

To investigate weather and climate on a local 1 km scale as well as evaluating RCMs, the Wegener Center at the University of Graz operates two high-resolution meteorological station networks (Fig. 1): the very high-density WegenerNet Feldbach Region (FBR) in southeastern Styria, Austria (Fig. 1a), and the high-density WegenerNet Johnsbachtal (JBT) in northern Styria, Austria (Fig. 1b); details are introduced in Sect. 2 below.

For both networks, diagnostic wind fields on a high-resolution grid of 100 m × 100 m are generated by a weather diagnostic application, the WegenerNet Wind Product Generator (WPG). Schlager et al. (2017) introduced the WPG and its performance evaluation for the WegenerNet FBR, which was then advanced by Schlager et al. (2018) to the WegenerNet JBT region and a longer-term evaluation in both FBR and JBT. Jointly these studies established the level of quality of the empirical WPG wind fields. In this study, we now make use of these empirical high-resolution wind fields as reference data in order to intercompare them with empirical–dynamical wind field analysis data and with dynamical regional climate model data.

In this study, we intercompare the empirical WegenerNet wind fields (Schlager et al., 2017, 2018) with empirical–dynamical wind field analysis data from the Integrated Nowcasting through Comprehensive Analysis (INCA) (Haiden et al., 2011) system and with regional climate model data from the Consortium for Small Scale Modeling Model in Climate Mode (CCLM) (Böhm et al., 2006; Rockel et al., 2008). The intercomparisons aim at obtaining useful and robust information about performance limits for these empirical and dynamical modeling approaches for regions with very different topographic characteristics and weather situations. Furthermore, we co-analyze the impact of different horizontal resolutions, which will inevitably always be a challenge for the wide diversity of data products typically available.

Besides traditional grid-point-based verification methods, we use a novel wind verification methodology, recently developed by Skok and Hladnik (2018). This neighborhood-based spatial verification method avoids the "double-penalty" problem and can distinguish forecasts depending on the spatial displacement of wind patterns (Skok and Hladnik, 2018). A double-penalty problem arises when using traditional statistical methods for datasets which contain an offset between the modeled and the reference data. In that case, the modeled data are penalized twice: first, for simulating an event where it did not occur and, second, for failing to simulate an event where it did actually occur (Roberts, 2008; Prein et al., 2013a; Skok and Hladnik, 2018). So our primary motivation for this study is indeed to explore and provide improved insight by careful intercomparisons of the relative performance strength and weakness of empirical and dynamical wind field modeling at high spatial resolution over complex terrain where actual wind station observations will generally be available at sparse station density.

The paper is structured as follows. Section 2 provides a description of the study areas and basic information about the model data. Section 3 presents defined evaluation cases and the methodology for the automatic selection of typical wind events followed by a description of the methods used to evaluate model results. In the subsequent Sect. 4, results are presented and discussed in detail. Finally, in Sect. 5 we summarize our results and draw our conclusions.

2 Study areas and model data

2.1 Study areas

The first study area, the WegenerNet FBR (indicated by the orange-framed white rectangle in the middle panel of Fig. 1, enlarged in a) lies in the Alpine foreland of southeastern Styria, Austria, centered near the town of Feldbach (46.93° N, 15.90° E). It covers a dense grid of 155 meteorological stations within an area of about 22 km × 16 km, in a hilly terrain, characterized by small differences in altitude (Kirchengast et al., 2014). The typical difference in altitude between the valleys and the crests is about 100 m and the highest peak is the Gleichenberger Kogel, with an elevation of 598 m.

This region, with a more Alpine climate at the valley floors and more Mediterranean climate along hillsides, is quite sensitive to climate change (Wakonigg, 1978; Kabas et al., 2011; Hohmann et al., 2018). Furthermore, it exhibits rich weather

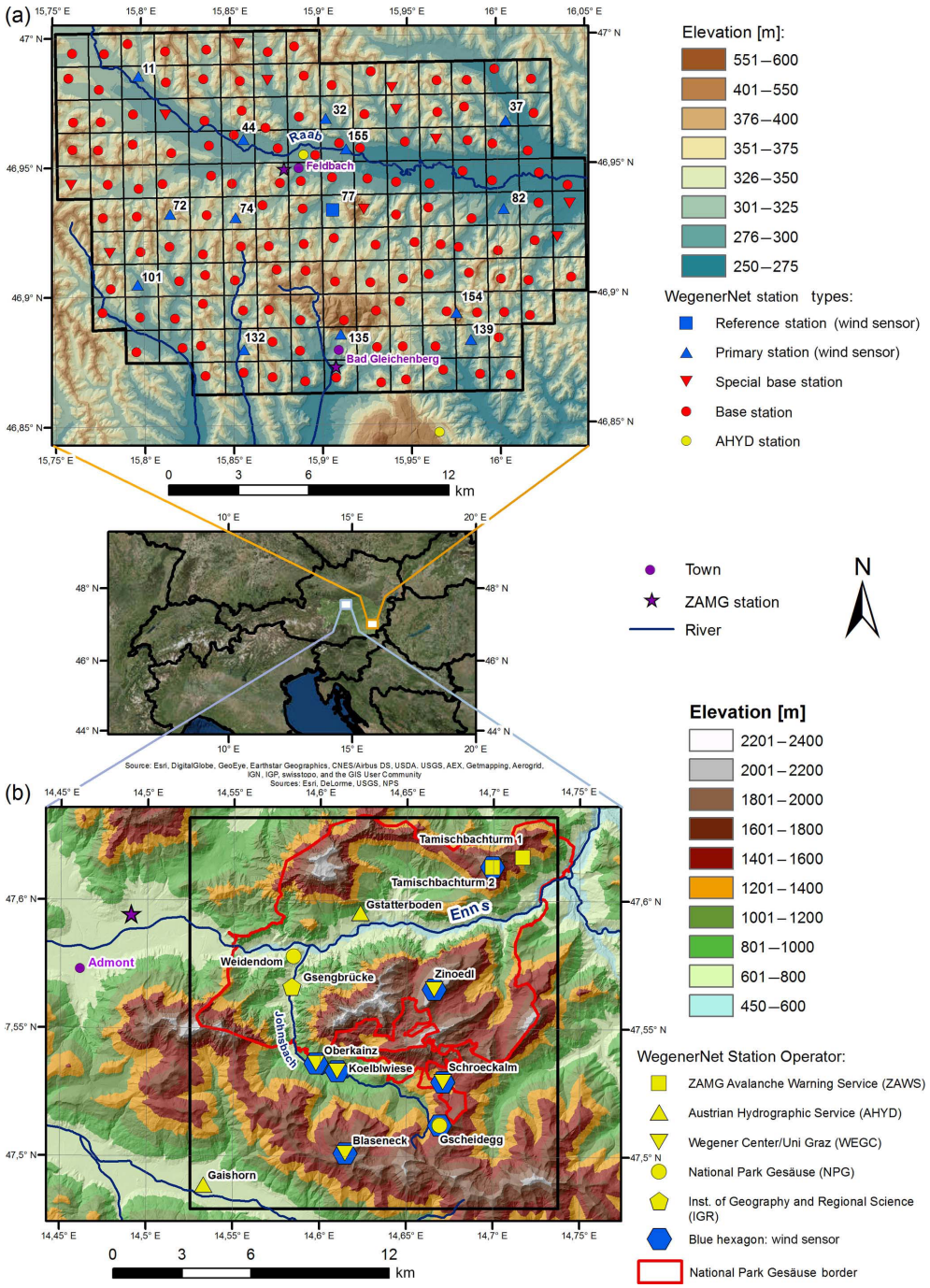

Figure 1. Location of the study areas in Austria (small middle panel between **a** and **b**), the WegenerNet Feldbach Region (FBR) in the southeast of the state of Styria and the WegenerNet Johnsbachtal (JBT) region in the north of Styria (white rectangles, enlarged in **a** and **b**). **(a)** The WegenerNet FBR with its 155 meteorological stations, with the legend explaining map characteristics and station types. **(b)** Map of the WegenerNet JBT region (black rectangle) including its meteorological stations, with the legend explaining map characteristics and station operators.

variability, especially through strong convective activity and severe weather in summer (Kirchengast et al., 2014; Kann et al., 2015a; O et al., 2017, 2018; Schroeer and Kirchengast, 2018). The wind fields in this study area are characterized by thermally induced local flows and influenced by thermally driven regional wind systems with weak wind speeds, caused by a dynamical process called Alpine pumping (Lugauer and Winkler, 2005). Furthermore, nocturnal drainage

winds, which lead to cold air pockets, are relevant for this region, which is dominated by agriculture. Especially in fall and winter, the nocturnal cold air production is amplified by temperature inversions in relation to high-pressure weather conditions. In the WegenerNet FBR, hillside locations are thermally preferred to valley locations at night. Results related to the WPG-diagnosed empirical wind fields in the WegenerNet FBR can be found in Schlager et al. (2017, 2018).

The second study area, the WegenerNet JBT (indicated by the gray-framed white rectangle in the middle panel of Fig. 1, enlarged in b), is named after the Johnsbachtal river basin (location of the village of Johnsbach: 47.54° N, 14.58° E) and situated in the eastern Alpine region, in the Ennstaler Alps and the Gesäuse National Park, in northern Styria, Austria. The terrain of this mountainous region is characterized by large differences in elevation. The Hochtor, with an elevation of 2369 m, is the highest summit, and the valleys lie roughly at a height of 600 to 800 m (Strasser et al., 2013; Schlager et al., 2018). This region spans an area of about 16 km × 17 km and comprises 11 irregularly distributed meteorological stations including two summit stations at altitudes of 2.191 and 1.969 m (Schlager et al., 2018).

The climate is Alpine with mean annual temperatures of around 8 to 0 °C and an annual precipitation of about 1.500 to 1.800 mm from the valley to the summit regions (Wakonigg, 1978; Prettenthaler et al., 2010). Typical for this region are thermally induced local flows and westerly flow synoptic weather conditions. Details related to initial studies and their results as well as to the cooperation and partnerships can be found in Strasser et al. (2013) and in their most up-to-date form in Schlager et al. (2018). Recently, Schlager et al. (2018) computed and evaluated WPG-generated empirical wind fields in this region.

2.2 WegenerNet data

The data acquired from the two WegenerNet regions FBR and JBT are automatically quality controlled and processed by the WegenerNet Processing System (WPS), consisting of four subsystems (Kirchengast et al., 2014): the Command Receive Archiving System transfers raw measurement data via wireless transmission to the WegenerNet database in Graz, the Quality Control System checks the data quality, the Data Product Generator (DPG) generates regular station time series and gridded fields of weather and climate products, and the Visualization and Information System offers the data to users via the WegenerNet data portal (https://wegenernet.org/portal/, last access: 2 July 2019).

Besides weather and climate time series, based on a spatial interpolation of the station observations, the DPG generates gridded fields of the variables temperature, precipitation, and relative humidity for the WegenerNet FBR. These gridded products of the WegenerNet FBR are available to users in near-real time with a latency of about 1–2 h. Kirchengast et al. (2014) and Kabas (2012) provide detailed information about the subsystems of the WPG.

The DPG furthermore includes a newly developed wind field application, the WPG, as briefly introduced in Sect. 1. The WPG provides high-resolution wind fields for the WegenerNet FBR as well as for the WegenerNet JBT. The WPG uses the freely available empirical California Meteorological Model (CALMET) as core tool and generates, based on meteorological observations, terrain elevations, and information about land use and mean wind fields at 10 and 50 m height levels with a spatial resolution of 100 m × 100 m and a temporal resolution of 30 min, again with a maximum latency of about 1–2 h. In order to keep the meteorological input data of the WPG independent from the data pertaining to the other operational station networks, observations from the Central Institute for Meteorology and Geodynamics (ZAMG) stations (violet stars in Fig. 1a and b) and other external stations are not used as WPG input. For the WegenerNet FBR, the gridded wind fields are available starting in 2007 and for the WegenerNet JBT starting in 2012. The wind fields at 10 m height level are used for the model intercomparisons.

The CALMET model is a diagnostic model that omits time-consuming integrations of nonlinear equations, such as the governing equations of dynamical models (Truhetz, 2010; Seaman, 2000; Ratto et al., 1994). It is hence not capable of simulating dynamic processes such as flow splitting and grid-resolved turbulence or of delivering prognostic information. Specific parameterizations allow the model to empirically take into account conditions such as the kinematic effects of terrain, slope flows, and terrain-blocking effects (Scire et al., 1998; Cox et al., 2005; Seaman, 2000). We enhanced the model by implementing methods developed by Bellasio et al. (2005) to as well take into account topographic shading through relief, topographic slope and aspect, and the sun position for the estimation of solar radiation. In addition, the modeling of temperature fields is now based on vertical temperature gradients, calculated from meteorological station observations located at different altitudes, and the influence of vegetation cover is taken into account. Details about these advanced algorithms can be found in Bellasio et al. (2005).

The quality of the generated wind fields depends above all on the quality and the spatial and temporal resolution of the meteorological observations and surface-related datasets which are used as model input (Schlager et al., 2017, 2018; Morales et al., 2012; Cox et al., 2005; Gross, 1996). A detailed description of the WPG application and the statistical results for the WegenerNet FBR can be found in Schlager et al. (2017). More information regarding statistical results related to the WegenerNet JBT as well as information regarding evaluation results from 5-year climate data of the WegenerNet JBT in comparison to 9-year climate data from the WegenerNet FBR can be found in Schlager et al. (2018).

2.3 INCA data

The INCA system has been developed at the ZAMG in Vienna, Austria, to provide realistic analyses and nowcasts of quantities of several meteorological variables for the highly mountainous and the overall complex terrain of Austria. In the case of the variable wind, the system operationally generates spatially distributed analysis wind fields in 3-D and for 10 m height above ground with a horizontal grid spacing of 1 km × 1 km and a temporal resolution of 1 h.

The basic idea of the INCA wind module is to statistically correct a numerical weather prediction (NWP) model first guess (i.e., in operational mode the latest available NWP model run) with the latest observational data, which do not enter the NWP data assimilation. Thus, the skill of the INCA analysis depends on the station density, their representativeness, and the spatial distribution of station observations, as well as on the skill of the NWP model providing the first guess. The impact of the NWP model on the analysis skill is further discussed in Kann et al. (2015b).

In this study, NWP model outputs used as a first guess for INCA were generated by the spectral ARPEGE-ALADIN (ALARO) model in a revised version (Wang et al., 2006). ALARO has a horizontal grid spacing of 4.8 km × 4.8 km (600 × 540 grid points) and includes 60 vertical layers up to the 2 hPa level (about 43 km altitude), covering central Europe, eastern France, and the northern part of the Mediterranean Sea. It is run with a temporal resolution of 180 s using a hydrostatic semi-implicit semi-Lagrangian dynamical solver (Bubnová et al., 1995) and the ALARO-0 physics package, which includes the 3MT microphysics-convection scheme (Gerard and Geleyn, 2005), the Interaction Soil Biosphere Atmosphere (ISBA) force restore 2 L soil scheme (Noilhan and Planton, 1989), and the Actif Calcul de Rayonnement et Nebulosité (ACRANEB) radiation scheme (Ritter and Geleyn, 1992). Soil temperature and moisture are initialized by a 6 h-cycle optimal interpolation data analysis taking into account the latest ALARO forecast as a first guess and 2 m relative humidity and temperature observations from synoptic (SYNOP) and national stations. The 2 m values are transferred to soil variables via empirical relations (Giard and Bazile, 2000). To reduce initial spin-up, a digital filter initialization is applied.

The model gets its lateral boundary and atmospheric initial conditions from the high-resolution deterministic operational global integrated forecast system (IFS) of the European Centre for Medium-range Weather Forecasts (ECMWF) model in lagged mode (i.e., ALARO 00:00 UTC is linked to IFS 18:00 UTC of the day before, ALARO 06:00 UTC to IFS 00:00 UTC, etc.). This is due to the rather late availability of the IFS data. Coupling is achieved by one-way nesting via Davies relaxation (Davies, 1976). Sea surface temperature is interpolated from the deterministic IFS model to the ALARO grid. More details about ALARO development and configurations can be found in Termonia et al. (2018).

The INCA wind fields have already been evaluated for a moderately hilly region in the north of Austria (47.78–49° N, 13.8–17° E), where the wind analyses show significantly higher errors compared to the statistical results from other meteorological variables (Haiden et al., 2011). These higher errors mainly root in the limited representativeness of station data, as well as on the low station density, which can be only partly compensated for by INCA's analysis algorithms (Haiden et al., 2011).

In the WegenerNet FBR area, INCA assimilates observations from the ZAMG Feldbach and Bad Gleichenberg stations (violet stars in Fig. 1a) to the NWP's first guess, and in the WegenerNet JBT region, observations from the ZAMG Admont station are used. However, data from WegenerNet FBR and JBT stations are not used in INCA data assimilation and hence the WPG fields can be used for independent evaluation (Haiden et al., 2011).

The coordinate system of the INCA datasets is transformed into WGS84/UTM zone 33° N coordinates. Furthermore, we resampled the wind fields at 10 m height levels from the INCA gridding onto the WegenerNet FBR and WegenerNet JBT grids, using a bilinear interpolation method. Based on extensive sensitivity tests regarding different interpolation methods, we concluded that the statistical results do not significantly depend on the interpolation method.

2.4 CCLM data

Regarding the CCLM (Rockel et al., 2008), we use available wind fields generated with the model version 5.0. These wind fields were generated during the course of a previous study and are available for the period 2008 to 2010. The data have a comparatively coarse horizontal resolution of 3 km × 3 km on an hourly basis that is nevertheless the highest resolution available to this study. This limited resolution leads to a smoothed orography, which may result in different wind patterns with errors in wind speed or direction. Furthermore, the winds may be displaced by an incorrect position of the topographic slopes (Skok and Hladnik, 2018; Prein et al., 2013b). The CCLM fields are provided for 40 vertical levels. The first level is simulated for 10 m above ground and the last level corresponds to the 100 hPa level (about 16 km altitude), whereby the vertical resolution is higher in the boundary layer and decreases towards the top level.

CCLM is a non-hydrostatic model with a Runge–Kutta dynamical core, which makes use of a third-order scheme with diffusion damping to discretize the advection term in the compressible Euler equations (Wicker and Skamarock, 2002). In order to avoid numerical instability, the model's orography is additionally smoothed via a 10th-order Raymond (1988) filter. The vertical coordinate system is a terrain-following, time-invariant Gal-Chen pressure-based sigma coordinate (Gal-Chen and Somerville, 1975). Deep and shallow convection are parameterized following Tiedtke (1989), and turbulence is parameterized based on Mellor

and Yamada (Raschendorfer, 2001). Vertical mixing comes from a prognostic formulation of the turbulent kinetic energy (TKE) with a 2.5 closure that accounts for grid- and subgrid-scale water and ice clouds. It uses a statistical cloud scheme for cloud cover and cloud water content (so-called Gaussian closure scheme). Horizontal diffusion follows the Smagorinsky approach.

Land cover data for CCLM are based on the Global Land Cover 2000 project (EEA, 2016) from SPOT4 satellite products (Bartalev et al., 2003). In the model setup used (3 km resolution), deep convection is resolved explicitly, which means that parameterization for deep convection was switched off. Shallow convection is still parameterized. In climate research, such simulations are referred to as convection-permitting climate simulations (CPCSs) (Prein et al., 2013a). To minimize decoupling effects from model-internal variability, which usually occurs in large model domains and if nudging techniques are not used (Kida et al., 1991), CCLM is operated in a small domain encompassing the greater Alpine region, and it is also driven by ECMWF's IFS. The data assimilation system IFS includes a wide range of observations and is assumed to provide perfect boundary conditions with a horizontal grid spacing of about 25 km at midlatitudes and at 91 vertical levels (Bechtold et al., 2008). Every 6 h (00:00, 06:00, 12:00, 18:00 UTC) of the IFS data is an analysis field from the assimilation system, and every alternate 6 h (03:00, 09:00, 15:00, 21:00 UTC) is a short-range forecast field. This procedure has already been used by Suklitsch et al. (2011) and keeps the modeled synoptic patterns in agreement with the observed ones.

In the course of the data preparation for the study, CCLM data at 10 m height level were also transformed into WGS84/UTM zone 33N coordinates, resampled and mapped onto the high-resolution WPG grid, and checked for sensitivity with respect to the interpolation method which was also found to be weak (see Sect. 2.3 above).

3 Evaluation events and methods

3.1 Events for wind field evaluation

The WegenerNet, INCA, and CCLM wind fields are intercompared for two representative types of wind events: thermally induced wind events and strong wind events. For this purpose, we defined eight evaluation cases, four for each of the two study areas (Table 1). For the cases shown in Table 1 we use the WegenerNet data as a reference, except for evaluating the CCLM wind fields for the WegenerNet JBT. The reason for this is that the CCLM data used in this study are available from January 2008 to December 2009, but the WegenerNet JBT data are available only as of January 2012, since this latter network has been sufficiently completed for long-term monitoring only since 2012 (Table 1, cases CCLMvsINCA_therm_JBT and CCLMvsINCA_strong_JBT).

In both study areas, autochthonous weather conditions mainly lead to thermally induced wind systems, meaning that the wind fields are controlled by small-scale temperature and pressure gradients. These small-scale gradients lead to characteristic interacting systems of air motion, like slope winds and mountain-valley winds, and create complex everyday flow patterns. The autochthonous days are characterized by small synoptic influences, cloudless or nearly cloudless skies, low relative humidity and increased radiation fluxes between the Earth surface and the atmosphere (Prettenthaler et al., 2010). Due to frequently occurring temperature inversions in relation to clear-sky and high-pressure weather conditions in winter, which often lead to a stable atmospheric stratification in the whole WegenerNet FBR and in the valley regions of the WegenerNet JBT, autochthonous days are only selected from spring, summer, and fall (March to October).

The automatic selection of thermally induced and strong wind events is done based on thresholds, which we defined based on sound physical and careful sensitivity checks summarized in Table 2. For the estimation of autochthonous days, we compared the observed daytime mean values of wind speed (v) and relative humidity (rh) as well as the nighttime mean values of net radiation (Q_{n}) from selected stations with the respective thresholds. A further criterion for the selection of such days is high daily global radiation, which indicates fair weather conditions. For this purpose, we compared the daily mean modeled global radiation ($Q_{\mathrm{g,m}}$) for clear-sky conditions with the observed daily mean net radiation ($Q_{\mathrm{n,o}}$) for the WegenerNet FBR and with the observed daily mean global radiation ($Q_{\mathrm{g,o}}$) for the WegenerNet JBT at defined station locations (Table 2, reference data). The reason for the comparison of $Q_{\mathrm{g,m}}$ with $Q_{\mathrm{n,o}}$ for the WegenerNet FBR is that this station network includes no global radiation sensors. Due to the almost linear relationship between the daytime $Q_{\mathrm{g,o}}$ and $Q_{\mathrm{n,o}}$ for clear-sky conditions, we find that the same selection method can robustly be applied to both study areas by defining different thresholds (Table 2, $Q_{\mathrm{g,m}}$–$Q_{\mathrm{n(g),o}}$). If all criteria are fulfilled for a given day, the data from the entire day are added to the thermally induced wind event dataset, leading to 24 h events (i.e., 24 h mean wind speed values).

The modeling of the global radiation is done based on ESRI's ArcGIS Area Solar Radiation Tool. This tool is designed for local landscape scales and derives the incoming solar radiation based on a digital elevation model. Small differences of daily mean values between $Q_{\mathrm{g,m}}$ and $Q_{\mathrm{n(g),o}}$ indicate fair weather conditions and high global radiations during the day. If all criteria are fulfilled for a given day, the data from that day are included in the thermally induced wind events dataset.

The strong wind events, caused by synoptic weather conditions such as cyclones and frontal system at a larger scale, are selected on an hourly basis from preselected days, by com-

Table 1. Characteristics of wind field evaluation cases used for the WegenerNet, INCA, and CCLM intercomparisons (top half for the WegenerNet FBR; bottom half for the WegenerNet JBT region).

Evaluation case	Type	Region	Modeled dataset	Reference dataset	Period
	WegenerNet FBR				
INCAvsWN_therm_FBR	thermally	FBR	INCA	WN	2008–2017
INCAvsWN_strong_FBR	strong	FBR	INCA	WN	2008–2017
CCLMvsWN_therm_FBR	thermally	FBR	CCLM	WN	2008–2010
CCLMvsWN_strong_FBR	strong	FBR	CCLM	WN	2008–2010
	WegenerNet JBT				
INCAvsWN_therm_JBT	thermally	JBT	INCA	WN	2012–2017
INCAvsWN_strong_JBT	strong	JBT	INCA	WN	2012–2017
CCLMvsINCA_therm_JBT	thermally	JBT	CCLM	INCA	2008–2010
CCLMvsINCA_strong_JBT	strong	JBT	CCLM	INCA	2008–2010

Table 2. Limits for the selection of thermally induced or strong wind events for the defined evaluation cases shown in Table 1 (top half for the WegenerNet FBR; bottom half for the WegenerNet JBT).

Evaluation variable[a] case	$\overline{v}$ ($\mathrm{m\,s^{-1}}$) (reference data[b])	v ($\mathrm{m\,s^{-1}}$) (reference data[b])	rh (%) (reference data[b])	$Q_{\mathrm{g,m}}$–$Q_{\mathrm{n(g),o}}$ ($\mathrm{W\,m^{-2}}$) (reference data[b])	Q_{n} ($\mathrm{W\,m^{-2}}$) (reference data[b])	Number of events[c]
	WegenerNet FBR					
INCAvsWN_therm_FBR	–	< 1.5 ($\mathrm{RS_{dm}}$)	< 65.0 ($\mathrm{RS_{dm}}$)	< 100.0 ($\mathrm{RS_{dm}}$)	< 30.0 ($\mathrm{RS_{nm}}$)	1632
INCAvsWN_strong_FBR	> 2.5 ($\mathrm{WN_{dm}}$)	> 3.0 ($\mathrm{WN_{hm}}$)	–	–	–	830
CCLMvsWN_therm_FBR	–	< 1.5 ($\mathrm{RS_{dm}}$)	< 65.0 ($\mathrm{RS_{dm}}$)	< 100.0 ($\mathrm{RS_{dm}}$)	< 30.0 ($\mathrm{RS_{nm}}$)	264
CCLMvsWN_strong_FBR	> 2.5 ($\mathrm{WN_{dm}}$)	> 3.0 ($\mathrm{WN_{hm}}$)	–	–	–	259
	WegenerNet JBT					
INCAvsWN_therm_JBT	–	< 2.0 ($\mathrm{SCH_{dm}}$)	< 65.0 ($\mathrm{SCH_{dm}}$)	< 20.0 ($\mathrm{SCH_{dm}}$)	< 30.0 ($\mathrm{SCH_{nm}}$)	2232
INCAvsWN_strong_JBT	> 9.5 ($\mathrm{WN_{dm}}$)	> 9.0 ($\mathrm{INCA_{hm}}$)	–	–	–	1450
CCLMvsINCA_therm_JBT	–	–	< 65.0 ($\mathrm{WEI_{dm}}$)	< 20.0 ($\mathrm{WEI_{dm}}$)	–	768
CCLMvsINCA_strong_JBT	> 6.0 ($\mathrm{INCA_{dm}}$)	> 6.0 ($\mathrm{INCA_{hm}}$)	–	–	–	182

[a] $\overline{v}$: average wind speed; v: wind speed; rh: relative humidity; $Q_{\mathrm{g,m}}$–$Q_{\mathrm{(n)g,o}}$: difference between mean modeled global radiation ($Q_{\mathrm{g,m}}$) and observed net radiation ($Q_{\mathrm{n,o}}$) for the WegenerNet FBR and difference between $Q_{\mathrm{g,m}}$ and observed global radiation ($Q_{\mathrm{g,o}}$) for the WegenerNet JBT; Q_{n}: net radiation. [b] RS: Reference Station (Nr. 77); SCH: Schroeckalm station; WEI: Weidendom station; dm: daytime mean value from observations (from sunrise until sunset); nm: nighttime mean value from observations (from sunset until sunrise); $\mathrm{WN_{dm}}$: daily mean value from gridded WegenerNet wind speed; $\mathrm{WN_{hm}}$: hourly mean value from gridded WegenerNet wind speed; $\mathrm{INCA_{dm}}$: daily mean value from gridded INCA wind speed; $\mathrm{INCA_{hm}}$: hourly mean value from gridded INCA wind speed. [c] Hourly wind events; i.e., hours are used as the base period for the statistical analysis.

paring hourly mean values from gridded reference datasets with defined minimum wind speeds. These preselected days were estimated by comparing the daily average wind speed from the gridded datasets with a defined minimum average wind speed (Table 2, $\overline{v}$ and v for strong wind speed cases). If the hourly mean value of this reference dataset is larger than the defined minimum wind speed, the data of this reference dataset and the corresponding model dataset are used as part of the hourly event data for evaluating strong wind events.

3.2 Statistical evaluation methods

In order to account for spatial differences and displacements between the model and the reference data and to analyze wind speed and direction in a combined way, we apply a novel wind verification methodology. This methodology extends the fractions skill score (FSS), a spatial verification metric developed by Roberts (2008), which is classified as a neighborhood-based approach and originally used for verifying precipitation. The FSS is based on the assumption that a model is useful when the model data and the corresponding reference data show a similar spatial frequency of precipitation events, which alleviates the requirement of the models to predict the events at exactly correct positions, which is an unduly strict assumption. Furthermore, this metric avoids the double-penalty problem and provides scale-dependent information about the level of model skill (Gilleland et al., 2010; Roberts, 2008).

In order to obtain information on how the skill of a model varies with spatial scale, the FSS is calculated for different neighborhood sizes. A neighborhood size of n defines a square consisting of $n \times n$ grid points; i.e., it denotes the side length of the square (e.g., for $n = 5$, the square contains 25 grid points). These squares of defined neighborhood sizes are moved as sliding windows over the datasets and centered

successively at each grid point, whereby the area outside the domain is assumed to contain no wind class. In terms of the FSS value, it is a 0-to-1 normalized metric; i.e., the lower limit of the FSS is 0 and the upper limit +1, with values approaching +1 representing a better degree of model performance.

The extended version of the FSS is called the wind fractions skill score, denoted WFSS, which has been developed by Skok and Hladnik (2018). The score is calculated based on user-defined wind classes. The definition of these classes is partly subjective and can significantly affect the WFSS. The wind vector field should be classified in such a way, that the definition reflects what a user wants to analyze. For example, a complex terrain leads to strong changes in wind directions; therefore, it is reasonable to define smaller class intervals regarding the wind directions. For upper-level winds the focus could be more on the magnitude of wind speed.

We defined eight wind direction classes with an interval size of 45° for a range of three wind speed categories, as shown in the wind roses of Fig. 2. Wind speeds $< 0.5\,\mathrm{m\,s^{-1}}$ were classified as calm, independently of the wind direction. The small interval size of 45° was chosen to be able to capture the varying wind directions in the study areas, especially for thermally induced winds. Because of the generally much lower wind speeds in WegenerNet FBR, we defined a smaller interval size of the wind speed categories for this region (Fig. 2a and b, lower panels) than for the WegenerNet JBT (Fig. 2c and d, lower panels).

Table 3 includes the equations for the calculation of the WFSS and the asymptotic WFSS (AWFSS). This AWFSS will always be reached for a neighborhood size $\geq 2N-1$, where N is the number of grid points of the largest domain size. At such a large neighborhood size, the estimated fractions within the domain are the same at all locations, and further enlarging this size will not affect the WFSS. A bias always leads to an AWFSS value < 1, which indicates systematic differences in the frequency of wind classes between the model and the reference wind classification.

The WFSS is calculated for each hourly field for the selected events. The event-averaged score values are calculated based on averaging these 1 h event WFSS values over all the hourly events within the analyzed multiyear period, for each evaluation case listed in Table 1.

As briefly explained above, the chosen thresholds of the classification and the number of classes influence the score. We found, in particular, that the wind direction thresholds can have a strong impact on the score values. For example, a small change in the wind direction value from prevailing northwesterly winds, which are close to a threshold to distinguish between W and N, could dramatically change the WFSS value. Such a small error in the model data could indicate a poor modeling performance, whereas a human analyst would assess the forecast as reasonably good. To avoid this problem we calculated the hourly WFSS for every rotation between 0 and 45° with an interval size of 5° (nine trail classes), in addition to the original class definition. As a next step, the maximum values of the hourly score values at each neighborhood size are always used for computing the final case-averaged score values. We applied this approach for 7597 selected events in total (Table 2, number of events) and estimated the case-averaged score value for each of the eight evaluation cases. A more detailed description of the wind fractions skill score metric can be found in Skok and Hladnik (2018).

Furthermore, we applied traditional grid-point-based statistical performance measures such as bias, root-mean-square error, and others, to each evaluation case. All statistical performance metrics used in this study are summarized in Table 3.

4 Results

4.1 Evaluation for selected wind events

Figure 2a–d illustrate typical examples of modeled wind fields (upper rows of panels) and the corresponding wind roses of relative frequency of wind directions divided by wind speed categories (lower rows of panels) from selected representative evaluation events. Each panel depicts the modeled and the associated reference data for the WegenerNet FBR (Fig. 2a and b) and the WegenerNet JBT (Fig. 2c and d), for thermally induced (Fig. 2a and c) and strong wind events (Fig. 2b and d). Figure 2e shows the WFSS values of these examples, estimated as explained in Sect. 3.2 above.

The thermally induced wind event on the 29 July 2009 from 16:00 to 17:00 UTC for the WegenerNet FBR (Fig. 2a) shows thermally driven regional flows caused by Alpine pumping. This flow is called "Antirandgebirgswind", which arises usually in the afternoon as southerly wind with maximum wind speeds of about $2.5\,\mathrm{m\,s^{-1}}$. The Antirandgebirgswind is a compensating flow between the bordering mountains of the eastern Alps, and the hilly countryside region of southeastern Styria (called Riedelland), which comprises the WegenerNet FBR (Wakonigg, 1978). The INCA (upper-left panel of Fig. 2a) and the WegenerNet wind fields (upper-right panel of Fig. 2a) show a similar distribution with generally low wind speeds and prevailing southerly wind directions. The intercomparison of these INCA data with WegenerNet data for this event shows the largest WFSS values for all neighborhood sizes, which indicates a good overlap of the wind classes (Fig. 2e, INCAvsWN_therm_FBR). Furthermore, it shows a nearly perfect asymptotic value of about 0.99. This large AWFSS indicates a very small bias, which is also reflected by the similar wind classification results (lower-left and lower-right panel of Fig. 2a).

The CCLM wind field shows similarly low wind speeds, compared to the WegenerNet wind field, but a shift in wind directions from the S sector mainly to the SE and partly to the E and NE sectors between the CCLM and the We-

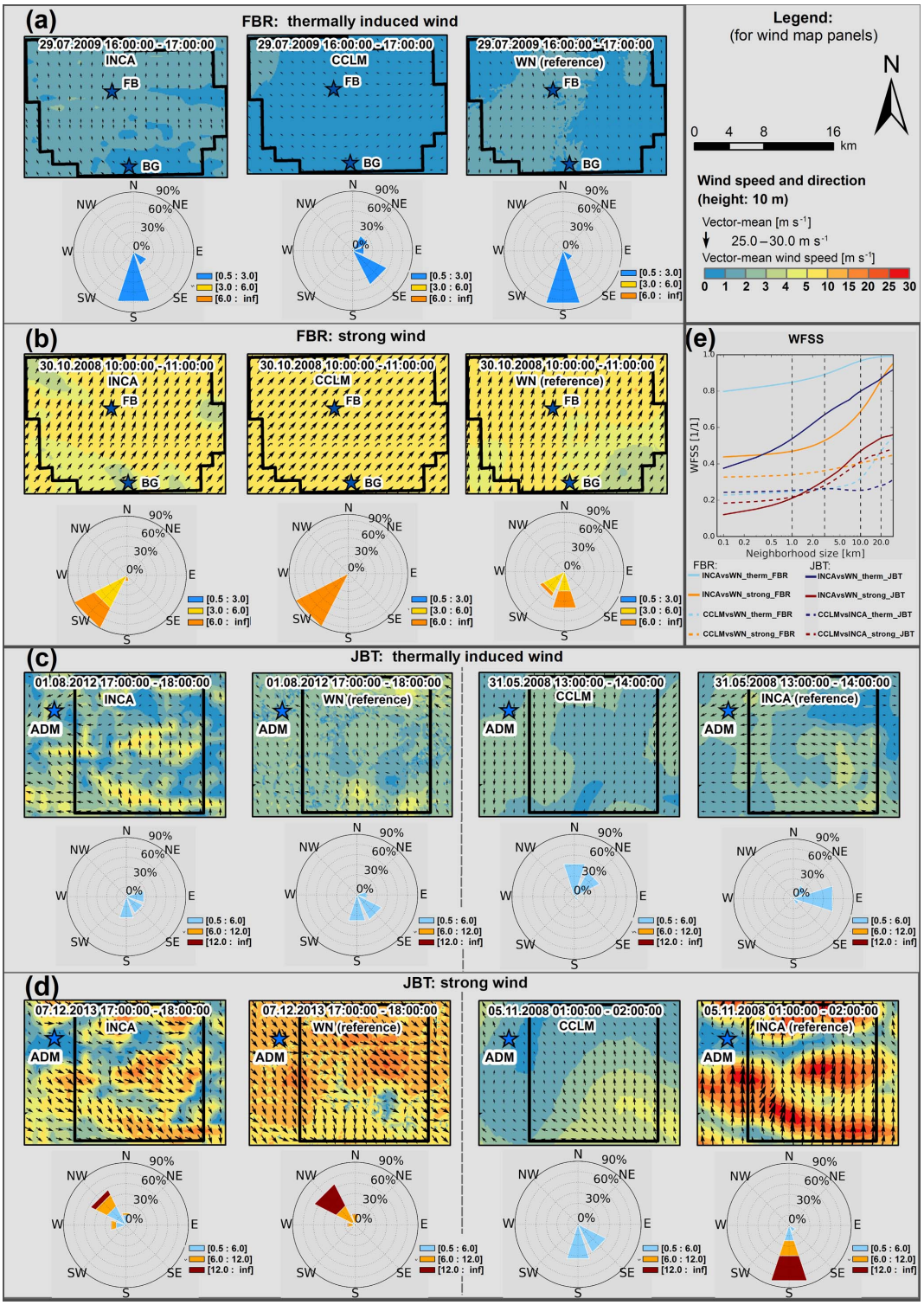

Figure 2. Wind fractions skill score (WFSS) analysis for selected 1 h wind fields for the WegenertNet FBR **(a, b)** and the WegenerNet JBT region **(c, d)**. **(a)**–**(d)** Modeled and reference wind fields (first row) and corresponding relative frequency of wind directions for a range of wind speed categories (second row) in each panel. **(e)** WFSS results for the modeled versus reference wind fields from **(a)** to **(d)**. See Table 1 for more information on the evaluation cases.

Table 3. Statistical performance parameters used for the intercomparison of the wind field modeling results.

Parameter	Equation	Remarks
Wind fractions skill score	$\mathrm{WFSS} = 1 - \frac{\sum_k \sum_{i,j} [O_k(i,j) - M_k(i,j)]^2}{\sum_k \left\{ \sum_{i,j} O_k(i,j)^2 + \sum_{i,j} M_k(i,j)^2 \right\}}$	O_k: fraction values for observations for wind class k at location i, j; M_k: fraction values for model data for wind class k at location i, j (Skok and Hladnik, 2018; Roberts, 2008)
Asymptotic WFSS	$\mathrm{AWFSS} = 1 - \frac{\sum_k \left(f_k^O - f_k^M\right)^2}{\sum_k \left\{ \left(f_k^O\right)^2 + \left(f_k^M\right)^2 \right\}}$	f_k^O: frequency of wind class k in the observations; f_k^M: frequency of wind class k in the model data (Skok and Hladnik, 2018)
Bias	$B = \frac{1}{N} \sum_{i=1}^{N} \left(v_{\mathrm{m},i} - v_{\mathrm{o},i}\right)$	v_m: modeled wind speed; v_o: observed wind speed
Standard deviation of observed wind speed	$\mathrm{SD_o} = \sqrt{\frac{1}{(N-1)} \sum_{i=1}^{N} (v_{\mathrm{o},i} - \overline{v_\mathrm{o}})^2}$	v_o: observed wind speed; $\overline{v_\mathrm{o}}$: mean observed wind speed
Root-mean-square error	$\mathrm{RMSE} = \sqrt{\frac{1}{N} \sum_{i=1}^{N} (v_{\mathrm{m},i} - v_{\mathrm{o},i})^2}$	v_m: modeled wind speed; v_o: observed wind speed
Correlation coefficient	$R = \frac{1}{(N-1)} \sum_{i=1}^{N} \left(\frac{v_{\mathrm{m},i} - \overline{v_\mathrm{m}}}{\sigma_\mathrm{m}}\right) \left(\frac{v_{\mathrm{o},i} - \overline{v_\mathrm{o}}}{\sigma_\mathrm{o}}\right)$	v_m: modeled wind speed; $\overline{v_\mathrm{m}}$: mean modeled wind speed; v_o: observed wind speed; $\overline{v_\mathrm{o}}$: mean observed wind speed; σ_m: standard deviation of modeled wind speed; σ_o: standard deviation of observed wind speed
Mean absolute error of wind direction	$\mathrm{MAE_{dir}} = \frac{1}{N} \sum_{i=1}^{N} \left\{ \arccos[\cos(\phi_{\mathrm{m},i} - \phi_{\mathrm{o},i})] \right\}$	ϕ_m: modeled wind direction; ϕ_o: observed wind direction

generNet data can be observed (lower-middle and lower-right panel of Fig. 2a). This shift is reflected by small WFSS values at all neighborhood sizes, especially below a scale of 10 km. The AWFSS shows the largest value of all CCLM intercomparisons but is still low compared to INCA evaluation cases, which indicates a large bias (Fig. 2e, CCLMvsWN_therm_FBR). Evidently, this regional climate wind field modeling at 3 km grid spacing is not adequately representative for the given challenging hilly terrain.

The strong wind speed event in the WegenerNet FBR on the 30 October 2008 from 10:00 to 11:00 UTC led to southwesterly to southerly winds (Fig. 2b). The INCA model data and the WegenerNet reference data show maximum 1 h vector-mean wind speeds of around 9–10 $\mathrm{m\,s^{-1}}$ (upper-left and right panel of Fig. 2b). Regarding the wind directions, differences in the wind sectors can be observed (lower-left and right panel of Fig. 2b). The INCA data show wind directions mainly from the SW sector (lower-left panel), while the WegenerNet data show wind directions from the S and SW sectors (lower-right panel). The WFSS for this case shows small values at small neighborhood sizes and increases with increasing neighborhood size (Fig. 2e, INCAvsWN_strong_FBR). These low WFSS values are mainly caused by the differences in wind direction classes, especially in the southern part of the domain and through some spatial displacements in wind speed classes. Despite low WFSS values at small neighborhood sizes caused by differences in wind sectors, the AWFSS shows a high asymptotic value (AWFSS > 0.97). This high value is caused by the prevailing wind directions in the WegenerNet data, which are close to the threshold values for distinguishing between S and the SW. Hence, in this case, the 5° azimuthal class rotation procedure avoids lower score values.

Regarding the CCLM data (lower-middle panel of Fig. 2b), the whole wind field shows wind speeds from about 6.5 to 7.5 $\mathrm{m\,s^{-1}}$ and is therefore assigned to the wind class with wind speeds higher than 6 $\mathrm{m\,s^{-1}}$, whereas, for the WegenerNet wind fields, a large proportion is assigned to the class with wind speeds from 3 to 6 $\mathrm{m\,s^{-1}}$ of this region (Fig. 2e, CCLMvsWN_strong_FBR) and indicates that the dynamically modeled CCLM wind speeds are systematically overestimated relative to the empirically diagnosed wind speeds.

This discrepancy leads to the smallest WFSS values at all neighborhood sizes for this region (Fig. 2e, CCLMvsWN_strong_FBR) and indicates that the dynamically modeled CCLM wind speeds are systematically underestimated relative to the empirically diagnosed wind speeds for this hourly event.

On the 1 August 2012 the winds were thermally driven and the local pressure and temperature gradients were causing varying wind speeds and wind directions in the WegenerNet JBT. This is illustrated for the late afternoon INCA and WegenerNet wind fields in the upper-left panels of Fig. 2c. The WFSS for the evaluation of the INCA wind field shows the second largest value at the 1 km neighborhood size, which in-

dicates overlapping areas at this neighborhood size, equal to the horizontal resolution of the INCA analysis (Fig. 2e, INCAvsWN_therm_JBT). The large AWFSS value again indicates a small bias, which is also reflected by the similar wind classification shown in the wind roses of the corresponding lower-left panels of Fig. 2c. The high asymptotic value (AWFSS > 0.9) indicates a small bias and that the WFSS is mostly influenced by the spatial displacement.

In a further example of a thermally induced wind event on the 31 May 2008, we intercompare the CCLM with INCA wind fields (right panels of Fig. 2c). Especially in the CCLM, the smoothed terrain leads to uniform wind speeds and directions. Regarding the INCA wind fields, some variability in wind speed can be observed, with higher values in the summit regions and lower values at lower altitudes in the valleys of this region. Furthermore, a valley wind in the Enns valley is simulated by INCA. Probably the analysis part of the INCA model with its higher-resolved digital elevation model (DEM) and assimilated ZAMG observations leads to a somewhat better representation of the wind field. Comparing wind directions, the largest part of the CCLM modeled flow is from the N and NE sectors, while the INCA system estimated wind directions mainly from the E sector and partly from the NE and SE sectors (bottom right panels of Fig. 2c). This simplistic pattern of wind directions in CCLM leads to low WFSS values for all neighborhood sizes, including the lowest asymptotic value of all examples, indicating a very poor representation of the wind field by the dynamical modeling of the CCLM in this challenging mountainous terrain.

The strong wind speed event for the WegenerNet JBT on the 7 December 2013 is caused by northwesterly weather conditions. These synoptic-scale flow conditions led to strong wind speeds with maximum 1 h mean wind speeds of around $20\,\mathrm{m\,s^{-1}}$ from 17:00 to 18:00 UTC. Both the INCA and the WegenerNet wind fields show wind directions mainly from the NW, with some proportions from the N and the W sectors, caused by a channeling of the air flow through the pronounced valleys of this study area. The INCA wind fields show much lower wind speeds in the valley regions compared to the WegenerNet wind fields, resulting from the observations of the ZAMG Admont (ADM) station that flow into the INCA analysis but are considered far off the area and not used by the diagnostic modeling (upper-left panels of Fig. 2d). As the neighborhood size increases, the WFSS also increases, but due to spatial displacements, the values are generally low (Fig. 2e, INCAvsWN_strong_JBT). The low AWFSS value is caused by the differences in wind speed categories (lower-left panels of Fig. 2d).

For the 5 November 2008 we intercompare the CCLM wind fields with INCA wind fields from 01:00 to 02:00 UTC, for a strong wind speed event (right panels of Fig. 2d). In this example, the influence of the smoothed terrain caused by the coarse horizontal resolution of the CCLM becomes obvious. This smoothed topography results in systematically lower wind speeds compared to the INCA wind fields. The WFSS shows similar results to the previous INCAvsWN_strong_JBT evaluation, with small values at all neighborhood sizes (Fig. 2e, CCLMvsINCA_strong_JBT), indicating the clear limits of the CCLM dynamical modeling fields also for strong wind events.

4.2 Statistical evaluation results

The statistical event-averaged WFSS values from the large ensemble of events over multiple years are represented for each evaluation case in Fig. 3. Overall, the WFSS values show a monotonic increase with neighborhood size for all cases so that the AWFSS is the largest value, indicating relatively the best performance at large scales.

For the WegenerNet FBR, the statistical WFSS values, calculated for the INCA wind fields compared to the WegenerNet wind fields, shows nearly the same behavior for both the thermally induced and strong wind events (Fig. 3a, INCAvsWN_therm_FBR and INCAvsWN_strong_FBR). The WFSS values for these cases indicate a reasonably good spatial matching at all neighborhood sizes. Furthermore, the AWFSS values are higher than 0.8, reflecting generally small INCA biases of wind classes.

The statistical WFSS estimated for the CCLMvsWN_therm_FBR case indicates that the CCLM clearly and systematically underperforms in the case of thermally induced wind events for the WegenerNet FBR. Evidently, due to the coarse horizontal resolution of the wind fields, the CCLM wind fields appear fundamentally unable to capture the varying wind directions for such events in this region. For the CCLMvsWN_strong_FBR case, however the results indicate a similar spatial matching as for the INCAvsWN_therm_FBR and INCAvsWN_strong_FBR cases, just with a somewhat higher bias of wind class differences. This similar performance despite the coarser horizontal resolution of the CCLM model is explained through a weaker influence of the terrain on the wind fields under strong wind conditions in this region.

Because of the challenging terrain of the WegenerNet JBT, the statistical WFSS values are generally low for this region, signalling large biases (Fig. 3b). These biases are indicated by low asymptotic values, which tend to be between 0.61 and 0.64, except for the INCAvsWN_strong_JBT case, which shows an even lower value (AWFSS $= 0.39$).

The spatial displacement and the biases for the INCAvsWN_therm_JBT case are mainly caused by the differences in wind directions for these thermally induced wind events. Especially at small neighborhood sizes at the 1 km scale, WFSS values indicate large spatial displacements.

The INCAvsWN_strong_JBT case shows the lowest values at all neighborhood sizes, but this time caused by the differences in the wind speed categories. These low values are caused by the INCA-analyzed wind speeds, which, in the case of strong winds, are overestimated in the summit regions and underestimated in the valley regions. Slightly overesti-

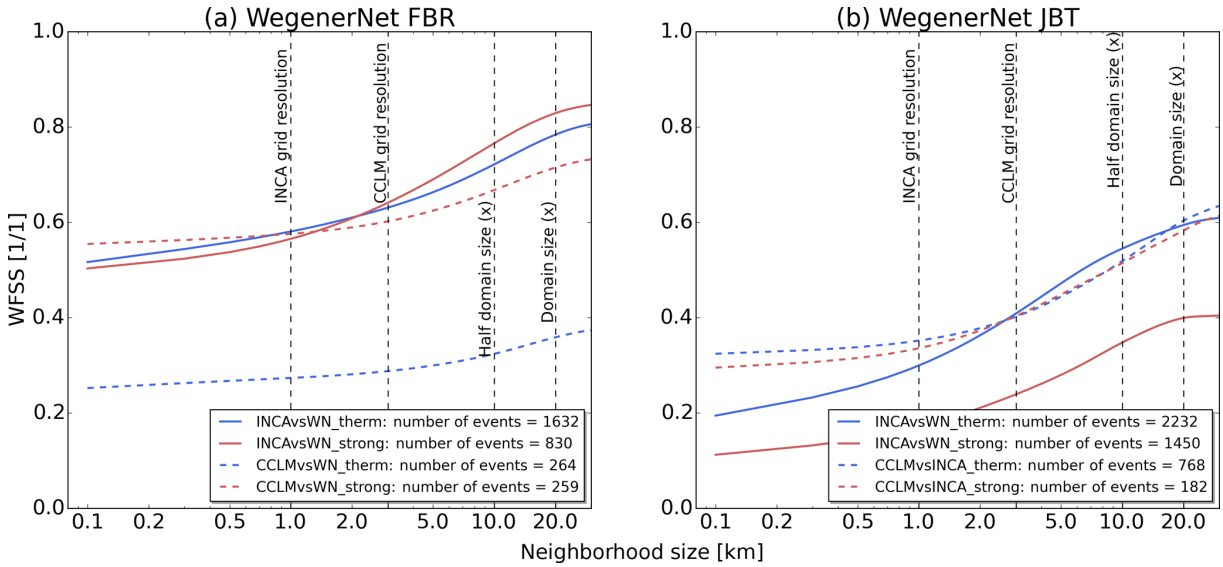

Figure 3. The event-averaged wind fractions skill score (WFSS) results for the WegenerNet FBR **(a)**, compared to the WegenerNet JBT **(b)**, for the four defined evaluation cases in each region (see legend; indicating also the number of events included). See Table 1 for more information on the evaluation cases.

mated WegenerNet wind speeds in the Enns valley somewhat reinforces the difference between the INCA and the WegenerNet wind speeds. These differences in wind speed especially in the valley and the summit regions become obvious in Fig. 4c and d and are discussed in further detail below.

The intercomparison of the CCLM wind fields with INCA delivers nearly the same (low) WFSS values for both types of wind events. In the case of thermally induced events (CCLMvsINCA_therm_JBT), the spatial displacements and biases are mainly caused due to differences in wind directions. For strong wind events (CCLMvsINCA_strong_JBT), the smoothed terrain caused by the coarse resolution of the CCLM leads to systematically underestimated wind speeds.

Table 4 summarizes, in addition to the AWFSS values, the results estimated with traditional statistical methods of the INCA analysis and CCLM dynamical fields. Due to the less challenging region of the WegenerNet FBR, all traditional statistical parameters show better performance for this region compared to the WegenerNet JBT. The absolute-value statistical metrics (bias B, standard deviation SD_o, root-mean-square error RMSE) applied to the hourly vector-mean wind speeds show higher values for the WegenerNet JBT, resulting from the generally higher wind speeds in addition to the effects of the complex mountainous terrain on the wind fields in this region. The B values are slightly positive for the WegenerNet FBR and negative for the WegenerNet JBT. The substantially negative B value for the INCAvsWN_strong_JBT case again reflects the underestimation of wind speed in the valleys, as explained above. Furthermore, the CCLMvsINCA_strong_JBT intercomparison also shows a negative bias, caused by the coarse resolution of the CCLM, which leads to lower wind speeds for strong wind events.

The RMSE values range from 0.79 to 1.85 $m\,s^{-1}$ for the WegenerNet FBR and from 1.3 to 8.6 $m\,s^{-1}$ for the WegenerNet JBT. The high value of 8.6 $m\,s^{-1}$ for the INCAvsWN_strong_JBT case is caused by the underestimation of wind speed in the valleys as well as the overestimation in the summit regions by the INCA model. The mean R values show a better correlation for the WegenerNet FBR than for the WegenerNet JBT. The mean absolute error of wind direction (MAE_{dir}) applied to hourly vector-mean wind directions also shows better performance (INCA and CCLM fields) for the WegenerNet FBR. Due to the varying wind directions caused by thermally induced circulations, the MAE_{dir} is higher for such events for both study areas, with the highest value of 68° for the INCAvsWN_therm_JBT case.

Figure 4 shows the mean wind speed bias spatial distributions for all evaluation cases, for the WegenerNet FBR (Fig. 4a and b) and the WegenerNet JBT (Fig. 4c and d). The distribution for the INCAvsWN_therm_FBR case, the case for thermally induced wind events for the WegenerNet FBR, shows large areas with nearly no B values (left panel of Fig. 4a). The maximum B value for this case can be observed in the area of the Gleichenberger Kogel, north of the ZAMG Bad Gleichenberg station with a value of around 1.4 $m\,s^{-1}$. The evaluation of the CCLM for the same thermally induced events shows an overestimation of wind speeds for the whole study area, with B values from 0.5 to 1 $m\,s^{-1}$ in the western part and from 1 to about 1.4 $m\,s^{-1}$ in the eastern part of the study area (right panel of Fig. 4a).

The overestimation of the wind speeds for the WegenerNet FBR can be explained by the too frequent flow-over patterns

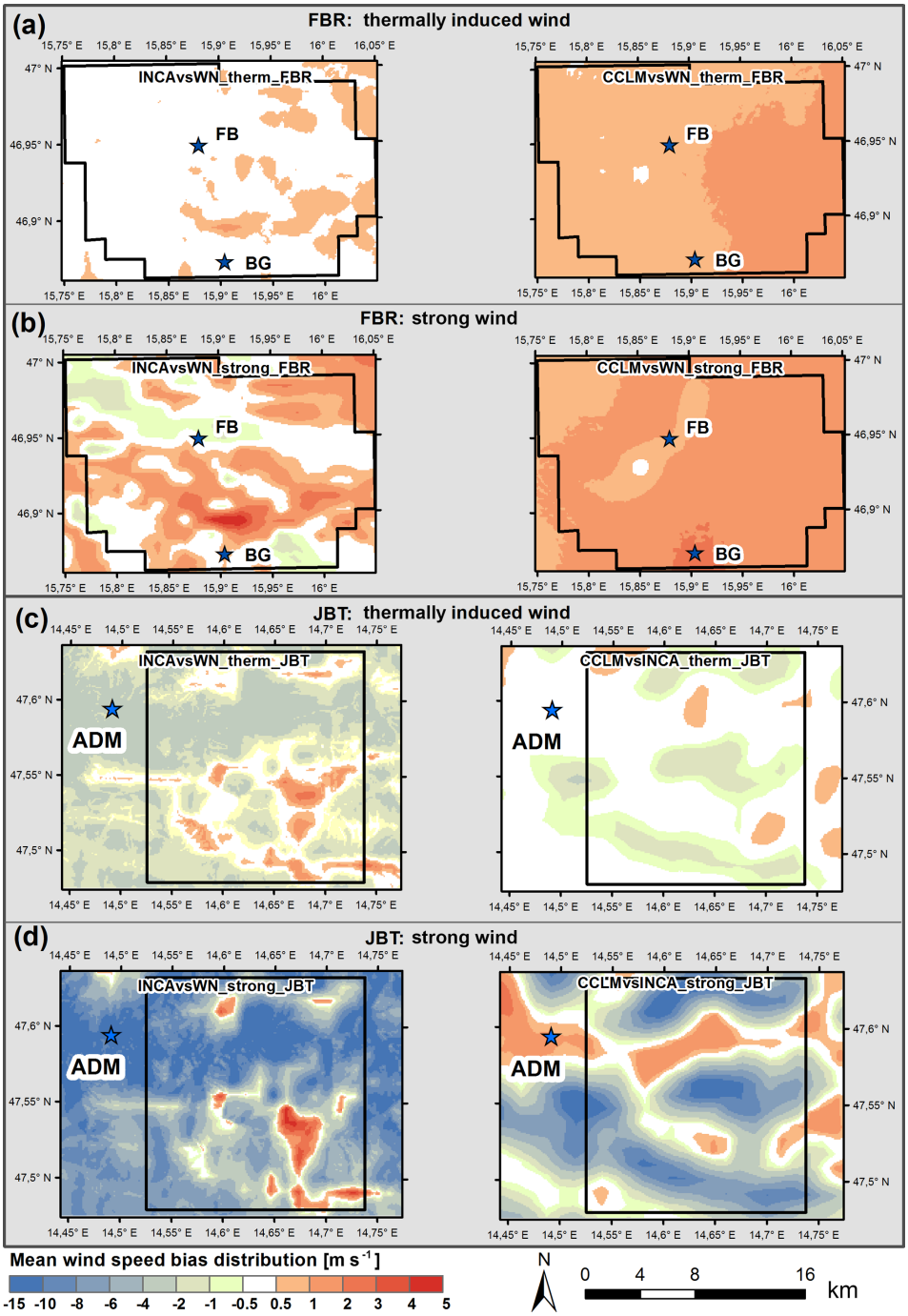

Figure 4. Mean wind speed bias distribution for the WegenertNet FBR **(a, b)** and the WegenerNet JBT **(c, d)**: **(a, b)** INCA versus WegnerNet (left) and CCLM versus WegenerNet (right) for **(a)** thermally induced wind events and **(b)** strong wind events and **(c, d)** WegenerNet versus INCA (left) and CCLM versus INCA (right) for **(c)** thermally induced wind events and **(d)** strong wind events.

simulated for this region, which lead to a more dominant orographic speedup effect. Due to orographic smoothing, flow-over patterns are generally more frequent than flow-around patterns, especially for the WegenerNet FBR with its small differences in altitude (Taylor et al., 1987).

The evaluation of the INCA model for strong wind speeds illustrates the strong influence of the terrain on this model. The results show a good agreement in the valleys of the study area, with partly small negative B values (left panel of Fig. 4b). The hilltop regions exhibit positive B values, with maximum values of around $5\,\mathrm{m\,s^{-1}}$ again in the area of the

Table 4. Statistical performance measures calculated for the evaluation cases from Table 1, for the WegenerNet FBR and the WegenerNet JBT region. See Table 3 for more information on the calculation of the parameters.

Evaluation case	AWFSS (1)	B ($m s^{-1}$)	SD_o ($m s^{-1}$)	RMSE (1)	R (1)	MAE_{dir} (°)
	WegenerNet FBR					
INCAvsWN_therm_FBR	0.81	0.34	0.74	0.79	0.67	38
INCAvsWN_strong_FBR	0.85	0.50	1.04	1.66	0.34	14
CCLMvsWN_therm_FBR	0.38	1.32	0.72	1.85	0.37	55
CCLMvsWN_strong_FBR	0.74	1.01	1.03	1.28	0.57	14
Mean value	0.70	0.79	0.88	1.40	0.49	30
	WegenerNet JBT					
INCAvsWN_therm_JBT	0.61	−1.37	2.37	2.97	0.20	68
INCAvsWN_strong_JBT	0.39	−6.69	3.97	8.60	0.16	39
CCLMvsINCA_therm_JBT	0.64	−0.23	1.32	1.31	0.40	56
CCLMvsINCA_strong_JBT	0.63	−3.79	4.24	5.52	0.08	25
Mean value	0.57	−3.04	2.98	4.62	0.20	47

Gleichenberger Kogel. Overall positive B values of CCLM dynamical wind speed fields for strong wind events are seen in the right panel of Fig. 4b, showing the systematic overestimating by CCLM fields in this case. These large B values are probably also due to the speedup effect explained for the above case CCLMvsWN_therm_FBR.

For the WegenerNet JBT, the strong influence of the terrain on the INCA-analyzed wind speeds can be observed in all evaluation cases in this region. The evaluation of the INCA model for thermally induced wind events exhibits negative B values in the valleys, whereby positive values partly occur in the summit regions (left panel of Fig. 4c). At lower elevations, the intercomparison of the CCLM with the INCA model shows nearly no B values for thermally induced events (right panel of Fig. 4c). Furthermore, small negative B values in the summit regions and some spots with positive values can be observed for this case. Due to these small bias values, similar results to these ones can be expected for a comparison of CCLM with WegenerNet data.

Similar bias distribution patterns as for the INCA evaluation for thermally induced wind events are present for strong wind events in the INCAvsWN_strong_JBT case, but this time with strong negative and positive B values ranging from -14.4 to $4.9\,m\,s^{-1}$ (left panel of Fig. 4d). These strong negative B values are again caused by the severely underestimated INCA wind speeds and the somewhat overestimated WegenerNet wind speeds in the valley regions of the WegenerNet JBT.

Opposite patterns can be seen for the intercomparison of the CCLM with the INCA model. This intercomparison exhibits small positive values in the valley regions and strong negative values in the summit regions (right panel of Fig. 4d). The main reason for these strong negative B values is the coarse resolution of the CCLM data and the resulting underestimation of wind speeds for strong wind events, as explained above. The negative B values are likely caused by negative orographic speedup effects, which are preferred in flow-around patterns and flow-splitting patterns that occur especially when the differences in the altitude of ridges of mountains are large (Hewer, 1998).

5 Conclusions

In this work we evaluated wind fields generated by two different modeling systems against empirically diagnosed wind fields from WegenerNet high-density network data: the INCA analysis system of the Austrian weather service Central Institute for Meteorology and Geodynamics (ZAMG) (Haiden et al., 2011) and the non-hydrostatic Consortium for Small Scale Modeling Model in Climate Mode (CCLM) (Schättler et al., 2016). The INCA wind fields have a horizontal resolution of 1 km × 1 km, and in the case of CCLM, 3 km × 3 km horizontal resolution was available. In both cases, the temporal resolution is 1 h. The empirical high-resolution wind fields from the WegenerNet were generated by the WegenerNet Wind Product Generator (WPG), recently developed by Schlager et al. (2017, 2018).

The WPG-diagnosed gridded wind fields are available with a temporal resolution of 30 min and a spatial resolution of 100 m × 100 m and can therefore serve well as a reference. The WegenerNet Feldbach Region (FBR) was used as study area, characterized by generally small differences in altitude in the hilly terrain of this region. The second study area was the WegenerNet Johnsbachtal (JBT) region, which is a mountainous region characterized by a very complex terrain.

The evaluation of the INCA and the CCLM wind fields was based on classifying the data separately into thermally induced and strong wind events. In the case of the INCA evaluation, we could select wind events within the period 2008–2017 for the WegenerNet FBR and within 2012–2017 for the WegenerNet JBT. For evaluating the CCLM data, events from the period 2008–2010 were selected for both study areas. Due to WegenerNet JBT wind fields not yet being available within 2008–2010, we intercompared the CCLM wind fields with INCA wind fields in this region.

Besides traditional performance measures such as bias, root-mean-square error, correlation coefficient, and mean absolute error of wind direction, in particular we applied a spatial wind verification methodology called the wind fractions skill score (WFSS) (Skok and Hladnik, 2018). This new score was used to detect spatial displacements of wind patterns and biases based on predefined wind speed and direction classes. The WFSS avoids the double-penalty problem and is able to distinguish between a "near miss" and large displacements between modeled and reference wind fields. Furthermore, a spatial-scale-dependent skill is determined by this score.

Due to the less challenging terrain of the Alpine foreland region, all statistical performance measures showed better INCA and CCLM performance for the WegenerNet FBR than for the challenging mountainous region of WegenerNet JBT. The spatial verification of all evaluation cases indicates an increasing skill with increasing scale (neighborhood size). For both study areas, the traditional statistical performance measures, applied to the wind speed, mostly show better performance of INCA and CCLM for thermally induced wind events than for strong wind events. On the other hand, the results related to wind direction indicate a better performance for strong wind events than for thermally induced events.

More specifically, the verification for the WegenerNet FBR shows that the INCA analysis wind fields are more skillful than the CCLM dynamical wind fields in this region. The INCA verification indicates a reasonably good performance for both thermally induced and strong wind events.

The CCLM clearly performs less well in the case of thermally induced wind events for this region. The reason for this weak performance is the limited resolution of the wind field dataset from this model. Although the difference in the numerical resolution between INCA (1 km grid spacing) and CCLM (3 km grid spacing) is only a factor of 3, CCLM is not able to resolve small-scale wind patterns. This occurs for multiple reasons: (1) due to the third-order advection scheme with its horizontal diffusion damping, the effective resolution in CCLM is several times coarser than the numeric grid spacing (Ogaja and Will, 2016); (2) the orography is smoothed as well, so that individual mountain ridge and valley structures are removed. For example, the mountain peak of the Hochtor with its 2396 m elevation at the center of the WegenerNet JBT region is lowered by about 500 m in the CCLM model.

Hence, with the resolution of 3 km × 3 km, the fields are not able to resolve the varying wind speeds and directions caused by thermally driven circulations. The wind speeds are overestimated by this model for both thermally induced and strong wind events, and large differences in wind directions are found for thermally induced events.

For the WegenerNet JBT region, the verification shows generally large spatial displacements at all scales and strong biases in wind classes for all evaluation cases. In the case of the INCA evaluation, large wind direction deviations for thermally induced wind events indicate that the analysis fields are not able to adequately capture the varying wind patterns such as slope and valley winds, which are rooted in the sparse station density to which INCA can be anchored and the coarse horizontal resolution of the first guess provided by the ARPEGE-ALADIN (ALARO) model in this complex-terrain region. Furthermore, the statistics show an substantial underestimation of wind speeds in the valleys and overestimated wind speeds in parts of the summit regions for both types of wind events.

The intercomparison of the CCLM dynamical fields with the INCA analysis fields for thermally induced wind events reflects the disadvantage of smoothed terrain, which is caused by the limited effective resolution being several times coarser than the 3 km × 3 km grid spacing of the CCLM as already noted above. Improvements can be expected from the latest developments in the numerical core of CCLM by Ogaja and Will (2016), which have enabled an improvement of the effective resolution by a factor of 2 by introducing a fourth-order advection scheme that allows us to circumvent the horizontal diffusion damping.

Based on these findings and underpinning the results of Haiden et al. (2011), we suggest that additional observed wind information in the summit and valley regions, especially in a complex terrain like the WegenerNet JBT, and a more comprehensive use of wind-constraining satellite data as well as a higher-resolution regional climate model (RCM) could help to systematically improve the INCA-analyzed wind fields. At higher resolutions, the topographic shading through the terrain becomes increasingly important, especially for the simulation of thermally induced wind events. Such methods have not yet been implemented into the ALARO model but may help to generate more realistic wind fields in the future.

Related to the CCLM dynamical modeling, a verification of CCLM-generated higher-resolution 1 km × 1 km wind fields and the application of the new fourth-order advection scheme from Ogaja and Will (2016) in a convection-permitting configuration would also be a promising issue for further investigations of how this may improve the modeling of wind patterns in a complex terrain.

Investigations regarding the WegenerNet JBT wind fields showed that an additional wind-observing station in the Enns valley would improve the results for this region (Schlager et al., 2018). Such an additional station would avoid the over-

estimation of WegenerNet wind speeds in the Enns valley, especially for strong wind events. In the WegenerNet FBR just recently (in May 2018), another wind station was added in the Raab valley (station Nr. 155 1b), which will further improve the WPG-derived fields in future. This adds further value to a valuable reference for the evaluation of important other data products such as the INCA operational analysis and dynamical climate model fields.

Code availability. The CALMET 6.5.0 model code is available from the website http://www.src.com (last access: 2 July 2019; Exponent, Inc., 2018). The INCA and the WPG code are not in the public domain and cannot be distributed. The source code for the CCLM is available on request via the website https://www.clm-community.eu (last access: 2 July 2019; Deutscher Wetterdienst, 2019). The code for the calculation of the wind FSS is available as part of the SpatialVx package (function calculate_FSSwind). SpatialVx is a R software package made by Eric Gilleland that enables the calculation of a large number of spatial verification scores (https://cran.r-project.org/package=SpatialVx, last access: 2 July 2019; Gilleland, 2019).

Data availability. CORINE land cover data for the study area were taken from https://www.eea.europa.eu/ (last access: 2 July 2019; EEA, 2016), digital elevation model data from http://www.landesentwicklung.steiermark.at/cms/ziel/141976122/DE/ (last access: 2 July 2019; Land Steiermark, 2019), and WegenerNet data from https://wegenernet.org/portal/ (last access: 2 July 2019; Wegener Center, 2019). The WegenerNet data contain the WPG wind field output data as introduced in this study. The INCA data are available on request from the Central Institute for Meteorology and Geodynamics (klima@zamg.ac.at). CCLM data are available on request from the Wegener Center, University of Graz (heimo.truhetz@uni-graz.at).

Author contributions. CS collected the data, performed the analyses and modeling, created the figures, and wrote the first draft of the paper. GK provided guidance and advice on all aspects of the study and significantly contributed to the text. JF provided guidance on technical aspects of the WegenerNet networks and its data characteristics and contributed to the text. AK provided INCA-related advice and contributed to the INCA part of the text, and HT provided information and advice on the CCLM setup and characteristics and contributed in particular to the CCLM part of the text. All authors commented on the final version of the paper.

Competing interests. The authors declare that they have no conflict of interest.

Acknowledgements. The authors thank Gregor Skok (Department of Physics, University of Ljubljana), for providing the R code to calculate the wind fractions skill score. Furthermore, the authors acknowledge the data providers at the Central Institute for Meteorology and Geodynamics (ZAMG) for the Integrated Nowcasting through Comprehensive Analysis (INCA) dataset. Andras Csaki (Wegener Center, University of Graz) is thanked for performing the CCLM modeling and extracting the wind field data. The authors are also grateful to the Jülich Supercomputing Centre (JSC) and the Vienna Scientific Cluster (VSC) for providing the necessary HPC resources. WegenerNet funding is provided by the Austrian Ministry for Science and Research, the University of Graz, the state of Styria (which also included European Union regional development funds), and the city of Graz; detailed information can be found online (http://www.wegcenter.at/wegenernet, last access: 2 July 2019). The CCLM simulation was funded by the Austrian Science Fund (FWF) under project NHCM-2 (project number P24758-N29).

Review statement. This paper was edited by Richard Neale and reviewed by two anonymous referees.

References

Abdel-Aal, R., Elhadidy, M., and Shaahid, S.: Modeling and forecasting the mean hourly wind speed time series using GMDH-based abductive networks, Renew. Ener., 34, 1686–1699, https://doi.org/10.1016/j.renene.2009.01.001, 2009.

Awan, N. K., Truhetz, H., and Gobiet, A.: Parameterization-induced error characteristics of MM5 and WRF operated in climate mode over the alpine region: An ensemble-based analysis, J. Climate, 24, 3107–3123, https://doi.org/10.1175/2011JCLI3674.1, 2011.

Bartalev, S., Belward, A., Ershov, D., and S. Isaev, A.: A new SPOT4-VEGETATION derived land cover map of Northern Eurasia, Int. J. Remote Sens., 24, 1977–1982, https://doi.org/10.1080/0143116031000066297, 2003.

Bechtold, P., Köhler, M., Jung, T., Doblas-Reyes, F., Leutbecher, M., Rodwell, M. J., Vitart, F., and Balsamo, G.: Advances in simulating atmospheric variability with the ECMWF model: From synoptic to decadal time-scales, Q. J. Roy. Meteor. Soc., 134, 1337–1351, https://doi.org/10.1002/qj.289, 2008.

Bellasio, R., Maffeis, G., Scire, J. S., Longoni, M. G., Bianconi, R., and Quaranta, N.: Algorithms to Account for Topographic Shading Effects and Surface Temperature Dependence on Terrain Elevation in Diagnostic Meteorological Models, Bound.-Lay. Meteor., 114, 595–614, https://doi.org/10.1007/s10546-004-1670-6, 2005.

Böhm, U., Kücken, M., Ahrens, W., Block, A., Hauffe, D., Keuler, B., Rockel, B., and Will, A.: CLM-The Climate Version of LM: Brief Description and Long-Term Applications, 225–236, Deutscher Wetterdienst (DWD), 6 Edn., available at: http://www.cosmo-model.org/content/model/documentation/newsLetters/newsLetter06/newsLetter_06.pdf (last access: 2 July 2019), 2006.

Bubnová, R., Hello, G., Bénard, P., and Geleyn, J.-F.: Integration of the Fully Elastic Equations Cast in the Hydrostatic Pressure Terrain-Following Coordinate in the Framework of the ARPEGE/Aladin NWP System, Mon. Weather Rev., 123, 515–535, https://doi.org/10.1175/1520-0493(1995)123<0515:IOTFEE>2.0.CO;2, 1995.

Cox, R. M., Sontowski, J., and Dougherty, C. M.: An evaluation of three diagnostic wind models (CALMET, MC-

SCIPUF, and SWIFT) with wind data from the Dipole Pride 26 field experiments, Meteor. Appl., 12, 329–341, https://doi.org/10.1017/S1350482705001908, 2005.

Davies, H. C.: A lateral boundary formulation for multi-level prediction models, Q. J. Roy. Meteor. Soc., 102, 405–418, https://doi.org/10.1002/qj.49710243210, 1976.

Deutscher Wetterdienst: Climate Limited-area Modelling Community, available at: https://www.clm-community.eu, last access: 2 July 2019.

EEA: Global land cover 2000 – Europe, Tech. rep., European Environment Agency (EEA), available at: https://www.eea.europa.eu/data-and-maps/data/global-land-cover-2000-europe (last access: 2 July 2019), 2016.

Exponent, Inc.: CALPUFF Modeling System, Exponent Engineering and Scientific Consulting, available at: http://www.src.com (last access: 2 July 2019), 2018.

Gal-Chen, T. and Somerville, R. C.: On the use of a coordinate transformation for the solution of the Navier-Stokes equations, J. Comput. Phys., 17, 209–228, https://doi.org/10.1016/0021-9991(75)90037-6, 1975.

Gerard, L. and Geleyn, J.-F.: Evolution of a subgrid deep convection parametrization in a limited-area model with increasing resolution, Q. J. Roy. Meteor. Soc., 131, 2293–2312, https://doi.org/10.1256/qj.04.72, 2005.

Giard, D. and Bazile, E.: Implementation of a New Assimilation Scheme for Soil and Surface Variables in a Global NWP Model, Mon. Weather Rev., 128, 997–1015, https://doi.org/10.1175/1520-0493(2000)128<0997:IOANAS>2.0.CO;2, 2000.

Gilleland, E., Ahijevych, D. A., Brown, B. G., and Ebert, E. E.: Verifying Forecasts Spatially, B. Am. Meteor. Soc., 91, 1365–1376, https://doi.org/10.1175/2010BAMS2819.1, 2010.

Gilleland, E: SpatialVx: Spatial Forecast Verification, The Comprehensive R Archive Network, available at: https://cran.r-project.org/package=SpatialVx, last access: 2 July 2019.

Gómez-Navarro, J. J., Raible, C. C., and Dierer, S.: Sensitivity of the WRF model to PBL parametrisations and nesting techniques: evaluation of wind storms over complex terrain, Geosci. Model Dev., 8, 3349–3363, https://doi.org/10.5194/gmd-8-3349-2015, 2015.

Gross, G.: On the applicability of numerical mass-consistent wind field models, Bound.-Lay. Meteor., 77, 379–394, https://doi.org/10.1007/BF00123533, 1996.

Haiden, T., Kann, A., Wittmann, C., Pistotnik, G., Bica, B., and Gruber, C.: The Integrated Nowcasting through Comprehensive Analysis (INCA) system and its validation over the eastern alpine region, Weather Forecast., 26, 166–183, https://doi.org/10.1175/2010WAF2222451.1, 2011.

Haylock, M. R., Hofstra, N., Klein Tank, A. M. G., Klok, E. J., Jones, P. D., and New, M.: A European daily high-resolution gridded data set of surface temperature and precipitation for 1950–2006, J. Geophys. Res., 113, D20119, https://doi.org/10.1029/2008JD010201, 2008.

Hewer, F.: Non-Linear Numerical Model Predictions of Flow Over an Isolated Hill of Moderate Slope, Bound.-Lay. Meteor., 87, 381–408, https://doi.org/10.1023/A:1000944817965, 1998.

Hiebl, J. and Frei, C.: Daily temperature grids for Austria since 1961 – concept, creation and applicability, Theor. Appl. Climatol., 124, 161–178, https://doi.org/10.1007/s00704-015-1411-4, 2016.

Hohmann, C., Kirchengast, G., and Birk, S.: Alpine foreland running drier? Sensitivity of a drought vulnerable catchment to changes in climate, land use, and water management, Clim. Change, 147, 179–193, https://doi.org/10.1007/s10584-017-2121-y, 2018.

Kabas, T.: WegenerNet climate station network region Feldbach: Experimental setup and high resolution data for weather and climate research (in German), Scientific Rep. 47-2012, Wegener Center Verlag, Graz, Austria, available at: http://wegcwww.uni-graz.at/publ/wegcreports/2012/WCV-WissBer-No47-TKabas-Jan2012.pdf (last access: 2 July 2019), 2012.

Kabas, T., Foelsche, U., and Kirchengast, G.: Seasonal and annual trends of temperature and precipitation within 1951/1971–2007 in south-eastern Styria, Austria, Meteor. Z., 20, 277–289, https://doi.org/10.1127/0941-2948/2011/0233, 2011.

Kann, A., Meirold-Mautner, I., Schmid, F., Kirchengast, G., Fuchsberger, J., Meyer, V., Tüchler, L., and Bica, B.: Evaluation of high-resolution precipitation analyses using a dense station network, Hydrol. Earth Syst. Sci., 19, 1547–1559, https://doi.org/10.5194/hess-19-1547-2015, 2015a.

Kann, A., Wittmann, C., Bica, B., and Wastl, C.: On the Impact of NWP Model Background on Very High–Resolution Analyses in Complex Terrain, Weather Forecast., 30, 1077–1089, https://doi.org/10.1175/WAF-D-15-0001.1, 2015b.

Kendon, E. J., Ban, N., Roberts, N. M., Fowler, H. J., Roberts, M. J., Chan, S. C., Evans, J. P., Fosser, G., and Wilkinson, J. M.: Do convection-permitting regional climate models improve projections of future precipitation change?, B. Am. Meteor. Soc., 98, 79–93, https://doi.org/10.1175/BAMS-D-15-0004.1, 2017.

Kida, H., Koide, T., Sasaki, H., and Chiba, M.: A New Approach for Coupling a Limited Area Model to a GCM for Regional Climate Simulations, J. Meteor. Soc. JPN, 69, 723–728, https://doi.org/10.2151/jmsj1965.69.6_723, 1991.

Kirchengast, G., Kabas, T., Leuprech, A., Bichler, C., and Truhetz, H.: WegenerNet: A pioneering high-resolution network for monitoring weather and climate, B. Am. Meteor. Soc., 95, 227–242, https://doi.org/10.1175/BAMS-D-11-00161.1, 2014.

Land Steiermark: Das Land Steiermark, Geoinformation aus dem Land für das Land, available at: http://www.landesentwicklung.steiermark.at/cms/ziel/141976122/DE/, last access: 2 July 2019.

Leutwyler, D., Fuhrer, O., Lapillonne, X., Lüthi, D., and Schär, C.: Towards European-scale convection-resolving climate simulations with GPUs: a study with COSMO 4.19, Geosci. Model Dev., 9, 3393–3412, https://doi.org/10.5194/gmd-9-3393-2016, 2016.

Lugauer, M. and Winkler, P.: Thermal circulation in South Bavaria – climatology and synoptic aspects, Meteor. Z., 14, 15–30, https://doi.org/10.1127/0941-2948/2005/0014-0015, 2005.

Morales, L., Lang, F., and Mattar, C.: Mesoscale wind speed simulation using CALMET model and reanalysis information: An application to wind potential, Renew. Energ., 48, 57–71, https://doi.org/10.1016/j.renene.2012.04.048, 2012.

Noilhan, J. and Planton, S.: A Simple Parameterization of Land Surface Processes for Meteorological Models, Mon. Weather Rev., 117, 536–549, https://doi.org/10.1175/1520-0493(1989)117<0536:ASPOLS>2.0.CO;2, 1989.

O, S., Foelsche, U., Kirchengast, G., Fuchsberger, J., Tan, J., and Petersen, W. A.: Evaluation of GPM IMERG Early, Late, and Final rainfall estimates using WegenerNet gauge data in southeastern Austria, Hydrol. Earth Syst. Sci., 21, 6559–6572, https://doi.org/10.5194/hess-21-6559-2017, 2017.

O, S., Foelsche, U., Kirchengast, G., and Fuchsberger, J.: Validation and correction of rainfall data from the WegenerNet high density network in southeast Austria, J. Hydrol., 556, 1110–1122, https://doi.org/10.1016/j.jhydrol.2016.11.049, 2018.

Ogaja, J. and Will, A.: Fourth order, conservative discretization of horizontal Euler equations in the COSMO model and regional climate simulations, Meteor. Z., 25, 577–605, https://doi.org/10.1127/metz/2016/0645, 2016.

Osborn, T. J. and Hulme, M.: Evaluation of the European daily precipitation characteristics from the atmospheric model intercomparison project, Int. J. Climatol., 18, 505–522, https://doi.org/10.1002/(SICI)1097-0088(199804)18:5<505::AID-JOC263>3.0.CO;2-7, 1998.

Prein, A. F., Gobiet, A., Suklitsch, M., Truhetz, H., Awan, N. K., Keuler, K., and Georgievski, G.: Added value of convection permitting seasonal simulations, Clim. Dynam., 41, 2655–2677, https://doi.org/10.1007/s00382-013-1744-6, 2013a.

Prein, A. F., Holland, G. J., Rasmussen, R. M., Done, J., Ikeda, K., Clark, M. P., and Liu, C. H.: Importance of regional climate model grid spacing for the simulation of heavy precipitation in the colorado headwaters, J. Climate, 26, 4848–4857, https://doi.org/10.1175/JCLI-D-12-00727.1, 2013b.

Prein, A. F., Langhans, W., Fosser, G., Ferrone, A., Ban, N., Goergen, K., Keller, M., Toelle, M., Gutjahr, O., Feser, F., Brisson, E., Kollet, S., Schmidli, J., Van Lipzig, N. P., and Leung, R.: A review on regional convection-permitting climate modeling: Demonstrations, prospects, and challenges, Rev. Geophys., 53, 323–361, https://doi.org/10.1002/2014RG000475, 2015.

Prettenthaler, F., Podesser, A., and Pilger, H.: Climate Atlas Styria, Period 1971–2000: An Application-Oriented Climatology, Vol. 4, Verlag der Oesterreichischen Akademie der Wissenschaften, Wien, 2010 (in German).

Raschendorfer, M.: The New Turbulence Parameterization of LM, 89–97, Deutscher Wetterdienst (DWD), 1 Edn., available at: http://www.cosmo-model.org/content/model/documentation/newsLetters/newsLetter01/newsLetter_01.pdf (last access: 2 July 2019), 2001.

Ratto, C., Festa, R., Romeo, C., Frumento, O., and Galluzzi, M.: Mass-consistent models for wind fields over complex terrain: The state of the art, Environ. Softw., 9, 247–268, 1994.

Raymond, W. H.: High-Order Low-Pass Implicit Tangent Filters for Use in Finite Area Calculations, Mon. Weather Rev., 116, 2132–2141, https://doi.org/10.1175/1520-0493(1988)116<2132:HOLPIT>2.0.CO;2, 1988.

Ritter, B. and Geleyn, J.-F.: A Comprehensive Radiation Scheme for Numerical Weather Prediction Models with Potential Applications in Climate Simulations, Mon. Weather Rev., 120, 303–325, https://doi.org/10.1175/1520-0493(1992)120<0303:ACRSFN>2.0.CO;2, 1992.

Roberts, N.: Assessing the spatial and temporal variation in the skill of precipitation forecasts from an NWP model, Meteor. Appl., 15, 163–169, https://doi.org/10.1002/met.57, 2008.

Rockel, B., Will, A., and Hense, A.: The Regional Climate Model COSMO-CLM (CCLM), Meteor. Z., 17, 347–348, https://doi.org/10.1127/0941-2948/2008/0309, 2008.

Schättler, U., Doms, G. U., and Baldauf, M.: A Description of the Nonhydrostatic Regional COSMO Model, Part VII: User's Guide, Deutscher Wetterdienst, 3004 Offenbach, Germany, 2016.

Schlager, C., Kirchengast, G., and Fuchsberger, J.: Generation of high-resolution wind fields from the dense meteorological station network WegenerNet in south-eastern Austria, Weather Forecast., 32, 1301–1319, https://doi.org/10.1175/WAF-D-16-0169.1, 2017.

Schlager, C., Kirchengast, G., and Fuchsberger, J.: Empirical high-resolution wind field and gust model in mountainous and hilly terrain based on the dense WegenerNet station networks, Atmos. Meas. Tech., 11, 5607–5627, https://doi.org/10.5194/amt-11-5607-2018, 2018.

Schroeer, K. and Kirchengast, G.: Sensitivity of extreme precipitation to temperature: the variability of scaling factors from a regional to local perspective, Clim. Dynam., 50, 3981–3994, 2018.

Scire, J. S., Robe, F. R., Fernau, M. E., and Roberto, Y. J.: A User's Guide for the CALMET Meteorological Model (Version 5), Earth Tech, Inc, 196 Baker Avenue, Concord, MA 01742, 1998.

Seaman, N. L.: Meteorological modeling for air-quality assessments, Appl. Energ., 34, 2231–2259, https://doi.org/10.1016/S1352-2310(99)00466-5, 2000.

Sfetsos, A.: A novel approach for the forecasting of mean hourly wind speed time series, Renew. Energ., 27, 163–174, https://doi.org/10.1016/S0960-1481(01)00193-8, 2002.

Skok, G. and Hladnik, V.: Verification of Gridded Wind Forecasts in Complex Alpine Terrain: A New Wind Verification Methodology Based on the Neighborhood Approach, Mon. Weather Rev., 146, 63–75, https://doi.org/10.1175/MWR-D-16-0471.1, 2018.

Strasser, U., Marke, T., Sass, O., Birk, S., and Winkler, G.: John's creek valley: A mountainous catchment for long-term interdisciplinary human-environment system research in Upper Styria (Austria), Environ. Earth Sci., 69, 695–705, https://doi.org/10.1007/s12665-013-2318-y, 2013.

Suklitsch, M., Gobiet, A., Truhetz, H., Awan, N. K., Göttel, H., and Jacob, D.: Error characteristics of high resolution regional climate models over the Alpine area, Clim. Dynam., 37, 377–390, https://doi.org/10.1007/s00382-010-0848-5, 2011.

Taylor, P. A., Mason, P. J., and Bradley, E. F.: Boundary-layer flow over low hills, Bound.-Lay. Meteorol., 39, 107–132, https://doi.org/10.1007/BF00121870, 1987.

Termonia, P., Fischer, C., Bazile, E., Bouyssel, F., Brožková, R., Bénard, P., Bochenek, B., Degrauwe, D., Derková, M., El Khatib, R., Hamdi, R., Mašek, J., Pottier, P., Pristov, N., Seity, Y., Smolíková, P., Španiel, O., Tudor, M., Wang, Y., Wittmann, C., and Joly, A.: The ALADIN System and its canonical model configurations AROME CY41T1 and ALARO CY40T1, Geosci. Model Dev., 11, 257–281, https://doi.org/10.5194/gmd-11-257-2018, 2018.

Tiedtke, M.: A Comprehensive Mass Flux Scheme for Cumulus Parameterization in Large-Scale Models, Mon. Weather Rev., 117, 1779–1800, https://doi.org/10.1175/1520-0493(1989)117<1779:ACMFSF>2.0.CO;2, 1989.

Truhetz, H.: High resolution wind field modelling over complex topography: analysis and future scenarios, Scientific

Rep. 32-2010, Wegener Center Verlag, Graz, Austria, available at: http://wegcwww.uni-graz.at/publ/wegcreports/2010/WCV-SciRep-No32-HTruhetz-Apr2010.pdf (last access: 2 July 2019), 2010.

Wakonigg, H.: Weather and Climate in Styria, Verlag fuer die Technische Universitaet Graz, Graz, 1978 (in German).

Wang, Y., Haiden, T., and Kann, A.: The operational Limited Area Modelling system at ZAMG: ALADIN-AUSTRIA, Vol. 37, Österreichische Beiträge zu Meteorologie und Geophysik, Wien, 2006.

Wegener Center: WegenerNet Data portal, WegenerNet – New data for research and society, available at: https://wegenernet.org/portal/, last access: 2 July 2019.

Whiteman, C.: Mountain Meteorology: Fundamentals and Applications, Oxford University Press, Graz, 2000.

Wicker, L. J. and Skamarock, W. C.: Time-Splitting Methods for Elastic Models Using Forward Time Schemes, Mon. Weather Rev., 130, 2088–2097, https://doi.org/10.1175/1520-0493(2002)130<2088:TSMFEM>2.0.CO;2, 2002.

9 Conclusions and discussion

Regional climate models are well-established tools used for analyzing and understanding climate on a regional scale, for conducting operational weather forecasting, and for carrying out practical planning of local projects. Innovations in computer software and the increased power of computer hardware have made possible simulations of RCMs at a near 1 km scale. At this scale, RCMs can accurately resolve topography and surface fields and simulate deep convection explicitly without parameterizations.

Several studies have demonstrated that, when it comes to numerical weather prediction, such convection permitting climate simulations (CPCSs) are more realistic than comparable coarse-resolution simulations, especially in cases of moist convection over mountainous regions (e.g. Langhans et al. 2013; Mass et al. 2002; Miura et al. 2007; Grell et al. 2000; Richard et al. 2007; Lean et al. 2008; Schwartz et al. 2009; Weusthoff et al. 2010; Baldauf et al. 2011; Hohenegger et al. 2008; Prein et al. 2013b). These simulations, however, are subject to various limitations and introduce various sources of uncertainty (Gómez-Navarro et al. 2015). As datasets in sufficiently high spatial and temporal resolution are often lacking, properly evaluating CPCSs also poses difficulties (Prein 2013; Schlager et al. 2017; Schlager et al. 2018).

Another challenge is the evaluation of the model outputs themselves, particularly the evaluation of high-resolution precipitation and surface wind fields (Skok and Hladnik 2018). Coarse-resolution outputs are generally favored over high-resolution fields by traditional verification methods, even if human analysts would tend to prefer a higher-resolution model (Gilleland et al. 2009).

In this vein, the present thesis, including the introductory chapters 1 to 4, the chapter 5 about the CALMET model's sensitivity to geophysical parameters, and the published paper chapters 6 to 8, have addressed the generation of high-resolution wind fields and the spatial evaluation of wind fields using empirical and dynamical modeling. This project has introduced the Wind Product Generator (WPG) application, the use of which has been applied to data from two networks of meteorological stations, the WegenerNet Feldbach Region (FBR), located in a hilly region, and the WegenerNet Johnsbachtal (JBT), located in a mountainous region.

The WPG produces wind fields with a spatial resolution of 100 m x 100 m and a temporal resolution of 30 minutes at 10 m and 50 m height levels with a maximum latency of about 1-2 hours. For the WegenerNet FBR, the generated gridded wind fields are available dating from 2007 and for the WegenerNet JBT dating from 2012. The WPG-produced wind fields were then used as evaluation

data and intercompared with wind field analysis data and dynamical climate model wind field data. A novel spatial verification methodology was used to evaluate the WPG-generated wind fields, namely the wind fractions skill score (WFSS); this methodology was chosen for its ability to avoid problems that tend to arise when verifying high-resolution vector fields.

In the first publication (chapter 6), the WPG was introduced and applied to the WegenerNet FBR. A core tool used by the WPG was the CALMET model (Scire et al. 1998). For this paper, the CALMET model was enhanced so that it could empirically take into account conditions such as topographic shading based on terrain height, the slope and aspect of topography, and the position of the sun. The model was also enhanced to take into account vertical temperature gradients and the influences of vegetation cover in the case of temperature fields (Bellasio et al. 2005).

The performance of the WPG was evaluated for two representative monthly periods; the wind fields produced by the WPG proved to be adequately accurate for both periods, such that the suitability of the WPG's use for this region was confirmed (Schlager et al. 2017).

The second publication (chapter 7) relates to the use of the WPG to generate high-resolution wind fields for the WegenerNet JBT study area. A gust model was also introduced and implemented within the WPG application in order to generates gridded fields representing peak gust speeds and corresponding gust directions at the 10 m height level. The wind fields generated by the WPG were again evaluated for two monthly periods, each consisting of representative weather conditions, and reasonable statistical agreement was found between the generated wind speeds and the observed data. Regarding wind direction, generating data for locations along mountain slopes was found to be particularly challenging.

Complementary investigations were made for a 5-year climate data record of the WegenerNet JBT (03/2012-02/2017) and a 9-year climate data record (03/2008-02/2017) of the WegenerNet FBR, regarding the statistical agreement between the WPG's generated wind fields and the corresponding station observations. Due to the greater density of the WegenerNet FBR network and its less challenging terrain, the WPG produced more accurate climatological wind fields for this region (Schlager et al. 2018).

In the third publication (chapter 8), an intercomparison was carried out for WPG wind fields in comparison with wind field analysis data from the Integrated Nowcasting through Comprehensive Analysis (INCA) system and with dynamical climate model wind field data from the non-hydrostatic climate model of the Consortium for Small Scale Modeling Model in Climate Mode (CCLM). The wind data considered were classified into thermally-induced winds and strong wind events, and a method for the automatic selection of such events was developed. Besides traditional performance measures, the evaluation was performed based using the WFSS methodology, which was used to estimate spatial displacements of wind patterns and biases based on predefined wind direction classes for a range of wind speed categories. The WFSS provides scale-dependent information regarding

a model's level of skill and allows for the avoidance of the double penalty problem. Furthermore, this score allows to distinguish between near misses and large spatial displacements between modeled and reference wind fields.

The results obtained with both the INCA and the CCLM model are more accurate for the Wegener FBR than for the WegenerNet JBT. This is explained by the less-challenging terrain of the FBR compared to the JBT. Meanwhile, INCA wind fields for the FBR were found to be more skillful than the dynamical wind fields generated by the CCLM, as the coarse 3 km x 3 km resolution available for CCLM wind fields is not able to capture the variations in wind speed and direction that thermally-driven circulations produce. Due to the challenging, mountainous terrain of the WegenerNet JBT network, large spatial displacements were observed at all scales, along with biases in wind classes for both models and types of wind events (Schlager et al. 2019).

Acronyms

AR5 Fifth Assessment Report.

CALMET California Meteorological Model.

CCLM Consortium for Small Scale Modeling Model in Climate Mode.

CMIP5 The Coupled Model Intercomparison Project Phase 5.

CPCSs Convection-Permitting Climate Simulations.

DPG Data Product Generator.

FBR Feldbach Region.

FSS Fractions Skill Score.

GCMs Global Climate Models.

ICP Coordinated Intercomparison Project.

INCA Integrated Nowcasting through Comprehensive Analysis.

IPCC Intergovernmental Panel on Climate Change.

JBT Johnsbachtal.

MCSCIPUF Mass Consistent Model associated with the Second Order Closure Integrated Puff transport/dispersion model.

RCMs Regional climate models.

RCPs Representative Concentration Pathways.

RF Radiative Forcing.

SWIFT Stationary Wind Field and Turbulence model.

WFSS Wind Fractions Skill Score.

WPG Wind Product Generator.

WPS WegenerNet Processing System.

List of Figures

List of Tables

Bibliography

Abdel-Aal, R., M. Elhadidy, and S. Shaahid (July 2009). "Modeling and forecasting the mean hourly wind speed time series using GMDH-based abductive networks". *Renewable Energy* 34.7, pp. 1686–1699. ISSN: 09601481. DOI: 10.1016/j.renene.2009.01.001.

Aebischer, U. and C. Schär (1998). "Low-Level Potential Vorticity and Cyclogenesis to the Lee of the Alps". *J. Atmos. Sci.* 55.2, pp. 186–207. DOI: 10.1175/1520-0469(1998)055<0186:LLPVAC>2.0.CO;2.

Alexander, G. D., J. A. Weinman, V. M. Karyampudi, W. S. Olson, and A. C. L. Lee (1999). "The Effect of Assimilating Rain Rates Derived from Satellites and Lightning on Forecasts of the 1993 Superstorm". *Mon. Wea. Rev.* 127.7, pp. 1433–1457. DOI: 10.1175/1520-0493(1999)127<1433:TEOARR>2.0.CO;2.

Alexandru, A., R. de Elia, R. Laprise, L. Separovic, and S. Biner (2009). "Sensitivity Study of Regional Climate Model Simulations to Large-Scale Nudging Parameters". *Mon. Wea. Rev.* 137.5, pp. 1666–1686. DOI: 10.1175/2008MWR2620.1.

Archer, C. L. and K. Caldeira (2008). "Historical trends in the jet streams". *Geophys. Res. Lett.* 35, L08803. DOI: 10.1029/2008GL033614.

Armstrong, L., K. Butler, J. Settelmaier, T. Vance, and O. Wilhelmi (2015). *Mapping and Modeling Weather and Climate with GIS*. California, USA: ESRI PR, p. 370. ISBN: 1589483766.

Awan, N. K., H. Truhetz, and A. Gobiet (June 2011). "Parameterization-induced error characteristics of MM5 and WRF operated in climate mode over the alpine region: An ensemble-based analysis". *J. Climate* 24.12, pp. 3107–3123. ISSN: 08948755. DOI: 10.1175/2011JCLI3674.1.

Baldauf, M., A. Seifert, J. Förstner, D. Majewski, M. Raschendorfer, and T. Reinhardt (2011). "Operational Convective-Scale Numerical Weather Prediction with the COSMO Model: Description and Sensitivities". *Mon. Wea. Rev.* 139.12, pp. 3887–3905. DOI: 10.1175/MWR-D-10-05013.1.

Barnes, E. A. (2013). "Revisiting the evidence linking Arctic amplification to extreme weather in midlatitudes". *Geophys. Res. Lett.* 40. DOI: 10.1002/grl.50880.

Barnes, E. A. and J. A. Screen (2015). "The impact of Arctic warming on the midlatitude jet-stream: Can it? Has it? Will it?" *WIRes. Clim. Change* 6.3, pp. 277–286. DOI: 10.1002/wcc.337.

Barriopedro, D., E. M. Fischer, J. Luterbacher, R. M. Trigo, and R. García-Herrera (2011). "The Hot Summer of 2010: Redrawing the Temperature Record Map of Europe". *Science* 332.6026, pp. 220–224. DOI: 10.1126/science.1201224.

Barry, R. G. (2008). *Mountain Weather and Climate*. 3rd ed. Cambridge: Cambridge University Press. DOI: 10.1017/CBO9780511754753.

Bartalev, S., A. Belward, D. Ershov, and A. S. Isaev (May 2003). "A new SPOT4-VEGETATION derived land cover map of Northern Eurasia". *Int. J. Remote Sens.* 24, pp. 1977–1982. DOI: 10.1080/0143116031000066297.

Bechtold, P., J.-P. Chaboureau, A. Beljaars, A. K. Betts, M. Köhler, M. Miller, and J.-L. Redelsperger (2004). "The simulation of the diurnal cycle of convective precipitation over land in a global model". *Quart. J. Roy. Meteor. Soc.* 130.604, pp. 3119–3137. DOI: 10.1256/qj.03.103.

Bechtold, P., M. Köhler, T. Jung, F. Doblas-Reyes, M. Leutbecher, M. J. Rodwell, F. Vitart, and G. Balsamo (2008). "Advances in simulating atmospheric variability with the ECMWF model: From synoptic to decadal time-scales". *Quart. J. Roy. Meteor. Soc.* 134.634, pp. 1337–1351. ISSN: 1477-870X. DOI: 10.1002/qj.289. URL: http://dx.doi.org/10.1002/qj.289.

Bellasio, R., G. Maffeis, J. S. Scire, M. G. Longoni, R. Bianconi, and N. Quaranta (Mar. 2005). "Algorithms to Account for Topographic Shading Effects and Surface Temperature Dependence on Terrain Elevation in Diagnostic Meteorological Models". *Boundary Layer Meteorol.* 114.3, pp. 595–614. ISSN: 0006-8314. DOI: 10.1007/s10546-004-1670-6.

Bendix, J. (July 2004). *Geländeklimatologie*. (in German). Stuttgart, Germany: Schweizerbart Science Publishers. ISBN: 9783443071394.

Bengtsson, L., K. I. Hodges, and E. Roeckner (2005). "Storm Tracks and Climate Change". *J. Climate* 19.15, pp. 3518–3543. DOI: 10.1175/JCLI3815.1.

Berry, D. I. and E. C. Kent (2011). "Air–Sea fluxes from ICOADS: the construction of a new gridded dataset with uncertainty estimates". *Int. J. Climatol.* 31.7, pp. 987–1001. DOI: 10.1002/joc.2059.

Bianco, L., B. Tomassetti, E. Coppola, A. Fracassi, M. Verdecchia, and G. Visconti (2006). "Thermally driven circulation in a region of complex topography: comparison of wind-profiling radar measurements and MM5 numerical predictions". *Ann. Geophys.* 24.6, pp. 1537–1549. DOI: 10.5194/angeo-24-1537-2006.

Böhm, U., M. Kücken, W. Ahrens, A. Block, D. Hauffe, B. Keuler, B. Rockel, and A. Will (2006). "CLM-The Climate Version of LM: Brief Description and Long-Term Applications". In: *COSMO Newsletter*. 6th ed. [Available online at http://www.cosmo-model.org/content/model/documentation/newsLetters/newsLetter06/newsLetter_06.pdf.]. Deutscher Wetterdienst (DWD), pp. 225–236.

Bracegirdle, T. J., E. Shuckburgh, J. B. Sallee, Z. Wang, A. J. Meijers, N. Bruneau, T. Phillips, and L. J. Wilcox (2013). "Assessment of surface winds over the atlantic, indian, and pacific ocean sectors of the southern ocean in cmip5 models: Historical bias, forcing response, and state dependence". *J. Geophys. Res. Atmos.* DOI: 10.1002/jgrd.50153.

Briggs, W. M. and R. A. Levine (1997). "Wavelets and Field Forecast Verification". *Mon. Wea. Rev.* 125.6, pp. 1329–1341. DOI: 10.1175/1520-0493(1997)125<1329:WAFFV>2.0.CO;2.

Brockhaus, P., D. Lüthi, and C. Schär (Aug. 2008). "Aspects of the diurnal cycle in a regional climate model". *Met. Z.* 17.4, pp. 433–443. DOI: 10.1127/0941-2948/2008/0316.

Brunner, L., G. C. Hegerl, and A. K. Steiner (2017). "Connecting atmospheric blocking to European temperature extremes in spring". *J. Climate* 30.2, pp. 585–594. DOI: 10.1175/JCLI-D-16-0518.1.

Bubnová, R., G. Hello, P. Bénard, and J.-F. Geleyn (1995). "Integration of the Fully Elastic Equations Cast in the Hydrostatic Pressure Terrain-Following Coordinate in the Framework of the ARPEGE/Aladin NWP System". *Mon. Wea. Rev.* 123.2, pp. 515–535. DOI: 10.1175/1520-0493(1995)123<0515:IOTFEE>2.0.CO;2.

Buzzi, A. and S. Tibaldi (1978). "Cyclogenesis in the lee of the Alps: A case study". *Quart. J. Roy. Meteor. Soc.* 104.440, pp. 271–287. DOI: 10.1002/qj.49710444004.

Casas-Prat, M., X. Wang, and N. Swart (2018). "CMIP5-based global wave climate projections including the entire Arctic Ocean". *Ocean Modell.* 123, pp. 66–85. ISSN: 1463-5003. DOI: https://doi.org/10.1016/j.ocemod.2017.12.003.

Cattiaux, J., R. Vautard, C. Cassou, P. Yiou, V. Masson-Delmotte, and F. Codron (2010). "Winter 2010 in Europe: A cold extreme in a warming climate". *Geophys. Res. Lett.* 37.20, L20704. DOI: 10.1029/2010GL044613.

Catto, J. L., N. Nicholls, C. Jakob, and K. L. Shelton (2014). "Atmospheric fronts in current and future climates". *Geophys. Res. Lett.* 41.21, pp. 7642–7650. DOI: 10.1002/2014GL061943.

Cheng, C. S., E. Lopes, C. Fu, and Z. Huang (2014). "Possible Impacts of Climate Change on Wind Gusts under Downscaled Future Climate Conditions: Updated for Canada". *J. Climate* 27.3, pp. 1255–1270. DOI: 10.1175/JCLI-D-13-00020.1.

Cheng, C.-H., F. Nnadi, and Y.-A. Liou (2015). "A Regional Land Use Drought Index for Florida". *Remote Sens.* 7.12, pp. 17149–17167. ISSN: 2072-4292. URL: http://www.mdpi.com/2072-4292/7/12/15879.

Cheng, F.-Y. and D. W. Byun (2008). "Application of high resolution land use and land cover data for atmospheric modeling in the Houston–Galveston metropolitan area, Part I: Meteorological simulation results". *Atmos. Environ.* 42.33, pp. 7795–7811. ISSN: 1352-2310. DOI: https://doi.org/10.1016/j.atmosenv.2008.04.055. URL: http://www.sciencedirect.com/science/article/pii/S1352231008004664.

Compo, G. P., J. S. Whitaker, P. D. Sardeshmukh, N. Matsui, R. J. Allan, X. Yin, B. E. Gleason, R. S. Vose, G. Rutledge, P. Bessemoulin, S. Brönnimann, M. Brunet, R. I. Crouthamel, A. N. Grant, P. Y. Groisman, P. D. Jones, M. C. Kruk, A. C. Kruger, G. J. Marshall, M. Maugeri, H. Y. Mok, Ø. Nordli, T. F. Ross, R. M. Trigo, X. L. Wang, S. D. Woodruff, and S. J. Worley (2011). "The Twentieth Century Reanalysis Project". *Quart. J. Roy. Meteor. Soc.* 137.654, pp. 1–28. DOI: 10.1002/qj.776.

Corby, G. A. (Oct. 1954). "THE AIRFLOW OVER MOUNTAINS. A review of the state of current knowledge". *MAUSAM* 80, pp. 491–521. DOI: 10.1002/qj.49708034602.

Coughlin, J. D. (Mar. 2005). "FORECASTING THE ONSET AND INTENSITY OF VERTICALLY PROPAGATING MOUNTAIN WAVES OVER THE ALPS". PhD thesis. Monterey California: Naval Postgraduate School.

Cox, R. M., J. Sontowski, and C. M. Dougherty (Dec. 2005). "An evaluation of three diagnostic wind models (CALMET, MCSCIPUF, and SWIFT) with

wind data from the Dipole Pride 26 field experiments". *Meteor. Appl.* 12.04, pp. 329–341. ISSN: 1350-4827. DOI: 10.1017/S1350482705001908.

Davies, H. C. (1976). "A lateral boundary formulation for multi-level prediction models". *Quart. J. Roy. Meteor. Soc.* 102.432, pp. 405–418. DOI: 10.1002/qj.49710243210.

Defant, F. (1949). "Zur Theorie der Hangabwinde nebst Bemerkungen zur Theorie der Berg- und Talwinde. [A theory of slope winds, along with remarks on the theory of mountain winds and valley winds]". In: *Arch. f. Meteorol., Geophys. u. Biokl.* 1st ed. [English translation: Whiteman, C.D., and E. Dreiseitl, 1984: Alpine meteorology: Translations of classic contributions by A. Wagner, E. Ekhart and F. Defant. PNL-5141 / ASCOT-84-3. Pacific Northwest Laboratory, Richland, Washington, 121 pp], pp. 421–450.

Defant, F. (1951). "Local Winds". In: *Compendium of Meteorology: Prepared under the Direction of the Committee on the Compendium of Meteorology*. Ed. by T. F. Malone. Boston, MA: American Meteorological Society, pp. 655–672. ISBN: 978-1-940033-70-9. DOI: 10.1007/978-1-940033-70-9_54.

Dickinson, M. J. and D. J. Knight (1999). "Frontal Interaction with Mesoscale Topography". *J. Atmos. Sci.* 56.20, pp. 3544–3559. DOI: 10.1175/1520-0469(1999)056<3544:FIWMT>2.0.CO;2.

Dong, B., R. T. Sutton, T. Woollings, and K. Hodges (2013). "Variability of the North Atlantic summer storm track: mechanisms and impacts on European climate". *Environ. Res. Lett.* 8.3, p. 034037. DOI: 10.1088/1748-9326/8/3/034037.

Dorninger M., M. P., E. Mittermaier, E. E. Gilleland, B. G. Ebert, Brown, and L. J. Wilson (2013). *MesoVICT:Mesoscale Verification Inter-Comparison over Complex Terrain*. Tech. rep. Technical Note NCAR/TN-505+STR, p. 23. DOI: 10.5065/D6416V21.

Durran, D. R. (1990). "Mountain waves and downslope winds". In: *Atmospheric Processes over Complex Terrain*. Ed. by W. Blumen. Meteorological Monographs. Boston, MA: American Meteorological Society, pp. 59–81. ISBN: 9781935704256.

Durran, D. R., M. O. G. Hills, and P. N. Blossey (2015). "The Dissipation of Trapped Lee Waves. Part I: Leakage of Inviscid Waves into the Stratosphere". *J. Atmos. Sci.* 72.4, pp. 1569–1584. DOI: 10.1175/JAS-D-14-0238.1.

Ebert, E. E. (2008). "Fuzzy verification of high-resolution gridded forecasts: a review and proposed framework". *Meteorol. Appl.* 15.1, pp. 51–64. DOI: 10.1002/met.25.

EEA (Dec. 2007). *CLC2006 technical guidelines*. Tech. rep. European Environment Agency (EEA). URL: http://www.eea.europa.eu.

EPA., U. (2004). *User's Guide for the AERMOD Meteorological Preprocessor (AERMET)*. U.S. Environmental Protection Agency. Research Triangle Park, North Carolina 27711.

EUMeTrain (2017). *Gravity Waves*. URL: http://www.eumetrain.org/data/4/452/navmenu.php?tab=4&page=1.0.0 (visited on 11/22/2018).

Fant, C., C. A. Schlosser, and K. Strzepek (2016). "The impact of climate change on wind and solar resources in southern Africa". *Atmos. Environ.* 161, pp. 556–564. ISSN: 0306-2619. DOI: https://doi.org/10.1016/j.apenergy.2015.03.042.

Feldstein, S. B. and S. Lee (2014). "Intraseasonal and Interdecadal Jet Shifts in the Northern Hemisphere: The Role of Warm Pool Tropical Convection and Sea Ice". *J. Climate* 27.17, pp. 6497–6518. DOI: 10.1175/JCLI-D-14-00057.1.

Förchgott, J. (1949). "Wave streaming in the lee of mountain ridges". *Bull. Meteor. Czech.* 3, p. 49.

Fosser, G., S. Khodayar, and P. Berg (2014). "Benefit of convection permitting climate model simulations in the representation of convective precipitation". *Climate Dyn.* 44.1-2, pp. 45–60. DOI: 10.1007/s00382-014-2242-1.

Francis, J. A. and S. J. Vavrus (2015). "Evidence for a wavier jet stream in response to rapid Arctic warming". *Environ. Res. Lett.* 10.1. DOI: 10.1088/1748-9326/10/1/014005.

Frey, C. M., E. Parlow, R. Vogt, M. Harhash, and M. M. Abdel Wahab (2011). "Flux measurements in Cairo. Part 1: in situ measurements and their applicability for comparison with satellite data". *Int. J. Climatol.* 31.2, pp. 218–231. DOI: 10.1002/joc.2140. eprint: https://rmets.onlinelibrary.wiley.com/doi/pdf/10.1002/joc.2140. URL: https://rmets.onlinelibrary.wiley.com/doi/abs/10.1002/joc.2140.

Fuchsberger, J., G. Kirchengast, T. Kabas, and C. Bichler (Mar. 2016). "WegenerNet climate station networks: overview and examples". In: *LTER-Austria Conference 2016*. Austrian Long-Term Ecosystem Research Network.

Gal-Chen, T. and R. C. Somerville (1975). "On the use of a coordinate transformation for the solution of the Navier-Stokes equations". *J. Comput. Phys.* 17.2, pp. 209–228. DOI: https://doi.org/10.1016/0021-9991(75)90037-6.

Galarneau Jr., T. J., T. M. Hamill, R. M. Dole, and J. Perlwitz (2012). "A Multiscale Analysis of the Extreme Weather Events over Western Russia and Northern Pakistan during July 2010". *Mon. Wea. Rev.* 140, pp. 1639–1664. DOI: 10.1175/MWR-D-11-00191.1.

Gao, Y., S. Weiher, T. Markkanen, H. Gregow, M. Helena, D. Jacob, and A. Laaksonen (2015). "Implementation of the CORINE land use classification in the regional climate model REMO". *Boreal Environ. Res.* 6095.April, pp. 261–282.

Gerard, L. and J.-F. Geleyn (2005). "Evolution of a subgrid deep convection parametrization in a limited-area model with increasing resolution". *Quart. J. Roy. Meteor. Soc.* 131.610, pp. 2293–2312. DOI: 10.1256/qj.04.72.

Giard, D. and E. Bazile (2000). "Implementation of a New Assimilation Scheme for Soil and Surface Variables in a Global NWP Model". *Mon. Wea. Rev.* 128.4, pp. 997–1015. DOI: 10.1175/1520-0493(2000)128<0997:IOANAS>2.0.CO;2.

Gibbon, J. D. and D. D. Holm (2011). "Extreme events in solutions of hydrostatic and non-hydrostatic climate models". *Phil. Trans. R. Soc. A* 369.1939, pp. 1156–1179. DOI: 10.1098/rsta.2010.0244.

Gilleland, E. (2013). "Testing Competing Precipitation Forecasts Accurately and Efficiently: The Spatial Prediction Comparison Test". *Mon. Wea. Rev.* 141.1, pp. 340–355. DOI: 10.1175/MWR-D-12-00155.1.

Gilleland, E., D. A. Ahijevych, B. G. Brown, and E. E. Ebert (2010). "Verifying Forecasts Spatially". *Bull. Amer. Meteor. Soc.* 91.10, pp. 1365–1376. DOI: 10.1175/2010BAMS2819.1.

Gilleland, E., D. Ahijevych, B. G. Brown, B. Casati, and E. E. Ebert (2009). "Intercomparison of Spatial Forecast Verification Methods". *Wea. Forecasting* 24.5, pp. 1416–1430. DOI: 10.1175/2009WAF2222269.1.

GLC2016 (2016). *Global land cover 2000 - Europe*. URL: https://www.eea.europa.eu/data-and-maps/data/global-land-cover-2000-europe (visited on 05/23/2019).

Gómez-Navarro, J. J., C. C. Raible, and S. Dierer (2015). "Sensitivity of the WRF model to PBL parametrisations and nesting techniques: evaluation of wind storms over complex terrain". *Geosci. Model Dev.* 8.10, pp. 3349–3363. DOI: 10.5194/gmd-8-3349-2015. URL: https://www.geosci-model-dev.net/8/3349/2015/.

Govindasamy, B. and K. Caldeira (2000). "Geoengineering Earth's radiation balance to mitigate CO2-induced climate change". *Geophys. Res. Lett.* 27.14, pp. 2141–2144. DOI: 10.1029/1999GL006086.

Grell, G. A., L. Schade, R. Knoche, A. Pfeiffer, and J. Egger (2000). "Nonhydrostatic climate simulations of precipitation over complex terrain". *J. Geophys. Res. Atmos.* 105.D24, pp. 29595–29608. DOI: 10.1029/2000JD900445.

Gross, G. (Feb. 1996). "On the applicability of numerical mass-consistent wind field models". *Boundary Layer Meteorol.* 77.3, pp. 379–394. DOI: 10.1007/BF00123533.

Haiden, T., A. Kann, C. Wittmann, G. Pistotnik, B. Bica, and C. Gruber (2011). "The Integrated Nowcasting through Comprehensive Analysis (INCA) system and its validation over the eastern alpine region". *Wea. Forecasting* 26.2, pp. 166–183. ISSN: 0882-8156. DOI: 10.1175/2010WAF2222451.1.

Hansen, J., D. Johnson, A. Lacis, S. Lebedeff, P. Lee, D. Rind, and G. Russell (1981). "Climate Impact of Increasing Atmospheric Carbon Dioxide". *Science* 213.4511, pp. 957–966. DOI: 10.1126/science.213.4511.957.

Harris, D., E. Foufoula-Georgiou, K. K. Droegemeier, and J. J. Levit (2001). "Multiscale Statistical Properties of a High-Resolution Precipitation Forecast". *J. Hydrometeorol.* 2.4, pp. 406–418. DOI: 10.1175/1525-7541(2001)002<0406:MSPOAH>2.0.CO;2.

Hasselmann, K. (1993). "Optimal Fingerprints for the Detection of Time-dependent Climate Change". *J. Climate* 6.10, pp. 1957–1971. DOI: 10.1175/1520-0442(1993)006<1957:OFFTDO>2.0.CO;2.

Haylock, M. R., N. Hofstra, A. M. G. Klein Tank, E. J. Klok, P. D. Jones, and M. New (2008). "A European daily high-resolution gridded data set of surface temperature and precipitation for 1950–2006". *J. Geophys. Res.* 113.D20, D20119. DOI: 10.1029/2008JD010201.

Hewer, F. (June 1998). "Non-Linear Numerical Model Predictions of Flow Over an Isolated Hill of Moderate Slope". *Bound.Layer Meteor.* 87.3, pp. 381–408. ISSN: 1573-1472. DOI: 10.1023/A:1000944817965.

Hiebl, J. and C. Frei (2016). "Daily temperature grids for Austria since 1961—concept, creation and applicability". 124.1-2, pp. 161–178. ISSN: 14344483. DOI: 10.1007/s00704-015-1411-4.

Hoffman, R. N., Z. Liu, J.-F. Louis, and C. Grassoti (1995). "Distortion Representation of Forecast Errors". *Mon. Wea. Rev.* 123.9, pp. 2758–2770. DOI: 10.1175/1520-0493(1995)123<2758:DROFE>2.0.CO;2.

Hohenegger, C., P. Brockhaus, and C. Schär (Aug. 2008). "Towards climate simulations at cloud-resolving scales". *Met. Z.* 17.4, pp. 383–394. DOI: 10.1127/0941-2948/2008/0303.

Hohmann, C., G. Kirchengast, and S. Birk (Mar. 2018). "Alpine foreland running drier? Sensitivity of a drought vulnerable catchment to changes in climate, land use, and water management". *Climatic Change* 147, pp. 179–193. ISSN: 1573-1480. DOI: 10.1007/s10584-017-2121-y.

Hughes, T. P. et al. (2017). "Global warming and recurrent mass bleaching of corals". *Nature* 543.7645, pp. 373–377. DOI: 10.1038/nature21707.

IPCC (2007). *Climate Change 2007: The Physical Science Basis. Contribution of Working Group I to the Fourth Assessment Report of the Intergovernmental Panel on Climate Change*. Ed. by S. Solomon, D. Qin, M. Manning, Z. Chen, M. Marquis, K. B. Averyt, M. Tignor, and H. L. Miller. Cambridge, United Kingdom and New York, NY, USA: Cambridge University Press.

– (2012). "Summary for Policymakers". In: *Managing the Risks of Extreme Events and Disasters to Advance Climate Change Adaptation – A Special Report of Working Groups I and II of the Intergovernmental Panel on Climate Change*. Ed. by C. Field, V. Barros, T. Stocker, D. Q. abd D.J. Dokken, K. Ebi, M. Mastrandrea, K. Mach, G.-K. Plattner, S. Allen, M. Tignor, and P. Midgley. Cambridge, UK, and New York, NY, USA: Cambridge University Press, pp. 1–19.

– (2013). *Climate Change 2013: The Physical Science Basis. Contribution of Working Group I to the Fifth Assessment Report of the Intergovernmental Panel on Climate Change*. Ed. by T. F. Stocker, D. Qin, G.-K. Plattner, M. Tignor, S. K. Allen, J. Boschung, A. Nauels, Y. Xia, V. Bex, and P. M. Midgley. Cambridge, United Kingdom and New York, NY, USA: Cambridge University Press. 1535 pp.

– (2014). *Climate Change 2014: Impacts, Adaptation, and Vulnerability. Part A: Global and Sectoral Aspects. Contribution of Working Group II to the Fifth Assessment Report of the Intergovernmental Panel on Climate Change*. Ed. by C. B. Field, V. R. Barros, D. J. Dokken, K. J. Mach, M. D. Mastrandrea, T. E. Bilir, M. Chatterjee, K. L. Ebi, Y. O. Estrada, R. C. Genova, B. Girma, E. S. Kissel, A. N. Levy, S. MacCracken, P. R. Mastrandrea, and L. L. White. Cambridge, United Kingdom and New York, NY, USA: Cambridge University Press. 1132 pp.

Jancewicz, K. (Aug. 2013). "Remote Sensing Data in Wind Velocity Field Modelling: a Case Study from the Sudetes (SW Poland)". *Pure Appl. Geophys.* 171.6, pp. 941–964. ISSN: 0033-4553. DOI: 10.1007/s00024-013-0698-2.

Kabas, T. (2012). *WegenerNet climate station network region Feldbach: Experimental setup and high resolution data for weather and climate research (in German)*. (in German). Scientific Rep. 47-2012. [Available online at http://wegcwww.uni-graz.at/publ/wegcreports/2012/WCV-WissBer-No47-TKabas-Jan2012.pdf.] Graz, Austria: Wegener Center Verlag, p. 177. 177 pp. ISBN: 978-3-9503112-4-2.

Kabas, T., U. Foelsche, and G. Kirchengast (June 2011). "Seasonal and annual trends of temperature and precipitation within 1951/1971-2007 in south-eastern

Styria, Austria". *Meteor. Z.* 20.3, pp. 277–289. ISSN: 09412948. DOI: 10.1127/0941-2948/2011/0233.

Kalyanapu, A. J., S. J. Burian, and T. N. McPherson (2009). "Effect of land use-based surface roughness on hydrologic model output". *Journal of Spatial Hydrology* 9.2, pp. 51–71. ISSN: 15304736.

Kann, A., I. Meirold-Mautner, F. Schmid, G. Kirchengast, J. Fuchsberger, V. Meyer, L. Tuechler, and B. Bica (2015a). "Evaluation of high-resolution precipitation analyses using a dense station network". *Hydrol. Earth Syst. Sci.* 19.3, pp. 1547–1559. ISSN: 1607-7938. DOI: 10.5194/hess-19-1547-2015.

Kann, A., C. Wittmann, B. Bica, and C. Wastl (2015b). "On the Impact of NWP Model Background on Very High–Resolution Analyses in Complex Terrain". *Wea. Forecasting* 30.4, pp. 1077–1089. DOI: 10.1175/WAF-D-15-0001.1.

Kendon, E. J., N. Ban, N. M. Roberts, H. J. Fowler, M. J. Roberts, S. C. Chan, J. P. Evans, G. Fosser, and J. M. Wilkinson (2017). "Do convection-permitting regional climate models improve projections of future precipitation change?" *Bull. Amer. Meteor. Soc.* 98.1, pp. 79–93. ISSN: 00030007. DOI: 10.1175/BAMS-D-15-0004.1.

Kennedy, D., T. Parker, T. Woollings, B. Harvey, and L. Shaffrey (2016). "The response of high-impact blocking weather systems to climate change". *Geophys. Res. Lett.* 43.13, pp. 7250–7258. DOI: 10.1002/2016GL069725.

Kent, E. C., S. Fangohr, and D. I. Berry (2012). "A comparative assessment of monthly mean wind speed products over the global ocean". *Int. J. Climatol.* 33.11, pp. 2520–2541. DOI: 10.1002/joc.3606.

Khodayar, S., N. Kalthoff, and G. Schädler (Aug. 2013). "The impact of soil moisture variability on seasonal convective precipitation simulations. Part I: validation, feedbacks, and realistic initialisation". *Met. Z.* 22.4, pp. 489–505. DOI: 10.1127/0941-2948/2013/0403.

Kida, H., T. Koide, H. Sasaki, and M. Chiba (1991). "A New Approach for Coupling a Limited Area Model to a GCM for Regional Climate Simulations". *J. Meteor. Soc. Japan* 69.6, pp. 723–728. DOI: 10.2151/jmsj1965.69.6_723.

Kirchengast, G., T. Kabas, A. Leuprech, C. Bichler, and H. Truhetz (Feb. 2014). "WegenerNet: A pioneering high-resolution network for monitoring weather and climate". *Bull. Amer. Meteor. Soc.* 95.2, pp. 227–242. ISSN: 0003-0007. DOI: 10.1175/BAMS-D-11-00161.1.

Kljun, N., M. Sprenger, and C. Schär (2001). "Frontal modification and lee cyclogenesis in the Alps: A case study using the ALPEX reanalysis data set". *Meteorol. Atmos. Phys.* 78.1, pp. 89–105. DOI: 10.1007/s007030170008.

Klok, E. J. and A. M. G. Klein Tank (2009). "Updated and extended European dataset of daily climate observations". *Int. J. Climatol.* 29.8, pp. 1182–1191. DOI: 10.1002/joc.1779.

Knote, C., G. Bonafe, and F. Di Giuseppe (2009). "Leaf Area Index Specification for Use in Mesoscale Weather Prediction Systems". *Mon. Wea. Rev.* 137.10, pp. 3535–3550. DOI: 10.1175/2009MWR2891.1. eprint: https://doi.org/10.1175/2009MWR2891.1. URL: https://doi.org/10.1175/2009MWR2891.1.

Kug, J.-S., D.-H. Choi, F.-F. Jin, W.-T. Kwon, and H.-L. Ren (2010). "Role of synoptic eddy feedback on polar climate responses to the anthropogenic forcing". *Geophys. Res. Lett.* 37.14. DOI: 10.1029/2010GL043673.

Kyselý, J. (2007). "Implications of enhanced persistence of atmospheric circulation for the occurrence and severity of temperature extremes". *Int. J. Climatol.* 27.5, pp. 689–695. DOI: 10.1002/joc.1478.

Lack, S. A., G. L. Limpert, and N. I. Fox (2010). "An Object-Oriented Multi-scale Verification Scheme". *Wea. Forecasting* 25.1, pp. 79–92. DOI: 10.1175/2009WAF2222245.1.

Lamptey, B. (2010). "An analytical framework for estimating the urban effect on climate". *Int. J. Climatol.* 30.1, pp. 72–88. DOI: 10.1002/joc.1873.

Langhans, W., J. Schmidli, O. Fuhrer, S. Bieri, and C. Schär (2013). "Long-Term Simulations of Thermally Driven Flows and Orographic Convection at Convection-Parameterizing and Cloud-Resolving Resolutions". *J. Appl. Meteor.* 52.6, pp. 1490–1510. DOI: 10.1175/JAMC-D-12-0167.1.

Langhans, W., J. Schmidli, and C. Schär (2012). "Bulk Convergence of Cloud-Resolving Simulations of Moist Convection over Complex Terrain". *J. Atmos. Sci.* 69.7, pp. 2207–2228. DOI: 10.1175/JAS-D-11-0252.1.

Lau, N.-C. and M. J. Nath (2014). "Model Simulation and Projection of European Heat Waves in Present-Day and Future Climates". *J. Climate* 27.10, pp. 3713–3730. DOI: 10.1175/JCLI-D-13-00284.1.

Lean, H. W., P. A. Clark, M. Dixon, N. M. Roberts, A. Fitch, R. Forbes, and C. Halliwell (2008). "Characteristics of High-Resolution Versions of the Met Office Unified Model for Forecasting Convection over the United Kingdom". *Mon. Wea. Rev.* 136.9, pp. 3408–3424. DOI: 10.1175/2008MWR2332.1.

Leutwyler, D., O. Fuhrer, X. Lapillonne, D. Lüthi, and C. Schär (2016). "Towards European-scale convection-resolving climate simulations with GPUs: A study with COSMO 4.19". *Geosci. Model Dev.* 9.9, pp. 3393–3412. ISSN: 19919603. DOI: 10.5194/gmd-9-3393-2016.

Lin, K. M., J. Y. Juang, Y.-W. Shiu, and L. F. W. Chang (2016). "Estimating the Bowen Ratio for Application in Air Quality Models by Integrating a Simplified Analytical Expression with Measurement Data". *J. Appl. Meteor.* 55.4, pp. 1041–1048. DOI: 10.1175/JAMC-D-15-0080.1.

Lin, Y.-L. (2007). *Mesoscale Dynamics*. North Carolina, USA: Cambridge University Press, p. 630. ISBN: 9780511619649.

Lucas-Picher, P., J. Cattiaux, A. Bougie, and R. Laprise (2016). "How does large-scale nudging in a regional climate model contribute to improving the simulation of weather regimes and seasonal extremes over North America?" *Climate Dyn.* 46.3-4, pp. 929–948. DOI: 10.1007/s00382-015-2623-0.

Lugauer, M. and P. Winkler (Feb. 2005). "Thermal circulation in South Bavaria – climatology and synoptic aspects". *Meteor. Z.* 14.1, pp. 15–30. ISSN: 09412948. DOI: 10.1127/0941-2948/2005/0014-0015.

Mahrt, L. (1982). "Momentum Balance of Gravity Flows". *J. Atmos. Sci.* 39.12, pp. 2701–2711. DOI: 10.1175/1520-0469(1982)039<2701:MBOGF>2.0.CO;2.

Marzban, C. and S. Sandgathe (2009). "Verification with Variograms". *Wea. Forecasting*. ISSN: 0882-8156. DOI: 10.1175/2009WAF2222122.1.

Mass, C. F., D. Ovens, K. Westrick, and B. A. Colle (2002). "Does Increasing Horizontal Resolution Produce More Skillful Forecasts?" *Bull. Amer. Meteor. Soc.* DOI: 10.1175/1520-0477(2002)083<0407:DIHRPM>2.3.CO;2.

McGowan, H. A. (2004). "Observations of Anti-winds in a Deep Alpine Valley, Lake Tekapo, New Zealand". *Arctic, Antarctic, and Alpine Res.* 36, pp. 495–501. DOI: https://doi.org/10.1657/1523-0430(2004)036[0495:OOAIAD]2.0.CO;2.

McVicar, T. R., M. L. Roderick, R. J. Donohue, L. T. Li, T. G. V. Niel, A. Thomas, J. Grieser, D. Jhajharia, Y. Himri, N. M. Mahowald, A. V. Mescherskaya, A. C. Kruger, S. Rehman, and Y. Dinpashoh (2012). "Global review and synthesis of trends in observed terrestrial near-surface wind speeds: Implications for evaporation". *J. Hydrol.* 416-417, pp. 182–205. DOI: https://doi.org/10.1016/j.jhydrol.2011.10.024.

Meleshko, V. P., O. M. Johannessen, A. V. Baidin, T. V. Pavlova, and V. A. Govorkova (2016). "Arctic amplification: does it impact the polar jet stream?" *Tellus A* 68.1, p. 32330. DOI: 10.3402/tellusa.v68.32330.

Miller, R. L., G. A. Schmidt, and D. T. Shindell (2006). "Forced annular variations in the 20th century Intergovernmental Panel on Climate Change Fourth Assessment Report models". *J. Geophys. Res. Atmos.* 111.D18. DOI: 10.1029/2005JD006323.

Miura, H., M. Satoh, H. Tomita, A. T. Noda, T. Nasuno, and S.-i. Iga (2007). "A short-duration global cloud-resolving simulation with a realistic land and sea distribution". *Geophys. Res. Lett.* 34.2. DOI: 10.1029/2006GL027448.

Morales, L., F. Lang, and C. Mattar (Dec. 2012). "Mesoscale wind speed simulation using CALMET model and reanalysis information: An application to wind potential". *Renewable Energy* 48, pp. 57–71. ISSN: 09601481. DOI: 10.1016/j.renene.2012.04.048.

Moss, R. H., J. A. Edmonds, K. A. Hibbard, M. R. Manning, S. K. Rose, D. P. van Vuuren, T. R. Carter, S. Emori, M. Kainuma, T. Kram, G. A. Meehl, J. F. B. Mitchell, N. Nakicenovic, K. Riahi, S. J. Smith, R. J. Stouffer, A. M. Thomson, J. P. Weyant, and T. J. Wilbanks (2010). "The next generation of scenarios for climate change research and assessment". *Nature* 463, pp. 747–756. DOI: 10.1038/nature08823.

Nicholas, F. and J. Lewis (1980). *Relationships between aerodynamic roughness and land use and land cover in Baltimore, Maryland*. Professional Paper 1099-C. U.S. Department of the Interior.

Nicholls, J. M. (1973). *The Airflow over Mountains. Research, 1958–1972*. WMO Technical Note No. 127. Geneva: World Meteorological Organization.

Noilhan, J. and S. Planton (1989). "A Simple Parameterization of Land Surface Processes for Meteorological Models". *Mon. Wea. Rev.* 117.3, pp. 536–549. DOI: 10.1175/1520-0493(1989)117<0536:ASPOLS>2.0.CO;2.

O, S., U. Foelsche, G. Kirchengast, J. Fuchsberger, J. Tan, and W. A. Petersen (2017). "Evaluation of GPM IMERG Early, Late, and Final rainfall estimates

using WegenerNet gauge data in southeastern Austria". *Hydrol. Earth Syst. Sci.* 21, pp. 6559–6572. DOI: 10.5194/hess-21-6559-2017.

O, S., U. Foelsche, G. Kirchengast, and J. Fuchsberger (2018). "Validation and correction of rainfall data from the WegenerNet high density network in southeast Austria". *J. Hydrol.* 556, pp. 1110–1122. ISSN: 00221694. DOI: 10.1016/j.jhydrol.2016.11.049.

O'Gorman, P. A. (2010). "Understanding the varied response of the extratropical storm tracks to climate change". *PNAS* 107.45, pp. 19176–19180. DOI: 10.1073/pnas.1011547107.

Ogaja, J. and A. Will (Oct. 2016). "Fourth order, conservative discretization of horizontal Euler equations in the COSMO model and regional climate simulations". *Meteor. Z.* 25.5, pp. 577–605. DOI: 10.1127/metz/2016/0645.

Oleniacz, R. and M. Rzeszutek (2014). "Determination of Optimal Spatial Databases for the Area of Poland to the Calculation of Air Pollutant Disperssion Using the CALMET/CALPUFF Model". *GaEE* 8.2, pp. 57–69. DOI: http://dx.doi.org/10.7494/geom.2014.8.2.57.

Omrani, H., P. Drobinski, and T. Dubos (2012). "Spectral nudging in regional climate modelling: How strongly should we nudge?" *Quart. J. Roy. Meteor. Soc.* 138.668, pp. 1808–1813. DOI: 10.1002/qj.1894.

Osborn, T. J. and M. Hulme (Apr. 1998). "Evaluation of the European daily precipitation characteristics from the atmospheric model intercomparison project". *IJC* 18.5, pp. 505–522. ISSN: 1097-0088. DOI: 10.1002/(SICI)1097-0088(199804)18:5<505::AID-JOC263>3.0.CO;2-7.

Pettre, P. (1982). "On the Problem of Violent Valley Winds". *J. Atmos. Sci.* 39.3, pp. 542–554. DOI: 10.1175/1520-0469(1982)039<0542:OTPOVV>2.0.CO;2.

Pichler, H. and R. Steinacker (Mar. 1987). "On the synoptics and dynamics of orographically induced cyclones in the Mediterranean". *Meteorol. Atmos. Phys.* 36.1, pp. 108–117. DOI: 10.1007/BF01045144.

Pierrehumbert, R. T. and B. Wyman (1985). "Upstream Effects of Mesoscale Mountains". *J. Atmos. Sci.* 42.10, pp. 977–1003. DOI: 10.1175/1520-0469(1985)042<0977:UEOMM>2.0.CO;2.

Prein, A. F., A. Gobiet, M. Suklitsch, H. Truhetz, N. K. Awan, K. Keuler, and G. Georgievski (Nov. 2013a). "Added value of convection permitting seasonal simulations". *Climate Dyn.* 41.9, pp. 2655–2677. ISSN: 1432-0894. DOI: 10.1007/s00382-013-1744-6. URL: https://doi.org/10.1007/s00382-013-1744-6.

Prein, A. F. (2013). *Added Value of Convection Resolving Climate Simulations*. Scientific Report 53-2013. [Available online at http://wegcwww.uni-graz.at/publ/wegcreports/2013/WCV-SciRep-No53-APrein-Jul2013.pdf.] Graz, Austria: Wegener Center Verlag, p. 164. ISBN: ISBN 978-3-9503608-0-6.

Prein, A. F., G. J. Holland, R. M. Rasmussen, J. Done, K. Ikeda, M. P. Clark, and C. H. Liu (July 2013b). "Importance of regional climate model grid spacing for the simulation of heavy precipitation in the colorado headwaters". *J. Climate* 26.13, pp. 4848–4857. ISSN: 08948755. DOI: 10.1175/JCLI-D-12-00727.1.

Prein, A. F., W. Langhans, G. Fosser, A. Ferrone, N. Ban, K. Goergen, M. Keller, M. Toelle, O. Gutjahr, F. Feser, E. Brisson, S. Kollet, J. Schmidli, N. P. Van Lipzig, and R. Leung (2015). "A review on regional convection-permitting climate modeling: Demonstrations, prospects, and challenges". *Rev. Geophys.* 53.2, pp. 323–361. ISSN: 19449208. DOI: 10.1002/2014RG000475.

Prettenthaler, F., A. Podesser, and H. Pilger (2010). *Climate Atlas Styria, Period 1971-2000: An Application-Oriented Climatology (in German)*. Vol. 4. Wien: Verlag der Oesterreichischen Akademie der Wissenschaften, p. 358. ISBN: 978-3-7001-6754-9.

Prusa, J. M., P. K. Smolarkiewicz, and A. A. Wyszogrodzki (2008). "EULAG, a computational model for multiscale flows". *Comput. Fluids* 37.9, pp. 1193–1207. DOI: https://doi.org/10.1016/j.compfluid.2007.12.001.

Radinovic, D. (1986). "On the development of orographic cyclones". *Quart. J. Roy. Meteor. Soc.* 112.474, pp. 927–951. DOI: 10.1002/qj.49711247403.

Radu, R., M. Déqué, and S. Somot (2008a). "Spectral nudging in a spectral regional climate model". In: *Tellus, Series A: Dynamic Meteorology and Oceanography*. DOI: 10.1111/j.1600-0870.2008.00341.x.

– (2008b). "Spectral nudging in a spectral regional climate model". In: *Tellus, Series A: Dynamic Meteorology and Oceanography*. DOI: 10.1111/j.1600-0870.2008.00341.x.

Randall, D., M. Khairoutdinov, A. Arakawa, and W. Grabowski (2003). "Breaking the Cloud Parameterization Deadlock". *Bull. Amer. Meteor. Soc.* 84.11, pp. 1547–1564. DOI: 10.1175/BAMS-84-11-1547.

Raschendorfer, M. (2001). "The New Turbulence Parameterization of LM". In: *COSMO Newsletter*. 1st ed. [Available online at http://www.cosmo-model.org/content/model/documentation/newsLetters/newsLetter01/newsLetter_01.pdf.]. Deutscher Wetterdienst (DWD), pp. 89–97.

Ratto, C., R. Festa, C. Romeo, O. Frumento, and M. Galluzzi (1994). "Mass-consistent models for wind fields over complex terrain: The state of the art". *Environ. Software* 9.4, pp. 247–268.

Raymond, W. H. (1988). "High-Order Low-Pass Implicit Tangent Filters for Use in Finite Area Calculations". *Mon. Wea. Rev.* 116.11, pp. 2132–2141. DOI: 10.1175/1520-0493(1988)116<2132:HOLPIT>2.0.CO;2.

Richard, E., A. Buzzi, and G. Zängl (2007). "Quantitative precipitation forecasting in the Alps: The advances achieved by the Mesoscale Alpine Programme". *Quart. J. Roy. Meteor. Soc.* DOI: 10.1002/qj.65.

Ritter, B. and J.-F. Geleyn (1992). "A Comprehensive Radiation Scheme for Numerical Weather Prediction Models with Potential Applications in Climate Simulations". *Mon. Wea. Rev.* 120.2, pp. 303–325. DOI: 10.1175/1520-0493(1992)120<0303:ACRSFN>2.0.CO;2.

Roberts, N. (2008). "Assessing the spatial and temporal variation in the skill of precipitation forecasts from an NWP model". *Meteorol. Atmos. Phys.* 15.1, pp. 163–169. ISSN: 1469-8080. DOI: 10.1002/met.57.

Roberts, N. M. and H. W. Lean (2008). "Scale-Selective Verification of Rainfall Accumulations from High-Resolution Forecasts of Convective Events". *Mon. Wea. Rev.* 136.1, pp. 78–97. DOI: 10.1175/2007MWR2123.1.

Rockel, B., A. Will, and A. Hense (Aug. 2008). "The Regional Climate Model COSMO-CLM (CCLM)". *Meteor. Z.* 17.4, pp. 347–348. DOI: 10.1127/0941-2948/2008/0309. URL: http://dx.doi.org/10.1127/0941-2948/2008/0309.

Rossa, A., P. Nurmi, and E. Ebert (2008). "Overview of methods for the verification of quantitative precipitation forecasts". In: *Precipitation: Advances in Measurement, Estimation and Prediction*. Ed. by S. Michaelides. Berlin, Heidelberg: Springer Berlin Heidelberg, pp. 419–452. ISBN: 978-3-540-77655-0. DOI: 10.1007/978-3-540-77655-0_16.

Rummukainen, M. (2010). "State-of-the-art with regional climate models". *WIRes. Clim. Change* 1.1, pp. 82–96. DOI: 10.1002/wcc.8.

Salifu, T. and W. A. Agyare (2012). "Distinguishing land use types using surface albedo and normalized difference vegetation index derived from the sebal model for the Atankwidi and Afram Sub- Catchments in Ghana". *ARPN Journal of Engineering and Applied Sciences* 7.1, pp. 69–80.

Schär, C., T. D. Davies, C. Frei, H. Wanner, M. Widmann, M. Wild, and H. C. Davies (1998). "Current Alpine Climate". In: *Views from the Alps: Regional Perspectives on Climate Change*. Ed. by P. Cebon, U. Dahinden, H. C. Davies, D. M. Imboden, and C. C. Jaeger. Cambridge, United Kingdom and Massachusetts, USA: Massachusetts Institute of Technology (The MIT Press), p. 170. ISBN: 026203252X, 9780262032520.

Schättler, U. Doms G, and M. Baldauf (2016). *A Description of the Nonhydrostatic Regional COSMO Model; Part VII: User's Guide*. Deutscher Wetterdienst. 3004 Offenbach, Germany.

Scheuerer, M. and T. M. Hamill (2015). "Variogram-Based Proper Scoring Rules for Probabilistic Forecasts of Multivariate Quantities". *Mon. Wea. Rev.* 143.4, pp. 1321–1334. DOI: 10.1175/MWR-D-14-00269.1.

Schlager, C., G. Kirchengast, and J. Fuchsberger (2018). "Empirical high-resolution wind field and gust model in mountainous and hilly terrain based on the dense WegenerNet station networks". *Atmos. Meas. Tech.* 11.10, pp. 5607–5627. DOI: 10.5194/amt-11-5607-2018.

Schlager, C., G. Kirchengast, J. Fuchsberger, A. Kann, and H. Truhetz (2019). "A spatial evaluation of high-resolution wind fields from empirical and dynamical modeling in hilly and mountainous terrain". *Geosci. Model Dev.* 12.7, pp. 2855–2873. DOI: 10.5194/gmd-12-2855-2019.

Schlager, C., G. Kirchengast, and J. Fuchsberger (Apr. 2017). "Generation of high-resolution wind fields from the dense meteorological station network WegenerNet in south-eastern Austria". *Wea. Forecasting* 32.4, pp. 1301–1319. DOI: 10.1175/WAF-D-16-0169.1.

Schneidereit, A., S. Schubert, P. Vargin, F. Lunkeit, X. Zhu, D. H. W. Peters, and K. Fraedrich (2012). "Large-Scale Flow and the Long-Lasting Blocking

High over Russia: Summer 2010". *Mon. Wea. Rev.* 140.9, pp. 2967–2981. DOI: 10.1175/MWR-D-11-00249.1.

Schroeer, K. and G. Kirchengast (June 2018). "Sensitivity of extreme precipitation to temperature: the variability of scaling factors from a regional to local perspective". *Climate Dyn.* 50.11, pp. 3981–3994.

Schultz, D. M. (2005). "A Review of Cold Fronts with Prefrontal Troughs and Wind Shifts". *Mon. Wea. Rev.* 133.8, pp. 2449–2472. DOI: 10.1175/MWR2987.1.

Schwartz, C. S., J. S. Kain, S. J. Weiss, M. Xue, D. R. Bright, F. Kong, K. W. Thomas, J. J. Levit, and M. C. Coniglio (2009). "Next-Day Convection-Allowing WRF Model Guidance: A Second Look at 2-km versus 4-km Grid Spacing". *Monthly Weather Review* 137.10, pp. 3351–3372. DOI: 10.1175/2009MWR2924.1.

Scire, J. S., F. R. Robe, M. E. Fernau, and Y. J. Roberto (1998). *A User's Guide for the CALMET Meteorological Model (Version 5)*. Earth Tech, Inc. 196 Baker Avenue, Concord, MA 01742.

Scorer, R. S. (1949). "Theory of waves in the lee of mountains". *Quart. J. Roy. Meteor. Soc.* 75.323, pp. 41–56. DOI: 10.1002/qj.49707532308.

Seaman, N. L. (2000). "Meteorological modeling for air-quality assessments". *Atmos. Environ.* 34, pp. 2231–2259. DOI: 10.1016/S1352-2310(99)00466-5.

Seibert, P., A. Frank, and H. Formayer (Jan. 2007). "Synoptic and regional patterns of heavy precipitation in Austria". *Theor. Appl. Climatol.* 87.1, pp. 139–153. DOI: 10.1007/s00704-006-0198-8.

Sfetsos, A. (Oct. 2002). "A novel approach for the forecasting of mean hourly wind speed time series". *Renewable Energy* 27.2, pp. 163–174. ISSN: 0960-1481. DOI: http://dx.doi.org/10.1016/S0960-1481(01)00193-8.

Shindell, D., J. C. I. Kuylenstierna, E. Vignati, R. van Dingenen, M. Amann, Z. Klimont, S. C. Anenberg, N. Muller, G. Janssens-Maenhout, F. Raes, J. Schwartz, G. Faluvegi, L. Pozzoli, K. Kupiainen, L. Höglund-Isaksson, L. Emberson, D. Streets, V. Ramanathan, K. Hicks, N. T. K. Oanh, G. Milly, M. Williams, V. Demkine, and D. Fowler (2012). "Simultaneously Mitigating Near-Term Climate Change and Improving Human Health and Food Security". *Science* 335.6065, pp. 183–189. DOI: 10.1126/science.1210026.

Shutts, G. (Aug. 1998). "Idealized models of the pressure drag force on mesoscale mountain ridges". *Contrib. Atmos. Phys.* 71, pp. 303–313.

Skok, G. and V. Hladnik (2018). "Verification of Gridded Wind Forecasts in Complex Alpine Terrain: A New Wind Verification Methodology Based on the Neighborhood Approach". *Mon. Wea. Rev.* 146.1, pp. 63–75. DOI: 10.1175/MWR-D-16-0471.1.

Smith, R. B. (1987). "Aerial Observations of the Yugoslavian Bora". *J. Atmos. Sci.* 44.2, pp. 269–297. DOI: 10.1175/1520-0469(1987)044<0269:AOOTYB>2.0.CO;2.

Steinacker, R. (1989). "Area-height distribution of a valley in its relation to the valley wind". 57, pp. 64–71.

Storch, H. von, H. Langenberg, and F. Feser (2000). "A Spectral Nudging Technique for Dynamical Downscaling Purposes". *Mon. Wea. Rev.* 128.10, pp. 3664–3673. DOI: 10.1175/1520-0493(2000)128<3664:ASNTFD>2.0.CO;2.

Strasser, U., T. Marke, O. Sass, S. Birk, and G. Winkler (2013). "John's creek valley: A mountainous catchment for long-term interdisciplinary human-environment system research in Upper Styria (Austria)". *Environ. Earth Sci.* 69.2, pp. 695–705. ISSN: 18666280. DOI: 10.1007/s12665-013-2318-y.

Suklitsch, M., A. Gobiet, H. Truhetz, N. K. Awan, H. Göttel, and D. Jacob (June 2011). "Error characteristics of high resolution regional climate models over the Alpine area". *Climate Dyn.* 37.1, pp. 377–390. ISSN: 09307575. DOI: 10.1007/s00382-010-0848-5.

Sun, L. and K. Schulz (2017). "Spatio-Temporal LAI Modelling by Integrating Climate and MODIS LAI Data in a Mesoscale Catchment". *Remote Sensing* 9.2. ISSN: 2072-4292. DOI: 10.3390/rs9020144. URL: http://www.mdpi.com/2072-4292/9/2/144.

Sütterlin, M., R. Stöckli, C. B. Schaaf, and S. Wunderle (2016). "Albedo climatology for European land surfaces retrieved from AVHRR data (1990–2014) and its spatial and temporal analysis from green-up to vegetation senescence". *J. Geophys. Res.* 121.14, pp. 8156–8171. DOI: 10.1002/2016JD024933.

Swart, N. C. and J. C. Fyfe (2012). "Observed and simulated changes in the Southern Hemisphere surface westerly wind-stress". *Geophys. Res. Lett.* 39.16. DOI: 10.1029/2012GL052810.

Takashi, H., U. Sathoshi, and K. Kazuo (1989). "Development of a system to estimate evapotranspiration over complex terrain using Landsat MSS, elevation and meteorological data". *Hydrol. Sci. J.* 34.6, pp. 635–649. DOI: 10.1080/02626668909491372.

Taylor, P. A., P. J. Mason, and E. F. Bradley (Apr. 1987). "Boundary-layer flow over low hills". *Bound.Layer Meteor.* 39.1, pp. 107–132. ISSN: 1573-1472. DOI: 10.1007/BF00121870.

Termonia, P., C. Fischer, E. Bazile, F. Bouyssel, R. Brožková, P. Bénard, B. Bochenek, D. Degrauwe, M. Derková, R. El Khatib, R. Hamdi, J. Mašek, P. Pottier, N. Pristov, Y. Seity, P. Smolıková, O. Španiel, M. Tudor, Y. Wang, C. Wittmann, and A. Joly (2018). "The ALADIN System and its canonical model configurations AROME CY41T1 and ALARO CY40T1". *Geosci. Model Dev.* 11.1, pp. 257–281. DOI: 10.5194/gmd-11-257-2018.

Thompson, D. W. J. and J. M. Wallace (2001). "Regional climate impacts of the Northern Hemisphere annular mode". *Science* 293, pp. 85–89. DOI: 10.1126/science.1058958.

Tiedtke, M. (1989). "A Comprehensive Mass Flux Scheme for Cumulus Parameterization in Large-Scale Models". *Monthly Weather Review* 117.8, pp. 1779–1800. DOI: 10.1175/1520-0493(1989)117<1779:ACMFSF>2.0.CO;2.

Truhetz, H. (2010). *High resolution wind field modelling over complex topography: analysis and future scenarios*. Scientific Rep. 32-2010. [Available online at http://wegcwww.uni-graz.at/publ/wegcreports/2010/WCV-SciRep-No32-HTruhetz-Apr2010.pdf.] Graz, Austria: Wegener Center Verlag, p. 170. ISBN: 978-3-9502940-0-2.

Truhetz, H., A. Gobiet, and G. Kirchengast (Apr. 2007). "Evaluation of a dynamic-diagnostic modelling approach to generate highly resolved wind fields in the Alpine region". *Meteor. Z.* 16.2, pp. 191–201. ISSN: 09412948. DOI: 10.1127/0941-2948/2007/0192.

Tsuang, B.-J. (2005). "Ground Heat Flux Determination according to Land Skin Temperature Observations from In Situ Stations and Satellites". *J. Hydrometeorol.* 6.4, pp. 371–390. DOI: 10.1175/JHM425.1. eprint: https://doi.org/10.1175/JHM425.1. URL: https://doi.org/10.1175/JHM425.1.

Tustison, B., D. Harris, and E. Foufoula-Georgiou (2001). "Scale issues in verification of precipitation forecasts". *J. Geophys. Res. Atmos.* 106.D11, pp. 11775–11784. DOI: 10.1029/2001JD900066.

Van Ulden, a. P. and a. a. M. Holtslag (1985). "Estimation of Atmospheric Boundary Layer Parameters for Diffusion Applications". *J. Climate Appl. Meteor.* 24, pp. 1196–1207. DOI: 10.1175/1520-0450(1985)024<1196:EOABLP>2.0.CO;2.

Vautard, R., J. Cattiaux, P. Yiou, J. N. Thépaut, and P. Ciais (2010). "Northern Hemisphere atmospheric stilling partly attributed to an increase in surface roughness". *Nature Geosci.* 3.11, pp. 756–761. DOI: 10.1038/ngeo979.

Vries, H. de, T. Woollings, J. Anstey, R. J. Haarsma, and W. Hazeleger (2013). "Atmospheric blocking and its relation to jet changes in a future climate". *Climate Dyn.* 41.9, pp. 2643–2654. DOI: 10.1007/s00382-013-1699-7.

Vuuren, D. P. van, J. Edmonds, M. Kainuma, K. Riahi, A. Thomson, K. Hibbard, G. C. Hurtt, T. Kram, V. Krey, J.-F. Lamarque, T. Masui, M. Meinshausen, N. Nakicenovic, S. J. Smith, and S. K. Rose (Aug. 2011). "The representative concentration pathways: an overview". *Climat. Change* 109.1, p. 5. DOI: 10.1007/s10584-011-0148-z.

Wakonigg, H. (1978). *Weather and Climate in Styria (in German)*. Graz: Verlag fuer die Technische Universitaet Graz, p. 473. ISBN: 3-7041-0049-8.

Waldron, K. M., J. Paegle, and J. D. Horel (1996). "Sensitivity of a Spectrally Filtered and Nudged Limited-Area Model to Outer Model Options". *Mon. Wea. Rev.* 124.3, pp. 529–547. DOI: 10.1175/1520-0493(1996)124<0529:SOASFA>2.0.CO;2.

Wang, W., W. J. Shaw, T. E. Seiple, J. P. Rishel, and Y. Xie (June 2008). "An evaluation of a diagnostic wind model (CALMET)". *J. Appl. Meteor. Climatol.* 47.6, pp. 1739–1756. ISSN: 15588424. DOI: 10.1175/2007JAMC1602.1.

Wang, Y., T. Haiden, and A. Kann (2006). *The operational Limited Area Modelling system at ZAMG: ALADIN-AUSTRIA*. Vol. 37. Wien: Österreichische Beiträge zu Meteorologie und Geophysik, p. 33.

Wedi, N. and S. Malardel (2010 2010). "Non-hydrostatic modelling at ECMWF". *ECMWF Newsletter* 125, pp. 17–21. DOI: 10.21957/rzojr98e. URL: https://www.ecmwf.int/node/17457.

Weusthoff, T., F. Ament, M. Arpagaus, and M. W. Rotach (2010). "Assessing the Benefits of Convection-Permitting Models by Neighborhood Verification: Examples from MAP D-PHASE". *Mon. Wea. Rev.* 138.9, pp. 3418–3433. DOI: 10.1175/2010MWR3380.1.

Wever, N. (2012). "Quantifying trends in surface roughness and the effect on surface wind speed observations". *J. Geophys. Res. Atmos.* 117.D11. DOI: 10.1029/2011JD017118.

Whiteman, C. D., S. Zhong, X. Bian, J. D. Fast, and J. C. Doran (2000). "Boundary layer evolution and regional-scale diurnal circulations over the and Mexican plateau". *J. Geophys. Res. Atmos.* 105.D8, pp. 10081–10102. DOI: 10.1029/2000JD900039.

Wicker, L. J. and W. C. Skamarock (2002). "Time-Splitting Methods for Elastic Models Using Forward Time Schemes". *Mon. Wea. Rev.* 130.8, pp. 2088–2097. DOI: 10.1175/1520-0493(2002)130<2088:TSMFEM>2.0.CO;2.

Willmott, C. J., S. M. Robeson, and K. Matsuura (Nov. 2012). "A refined index of model performance". *Int. J. Climatol.* 32.13, pp. 2088–2094. ISSN: 08998418. DOI: 10.1002/joc.2419.

Winterfeldt, J. and R. Weisse (2009). "Assessment of Value Added for Surface Marine Wind Speed Obtained from Two Regional Climate Models". *Mon. Wea. Rev.* 137.9, pp. 2955–2965. DOI: 10.1175/2009MWR2704.1.

Woollings, T. (2010). "Dynamical influences on European climate: an uncertain future". 368.1924, pp. 3733–3756. ISSN: 1364-503X. DOI: 10.1098/rsta.2010.0040.

Wu, J., J. Zha, D. Zhao, and Q. Yang (Sept. 2018). "Changes in terrestrial near-surface wind speed and their possible causes: an overview". *Climate Dyn.* 51.5, pp. 2039–2078. DOI: 10.1007/s00382-017-3997-y.

Yin, J. H. (2005). "A consistent poleward shift of the storm tracks in simulations of 21st century climate". *Geophys. Res. Lett.* 32.18. DOI: 10.1029/2005GL023684.

Zardi, D. and C. D. Whiteman (2013). "Diurnal Mountain Wind Systems". In: *Mountain Weather Research and Forecasting: Recent Progress and Current Challenges*. Ed. by F. K. Chow, S. F. De Wekker, and B. J. Snyder. Dordrecht: Springer Netherlands, pp. 35–119. ISBN: 978-94-007-4098-3. DOI: 10.1007/978-94-007-4098-3_2.

Zhang, H.-M., J. J. Bates, and R. W. Reynolds (2006). "Assessment of composite global sampling: Sea surface wind speed". *Geophys. Res. Lett.* 33.17. DOI: 10.1029/2006GL027086.

Zhao, C., Q. Jiang, Z. Sun, H. Zhong, and S. Lu (2013). "Projected Urbanization Impacts on Surface Climate and Energy Budgets in the Pearl River Delta of China". *Advances in Meteorol.* 10, p. 10. DOI: 10.1155/2013/542086.